Novel Indirect Additive Manufacturing for Processing Biomaterials

Shah Fenner Khan Mohamad Khan

This dissertation is submitted for partial fulfilment for the degree of Doctor of Philosophy.

School of Mechanical and System Engineering

Newcastle University

Newcastle upon Tyne, United Kingdom.

September 2015

Abstract

The aim of this work was to identify methods for the production of patient-specific biomedical devices via indirect additive manufacturing (AM) methods. Additive manufacturing has been shown to provide a good solution for the manufacture of patient specific implants, but in a limited range of materials, and at a relatively high cost. This research project considered what are known as “indirect” AM approaches, which typically consider AM in combination with one or more subsequent processes in order to produce a part, with a maxillofacial plate and mandible resection used as a demonstrator application.

Three different approaches were considered: (i) using AM to produce moulds for powder pressing of bioceramic green parts for subsequent sintering; (ii) using AM to produce moulds for biopolymer sintering; and (iii) 3D printing of bioceramic powders into green parts for subsequent sintering.

Apatite wollastonite glass ceramic (AW) and poly-Lactide-co-glycolide (PLGA) were selected as the bioceramic and biopolymer materials to process. These were characterised before and after processing in order to ensure that the processing route did not affect the material properties. Geometric dimensions, the morphological structure and mechanical properties were studied to establish the accuracy, shrinkage and strength of the fabricated biomaterial implants.

The use of AM processes to produce moulds for PLGA sintering, and the 3D printing of bioceramic powders formed the best overall results in terms of the definition and properties of the manufactured parts. Parts produced were accurate to within 5% of the as designed dimensions for both the PLGA sintering and the bioceramic powders 3D printing. The indirect AM methods are considered to be promising processing routes for medical devices.

Dedication

This work is dedicated to my beloved late parents,

Noor Aini Abdullah

1939 – 1984

Mohamad Khan Shoumuz Khan

1937 – 2014

"Semoga Allah swt mencucuri rakhmat ke atas roh mereka.

Tiada yang mustahil dicapai sekiranya berusaha tanpa mengalah."

Nothing is impossible to accomplish if one persevere without giving in.

Personal statement

During the time spend in doing this research it had broadened my view as an academician as well as a human being. Doing research is just not about academic materials purely but also involved the interpersonal domain. How one communicates and respects others that surround the daily activities in carrying out the research play an important and significant role in the success of the research. The more one seek to understand one thing the more one will realise the need to understand a lot of others related things.

Declaration

This dissertation is the result of my work and includes nothing, which is the outcome of the work done in collaboration except where specifically indicated in the text. It has not been previously submitted, in part or whole, to any university of institution for any degree, diploma, or other qualification.

In accordance with the Faculty of Science, Agriculture and Engineering guidelines, this thesis does not exceed 80,000words.

Signed: _.....

Date: 23rd September 2015

Shah Fenner Khan Mohamad Khan MSc. (UK), BSc. (USA)

Student ID: A079082150

School of Mechanical and Systems Engineering

Newcastle University, UK.

Acknowledgements

In the duration of my study in Newcastle University, I am ever grateful to all the individuals who have contributed to my quest of knowledge as a Ph.D. student.

First of all, I would to extend gratitude and appreciation to my supervisors Prof. Dr. Kenneth W. Dalgarno and Dr. Matthew German (School of Dental Sciences) for their insightful inputs, invaluable assistance, guidance and supports throughout this research journey. This research would not have been possible without their supervision and encouragement as supervisors and as friends.

I too would like to express my appreciation to the technical team; Ken Madden, Malcolm Black, Michael Foster, Stephen Charlton and Brian Stoker for all the technical assistances and helpful advices during practical works. I would also like to thank Andrew Yates (School of Dental Sciences) for assistance in the operation of DSC analysis and Instron tensile testing equipment, Maggie White (School of Chemical Engineering and Advanced Materials) for helping in XRD analysis, Pauline Carrick (ACMA) and Tracey Davey (Medical School) for SEM works and Neville Dickman (School of Chemical Engineering and Advanced Materials) for assistance in operation of Carbolite furnace. My gratitude also extended to Phil Heslop (Computing Science) for 3D printing the parts that were used in the research.

I would also like to thanks to my colleagues for their suggestions, wishes and help during the four years study.

Furthermore, I would like to thank University Malaysia Perlis and the Malaysian Higher Education Ministry for sponsoring me and giving me the opportunity for doing research in Newcastle University.

And most of all, I would like to express my endless love to my family for their understanding and support through the duration of my study. Very special thanks to my children; Nurdiyanah Nasuha, Muhammad Zulhanis, Nurliyanah Atiqah, NurIffah Syahirah and NurIzzah Syakirah, for bringing smiles and laughter. For them, there are my sparks of encouragement to carry on when I am down.

Finally, for my ever dearest wife, Salma Mohamad Isa for the wishes, love and support, as well as being always by my side.

Table of Contents

Abstract iii

Dedication iv

Personal statement v

Declaration vi

Acknowledgements vii

Table of Contents ix

List of Tables xv

List of Figures xvi

List of Abbreviations and Acronyms xxi

Chapter 1: Introduction 1

1.1 Introduction 1

1.2 Research Problem 2

1.3 Research Aim and Objectives 4

1.3.1 Aim 4

1.3.2 Objectives 4

1.4 Research Framework 4

1.5 Thesis Outline 5

Chapter 2: Literature Review 7

2.1 Introduction 7

2.2 Fundamentals of Additive Manufacturing (AM) 7

2.3 Process categories of AM Systems 10

2.3.1 Vat photopolymerisation 10

2.3.2 Powder bed fusion 11

2.3.3 Directed energy deposition 12

2.3.4 Binder jetting 14

2.3.5 Material Jetting 15

2.3.6 Material Extrusion 15
2.3.7 Sheet Lamination 17
2.4 Type of Application in AM 18
2.4.1 Rapid prototyping 20
2.4.2 Rapid tooling 20
2.4.3 Rapid manufacturing 21
2.5 Indirect AM 22
2.6 Design in AM 23
2.7 STL file format 26
2.8 Natural Bone 28
2.8.1 Bone Graft Substitute (BGS) Materials. 29
2.8.2 Fixation of bone graft substitute. 31
2.9 Bioceramic and glass-ceramics 32
2.9.1 Glass-Ceramic 34
2.9.2 Apatite Wollastonite glass-ceramics 37
2.10 Biodegradable polymer 39
2.10.1 Polylactide-co-Glycolide Acid (PLGA) 43
2.11 Biocomposite 44
2.12 Forming Processes of Biomaterials in the Manufacturing of Medical Devices and Implants 44
2.12.1 Fabrication methods in ceramic material 45
2.12.2 Methods in processing of biopolymers 46
2.13 Sintering 47
2.13.1 Solid-state and liquid state sintering 48
2.14 Materials Characterisations and Analysis 50
2.14.1 Density Measurement using Pycnometer 51
2.14.2 DSC 52
2.14.3 SEM 54

2.14.4 XRD 56
2.14.5 Mechanical Testing 57
2.15 Methodology 59
Chapter 3: 3D Printed Moulds for Lost Wax Casting of Apatite Wollastonite Powder 61
3.1 Introduction 61
3.2 Material Characterisations and Methods 61
3.2.1 Materials 62
3.2.2 Powder Mixing 66
3.2.3 DSC Analysis 68
3.2.4 Fabrication of AW glass ceramic specimens 69
3.2.5 Characterisation of sintered specimens 70
3.2.6 XRD and EDX evaluation of material after fabrication process 83
3.3 Assessment of moulding process 88
3.3.1 SLA mould 90
3.3.2 Aluminium (Al) block mould 91
3.3.3 Aluminium shell mould 91
3.3.4 FDM with aluminium sheet shell mould 92
3.3.5 Different moulding system outcome 94
3.4 Case Study 95
3.4.1 Specific Case Study Background 95
3.4.2 Design and AM manufacturing of Implant Moulding System 96
3.4.3 DFMA methodology in design of mandible implant 97
3.4.4 Design of Implants for mandible reconstruction 98
3.4.5 Fabrication and Attachment of Implants for mandible reconstruction 98
3.4.6 Integration Indirect AM and lost wax process. 100
3.4.7 AM Indirect tooling. 100
3.4.8 AM in soft tooling 104

3.5 Discussion 107
3.5.1 Comparison of AM in indirect tooling and soft tooling 107
3.6 Conclusions 108
Chapter 4: 3D Printing of bioceramics powder 110
4.1 Introduction 110
4.2 Materials and Methods 110
4.2.1 Process 111
4.2.2 Materials 113
4.2.3 Powder Blending 115
4.2.4 Binder Preparation 117
4.3 Process Development 117
4.3.1 Binder Evaluation 117
4.3.2 Powder Blend Evaluation 120
4.3.3 Sintering 130
4.3.4 Accuracy 132
4.3.5 Mechanical Properties 136
4.3.6 XRD analysis of sintered parts fabricated using 3DP 140
4.4 Discussion 143
4.5 Conclusion 143
Chapter 5: 3D Printed Moulds for Biopolymers 145
5.1 Introduction to Chapter 145
5.2 Material Characterisation 145
5.2.1 Material and DSC Analysis 145
5.3 Moulding Process Development 151
5.3.1 Load and Temperature Combination Optimum Process Setting 152
5.3.2 Evaluation and Analysis 154
5.3.3 Results 155

5.3.4 DSC Evaluation of material after fabrication process 163
5.4 Case Study 164
5.4.1 Specific Case Study Background 164
5.4.2 Design and AM manufacturing of Patch Moulding System..... 166
5.4.3 Mould Design and Manufacture 170
5.4.4 Attachment of a personalised fixation patch 171
5.5 Results 171
5.6 Discussion..... 173
Chapter 6: General Discussion 175
6.1 Introduction 175
6.2 Discussion..... 175
6.2.1 Moulding of AW scaffolds by aluminium sheet mould 176
6.2.2 Shell moulding Process of AW 3D artefacts by mean of Rapid Tooling (RT) 177
6.2.3 Lost wax casting (LWC) process of bioceramic 3D artefacts by mean of Rapid Tooling (RT) 177
6.2.4 3D printing process of bioceramic 3D artefacts by indirect AM 177
6.2.5 Crystallography Phase Comparison of Sintered AW parts from Moulding and 3D Printing. 178
6.2.6 Melt moulding processing of biopolymer 3D artefacts by mean of Rapid Tooling (RT)..... 179
Chapter 7: Conclusion and Future Work. 181
7.1 Conclusion 181
7.2 Future Work..... 182
References 184
Appendix A – Academic contribution. 203
Appendix B Data 206
Appendix C Mould drawing and RTV moulding steps. 233

List of Tables

Table 3.1 List of equipment used in the study..... 62
Table 3.2 Average Tg of PMMA at midpoint. 69
Table 3.3 Samples average geometrical measurements. 75
Table 3.4 Density and porosity measurements of AW as determine using pycnometer. 77
Table 3.5 Flexural Modulus and Modulus of Rupture (Flexural Strength)..... 82
Table 3.6 Samples of different AW-PMMA ratio tested on different mould..... 94
Table 3.7 Materials cost for fabricating a unit of AM soft tooling. 105
Table 3. 8 Mechanical Properties of Natural bone and bioceramics. 107

Table 4.1 List of equipment used in the study..... 110
Table 4.2 Ratio of AW mixture preparation..... 115
Table 4.3 Components of ZP18 binder solution..... 117
Table 4.4 Result of spraying different binder solution to AW maltodextrine powder mixture..... 118
Table 4.5 Accuracy of 3D printed green specimens..... 133
Table 4.6 Accuracy of sintered 3D printed specimens..... 134
Table 4.7 Young's modulus and Flexural strength of printed 3D specimens. 140

Table 5.1 Properties of Lactide:Glycolide co-polymer. 146
Table 5. 2 Glass transition temperature of biopolymer PLGA..... 146
Table 5.3 Glass transition temperature of SLA material..... 151
Table 5.4 Results of different parameter settings in melt moulding of PLGA pellets. 153
Table 5.5 Statistical Analysis for Mechanical Properties of PLGA fabricated under heating profile and load of 15lbs (kg) as described in 5.3.1..... 158
Table 5.7 Mean value for 95% confidence interval for sintered test sample of PLGA.160

List of Figures

Figure 2.1 Generalised AM process flow from the CAD model created from data captured to AM fabricated artefact. 9
Figure 2.2 Vat photopolymerisation AM system configuration for stereolithography apparatus (SLA)(SD3DPrinting, 2013)..... 11
Figure 2.3 Powder bed fusion AM system for Selective Laser Sintering (SLS) Process overall configuration (VG, 2012)..... 12
Figure 2.4 Direct energy deposition AM system, (a) Electron beam melting (EBM) (Arcam, 2013) (b) laser engineered net shape (LENS) (Mechanicalengineeringblog, 2012). 13
Figure 2.5 Binder jetting AM system, Colour 3DP (dreams.me.vt.edu, 2009). 14
Figure 2.6 Material jetting schematic arrangement (Objet, 2008)..... 15
Figure 2.7 Material extrusion Fused Deposition Modeling (FDM) System overall configuration (3DParts, 2011)..... 16
Figure 2.8 Sheet lamination AM system configuration LOM (Custompartnet, 2012)... 17
Figure 2.9 Sheet lamination AM system configuration UAM. (Fabrisonic, 2012). 18
Figure 2.10 Applications areas in general subset of AM. These include RP, RT and RM in various form of usage in the medical fields (Khan, 2010)..... 19
Figure 2.11 Titanium implants with original RP as a master pattern in investment casting(a) and injection mould inserts(b) (CUT-CRPM, 2014, Turner, 2007)..... 21
Figure 2.12 Some RM customised parts dental coping (a) and Cranial Implants(b) (EOS, 2011).(Source: EOS GmbH). 22
Figure 2.13 Format of a triangular facet for STL file. 27
Figure 2.14 An STL file format model of a section of a mandibular image showing the surface triangulation with mesh reduction using Meshlab software. (a) Low number of triangulation and (b) High number of triangulation. 27
Figure 2.15 Bone remodelling cycle(Umich.edu, 2005)..... 30
Figure 2.16 Manufacturing schedule for the production of glass ceramics. 35
Figure 2.17 Clinical uses of bioceramics (Hench and Wilson, 2013)..... 36
Figure 2.18Categories of sintering in a phase diagram..... 48
Figure 2.19 Classical sintering model of two adjacent particles (German, 1996)..... 49
Figure 2.20 Diffusion pathways (German, 1996). 50
Figure 2. 21 Density bottle (Impact-test, 2013, Jaytecglass, 2012)..... 51

Figure 2.22 Schematic of a DSC (Colby, 2007). 53
Figure 2.23 Schematic DSC thermogram of semi-crystalline polymer which denote the point of glass transition temperature T_g, crystallisation temperature T_c, melting temperature T_m and decomposition temperature T_d (Braun et al., 2012). 53
Figure 2. 24 Various signal from electron-sample interactions when the incident electrons are decelerated in the solid sample (Nanoscience, 2014). 54
Figure 2.25 schematic of SEM and x-ray optics (Swapp, 2007). 55
Figure 2. 26 Bragg's Law reflection. The diffracted X-rays exhibit constructive interference when the distance between paths ABC and A'B'C' differs by an integer number of wavelengths (λ) (Henry et al., 2007). 57
Figure 2.27 Typical stress-strain diagram for ductile materials. 58
Figure 2.28 Specimen's initial position at start of test (BSI, 2011). 59
Figure 2.29 Methodology flow chart used in the proposed study. 60

Figure 3.1 AW frits as obtained (a)batch1 and (b)batch2, mostly in the range of 53-90μm with few larger than 90μm; scale bar at top left, top right, bottom left and bottom right are 500μm, 200μm, 100μm and 20μm respectively. 64
Figure 3.2 PMMA particles of mostly below the size 4um as obtained (a) GM0600 fairly dispersed and (b) GM0800 closely lumped; scale bar at top left, top right, bottom left and bottom right are 500μm, 200μm, 50μm and 20μm respectively. 65
Figure 3.3 AW-PMMA powder mixtures (a) PMMA GM0600 adheres well to A-W and (b) PMMA GM0800 did not blend well with A-W. The scale bar at top left, top right, bottom right and bottom right are 500μm, 200μm, 50μm and 20μm respectively. 67
Figure 3.4 DSC tests of four out of six PMMA powder samples. 68
Figure 3.5 Process flow in preparing sintered test specimens. 71
Figure 3.6 Heating Profile for sintering AW green parts. 72
Figure 3.7 Three Measurements were taken on sintered specimens (a), (b), (c) and (d) where variation is not significant; scale bar on images is 1000μm. 74
Figure 3. 8 Image (a) and (b) of the cross section of sintered AW samples. 77
Figure 3.9 SEM images (a) and (b) of sintered porous A-W glass ceramic 80%wt on the external surface of two samples at 500X and 5000X magnification indicating micro-porosity; scale for left image and right image are 50μm and 5μm respectively. 78

Figure 3.10 Scaffolds as produced by the proposed method (top) and scaffolds produced by SLS. 79
Figure 3.11 Bending test diagram as based on BS (BSI, 2008). 80
Figure 3.12 Load versus Deflection for 2 batches of AW cylindrical specimens from 3 Point bending test. 81
Figure 3.13 XRD analysis of the sintered AW cylindrical specimens indicating the consistent peaks pattern using newer ICDD database (a-b) 2003 and (c-d) 2009. 86
Figure 3.15 EDX results for sintered two samples specimen fabricated using aluminium sheet mould using the same batch of AW-PMMA powder mixture. 88
Figure 3.16 Different moulds designed to assess the viability for used in AW scaffold round specimens fabrication; (a) two different designs for aluminium block mould without ejector, (b) CAD design (left) and SLA mould (right)for moulding system with ejector, (c) alternative CAD designs and (d) simple Al sheet mould. 89
Figure 3.17 Greenpart inside (a) SLA mould, and (b) greenpart as removed from mould. 90
Figure 3.18 Simple rolled-up Aluminium sheet mould of diameter 3.0mm. 92
Figure 3.19 Two designs of mould that use aluminium foil to ease removal of moulded part (a) 2-piece Al mould with end-cover (b) 2-piece mould incorporating end cover, and (c) Al sheet on the fabricated mould with top view and assembled front view. 93
Figure 3.20 (a) Conventional implant fixation method. (b) A section cut-out for implant with slotted joint. 97
Figure 3.21 (a) CAD implants model, (b) CAD multiple parts mould of implants and (c) FDM fabricated mould with one-half of the mould filled with modelling wax as used in LWC. 98
Figure 3.22 Aluminium foil as pressed into the cavity of the AM mould. 99
Figure 3.23 Sintered AW implant from green part of implant produced from FDM mould with Al sheet shell mould. 99
Figure 3.24 (a) Initial design and (b) redesign for better heat penetration. 100
Figure 3.25 (a) Show Comparison between FDM model (left) with a wax model (middle) and AW part, while (b) show the outcome of several AW parts that were produced. Some improvements were noted on the parts in term of reducing crack, and the geometrical shape is near to the model geometry. 102
Figure 3.26 Processing flow in indirect fabrication of customised AW medical implants. 103

Figure 3.27 (a) Preparation for soft tooling moulding with FDM master pattern and (b) wax pattern as duplicated from RTV silicone mould of the FDM master pattern. 104
Figure 3.28 (a) Wax model (left) obtained from RTV silicone moulding process comparing to the FDM master pattern (b) minor deviation of features..... 105
Figure 3.29 Processing flow in fabricating customised AW medical implants by indirect AM with the integration of RTV silicone mould and LWC process..... 106
Figure 3.30 Comparison of the wax model with FDM model. Model from modelling wax showing higher loss definition of the feature as compared to the wax model from RTV soft tooling..... 108

Figure 4.1 Ball mill machine that was used in the milling process of AW powders. .. 112
Figure 4.2 Process Flow and Characterisation of AW powder mixture..... 113
Figure 4.3 Particles of AW 53μm -90μm and maltodextrine below 53mm as received114
Figure 4.4 SEM images of different preparations. 116
Figure 4.5 The influence of the amount of binder solution to the layer thickness. 120
Figure 4. 6 (a)Printing orientation of AW test specimens on Z-Corp 310Plus 3D printer, (b) different distortion in green part specimens and (c)samples of sintered part where the bottom surface are straighter than the top surface. Circled areas showing the effect of curling..... 121
Figure 4.7 Printing effects (a), (b) and (c) on the geometrical accuracy of 3D artefacts. 124
Figure 4.8 Surface texture of top, bottom and side of printed samples (a), (b) and (c).129
Figure 4.9 Specimens printed using the prepared AW-maltodextrine mixture with ethanol-Darvan-C based binder solution. 130
Figure 4.10 Equipment used in sintering AW green parts. 131
Figure 4.11 SEM images of sample at (a) outer surface and (b) at bending failure surface (from left to right) at 20X magnification (2mm scale bar), 117X (200μm scale bar), and 1170X (20μm scale bar) 132
Figure 4.12 3D printed artefacts showing minor geometrical deviation from the CAD model, (a) curling of printed parts, and (b) different in surface profile in top and bottom surface of AW fracture patch..... 135
Figure 4. 13 Comparison of outcomes from two different approaches; indirect tooling and 3D printing..... 136
Figure 4.14 AW green parts stress-strain curve. 137

Figure 4.15 AW sanded sintered parts stress-strain curve. 138
Figure 4. 16 AW unsanded sintered parts stress-strain curve. 139
Figure 4.18 XRD analysis using 2 different ICCD database for samples which used maltodextrine binder and PVA solution..... 143

Figure 5.1 DSC analysis of various ratio of PLGA. 150
Figure 5.2 Processing of PLGA Specimens..... 152
Figure 5.3 (a) SLA mould in the heating setup and (b) PLGA pellets in SLA mould.. 152
Figure 5.4 Heating profile for the sintering process of PLGA..... 154
Figure 5.5 Bending test diagram and the actual test on a universal testing machine rig.154
Figure 5.6 Stress-Strain curves of PLGA co-polymers..... 157
Figure 5.7 Fracture of PLGA 50:50(above) and PLGA 65:35 (below) obtained from bending test showing the region of tension at the top with craze. 161
Figure 5.8 SEM images at outer surface of specimens 162
Figure 5.9 SEM images at fracture surface from 3 point bending test. 162
Figure 5.10 Comparison of virgin to sintered PLGA 65:35. 163
Figure 5.11 Fracture Occurrence for Regions of the Mandible (Natu et al., 2012). 164
Figure 5.12 Bone Plate Used in an Open Reduction Internal Fixation Procedure(ORIF) (Bhagol et al., 2013)..... 165
Figure 5.13 Step in reverse engineered the fracture patch. 168
Figure 5. 14 Process flow in design and manufacture of moulding for customised fracture patch..... 167
Figure 5.15 Various fixation plates were created for high occurrence sites of fracture.169
Figure 5.16 FDM model of the fixation plate for form fitting test. 169
Figure 5.17 Individual part of the mould assembly as design from Autodesk Inventor. Design steps are as displayed in Browser Panel. 170
Figure 5.18 CAD model of the moulding assembly and exploded view. 171
Figure 5.19 PLGA before and after sintering in SLA mould..... 172
Figure 5.20 (a) PLGA 50:50, (b) PLGA 65:35 and (c) CAD model of the fracture plate. 172

List of Abbreviations and Acronyms

3D - Three dimensional

3DP - 3D Printing/Printer

ABS - Acrylonitrile butadiene styrene

AM - Additive Manufacturing

ASTM - American Society for Testing and Materials

AW-GC - Apatite-Wollastonite glass ceramic

BGS – Bone graft substitute

CAED - Computed Aided Engineering Design

CAD - Computed Aided Design

CNC - computer numerical control

CT – Computer tomography

DLS - Direct Laser Sintering

DMLS - Direct Metal Laser Sintering

DOF - Degree Of Freedom

EBM - Electron Beam Melting

FDM - Fused Deposition Modelling

FE – Finite element

FGM - functional graded material

HIP - Hot Isostatic Pressing

IC - Investment Casting

LWC - Lost wax casting

LENS - Laser Engineering Net Shape

LOM - Laminated Object Manufacturing

MJM - Multi-Jet Modelling

MRI - Magnetic Resonance Imaging

MVA - motor vehicle accidents

PE - Polyethylene

PLGA - poly-lactide-co-glycolide

RE - Reverse Engineering

RM - Rapid Manufacturing

RP - Rapid Prototyping

RT - Rapid Tooling

SFF - Solid Freeform Fabrication

SLA - Stereolithography

SLM - Selective Laser Melting

SLS - Selective Laser Sintering

STL – Stereolitographic /surface tessellation (triangulation) language file format

UAM –Ultrasonic AM

UV - ultra violet

Chapter 1: Introduction

1.1 Introduction

Additive manufacturing technologies were initially envisioned to be tools for rapid fabrication of prototypes. Hence, in the early development of these technologies, the phrase *rapid prototyping system* was often used to describe additive manufacturing technologies. After almost 30 years of development, advancements in materials development for additive manufacturing systems have pushed the boundary of these technologies from merely producing prototypes to producing functional parts. In 2009, ASTM agreed upon the term additive manufacturing as the standard term in acknowledging this recent development (ASTM, 2012). However, it is still far from being able to use all the traditional materials available in a typical manufacturing environment. Additive manufacturing (AM) technologies allow physical three dimensional (3D) artefacts to be built directly from virtual models of almost any geometry created from computer aided design (CAD) systems (Mavili et al., 2007). These 3D artefacts are built in a layer wise manner where materials are added layer-by-layer. Therefore, needs for dedicated moulds, dies, or tooling are not required during fabrication. As AM systems' main source of data input are from CAD models, these technologies are well suited for the medical field. Computed tomography (CT) and magnetic resonance imaging (MRI) methods for scanning bodies and creating computer images of the skeletal structure use slicing technique to capture images in layers, much like the way AM build 3D artefacts. The images are used to generate 3D computer models and can be used as input data for the AM system. This method had been established in creating 3D models for surgical visualisation, planning and communication (Esses et al., 2011, Sanghera, 2001, Winder, 1999).

The changing role of additive manufacturing technologies from rapid prototyping to rapid manufacturing have influenced the optimistic view of medical practitioners of using additive manufacturing technologies for medical applications far beyond the scope of pre-surgical visualization and planning. Defects of the skeletal system caused by trauma, disease, congenital abnormalities or bone deficiency, osteoarthritis and wear, pose a major challenge to overcome. Clinical needs for anatomically shaped biomaterials to replace the skeletal defects not only confined to the healing of bone but also to the functional and aesthetical aspects. Recent developments have shown the capabilities of additive manufacturing methods in providing improvements for patients care in traumatic injuries and congenital defects

(Douglas, 2014, Melchels et al., 2010, Wang et al., 2009, Parthasarathy et al., 2009, Cohen et al., 2009). Even though AM systems are capable of fabricating freeform shape, replacement of human parts that mimic nature in structure and function remains distant.

Bone as a living tissue, considered a composite material, is comprised of trabecular (cancellous) bone and cortical (compact) bone. It can heal and remodel by responding with adaptation in its structure to loading stress or injury such as fracture. Even though bone has this natural ability to heal and remodel; external mechanical means are required in helping to stabilize and realign fractured bone during the healing process, thus encouraging faster healing. In addition, bone is only capable of automatically fulfilling their regenerative function within voids of limited size. Therefore, bone is unlikely to remodel itself in major bone losses. Hence, if the defect is too large, bone replacements are required to fill the gap and bridge the defects. Most of these types of major bone repairs are treated by bone grafting that use the patient's bone (autografts) or donor bone (allografts). The advantages of these grafts include rapid and excellent osseous integration, which justified their usage in more than half of bone grafting procedures. However, the need of further surgery, risk of transmitted disease, immunogenic rejection, donor site morbidity and limited material from donor site pose some limitations to the current practices (Zwingenberger, 2012, Ogilvie et al., 2009, Goldberg, 2005, Getty and Peabody, 1999, Strong, 1996). Therefore, increasing attention towards alternative techniques and implant materials and devices as solutions to these problems has encouraged much research over recent years.

Bone graft substitute (BGS) of synthetic materials such as metals, alloys, polymers, glass and ceramics have been applied and studied as reinforcement or replacement in bone defects. Although, an ideal to date, the traditional methods for producing these devices that mimics the natural bone and the anatomy of the recipients are yet to be fully achieved.

1.2 Research Problem

AM systems had seen a flourishing development in recent research and usage for medical applications in which an increase from 8.8% in 2001 to 16.4% in 2013 was noted (Wohlers, 2013). Depending on the parts and materials required, different approaches are used in producing the medical artefacts. Additive manufacturing (AM) can produces parts by either using the direct or indirect method. Additive manufacturing used to produce directly end user parts is termed as rapid manufacturing (RM). However, the cost of acquiring such a machine is high. A couple of the AM machines that have been used in recent research for RM are

electron beam melting (EBM) and direct metal laser sintering (DMLS) which cost from £723,000 and £482,000 upward, respectively. The EBM machine was used in studies to produce implantable parts for the application in maxillofacial surgery (Jamshidinia et al., 2014, Poukens et al., 2010) while DMLS system was used in orbital implants fabrication (Salmi et al., 2012). Since most of the systems used for direct additive manufacturing are costly, the overhead cost for producing patient specific part tends to increase. It was pointed out from a comparison study between EBM and conventional method that the manufacturing cost contribution of parts produced by EBM as compared to conventional method is 130% even though the total cost to produce the parts is only 65% overall of the conventional method (Cronskar et al., 2013). Furthermore, fixation and reconstruction of defective bone involved high health care costs and, therefore, are often not easily reachable for patients in most of the developing countries. The cost of surgery is very high due partly to the cost of the device used as well as the time needed for pre- and post-operation. Patients facing this ordeal find it difficult to afford a corrective action; especially for patients from the low income and newly developed countries as well as lower income group in developed countries. The appearance of the facial features cause by fracture and deformation to the mandible often produce undesirable emotional stress and discomfort. Thus, healthy life style can be jeopardised. Patients will have serious problems with ingestion and communication as well as appearance that have negative effects on their social life (Simon et al., 2013). It has been highlighted that high occurrences of bone fractures are caused by motor vehicle accidents (MVA) involving motorbikes and alcohol abuse and of these incidents; most are from the lower income group (Nordin et al., 2014, Rahman et al., 2007, Brasileiro and Passeri, 2006).

Even though AM systems are capable of producing end-user products and at reducing manufacturing time, AM use is dampened by the high initial investment cost and the high cost of producing usable raw materials for the AM systems (White and Lynskey, 2013). Hence, in order to contribute to the achievement of healthy life style, affordable and reasonable customised devices which can indirectly reduce the time and cost for reconstruction of defective mandibular bone of these patients would contribute toward improving their quality of life. In order to do these, new manufacturing routes to produce affordable customised implantable devices need to be addressed. One approach is to use indirect AM method as indirect application of AM method has been proven in studies conducted at producing tooling and patterns for industrial applications (Park et al., 2014, Eggbeer et al., 2012, Pham and Dimov, 2003).

1.3 Research Aim and Objectives

1.3.1 *Aim*

The aim of this research is to establish alternatives route in the fabrication of patient specific devices within the implantable medical devices area. This research will demonstrate that the integration of indirect AM with conventional methods can contribute to new functionality and relatively lower cost of producing fracture fixations devices and bone replacements.

1.3.2 *Objectives*

The objectives that have been developed to support the aim are as follows: -

i. Reviewing and investigating suitable additive manufacturing processes that are adopted by the industries that service the medical community and new emerging technologies in this field.

ii. Identifying and establishing process parameters of the selected biomaterials.

iii. Characterising the selected biomaterials' properties prior to the fabrication process and after it.

iv. Exploring design freedom in AM for producing tooling.

v. Developing indirect additive manufacturing process for biomaterials.

vi. Applying and testing the developed process model in the fabrication of maxillofacial devices.

1.4 Research Framework

In order to fulfil the aim and objectives of this research, the scopes of work performed were separated in stages. The initial stage was to review the relevant AM systems and conventional methods that can be integrated in low cost fabrication of customised devices. In the second stage, investigation into biomaterial that can be used was performed. In this stage, characterisation and mechanical testing on the biomaterial that need to be performed were to establish that no changes or degradation in the material properties occurred after the fabrication process. In this stage, processing parameters were also established to produce an

optimum setting for the fabrication process. The next stage was to identify suitable applications where contributions and opportunities of using AM can be tapped. In the final stage, case studies were presented.

1.5 Thesis Outline

This thesis consists of seven chapters. The first chapter is the introduction in which the general idea of the research project is presented. The second chapter proceed with the bulk of the information essential for understanding the research study. It provides comprehensive reference materials and literatures which encompasses additive manufacturing methods and applications, and the range of conventional manufacturing processes of biomaterials. In addition, physiology of human bone and causes of defect to the bone as well as the fixation of it are described. Experimental methods used in this research are presented toward the end of this chapter. Finally, the generalised methodology for this research project is outlined.

The third chapter establishes the appropriate process parameters and material characterisation and properties from AM processed bioceramics. It describes the new route for producing patient specific bioceramic medical devices where the integration of CAD, AM technologies and lost wax casting (LWC) are used. Two different approaches of indirect AM tooling were implemented and described. The mandibular geometry created using the proposed route was assessed for feature definition and repeatability as well as accuracy. The results are presented and discussed.

The fourth chapter describes the steps taken for developing the process of indirect three dimensional printing (3DP) of bioceramic. Process parameters and characterisation for the in-house medium used are established prior to using a commercial 3D Printer (3DP) machine. Morphology analysis and mechanical testing are performed to study the characteristics of the printed artefacts. Mandible implant and fracture fixation patch are used as case studies to determine the feasibility of the indirect AM process using 3DP for bioceramic.

In chapter five, the research work was on creating artefacts from biopolymer. It describes the method developed for the fabricating personalised polymer structures by sintering poly-lactide-co-glycolide (PLGA) granules in a mould manufactured from stereolithography (SLA) process. The explanations on the indirect AM method utilising the tooling created from SLA and adoption of the melt-moulding process as the overall process for fabrication are exemplified by the steps taken in the evaluation of the manufacturing parameters with

material and mechanical properties assessments. A customised fracture patch was moulded to illustrate the feasibility of this process and its ability to create and maintain physiologically shaped parts throughout the process.

The results are then summarised and discussed in chapter six. The thesis then concludes with chapter seven in which conclusion are drawn, and impending works are suggested.

This thesis itself is based on research articles presented and published in refereed conferences and journals. The listing of the research articles are as in appendix A.

Chapter 2: Literature Review

2.1 Introduction

The literature survey presented in this chapter forms the basis for conducting this research study. It serves as the foundation from which the rationales for this research study; and subsequently aims and objectives, are established and justified.

In order to implement a recent technology of manufacturing such as additive manufacturing (AM) techniques into the mature manufacturing industries for medical devices, a thorough understand of the techniques is deemed appropriate. In addition, it is also necessary to gain knowledge in a broad range of subjects including: common additive manufacturing techniques, bone physiology and transplantation, bone fracture and fixation methods, medical biomaterials and manufacturing techniques, medical applications using additive manufacturing techniques, methods in characterisation and mechanical testing of materials as well as AM in design and manufacturing.

The chapter starts with describing the working principle of each different AM techniques and discussing the various applications of AM. A review of AM roles in design and manufacturing is presented besides medical applications of AM. Traditional medical devices manufacturing methods are also reviewed and discussed to form the foundation to which AM techniques to use. This chapter also addresses the tools used in the materials' characterisation and analysis.

2.2 Fundamentals of Additive Manufacturing (AM)

In manufacturing industries, objects/parts can be manufactured either by removing or by adding materials. The addition of materials in conventional manufacturing methods can be performed by joining such as either through adhesion, welding or mechanical joint of subcomponents to make up the end objects/parts. However, the subcomponents are normally fabricated using subtractive methods where materials are removed to create the object. Besides these conventional additive methods, another technique that is considered an additive method is additive manufacturing (AM). However, its' working principle is different. The stark difference in AM as opposed to conventional manufacturing processes by additive methods are that the automatic process of adding material is in the form of predefined layer by layer manner to incrementally shape the three dimensional (3D) objects. AM normally

does not involve subtractive method at all. Although there are research conducted to create hybrid AM systems which integrate both additive and subtractive processes (Yan et al., 2009), it is not as widespread.

In general, AM systems typically add materials in the form of powder, liquid or solid-sheet during the creation process of 3D objects. AM systems normally process single build materials with support materials either from the same or different materials as the build materials. Although various works had been performed to incorporate different build materials (Vaezi et al., 2013, Gibson et al., 2010, Hague et al., 2004), most are single/mono material AM systems. Currently only Statrasys offer one commercial printer marketed as true multimaterial from 3D Object Connex series (Object, 2014) and 3DSystem through its ProJet 5500X series (3DSystem, 2014) are capable of producing multimaterial 3D objects. In addition, there are some hobbyist open source 3D fused filaments fabricators using multiple heads to extrude different materials to build the 3D objects.

AM systems allow the user to generate physical parts from 3D data which can be obtained from computer aided design (Mavili et al., 2007) models, scanned data manipulated from computed tomography (CT) or magnetic resonance imaging (MRI) scans, and from 3D digitizing systems. This technique has frequently been labelled as solid free-form manufacturing/fabrication, computer automated manufacturing, digital desktop manufacturing, additive layer manufacturing and numerous others names. Clarification of terms use in this technique can be referred from ASTM. Even though this technique goes by numerous names, a typical process flow of AM can be described as the process in which virtual part or model is designed using computer aided design (Mavili et al., 2007) software and is converted to stereolithography file format (STL); the industry standard file format for additive manufacturing systems. An STL format is a multifaceted triangulation approximation of a 3D object as shown in Figure 2.14 and is explained in detail in section 2.6.2.2.

The CAD file in STL format is then uploaded into an additive manufacturing system. Orientation for the creation of the physical parts are set for optimal processing with respect to build time, material properties, surface finish or support structure (Chua et al., 2010, Hopkinson et al., 2005, Pham and Dimov, 2001). Intersecting planes are then used to slice the data into successive linear contours which define the composite layers for the object (Choi and Samavedam, 2002). This process flow is as illustrated in figure 2.1.

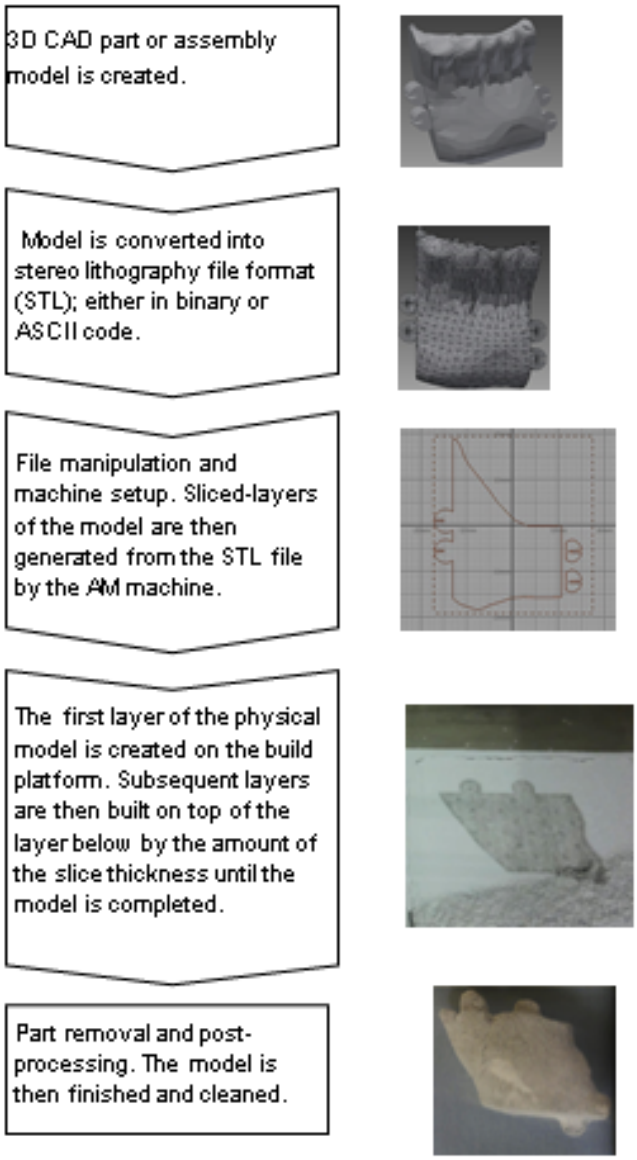

Figure 2.1 Generalised AM process flow from the CAD model created from data captured to AM fabricated artefact.

The development of commercial additive manufacturing systems started approximately three decades ago. 3D Systems of Valencia, CA, developed the first AM technique in the USA using the Stereolithography (SLA) method. Initially, this technique was known as Rapid Prototyping (RP) for it is mainly used to make prototypes. This is partly because a substantial amount of time and resources are spent on tooling and specialised craftsman for making prototypes. Hence, the logical choice is to use this technique to produce prototypes at a faster rate than the conventional methods; thus reducing the cost and the design cycle time. This is truer in small production runs or products of one-off with complicated and complex geometrical designs. Application of additive manufacturing techniques can be a quick and

cost effective manufacturing processes (Pham and Dimov, 2003, Hopkinson and Dicknes, 2003) in these instances. Since then, a number of different methods have become available.

2.3 Process categories of AM Systems

There are 24 different commercial AM technologies offering different functionality to different segments of industries or user groups (Wohlers, 2010) with significant numbers of research on processes and materials for AM conducted up to now. Since AM technologies depend on the materials and methods used, the industries as well as academic seem to have differences in conjugating a common term for the technologies used in AM. Initial classification on AM was based on the physical state of the pre-process build materials and was characterised into liquid, powder and solid (Kruth et al., 1998, Pham and Gault, 1998). As of 2011, AM systems were reclassified based on process similarity and characterised into vat photopolymerization, powder bed fusion, direct energy deposition, binder jetting, material jetting, material extrusion and sheet lamination (ASTM, 2012). All these technologies are described in the following subsections.

2.3.1 *Vat photopolymerisation*

Vat photopolymerization is an AM process in which liquid photopolymer in a vat is selectively cured by light-activated polymerisation (Figure 2.2). The technique produces models from liquid photosensitive polymers that solidify when exposed to ultraviolet light from helium-cadmium or argon ion laser. A highly focused laser beam is used to trace out the 2D cross-sectional profile of the model in a vat of liquid epoxy or acrylate resin which containing a vertically moving platform situated just below the vat surface. The model under construction is supported by the platform that moves downward once a layer is fully traced by a layer thickness for each layer. The process is repeated until the model is fully built. Parts of the model that need support are built the same way at the same time as the model. When the model is completed, the base plate is then raised to lift the model out. Any supports for overhang are removed. The model is then placed in an ultraviolet oven for complete curing (Noorani, 2006, Pham and Dimov, 2003) to avoid toxicity. The advantage of using vat photopolymerisation is that it provides better accuracy among all the AM processes (Melchels et al., 2010). However, it is limited to direct production of plastic parts, although attempts had been made to indirectly produce ceramic parts by suspension of ceramic particle in light sensitive monomer/oligomer resin (Tomeckova and Halloran, 2012, Chartier, 2012).

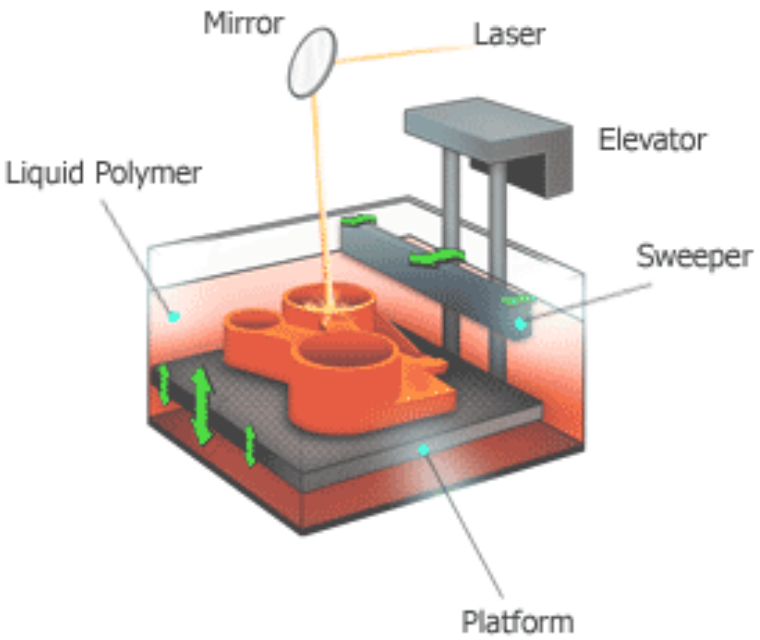

Figure 2.2 Vat photopolymerisation AM system configuration for stereolithography apparatus (SLA)(SD3DPrinting, 2013).

2.3.2 *Powder bed fusion*

The process in this AM system involves selective fusing of regions of a powder bed by thermal energy. AM system such as Selective Laser Sintering (SLS), and Direct Metal Laser Sintering (DMLS) are examples of this process and are comparable in principle to SLA where fine heat-fusible compacted powder is used instead of liquid resin. Once the powder is spread on to a build platform by the roller from the powder-feed platform, a concentrated heating laser beam selectively sintered the powder into the desired shape for each layer. The entire fabrication is performed in a sealed nitrogen atmosphere chamber with maintained temperature-control. The build platform moves down along with loose powder around the formed layer; acting as a support for the next powder layer. Thus, no supports are required with this method since the solid powder bed supports both overhangs and undercuts. This saves some finishing time compared to vat photopolymerisation. Powder is spread with a roller for the next layer and the process repeats until full object is formed. Excess powder is simply brushed away, and final manual finishing may be carried out. Process parameters, such as laser scanning speed and power, can be adjusted to control the strength and porosity of the material (Hon and Gill, 2003, Pham and Dimov, 2003). No final curing is required as in vat photopolymerisation; however, it may be necessary to infiltrate the object with another material to improve the mechanical properties. SLS has a wider variety of materials available

as compare to SLA. Part of the materials available in SLS includes Nylon (Duraform PA), Glass-Filled Nylon (Duraform GF), Flame Retardant Nylon, Durable Nylon (Duraform EX), and SLS Flex.) (Quickparts, 2013, VG, 2012). The general configuration of a typical SLS system is as illustrated in figure 2.3.

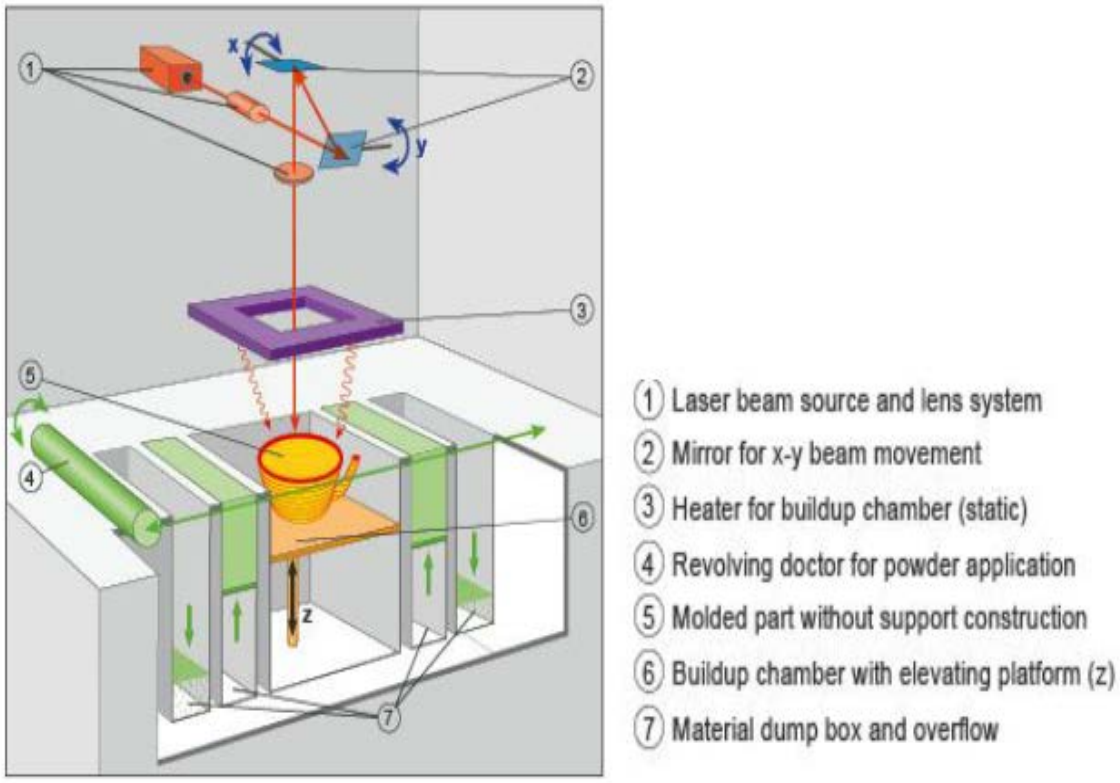

Figure 2.3 Powder bed fusion AM system for Selective Laser Sintering (SLS) Process overall configuration (VG, 2012).

2.3.3 *Directed energy deposition*

Directed energy deposition AM is a process in which focused thermal energy (laser, electron beam, or plasma arc) is focused to melt the powdered materials as they are being deposited. A high thermal energy is used to produce a molten pool as a precise amount of powder is added into the pool to build the part volume. The process repeats the deposits layer upon layer until it has produced a physical version of the CAD model. The process needs to occur inside a sealed chamber to prevent oxidation that causes material from properly wetting to the previous deposited layer. The chamber is purged with argon so that the oxygen and moisture levels stay below 10 parts per million(ppm) for laser engineered net shape (LENS) (Optomec, 2013) and below 50ppm for electron beam melting (EBM) (Yamamoto and Sakai, 2005).

The AM systems included in this category are selective laser melting (SLM), electron beam melting (EBM) (Figure 2.4a) and laser engineered net shape (LENS) (Figure 2.4b). Materials that can be processed include stainless steel, aluminium alloys, titanium, cobalt-chrome and tool steel (Wohlers, 2010). This AM method has an advantage over the powder bed fusion as it can directly produce fully dense parts approaching the bulk material properties (Yasa et al., 2011, Zhao et al., 2009). However, these AM systems are among the costliest with high maintenance cost (refer Table 2.1)

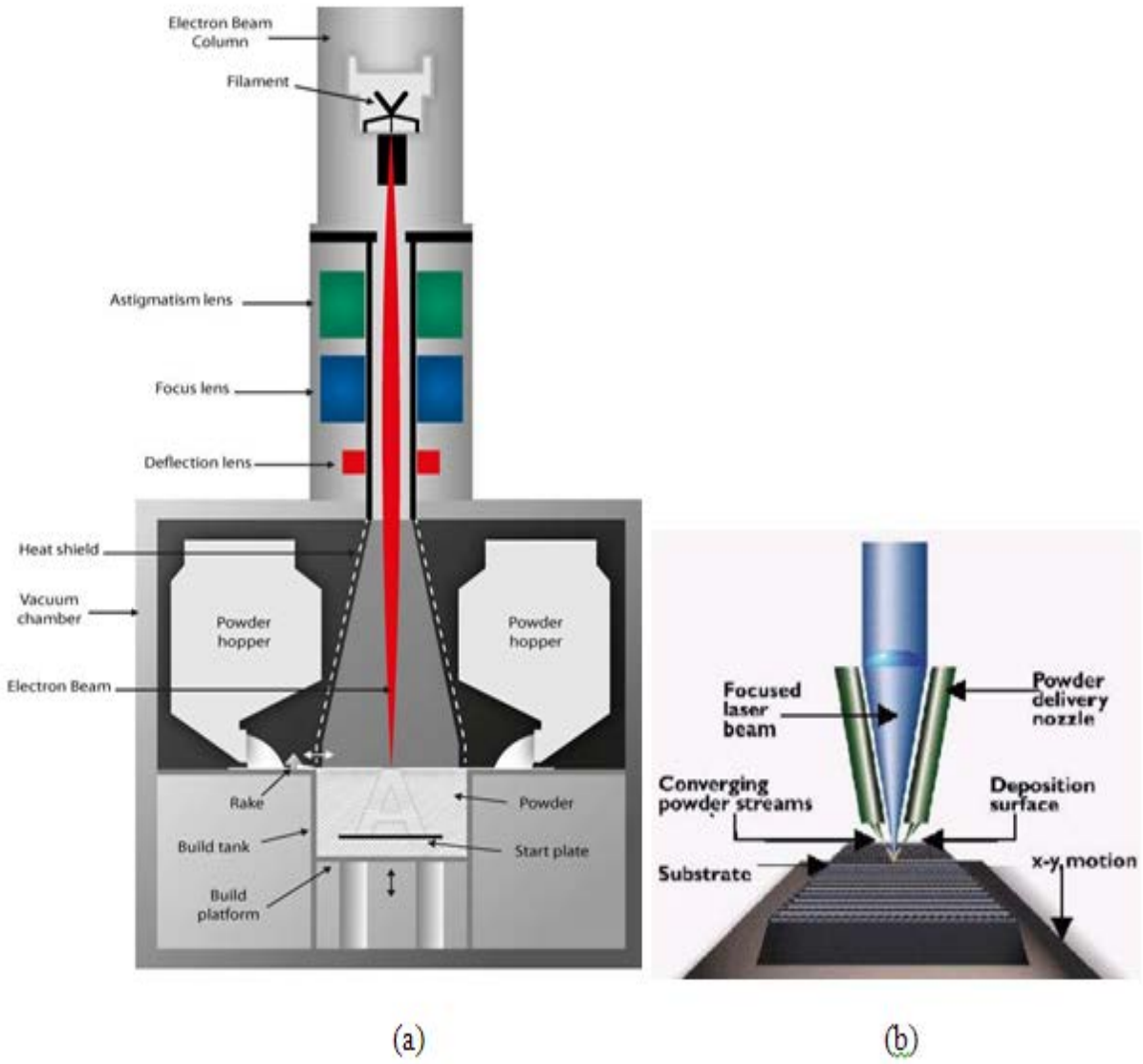

Figure 2.4 Direct energy deposition AM system, (a) Electron beam melting (EBM) (Arcam, 2013) (b) laser engineered net shape (LENS) (Mechanicalengineeringblog, 2012).

2.3.4 *Binder jetting*

The AM systems under binder jetting is rather similar to selective laser sintering, except that an inkjet head is used to deposit a liquid adhesive compound onto the top layer of a bed of compacted powder object material in place of the laser (Figure 2.5). This AM system derived its concept from the printer and plotter industry. It utilizes inkjet technology to spurt minuscule droplets to form layers of a 3D AM model onto a platform from the print head. The particles of the powder become bonded in the areas where the adhesive is deposited. Once a layer is completed, the piston moves down by the thickness of a layer. The ZPrinter from Z-Corp uses this process. The materials available from this system are generally made from starch.

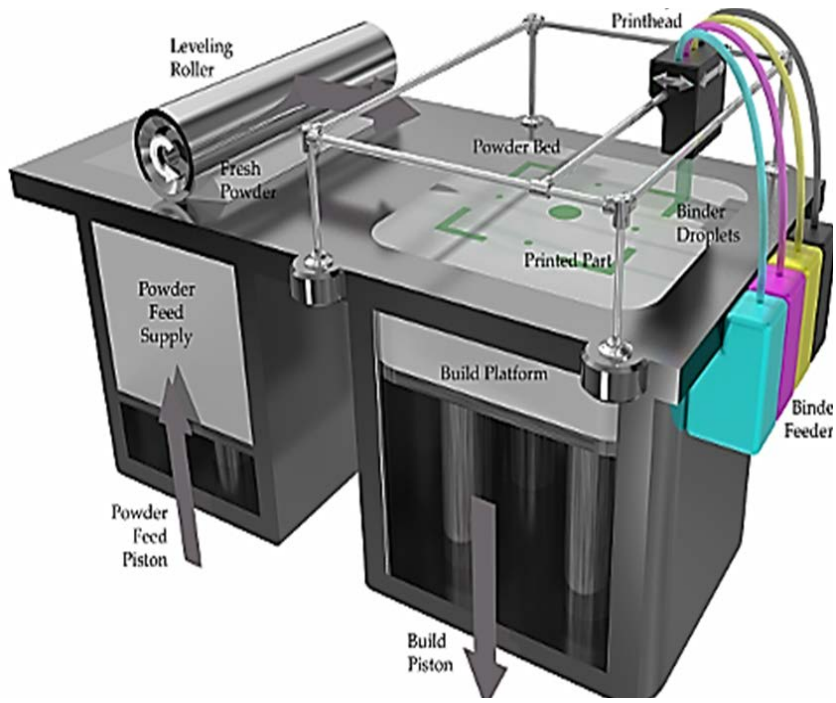

Figure 2.5 Binder jetting AM system, Colour 3DP (dreams.me.vt.edu, 2009).

Besides the normally uses natural polymers as well as plaster of Paris in combination with a water-based ink, starch-based polymer and ceramic with organic binder had been used for 3D printing (Warnke et al., 2010, Klammert et al., 2010, Khalyfa et al., 2007, Derby, 2005, Lam et al., 2002). These AM systems are price at the lower end as compare to others AM systems (Table 2.1).

2.3.5 *Material Jetting*

As with binder jetting AM system, this AM process too derived it concept from the printer industry. Each individual jet dispenses on demand droplets of thermoplastic build material to selective regions (Figure 2.6). Once the material is jetted on the build platform ultraviolet lights (UV) that turn the resin into solid layer cure it. UV light, which is mounted alongside the jetting head, is use to cure and harden each layer. The jetting head and platform which are numerically controlled by the computer moves relatively to each other in the X, Y and Z coordinate system to form each layer. Depending on the technique used either the jetting head or the platform move in the Z direction to allow the jets to form subsequent layers. There are various material jetting systems in the market, such as Sanders ModelMaker™, 3DS Multi-Jet Modeling™, and 3DObject PolyJet™.

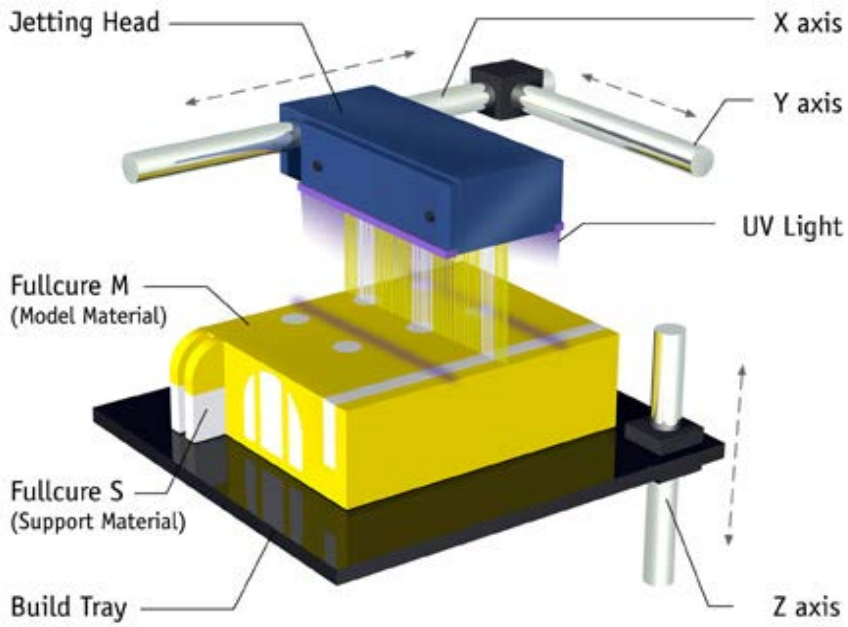

Figure 2.6 Material jetting schematic arrangement (Objet, 2008)

2.3.6 *Material Extrusion*

The AM process in which material is selectively dispensed through a nozzle or orifice is classified as material extrusion AM system (Figure 2.7). Stratasys' Fused Deposition

Modelling system (FDM) is an example of this process as well as numerous open-source material extrusions AM systems such as Fab@home, RepRap, Makerbot and Replicator.

The working principle of most material extrusion AM systems; except Fab@home that extrude putties, involves heating thermoplastic polymer filament wire which is fed through a heated extrusion nozzle head that is controlled numerically. The first layer is formed by the deposition of very thin droplet of material onto the build platform. The temperature at the platform is maintained lower than the heated thermoplastic filament in order for the deposition to quickly harden. Consecutive layers are built layer by layer in the increment of the slice thickness generated from the STL file by the FDM machine. Supports are built along the way, fastened to the part either with a second, weaker material or with a perforated junction. Upon removal of the part from the chamber, it hardens immediately when exposed the temperature of the environment. Acrylonitrile butadiene styrene (ABS) elastomer, polycarbonate, polyphenolsulfone, and investment casting wax are some of the materials use in FDM. Material choices include production-quality ABS (red, yellow, green, blue, white, and black), Polycarbonate (white), PC-ABS (black) and Food-grade ABSi material (Stratasys, 2014, Novakova-Marcincinova and Kuric, 2012).

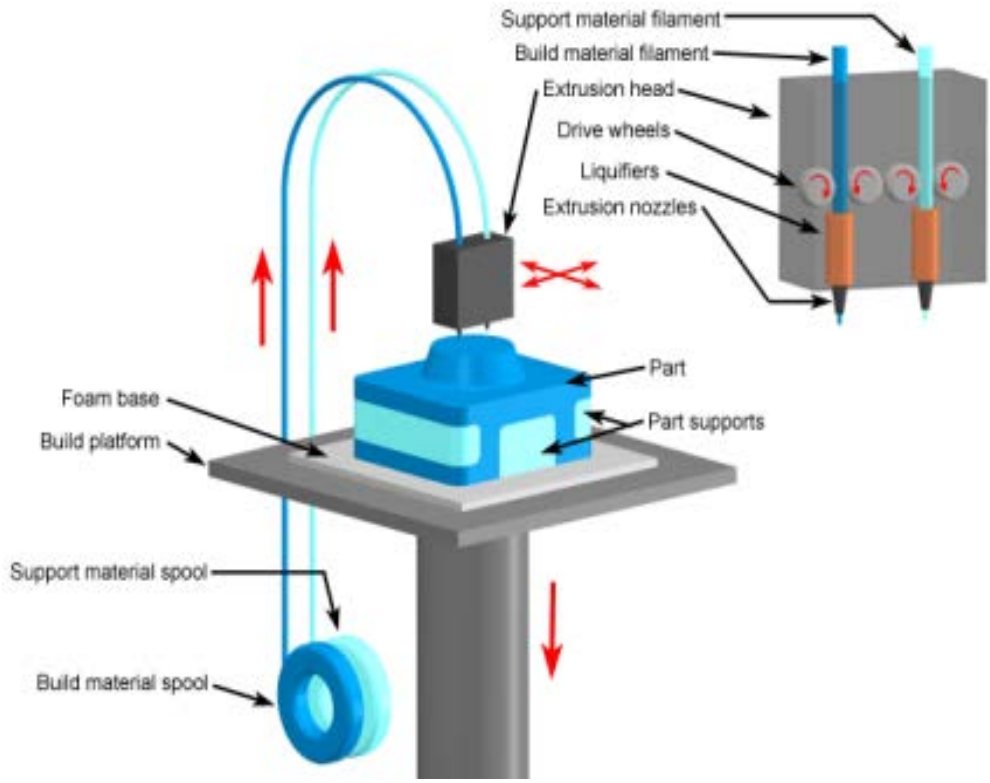

Figure 2.7 Material extrusion Fused Deposition Modeling (FDM) System overall configuration (3DParts, 2011)

2.3.7 *Sheet Lamination*

Sheet lamination AM process uses adhesive bonding or interfacial bonding (ultrasonic) to form 3D objects. The first step is to create a base on which the sheet/foil can attach itself. For adhesive bonding, a heated roller is used to melt the adhesive/polyethylene coating on the paper so that each new layer will adhere to the previous layer whereas for interfacial bonding, ultrasonic vibrations are locally applied to consolidate metal foil materials as solid-state welding, held together under pressure. Materials are fed through with the aid of rollers. Excess materials are trimmed off to create the required shape for the given layer in which, for adhesive bonding, carbon-dioxide laser is used while in interfacial bonding, a computer numerical control (CNC) contour milling is used. The deposit, trim and finish cycle continues until the finished object has been manufactured; at which point it is taken off the base plate and finished. Figure 2.8 shows the adhesive bonding AM process of a laminated object modelling (LOM) system while figure 2.9 shows the interfacial bonding AM process of a ultrasonic consolidation AM (UAM) system (Obielodan et al., 2010).

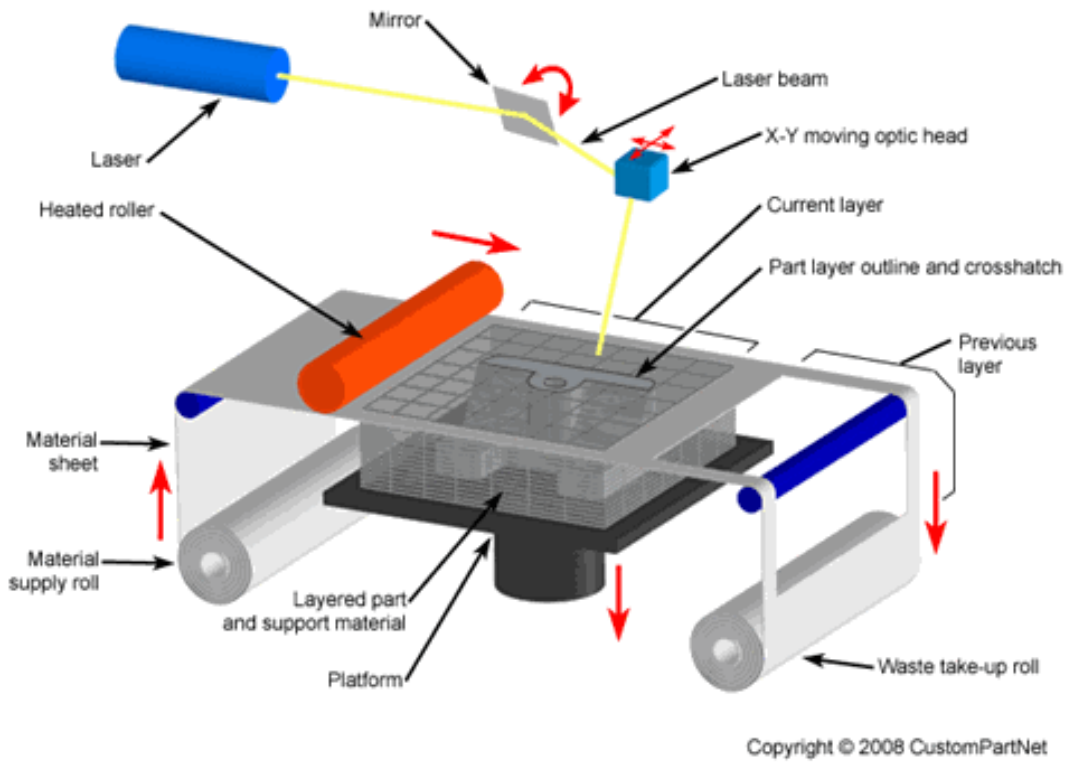

Figure 2.8 Sheet lamination AM system configuration LOM (Custompartnet, 2012).

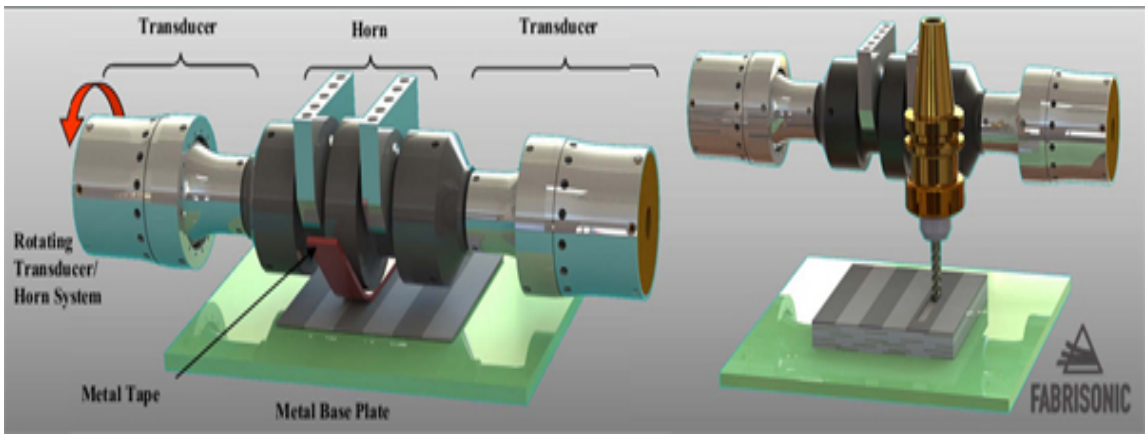

Figure 2.9 Sheet lamination AM system configuration UAM. (Fabrisonic, 2012).

2.4 Type of Application in AM

Since AM depends on the materials and methods use, the industries as well as academic seem to have differences in conjugating a common term for this technique. Additive manufacturing had been classified into liquid photopolymer solidification, molten material deposition, discrete powder solidification, and solid sheets lamination (Levy et al., 2003, Pham and Dimov, 2003, Pham and Dimov, 2001, Kruth et al., 1998). Depending on the material that is being used, AM can be further subset into three general areas of applications; rapid prototyping (RP), rapid tooling (RT), and rapid manufacturing (RM) (Mellor et al., 2014, Gibson et al., 2010, Hon, 2007, Kamrani and Nasr, 2006, Noorani, 2006, Levy et al., 2003, Kruth et al., 1998) as shown in figure 2.10 (Khan, 2010). Figure 2.10 illustrate AM applications and their usage in numerous fields. The use of AM in the medical field can be seen to being applied from the visualisation to mass customisation. This is not an exhaustive list as further researches and new developments are realised; the application areas can be expanded.

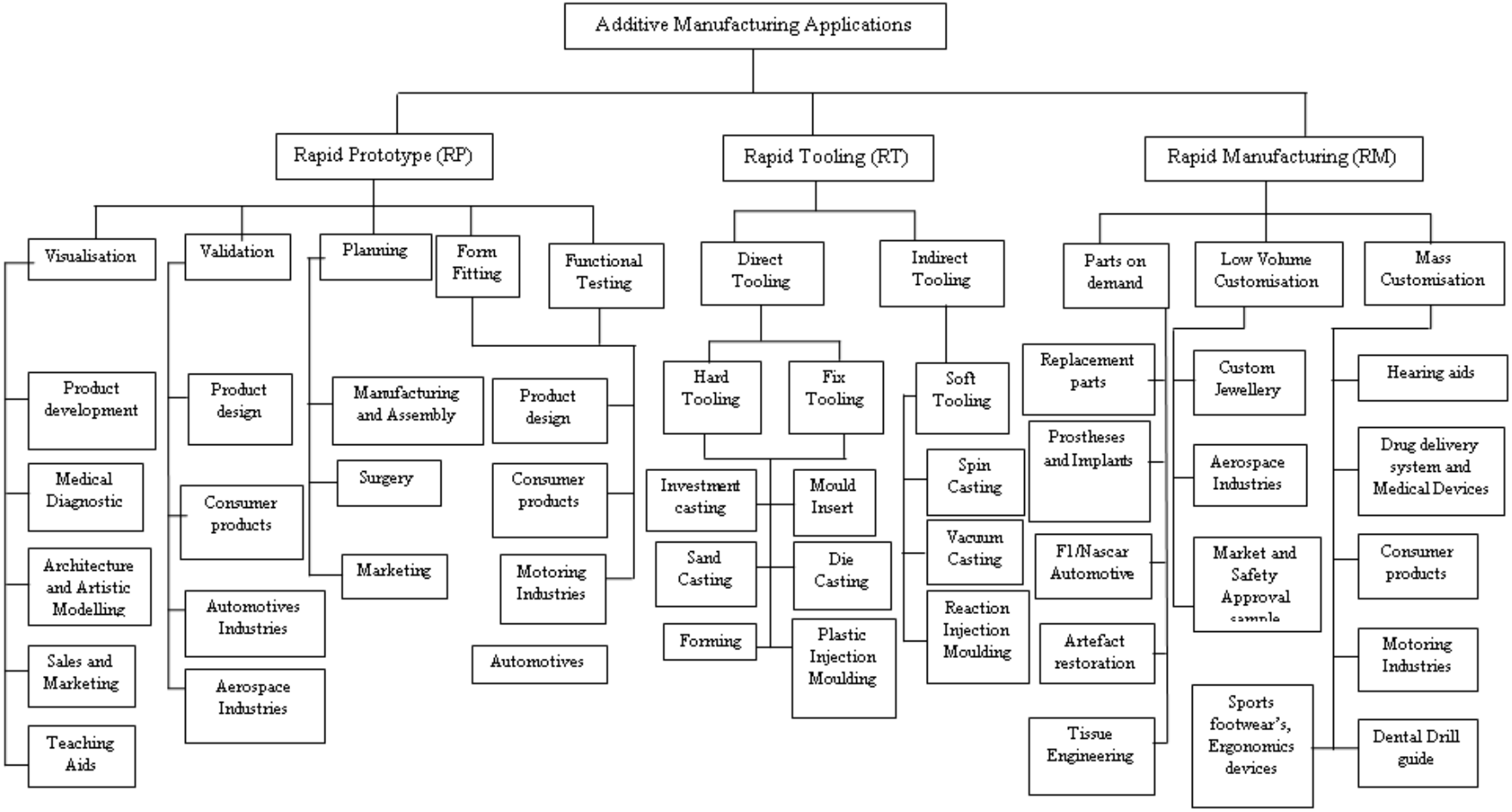

Figure 2.10 Applications areas in general subset of AM. These include RP, RT and RM in various form of usage in the medical fields (Khan, 2010).

2.4.1 *Rapid prototyping*

Rapid Prototyping (RP) can be defined as building three-dimensional physical models directly from 3D computer-aided design (Mavili et al., 2007) for the purpose of prototyping, visualising, validating, form fitting, testing, surgical planning, diagnostic visualisation, and training aids. These models can simplify significantly specialist communication on all levels, minimise miscommunication and breakdown in communication between designers, manufacturing engineers, and end-users during the design process became possible; or between members of a surgery teams; the doctor, the radiologist and surgeon as well the patient during surgical planning (Douglas, 2014, Melchels et al., 2010, Truscott et al., 2008, Berce et al., 2005)

Moreover, RP process provide an alternative route for making prototypes of complex shapes, intricate internal structures, parts within parts, and very thin-wall features and functional models in a relatively cost-effective manner and faster as compared to the conventional methods as prototype's tooling is not required (Gibson et al., 2010, Bartolo and Bidanda, 2008, Hopkinson et al., 2005).

Uses of AM in product design development cycle have a positive influence on time and cost (Wohlers, 2010, Bibb et al., 2000, Webb, 2000)

2.4.2 *Rapid tooling*

The utilizing of AM to produce tooling is referred to as rapid tooling (RT). RT constitute two main categories, indirect tooling that use master patterns to produce a mould or die and direct tooling that fabricate the actual core and cavity mould inserts (Nyembwe et al., 2013, Nagahanumaiah et al., 2008, Dotchev and Soe, 2006). As AM began to evolve in terms of materials and process, foundry and plastics industries began to apply AM to produce rapidly patterns for casting in foundry and plastics industries, investment and die casting for medical and dentistry, moulds and mould inserts, and small lot cast parts (Maji et al., 2008, Cheah et al., 2005, Pham and Dimov, 2003, Levy et al., 2003). Figure 2.11 shows a couple of AM methods that are used in RT applications.

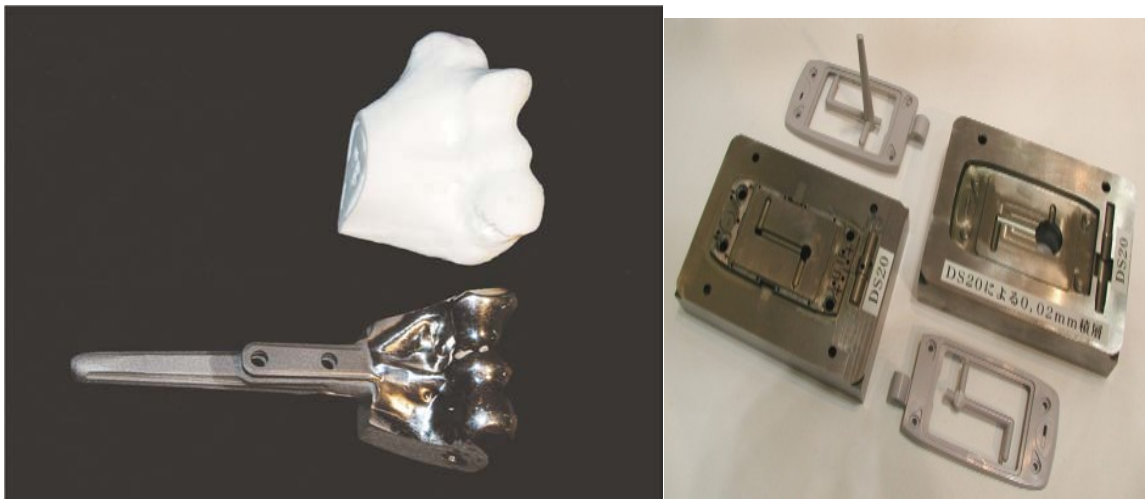

(a) (b)

Figure 2.11 Titanium implants with original RP as a master pattern in investment casting(a) and injection mould inserts(b) (CUT-CRPM, 2014, Turner, 2007)

Not only have numerous studies had been carried out on RT for use in the manufacturing and engineering fields but also various works had been done in using RT for the production of customised medical devices and implants such as stent and bone replacement applications such as jaw bone, elbow bone, and knee (Melgoza et al., 2014, Warnke et al., 2010, Cohen et al., 2009, Maji et al., 2008, Goodridge et al., 2006b, Chiang et al., 2005).

2.4.3 *Rapid manufacturing*

The application of using additive manufacturing system to produce end user products or parts from CAD data directly is termed as Rapid Manufacturing (RM). It is the use of a CAD based automated AM process to build or produce parts that can be directly used (Yan et al., 2009, Hon, 2007). The underlying advantages of RM over CNC machining and injection moulding are that; it provides geometric freedom in part design, capability of functional graded material (FGM), potential of zero tooling, lowered or zero inventory requirements, single material, single piece component in place of an assembly and after post sale, and mass customisation (Hopkinson, 2006). Designers will have the creative freedom for producing new designs that were impossible or impractical to manufacture with the removal of tooling and manufacturing constraints. Rapid Manufacturing for customisation may involve the production of custom part, replacement part, low volume part, or a series of mass produce parts. Increasingly, rapid manufacturing is being applied to automotive, motor sports, jewellery, dentistry, orthodontics, medicine, consumer products, and collectibles where there

is a high degree of customisation. Some examples of RM customised parts for medical and consumer application are as shown in figure 2.12.

2.5 Indirect AM

The approach of direct AM is more achievable for fabrication of metal-based and polymeric-based artefacts rather than ceramics-based. Works on creating dense ceramic artefacts had begun since the early nineties on this approach using SLS system. However, building crack free dense ceramic parts for commercial applications are yet to be realised (Bertrand et al.,

(a) (b)

Figure 2.12 Some RM customised parts dental coping (a) and Cranial Implants(b) (EOS, 2011).(Source: EOS GmbH).

2007, Wu et al., 2007). This is due to several facts such as a high melting temperature, low or no plasticity and low thermal shock resistance of ceramics. Hence, the indirect approach is used.

In indirect AM, two methods can be adopted; the first is by using a sacrificial organic polymer binder as a starting material while the second is by RT. In the sacrificial binder method, thermal energy from the laser melts the organic binder, bonding the ceramic particles. Subsequently the produced green parts are debinded and sintered to increase density and strength. The used of this method had been demonstrated in the fabrication of artefacts from alumina (Shahzad et al., 2013, Deckers et al., 2012), zirconia (Shahzad et al., 2014, Ebert et al., 2009), and glass-ceramics (Tesavibul et al., 2012, Xiao et al., 2008, Goodridge et al., 2006b). With this method, further enhancement to the mechanical properties can be performed by post-processing (Shahzad et al., 2013, Maleksaeedi et al., 2014).

As for the second method, AM parts are used as master patterns (positive) or as sacrificial patterns as practice in traditional casting techniques. Special materials have been created precisely for this purpose, and it is a fast and inexpensive method in comparison to some traditional methods, such as high-speed milling (Pham and Dimov, 2003). In this method where special materials (Quickcast, RapidTool) are used, it is usually for validation of the tool design before final production tooling is made. Conventional manufacturing processes such RTV silicone rubber moulding, vacuum casting, reaction injection moulding (RIM), spin casting, cast resin tooling were revised toward AM pattern-based processes for developing mould rapidly, with varying costs, lead-times and process capabilities. The accuracy of these processes depends much in part on the accuracy of the AM process used to create the pattern (Dickens et al., 2000). Quail et. al (Quail et al., 2010), Rahmati et. al (Rahmati et al., 2007) and Ramos and Simoes (Ramos and Simoes, 2009) performed research work in evaluating the accuracy wax patterns created through RTV rubber moulding of AM master-pattern in the suitability of this technique for the manufacturing of lost wax parts.

Table 2.1 list some of the AM systems that are can be used in direct and indirect rapid tooling. The AM systems that are capable of direct RM of polymer and metal are expensive with price starting from £130,000 onward especially for direct metal AM systems.

2.6 Design in AM

The approach in producing artefacts using AM is the opposite of subtractive manufacturing processes. A lot of design guides have been developed for these subtractive processes. However, when designing artefacts that are to be manufactured by utilising AM as the manufacturing process, designers need a different approach. Most AM systems have the benefits of freedom in geometrical shape definition as well as tooling independent (Hoque et al., 2012, Mansour and Hague, 2003, Hollister et al., 2002, Bernard and Fischer, 2002). Hence, one of the pulling factors for using AM is in the design environment as it offers the capacity of producing parts with unlimited geometry complexity and shape of complex organic structures can be designed and be fabricated (Liu et al., 2014, Rainer et al., 2012, Parthasarathy et al., 2011, De Beer et al., 2008). Conventional manufacturing's cost is highly dependent to the geometry complexity, therefore with lower cost combined with design freedom; both manufacturer and customer will benefit (Hoque et al., 2012, Truscott et al., 2008, Ruffo et al., 2006). With the help from AM, designers have unrestrained freedom to design for customisation rather than to design for manufacturing and assembly. So products

can be designed to fit the user rather than the other way around. The only limitation is the designer's imagination and the design tools. So with the opportunities created from AM technologies, the concept of Design-for-Manufacturing and Assembly (DFMA) can evolve into Manufacturing-for-Design using AM (AMFD) with new design guidelines (Hoque et al., 2012, Diegel et al., 2011, Hopkinson et al., 2006, Hague et al., 2004).

The AM design rules can be summarized as the following (Atzeni et al., 2010):

- Avoid observing, reverse engineering, and designing to conventional manufacturing guidelines and design principles,
- Take advantages from AM technologies capabilities,
- Rethink the whole assembly towards integrated freeform design,
- Reduce the parts count by intelligent integration of functions and
- Optimise the design towards maximum strength with minimal materials usage (and therefore as little energy as possible).

Ponche et al. (Ponche et al., 2012) suggested that a global approach in DFM be structured on the issues of manufacturing process characteristics and parts design functional specifications. Thus, designers can optimise the geometry to address functional specifications and choose the ideal AM process characteristics for fabrication. Various research works had been conducted on these issues which involved developing tools for the selection of AM system with regard to design (Borrille and Gomes, 2011, Ghazy, 2012) and topology optimisation using AM (Brackett et al., 2011, Gardan, 2014).

Table 2.1 AM machine specifications as adapted (Aniwaa, 2014, Namii, 2013).

AM Process Categories	**Entry Level**			**Method**		**Printable Materials**			
	Price USD1000(£1000)	**Built Area inches (mm)**	**Resolution (mm)**	**Direct**	**Indirect**	**Metals**	**Plastics**	**Ceramics**	**Bio**
Binder Jetting									
Z-Corp	USD15 (£9.3)	9.3x7.3x5.0 (236x185x127)	0.1		X			X	
ExOne	USD150 (£95)	1.5x2.3x1.5 (38x58x33)	0.100		X	X		X	

Directed Energy Deposition									
Electron Beam Direct Manufacturing (EBDM)	See manufacturer	7.87x7.87x7.09 (200x200x180)	0.050	M, P	X	X			
Direct Metal Deposition (DMD)	See manufacturer	See manufacturer		M	X	X			
Laser Engineered Net Shaping (LENS)	See manufacturer	See manufacturer		M, P	X	X			
Material Extrusion									
Fused Deposition Modeling (FDM)	USD35 (£23)	10x10x12 (254x254x305)	0.178	P	X		X		
Fused Filament Fabrication (FFF)	USD10 (£6.3)	5x5x5 (127x127x127)	0.178	P	X		X	X	
Bio plotter	USD125 (£77.7)	5.91x5.91x5.51 (150x150x140)	0.001	X					X
Powder Bed Fusion									
Direct Metal Laser Sintering DMLS	USD210 (£130.6)	1.97x1.97x3.15 (50x50x80)	0.05	M	X	X			
Selective Laser Sintering (SLS)	USD725 (£559)	22x22x18 (560x560x457)		P	X		X	X	
Sheet Lamination						X	X		
LOM	USD39 (£24.2)	10.08x6.65x5.91 (256x170x150)	0.19		X		X		
UAM				P, M	X	X	X		
Vat Photopolymerization									
Stereolithography Apparatus (SLA)	USD200 (£132)	10x10x10 (254x254x254)	0.050	P	X		X	X	
Digital Light Projection(DLP)	USD15 (£9.3)	1.57x1.18x3.94 (40x30x100)	0.100	P	X		X	X	
Material Jetting									

Aerosol Jet (AJ)	USD299 (£127)	3.9x3.9x3.9 (99x99x99)	0.025	M	X	X	X	X	
Thermal Spray (TS)				M		X			
Ink jet (IJ)	USD30 (£19.8)	8x10x8 (203x254x203)	0.100		X	X	X	X	
Laser Direct Structuring (LDS)	See manufacturer	See manufacturer		M		X			

2.7 STL file format.

The common factor in all of the AM technologies uses the same file format to print the 3D artefacts. Standard Tessellation Language or commonly known as stereolithography file format (STL) is the use of surface tessellation to define the original 3D part. The STL model is essentially a triangulated surface model of the original part. The STL format is an approximate representation of a true solid-surface model, and a huge amount of STL data is needed to provide sufficient accuracy for AM. STL files are surface approximations of models generated by CAD, reverse engineering (RE) data or 3D reconstruction data from 3D image processing.

As mentioned, the STL format is the dominating data format in AM data processes. The basis of an STL data set is the description of model surfaces by triangulation. The STL format is a tessellation representation, which defines a 3D object by a series of triangular facets. Each triangular facet is defined by three vertices and a unit normal vector for the facet where the normal vector direction indicates the outside of the object (Lin and Liang, 2002). Figure 2.13 shows the description of a triangular facet needed for triangulation. The attributes and coordinates of an STL data set can be written as an ASCII (American Standard Code for Information Interchange) file or a binary file. The STL format allows for both ASCII and binary representations. A binary file creates a small data volume as compared to ASCII source code; which is easier to read.

In a triangulated model, all surfaces of the part are transformed to a mesh of triangles. Generally, increasing the number of triangles increase the dimensional accuracy of the complex and curved surfaces in the original part but also the amount of data.

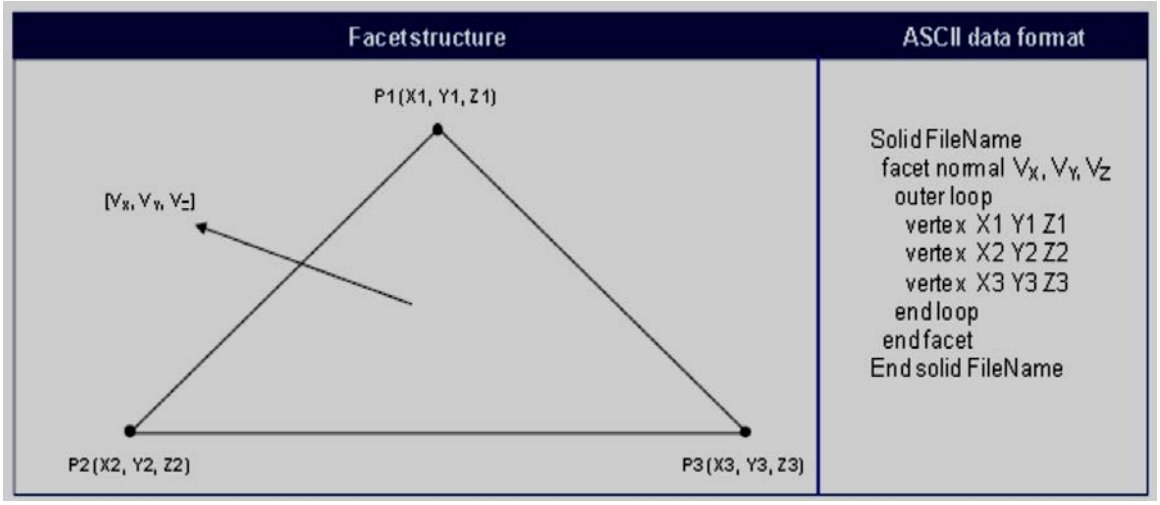

Figure 2.13 Format of a triangular facet for STL file.

The more triangles are used; the more accurate the representation is (Figure 2.14). As shown in Figure 2.14a the number of vertices and faces are 622 and 1240 with a file size of 61KB respectively while in Figure 2.14b the number of vertices and faces are 2481 and 4958 with a file size of 243KB, an increase of 4 folds. Thus, when higher surface qualities are required, the volume of data tends to increase disproportionately to the designated accuracy.

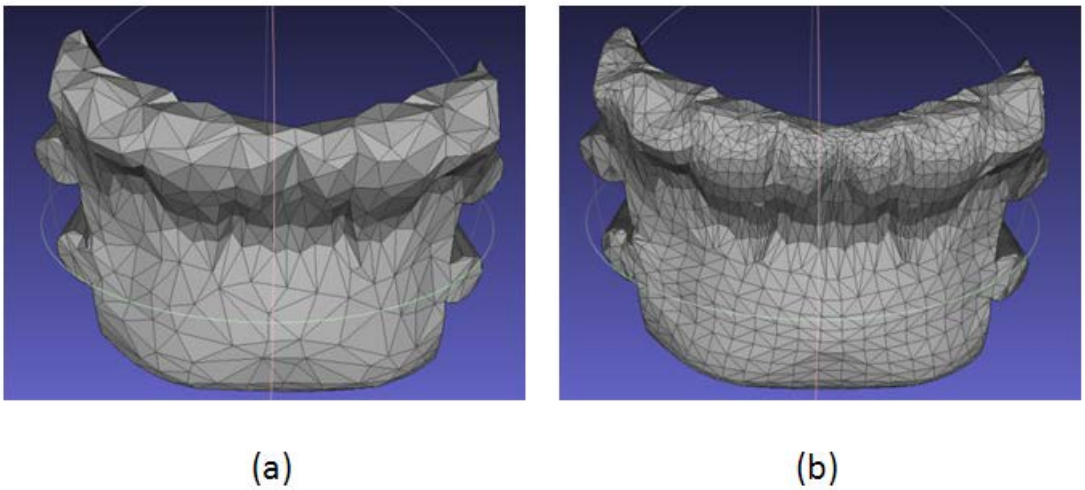

Figure 2.14 An STL file format model of a section of a mandibular image showing the surface triangulation with mesh reduction using Meshlab software. (a) Low number of triangulation and (b) High number of triangulation.

Various algorithms are used in extracting medical imaging data. One of which is marching cubes algorithms (Lorensen and Cline, 1987) and is normally used in extracting isosurfaces from MRI or CT datasets for reconstruction of the human organs in medical visualisation. But the marching cubes algorithms produce meshes with redundant information as with other algorithms. Hence, the amounts of data from 3D reconstructions medical imaging are predictably high. To improve work with medical models, mesh reduction and smoothing algorithms are frequently used before the models are imported into virtual reality environment (Riener and Harders, 2012). In order to utilise low-to-midrange software and hardware, some compromises need to be made such that the data generated are within the capability of the low-to-midrange CAD system and the acceptable accuracy of the medical model. Otherwise, without post-processing of the acquired imaging data, specialised software and hardware will be required to create and model medical artefacts. This will increase the initial fix cost and the computing cost. However, it should be pointed out that it is crucial to keep the CAD model accuracy as close to the medical imaging data model as possible. With accurate post-processing using suitable algorithms on medical imaging, the dataset can be maintained low and aided in faster arithmetic operations for the CAD system. This has been proven with work by Young (Young, 2008) in which by using grid-based segmentation algorithm for mesh reduction, inexpensive and commonly available hardware platforms can generate structural models from scaffolds through to complete human head in a straightforward, robust, accurate and efficient manner. Difficult problems in CAED simulations and numerical analysis can now be performed from on accurate medical models generated from mesh reduction algorithm.

In AM for medical applications, most of the CAD software can translate the original CAD model into STL format and is usually sufficient for practical purposes. However, 3D scanner data model either from magnetic resonance imaging (MRI), 3D scanner or computed tomography (CAT) scanner is not suitable to be used as design model for CAD software as it is always exported in 3D stl format. The STL file needs to be post-processed before it can be used in CAD software as most CAD software are either based on parametric constructive solid geometry (CSG) or non-uniform boundary representation solid (NURBS).

2.8 Natural Bone

Natural bone is a dense connective and highly vascular tissue that plays a vital part providing essential functions and protection for both muscles and organs. Bone is a composite material

containing both organic (living cells such as osteoblasts, osteocytes and osteoclasts and extracellular matrix) and inorganic components (mineral; predominantly calcium phosphate) which by weight contains about 60% mineral, 30% matrix and 10% water (Athanasiou et al., 2000). The organic component is predominantly responsible for the tensile strength while the mineral component of calcium phosphate is accountable for the compressive strength. In general, bone consists of two different structures: compact bone (cortical bone) and spongy bone (trabecular or cancellous bone). Cancellous, the inner part of the bone is spongy in nature having 50% to 90vol% porosity while cortical bone is the dense outer layer of bone with less than 10vol% porosity. Compact bone has a compressive strength in the range of 131 to224 MPa, and a Young's modulus ranging from 17 to 20GPa, while compressive strength and Young's modulus for trabecular bones are 5 to 10MPa and 50 to 100MPa, respectively (Navarro et al., 2008, Athanasiou et al., 2000, Yaszemski et al., 1996). Thus, bone is also a porous material with continuously varying degree of porosity in the mature bone at 5% to 95%. The porosity and pore size of cancellous bone is much greater than that of cortical bone: cancellous bone has 75% to 85% porosity with 300 to 600µm diameter pores and cortical bone has 5% to 10% porosity with 10 to 50µm diameter pores. In its natural hydrated state, cortical bone has a compressive strength (σ) of 110 to 150MPa, and Young's modulus (E) of 18 to 22GPa, while cancellous bone has a compressive strength and Young's modulus of 2 to 6MPa and 0.1 to 0.3GPa, respectively (Novitskaya et al., 2011, Chen and McKittrick, 2011).

2.8.1 *Bone Graft Substitute (BGS) Materials.*

As bone is a living tissue that continuously remodels, bone undergoes dynamic remodelling, maturation, differentiation, and resorption. Figure 2.15 shows the cycle of bone remodelling. Remodelling tend to occur on bone surfaces in which the removal of old bone tissues by osteoclasts are replaced with mineralised osteoblast cells within the formed cavity.

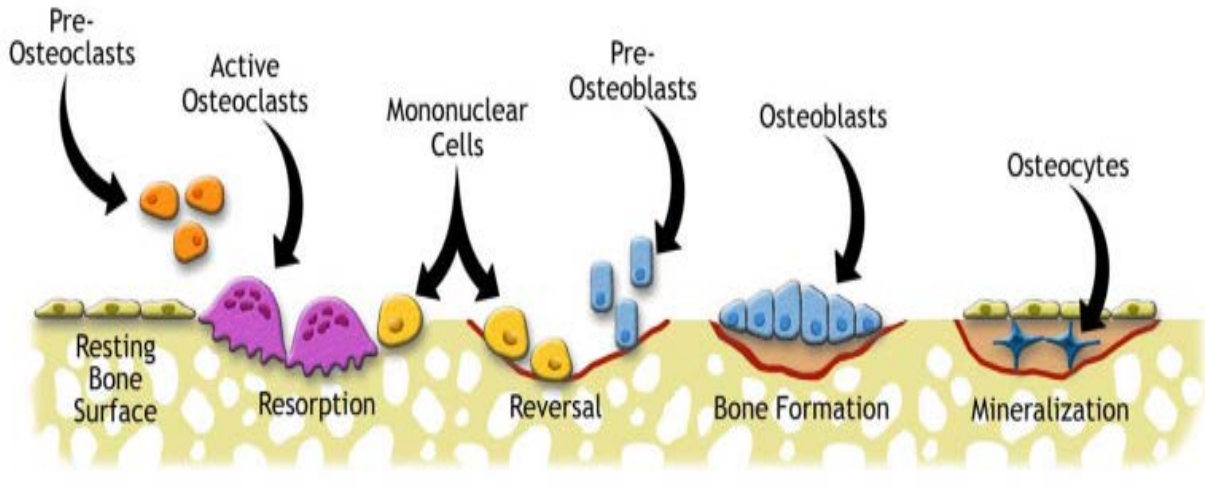

Figure 2.15 Bone remodelling cycle(Umich.edu, 2005).

The remodelling process is governed and induced by biological and mechanical means (Hill, 1998). As bone and bone tissue are prone to degradation due to aging and damage from trauma, disease wear or congenital defects, replacement materials are needed to support the bone regeneration. However; for large-scale bone defects, it cannot be healed completely by the body. In most cases, external intervention is needed to restore normal operations (Seitz et al., 2009, Jones et al., 2007).The surgical procedure of autografts (bone taken from the same person's body) and allografts (bone tissue from donor) as well as artificially synthesized materials are the main methods use for bone repair. The pre- and post-surgical procedures of bone repair and implantation through bone grafting are costly. In 2005 there were more than 500,000 bone graft procedures performed in the U.S. costing USD2.5 billion (Laurencin et al., 2006) and in the United Kingdom 150,000 fractures each year costing £900 million (Chrischilles et al., 1994) This will tend to increase as the populations are living longer. Although autografting has been the golden standard, it has several limitations including patient pain, cost, and limited supply. As alternatives, allograft and xenograft have been studied due to its abundant source. However, both alternatives had theirs drawbacks that include the uncertainty of compatibility and disease transmission. To overcome the limitations of autograft, allograft and xenograft, synthetic materials have been developed as replacements. As it is essential not only to replace bone tissues with materials that provide mechanical support but also a mechanism for tissue propagation. Hence, increasing bone

tissue engineering or bone scaffolds researchers are focusing in methods to synthesize, regenerate bone for restoration, maintenance or improvement from biocompatible and bioactive materials. Thus, in order for defective bone to be remodelled and regenerated, the bone graft substitute must not only be biocompatible but must also needs to be integrated with the host tissues *(osseointegration)* and provide a 3D template upon which cells may adhere, proliferation and eventually produce (ECM) (*osteoinductive and osteoconductive)*. With these requirements, a move toward 'bioactive' materials from 'bio-inert' materials in the design of implantations have prompt much research work in the last two decades in materials such as either bioactive ceramics, bioactive glasses, biological or synthetic polymers, biodegradable polymers, and composites of all these bioactive and biodegradable materials (Tan et al., 2013, Hench and Polak, 2002).

2.8.2 *Fixation of bone graft substitute.*

Attachment of BGS can be categorised as temporary implants and permanent implants. Temporary implants require the use of removable parts such as plates, nails, screws, pins, wires, and rods in order to secure the fixation. A secondary operation is often performed to remove temporary fixator after bone healing. This often creates additional discomfort to the patient and extra financial burden.

Permanent implants on the hand do not require a secondary operation after healing as these implants will last much longer than the temporary implants. More often it will last longer with little wear in 20 years (Dowson, 2006). Hence, the permanent implants need to be durable. As such most of the permanent implants are made from bioinert metal. These metal prostheses frequently deployed in the treatment of hip and knee replacement are normally fabricated as solid, dense components. Therefore, the fixations of the prostheses are by morphological technique. In this technique the implants are secured by bone in-growth on to the surface irregularities either from press–fitting, cementing using bone cement like PMMA or joining using threaded components. However, there is a compromise as most of these implants usually has much higher modulus than the bone. This resulted in implants loosening due to stress shielding as load is relocated from the bone to the implants, a condition known as bone resorption.

Due the shortcoming in metallic implants, biomimetic implants have been foreseen as the most logical solution. Biomimetic scaffolds are defined as scaffolds that have material

characteristics, morphology, and structural properties that mimic the natural bone graft (Simske et al., 1997). Hence, a secure fixation can be achieved by having the scaffolds fulfil the biological, mechanical and geometrical constraints of the natural bone. The fixation can be achieved through biological fixation technique or bioactive fixation.

In biological fixation technique, textured or porous implant allows tissue ingrowth into the openings, thus stabilising it. In order to encourage bone regeneration, the pores size should be in the range of between 100-500μm and interconnected (Karageorgiou and Kaplan, 2005). However, the manufacturing complexity in producing this type of porous implants using conventional manufacturing methods cause the price of the prostheses to be costlier than dense prostheses. As for bioactive fixation technique, fixations are attained through the formation of direct physiochemical bond with the bone tissue. The material used in forming these types of prostheses is bioactive ceramics or bioactive composite.

In order to satisfy bone healing and regeneration mechanisms, various research works conducted using different materials and designs were based on either biodegradable, bioactive or biocomposite (Butscher et al., 2011b, Warnke et al., 2010, Saito et al., 2010, Wang et al., 2009, Ramin and Harris, 2009, Porter et al., 2009). These materials are mainly from the bioceramics families and biopolymers families.

2.9 Bioceramic and glass-ceramics

Ceramics and glasses have been used for a long time in the medical industry, and the first cited implementation of bioceramics as biomaterials was in 1963 (Smith, 1963, Hulbert et al., 1982). Ceramics and glasses utilized in the repair and reconstruction of diseased, damaged, or worn-out parts of the body musculoskeletal system are termed bioceramics. Bioceramics may be bioinert such alumina and zirconia; resorbable such tricalcium phosphate; bioactive such hydroxyapatite, bioactive glasses, and apatite-wollastonite glass ceramics; or porous for tissue ingrowth such metal-coated hydroxyapatite and alumina (Hench, 1998). The potential of bioceramics as implants is based on their compatibility with the physiological environment. The biocompatibility is related to their compositions that contain ions, such as sodium, potassium, calcium, magnesium, phosphorus, and ions showing limited toxicity to body tissues, such as alumina, zirconium, and titanium, commonly found in the physiological environment (Hench and Wilson, 1995, Hench and Andersson, 1993, Hench, 1991). Bioceramic applications included replacement of hips, knees, teeth, tendons, and ligaments

and repair of periodontal disease, maxillofacial reconstruction, augmentation and stabilization of the jaw skeletal substance, iliac spacers, spinous spacer, intervertebral spacers, middle-ear implants and bone fillers after tumour surgery and to augment both hard and soft tissues. Table 2.2 and figure 2.17 summarized the forms and phases of bioceramics and their many different functions in the repair of the body (Hench and Wilson, 2013). In many applications, bioceramic materials in bulk form are used for implants and prosthetic devices while the granule and powder are used for space fillers and coating, or as a secondary phase in the production of composite to improve both mechanical and biochemical properties (Hench and Wilson, 1995, Kokubo, 1991a). Glass-ceramics have generated interest as possible choice material for the repair and reconstruction of diseased, damaged, or worn out parts of the hard tissues of the body, owing to their biocompatibility with living tissues (Chevalier and Gremillard, 2009, Arcos et al., 2009, Vitale-Brovarone et al., 2007, Navarro et al., 2004). Some of the approved glass-ceramics have been marketed under commercial trade name such as Bioglass®45S5 Novamin, Cerabone® (apatite-wollastonite), BonAlive®, NovaBone®, Dicor® (mica glass-ceramic), Ceravital® (apatite devitraite glass-ceramic), Ilmaplant L1, Bioverit® I (mica-apatite glass-ceramic) and Bioverit® II (mica glass-ceramic). Table 2.3 gives some of the mechanical properties of natural and bioceramics materials.

Table2.2 Form, Phase and Function of Bioceramics (Hench and Wilson, 2013, Hench and Kokubo, 1998).

Form	**Phase**	**Applications**	**Function**
Powder	Polycrystalline, Glass	Repair of periodontal defects, fixation of revision arthroplasty, cranial repair	Space-filling, therapeutic treatment, regeneration of tissues
Coating	Polycrystalline, Glass	Fixation of hip prostheses	Tissue bonding, thromboresistance, Corrosion protection
	Glass-Ceramic		
Bulk	Single Crystal	Middle ear prostheses, vertebral prostheses, orbital floor prostheses, Iliac crest prostheses	Replacement and augmentation of tissue, replace functioning parts
	Polycrystalline, Glass		
	Glass-Ceramic Composite (Multi-Phase)		

2.9.1 *Glass-Ceramic*

Materials which are produced as glasses initially and then converted to ceramics by rearrangement of a random structure (glass) to an ordered structure (crystalline) through heating to improve their properties are known as glass-ceramics. Glass-ceramics are polycrystalline materials formed by controlled crystallization of a base glass, in which the crystalline phases are nucleated and grown in a glass by means of a heat treatment or heat treatment together with pressure application (El-Meliegy and van Noort, 2012, Holand and Beall, 2012, Rawlings et al., 2006). Their properties are controlled by the mineral phases created. The relation between the mineral phases (the primary phases), the glassy phase (the secondary phases), and the incorporated porosity in medical ceramic is termed ceramic microstructure. The microstructure and chemical composition of a glass-ceramic both determine the general physical, chemical, optical, biological, and mechanical properties of the final material (El-Meliegy and van Noort, 2012, Holand and Beall, 2012). Thus, glass-ceramic materials share many properties with both glasses and ceramics.

Glass–ceramics are generally fabricated from starting materials, which naturally occur as minerals and rocks or their extracted reagent grade derivatives. The manufacture of a glass-ceramic involves three general steps (El-Meliegy and van Noort, 2012, Holand and Beall, 2012):

1. Raw materials, oxides, and nucleating agents are prepared for a glass-forming batch.
2. The batch is melted and then cooled to a temperature within the transition range to yield a glass.
3. The glass is then heated to a temperature above the transition range to perform glass crystallization.

The crystallisation process occurs when an ordered crystalline array is generated from the less ordered glass structure through the processes of nucleation and crystal growth (crystallization). In the nucleation process, longer range atomic order than the amorphous glass matrix regions are formed and developed spontaneously into a stable crystalline phase. Nucleation is presumably influenced by two general factors (Holand and Beall, 2012):

1. Appropriate selection of the chemical composition of the base glass with the usual addition of a nucleating agent
2. Controlled heat treatment of the base glass.

Frequently, the glass body is exposed to a two-stage heat treatment. In this treatment, the glass needs to be heated initially to a temperature within or somewhat above the transition range for a period of time sufficient to induce the development of sufficient nuclei in the glass. Thereafter, the temperature needs to be increased to levels approaching or above the softening point of the glass to induce the growth of crystals upon the nuclei. The general profile for the production of glass ceramics manufacturing schedule is shown in figure 2.16, where it starts with melting of the base glass. It is crucial that nucleation be optimised during the manufacturing schedule as it is a key factor in the controlled crystallization of a glass-ceramic (El-Meliegy and van Noort, 2012, Holand and Beall, 2012). Current bioactive glass ceramics include apatite glass ceramics, apatite–mullite glass ceramics, apatite–wollastonite glass ceramics, fluorcanasite glass ceramics, and potassium fluorrichterite glass ceramics.

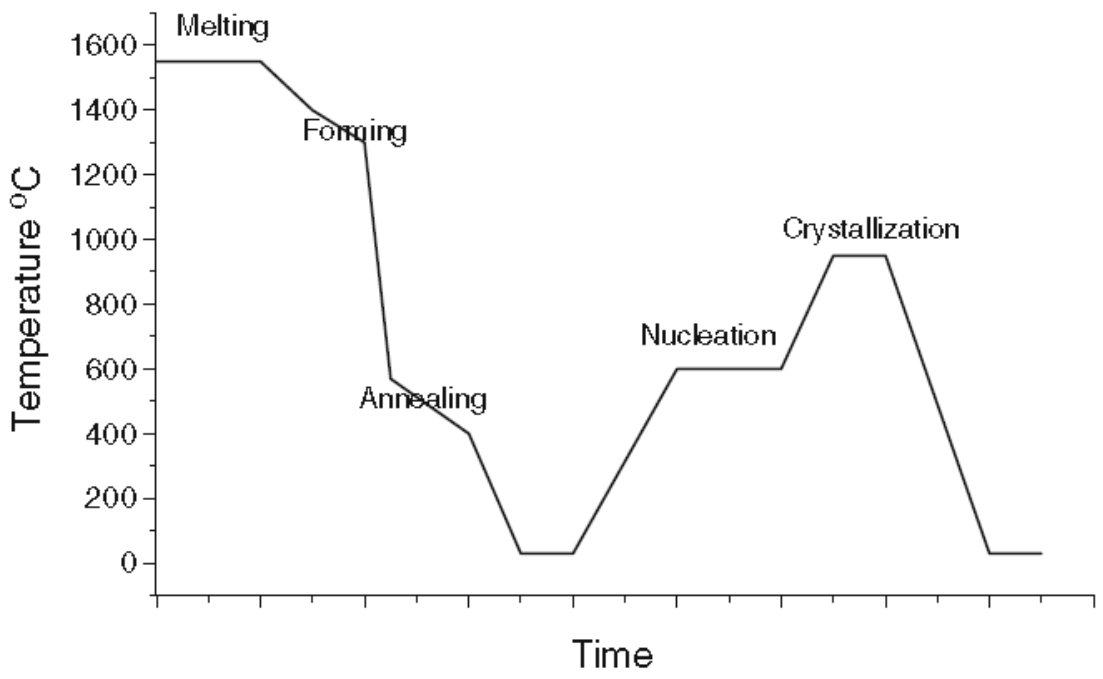

Figure 2.16 Manufacturing schedule for the production of glass ceramics.

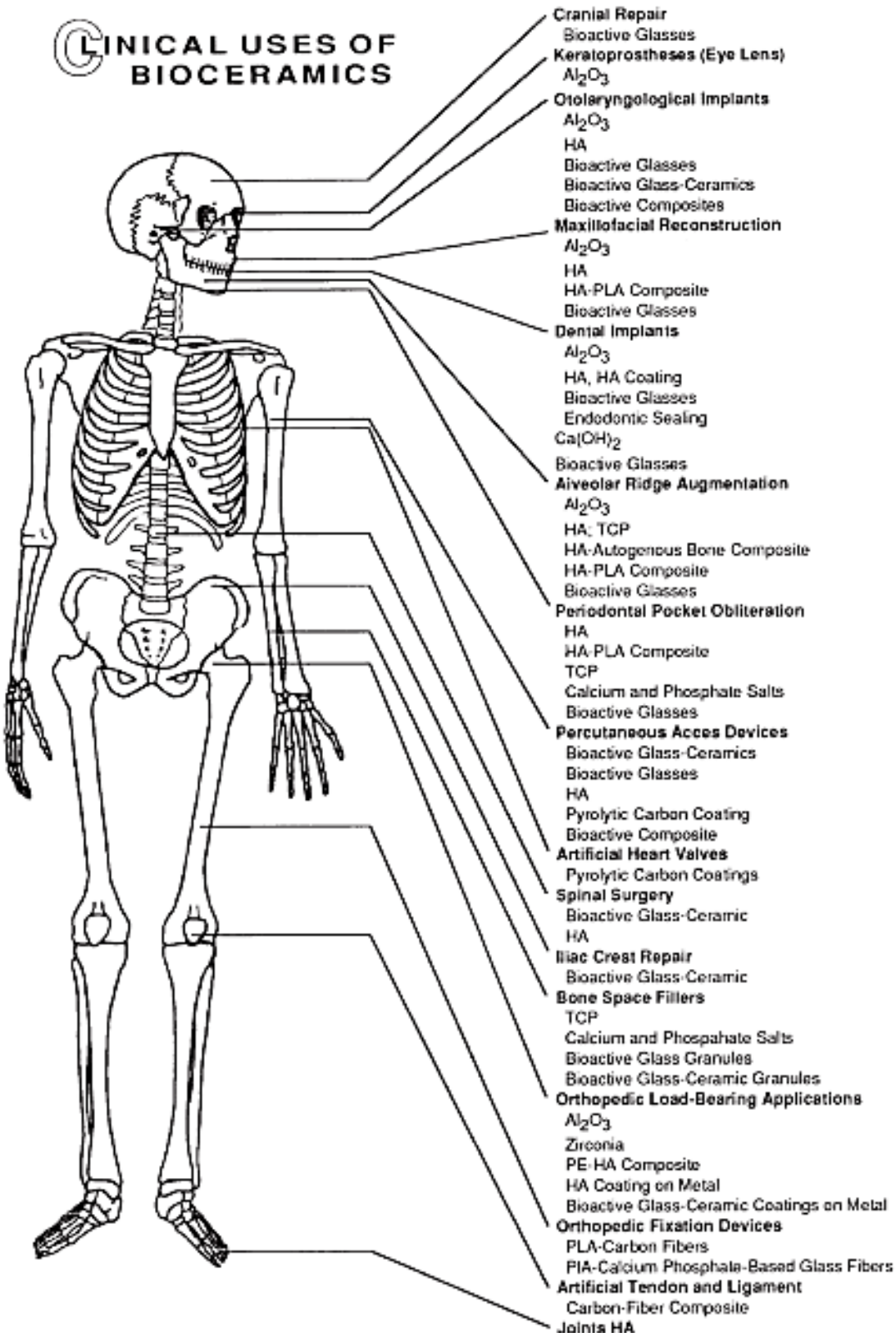

Figure 2.17 Clinical uses of bioceramics (Hench and Wilson, 2013).

Table 2.3 Mechanical properties of Bioceramics and Bone (Hench and Kokubo, 1998, Zanotto, 2010, Ben-Nissan and Pezzotti, 2004).

	Young's Modulus E (GPa)	Compressive Strength (MPa)	Tensile Strength (MPa)	Density (g/cm^3)	Fracture Toughness (MPa√m)
Bioceramics					
Alumina Al_2O_3	366 - 420	4400	282 -551	3.98	3 – 5.4
Zirconia ZrO_2	201 - 220	1990	800 – 1500	5.74 – 6.08	6.4 -10.9
Silicon Nitride	304	3700	700 – 1000	3.3	3.7 – 5.5
Hydroxyapatite	7 - 13	350 - 450	38 - 48		3.05 – 3.15
Dense sintered β-$3CaO.P_2O_5$[4]	7		21		
Glass-ceramics					
BioGlass 45S5	35	-	42	2.66	
Cerabone	118 - 120	1080	215 *(3-point flexural test)	3.07	2.0
Bioverit I	70 -90	500	140 - 180*(3-point flexural test)	2.8	0.5 - 2.1
Na-Ca-Si-P-O system based Highly bioactive glass ceramic	70	210*(3-point flexural test)		2.6	0.95
Natural Bone					
Cortical Bone	3.8 - 11.7	88 - 164	82 - 114	1.7 – 2.0	2 - 12
Cancellous	0.2 – 0.5	23	10 -20		

2.9.2 *Apatite Wollastonite glass-ceramics*

AW glass ceramics (AW-GC) discovered in 1982 by Kokubo et al. (Kokubo et al., 1982) has generated much responses and interests among the bioceramic community in the biomedical field due the biological ability to bond spontaneously to living bone in a short period, and maintenance of high mechanical properties such as toughness and strength for a long period in a body environment (Yamamuro, 2013, Kokubo et al., 2003, Kokubo et al., 1986). The microstructure of AW-GC contains apatite, wollastonite and whitlockite crystalline phases. The crystallinity in AW-GC influences the mechanical properties as with most glass-ceramics (Hench and Wilson, 2013, El-Meliegy and van Noort, 2012, Holand and Beall, 2012). AW-

GC is a matrix of small apatite particles effectively reinforced by wollastonite phase. The apatite induces the biological ability of AW-GC to bond instinctively to living bone, while the wollastonite prevents straight propagation of cracks and promotes a reinforcing effect (Kokubo, 2008, Kokubo et al., 1986) AW-GC has higher value of the bending strength, fracture toughness and Young's modulus among bioactive glass and glass ceramics which makes it useful in major compression load bearing applications (Best et al., 2008). As AW-GC exhibit good mechanical and biological ability, clinical use of AW-GC in either powder form or bulk materials are found in specific applications such as bone filler, iliac crest prostheses, artificial vertebrae, intramedullary plug, spinal spacers, and intervertebral spacers (Fujita et al., 2000, Kobayashi et al., 1998, Kitsugi et al., 1989, Ono et al., 1988). Table 2.4 shows some of the physical and mechanical properties of AW-GC. As shown in Table 2.4, the high degree of mechanical properties as compared to human cortical bone is due to the existence of β-wollastonite phase which increases the fracture energy, a result from precipitation of wollastonite crystals (Kokubo et al., 1986).

The bioactivity of AW-GC through the apatite phase encourages growth and proliferation of bone tissue on the surface. Kokubo demonstrated the dissolution of calcium (Ca) and silicate (SiO_2) ions from glass ceramics as a critical part of forming bone-like apatite layer on the surface in an *in vivo test* (Kokubo, 1991a). The mechanism of apatite layer formation has been thoroughly described by Jones and Hench (Jones and Hench, 2001). AWGC contains a glassy phase which releases more Ca ions in the early post-implantation stage than hydroxyapatite (HA), and it releases silicate ions which initiate crystallization of apatite as their nuclei on the surface of the implant.

Table 2.4 Physical and mechanical properties of A-W glass-ceramic (Kokubo, 2008, Kokubo et al., 1986)

Property	Value
Density (g/cm^3)	3.07
Bending strength (MPa)	215
Compressive strength (MPa)	1080
Young's modulus (GPa)	118
Vickers hardness (Hv)	680
Fracture toughness ($MPa.m^{0.5}$)	2.0

Table 2.5 shows the bonding ability of selected bioceramic materials in *in vitro studies*. It show that AWGC bonding ability to bone is better and that AWGC binds to bone more tightly than hydroxyapatite, which is currently available for the repair of bone and joints defects

(Yamamuro, 2013, Kokubo, 1991a). The chemical composition of AWGC is in the MgO-CaO-SiO_2-P_2O_5 system and made from reagent grade chemicals of MgO, $CaCO_3$, SiO_2, $CaHPO_4 \cdot 2H_2O$, and CaF_2 (Kokubo et al., 1986).

Table 2.5 Failure loads obtained by detaching test between rabbit tibia bones and bioceramics after 8 weeks implantation (Yamamuro, 2013, Hench and Kokubo, 1998).

Bioceramic.	Failure Load ± Standard deviation(kg)
Alumina	0.18 ± 0.018
BioGlass®	2.75 ± 1.80
Ceravital® KGS-type glass-ceramic	3.52 ± 1.48
Natural polycrystalline calcite	4.11 ± 0.98
Dense hydroxyapatite	6.57 ± 1.36
Dense sintered β-3CaO.P_2O_5[4]	7.58 ± 1.97
Cerabone® A-W glass-ceramic	7.44 ± 1.91

2.10 Biodegradable polymer

Polymers are macromolecules of repeated subunits forming molar masses ranging from thousands to millions. Polymeric materials occurred naturally or as synthetic, are created via polymerisation of monomers. A polymer is synthesized by chemically joining together many small molecules into one giant molecule. Cellulose, collagen, keratin, starch, lignin, chitin, and various polysaccharides are natural polymers and as such provide specific biological activities in tissue engineering (TE). But natural polymers lack controllability over molecular weight that influence the degradation rate, and mechanical properties (Matthew, 2002) hindered its full usage in TE. In contrast, synthetic polymers can be designed with specific molecular and physical properties by a wide range of different monomers combined to form copolymers and to control the polymerisation. Therefore, synthetic polymers can achieve batch-to-batch uniformity, predictability and reproducibility in mechanical and physical properties. However, synthetic polymers lack the biological activities associated with natural polymer and thus pose the risks of toxicity and immunogenicity as opposed to natural polymers which degrade enzymatically to nontoxic subunits which can be utilised by adjacent cells (Matthew, 2002). Synthetic polymers are generally preferred as implants due to the minimal site-to-site and patient-to-patient variations as compared to enzymatically degradable polymers (Katti et al., 2002).

Both types of polymers have gained much attention in industrial and medical applications in the past decades in which they are used extensively as biomedical materials in prosthetic,

dental, implants, dressings, pacemakers, polymeric drug delivery systems, and tissue engineered. Typical polymeric biomaterials (biopolymers) used as TE materials are bioresorbable and biodegradable polymers. These polymers do not require surgical removal and hence are preferred for biomedical applications. However, since they degrade to smaller absorbable molecules, it is vital to ensure that the monomers are non-toxic in nature and must meet the followings (Lloyd, 2002):

1) The implantation of the material should not induce inflammatory or toxic response in the body.

2) The shelf life of the material should have acceptable duration.

3) The degradation time of the material should match the healing or regeneration process.

4) The material should have appropriate mechanical properties for the designated application and the variation in mechanical properties with degradation should be compatible with the healing process.

5) The degradation products should be nontoxic, and be able to metabolize and cleared from the body.

6) The material should have appropriate permeability and processibility for the intended application.

Biodegradable polymers with differ molecular weight (MW), polydispersity, crystallinity, structure and thermal transition allowing mechanical properties and degradation kinetic are well tailored for bone defects generation. Synthetic biodegradable polymers are poly (α–hydroxy acids), polycaprolactone (PCL) and poly (ester-urethane) urea (PEUU). The most commonly used biodegradable polymers in bone regeneration are from the poly (α-hydroxy acids) which includes poly (lactic acid) (PLA) and poly (glycolic acid) (PGA) homopolymers as well their co-polymers poly (Lactide-co-glycolide) (PLGA) as they promote biocompatibility and biodegradability which allow cell growth (Nair and Laurencin, 2007). The structural formulas of the four basic polymers are given in table 2.6.

Table 2.6 Chemical Structure of biodegradable polymers.

Biopolymer	Chemical Structure
PLA	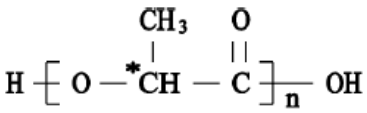
PGA	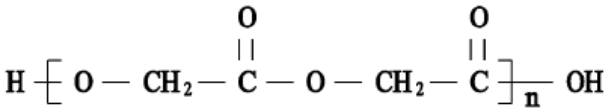
PCL	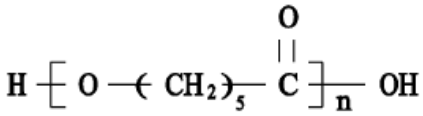
PLGA	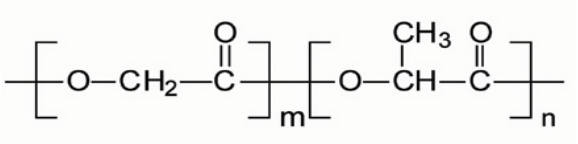

The earliest biodegradable poly (α–hydroxy acid) that has been used for three decades as suture and reinforcement material in surgical operation is PGA (Lewandrowski, 2002). PGA is a biodegradable, thermoplastic polymer of highly crystalline polymer (45-50 % crystallinity) with simple linear, aliphatic polyester. However, with its rapid degradation, acidic degradation products and low solubility, PGA application is limited even though it has excellent mechanical properties due to high crystallinity. Due to its good initial mechanical properties, polyglycolides have been investigated as a self-reinforced composite materials for bone internal fixation devices (Tormala, 1992). Thus to widen the application of biodegradable polymers, longer biodegradation period polymers have been developed, one of which is PLA. PLA an agro-based polymer type is derived from plants such as corn, tapioca and sugarcane. It is a renewable resource and environmentally responsible. PLA is a chiral molecule and therefore it exists in two stereo-isomeric forms, l-lactide and d-lactide, D, L-PLA, is also available. The polymers derived from the optically active D and L monomers are semi-crystalline materials, while the optically inactive D, L-PLA is always amorphous. Poly(*l*-lactide) has good tensile strength, low extension and a high modulus (approximately 4.8GPa) with slow-degradation as compared to polyglycolides, and hence, has been considered for load-bearing applications, such as orthopaedic fixation devices (Middleton and Tipton, 2000, Bergsma et al., 1995). However as PLA warps and degrades more quickly when exposed to excessive heat or humidity and lose its strength in approximately 6 months when

hydrolysed with no significant changes in mass for total resorption *in vivo* between 2 and 5.6 years (Middleton and Tipton, 2000) , there is a significant obstacle in using PLA in specific applications. Therefore, current development of biopolymers with better property variation is under investigation for several co-polymers of l-lactide or dl-lactide with glycolide. Table 2.7 displays the mechanical properties of biodegradable polymers. The glass transition temperatures (T_g) of the PLGA copolymers are slightly above the physiological temperature of 37°C and hence they are glassy in nature. Thus, they have a fairly rigid chain structure which gives them significant mechanical strength to be formulated as drug delivery devices. The lactide-rich PLGA copolymers are less hydrophilic, absorb less water, and subsequently degrade more slowly (Jain, 2000a) as lactic acid is more hydrophobic than glycolic acid.

Table 2.7 Compilation of biodegradable polymers properties (Gentile et al., 2014, Van de Velde and Kiekens, 2002).

Properties	PLA	L-PLA	PGA	DL-PLGA 50:50	DL - PLGA 75:25	PCL
Young's modulus E (GPa)	0.35 – 3.5	2.7 – 4.14	6 - 7	1 – 4.34	1.38 – 4.13	0.21 – 0.44
Tensile strength σ (MPa)	21 - 60	15.5 - 150	55 – 99.7	41.4 – 55.2	41.4 -55.2	20.7 - 42
Elongation ε (%)	2.5 - 6	3 - 10	1.5 - 20	2 - 10	2.5 - 10	300 - 1000
Bending strength (MPa)	0.89 - 1.03	-	-	-	-	-
Impact strength (J/cm)	0.16 - 1.35	-	0.16 – 1.35	-	-	-
Melting temperature (°C)	150 - 162	170 -200	220 -233	amorphous	amorphous	58 - 65
Glass Transition temperature (°C)	45 - 65	55 - 65	35 -45	40 - 50	50 - 55	-65 - -60

Density (g/cm^3)	1.21 – 1.43	1.24 – 1.30	1.50 – 1.71	1.30 – 1.40	1.30	1.11 – 1.146
Water absorption (%)	0.5 - 50	-	-	-	-	-
Degradation Time (Weeks)	11 - 15	12 - 18	6 - 12	1 - 2	4 - 5	

2.10.1 *Polylactide-co-Glycolide Acid (PLGA)*

Poly (DL-lactide-co-glycolide) (PLGA); a bioresorbable biodegradable aliphatic polyester, is formed from the combination of lactic and glycolic. Controlled co-polymerisation of lactic and glycolide can produce tailored mechanical properties and degradation rate by varying the molecular weight. PLGA with composition of 25%- 75% lactide-to-glycolide ratio forms amorphous polymers while a 50-50% PLGA is very hydrolytically unstable. PLGA is a widely investigated polyester and used in a number of clinical applications such as for bone repair and substitute applications. PLGA has been well documented for its excellent biodegradability, biocompatibility, nontoxicity properties and favourable regulator status (Makadia and Siegel 2011, Miao et al., 2007, Landes et al., 2006, You et al., 2005, Domb et al., 2001, Lu et al., 1999).

The main advantage of PLGA is it extensive variety of disintegration times and has tuneable mechanical properties. Researchers had used various ratios PLGA in different applications to understand the behaviour of PLGA(Landes et al., 2006). Most of the likely usages of PLGA under study are for minimal load bearing applications. One such area is craniofacial surgery to provide secure fixation while eliminating much of the concern over intracranial migration of metallic plates and screws that are normally used(Peltoniemi et al., 2002). In addition, PLGA is also widely studied as a scaffold material for osteogenesis (Gentile et al., 2014, Leung et al., 2008, Callaghan et al., 2004, Vozzi et al., 2003, Thomson et al., 1996) besides being used in research work relating to drug delivery (Makadia and Siegel 2011, McDonald et al., 2009, Chung et al., 2006, Alexis, 2005).

Most of the biopolymers; PGA, PLA and co-polymers PLGA, have lower strength than natural bone and not propagator of cell bone for bone regeneration. As apatite is part of natural bone composition, most of the biopolymers are reinforcing with apatite containing bioceramic such as hydroxyapatite (HA) and apatite-wollastonite to form biocomposite. In addition as reinforcement, apatite containing bioceramic also induce bone in-growth.

2.11 Biocomposite

As research into singular biomaterials for scaffolds are maturing with new findings regarding their usages in the medical field, more research are looking toward new types of biomaterials that can mimics natural bone. This development has been the hottest topic in both advanced composites and biomaterials communities (Cheung et al., 2007). High-strength and durable biocomposite can be fabricated from either biodegradable polymer or bioactive ceramic as parent material. Depending on the applications requirements, the biocomposite can be enhanced either by reinforcing the parent materials with fibre of the same or different materials or by combining with other biomaterials. With the knowledge of regenerative medicine in term of porous size, degradation rate and surface morphology, researcher and engineers can develop new biocomposites and fabrication techniques. In the fabrication process of the biocomposite, researchers had investigated various manufacturing process ranging from conventional to advanced manufacturing methods. In the fabrication of Bioglass®45S5-HDPE composite, a conventional approach was used where the composite mixture were blended, compounded and compression moulded. While in advanced techniques, one of the AM methods was used. Biocomposite of PEEK-HA scaffolds were successfully fabricated using SLS with promising results in microscopic analysis, porosity analysis, bioactivity and cell viability analysis (Tan et al., 2005).

Biocomposites that are based on polymers can be categorised into three groups: bioinert composites, such as carbon/high density polyethylene (HDPE) and β-TCP/HDPE; bioactive composites, such as HA/HPDE, poly-(DL-lactic acid)-wollastonite and AW-PMMA; bioresorable composites such as TCP/PLA and PLGA/TCP. Much research work were performed to improve the mechanical properties and the bone bonding properties (Keshaw et al., 2009, Roeder et al., 2008, Miao et al., 2007, Georgiou et al., 2007a, Ignjatovic et al., 2004).

2.12 Forming Processes of Biomaterials in the Manufacturing of Medical Devices and Implants

As been mentioned earlier, various manufacturing processes have been proposed and investigated in processing biomaterials. The next two sub-sections described the conventional processes that have been used.

2.12.1 *Fabrication methods in ceramic material*

There are many methods that can be used in shape forming ceramic powder. The simplest form is by pressing fine ceramic powder mixed with additives. Powder pressing can be carried out in a number of ways which includes uniaxial pressing, wet pressing, hot pressing and isostatic pressing. Table 2.8 describes the process and the area of applications this process was used. In addition, other methods too are used such as Robocasting and AM.

Table 2.8 Processing of Ceramics Materials.

Process	Description	Applications
Uniaxial (Die) Pressing	Die pressing is the powder compaction method involving uniaxial pressure applied to the powder placed in a die between two rigid punches. Various binders (organic as well as inorganic) may be added in the mixture depending on the requirement.	Used for mass production of simple shapes such as abrasive products and white-wares.
Isostatic Pressing	In isostatic pressing, powder mixture compaction is achieved by applying pressure from multiple directions through a liquid or gaseous medium surrounding the compacted part placed around a central mandrel pin in a flexible mould.	Used to obtain uniform density in the product.
Injection Moulding	In this method, a rotating screw inside cylinder compacted and fed the mixture of ceramics with binder (usually thermoplastic polymer or wax).The mixture is heated until the correct temperature to attain sufficiently low viscosity before injection by pressure into the mould cavity.	Used for precision forming of complex shape.
Extrusion	Extrusion ram forces the ceramic paste through a die, resulting in a long product (rods, bars, long plates, pipes) of regular cross-section,	Used in the production of constant cross-section and hollow shapes with limited thickness parts such furnace tubes, thermocouple components, and heat exchanger tubes.
Slip Casting	Slip casting technique is used for shape	Used to produce replication of

	forming ceramic slurry - a stable suspension, consisting of ceramic powders, processing additives and 20-35% of liquid (water or solvent).	cancellous bone from bioceramic and its' compositions including HA,β-TCP, and HA/β-TCP (Tancred et al., 1998).
Gel Casting	Gel Casting is a process of shape forming slurry prepared from ceramic powder mixed with a solution of organic monomer.	Used of highly porous gel-cast ceramics in medical applications, bone repair implants and non-oxide ceramics with reactive surfaces of zirconia for dental application.
Tape Casting (Doctor-blade process)	Tape Casting is a process of forming a thin film of ceramic slurry spread over a flat surface. Tape casting process can be divided aqueous and non-aqueous systems according to the types of solvents used.	Used in large-scale fabrication of ceramic-based substrates and multi-layered structures, such as multi-layered ceramic capacitors and multichip ceramic modules, solid fuel cells, photovoltaic cells and laminated object moulding (Hotza D., et al., 1995; Mister R. E., 1998)

2.12.2 *Methods in processing of biopolymers*

In bone application, biodegradable polymer or its composite can be prepared in two forms, scaffold and dense. Dense form of biodegradable polymer can be obtained from forging, hot or cold pressing. Extrusion, injection and compression moulding as well as particulate leaching and solvent casting, are some of the techniques used to develop polyglycolides-based structures for biomedical applications. Polylactic acid-phosphate glass (PLA-PG) composite foams was fabricated with various PG content by melt-extrusion, and either compression-moulded or foamed through supercritical CO_2 as scaffolds for bone tissue engineering applications (Georgiou et al., 2007b).

Table 2.9 Fabrication of biodegradable polymer materials (Gentile et al., 2014).

Polymer	Solvent	Applications
Polyglycolide / Polyglactine	Hexafluoroispropanol	Suture anchors, meniscus repair, medical devices, drug delivery, orbital floor
Poly(l-lactide)	*Benzene, *dioxane tetrahydrofuran (THF).	Fracture fixation, interference screws, suture anchors, meniscus repair
Poly(d,l-lactide)	Methanol, dimethyl-formamide (DMF)	Orthopaedic implants, drug delivery
Poly(d,l-lactide-*co*-glycolide) 85:15	Ethyl acetate, *chloroform, acetone, THF	Interference screws, suture anchors, anterior cruciate ligament (ACL) reconstruction
Poly(d,l-lactide-*co*-glycolide) 75:25	Ethyl acetate, chloroform, acetone, DMF, THF	Plates, mesh, screws, tack, drug delivery
Poly(d,l-lactide-*co*-glycolide) 50:50	Ethyl acetate, chloroform, acetone, DMF, THF	Orthopaedic implants, drug delivery

Note: *(use with high precaution as these are nasty carcinogen/cancer causing agent)

2.13 Sintering

As sintering is part of the approach use to densify the powder in this research, it is necessary to have an understanding of the sintering process. Sintering is the technique in which the non-compacted material is heated to a specific temperature below its melting point to form concentrated agglomerate (Rahaman, 2008, German, 1996). For most sintering process, loose fine particles of less than 1mm in diameter are compacted in a mould before heated to a temperature below the melting point of the powder. The compacted particles are terms green part while once sintered it is called brown part. In sintering, the main mechanisms which cause bonding is by diffusion, although other mechanisms such as plastic flow, recrystallization, grain growth, liquid and vapour phase material transport may happen. Sintering can be broadly categorised into solid-state sintering and liquid-state sintering. Figure 2.18 illustrate the different sintering category on a phase diagram (Kang, 2005).

2.13.1 *Solid-state and liquid state sintering*

In solid-state sintering when two adjacent rigid particles that were initially in contact are induced with thermal energy, the material at the atomic level gains enough energy to diffuse away from the material and join together. During this stage of sintering, necking occurs within the loose powder particles. If thermal energy is continuously supplied, the next stage of sintering occurs where the initial necking will grow until the particles become smooth and develops, nearing cylindrical shape. The particle will eventually coalesce into a single, larger particle as shown in figure 2.19 (German, 1996).

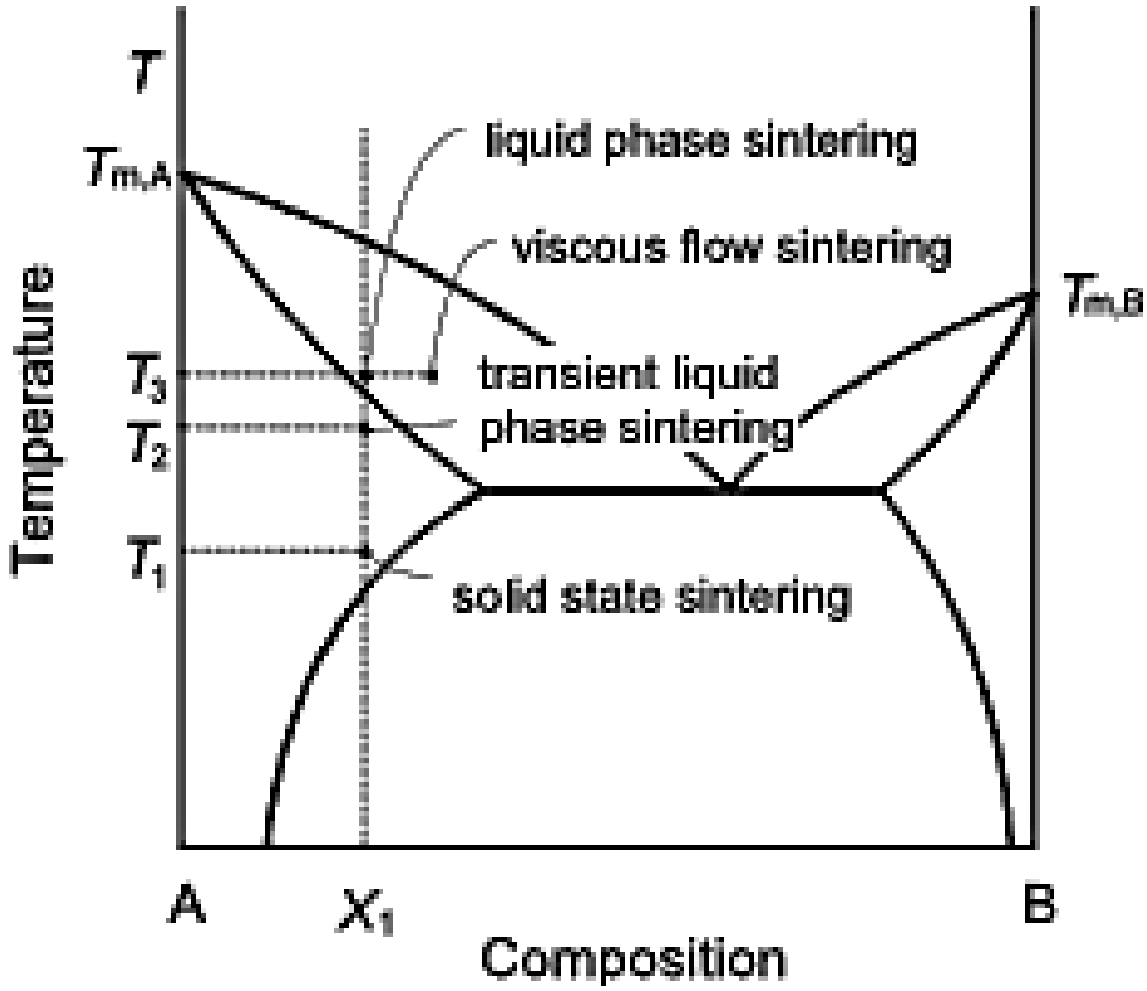

Figure 2.18Categories of sintering in a phase diagram (Kang, 2005).

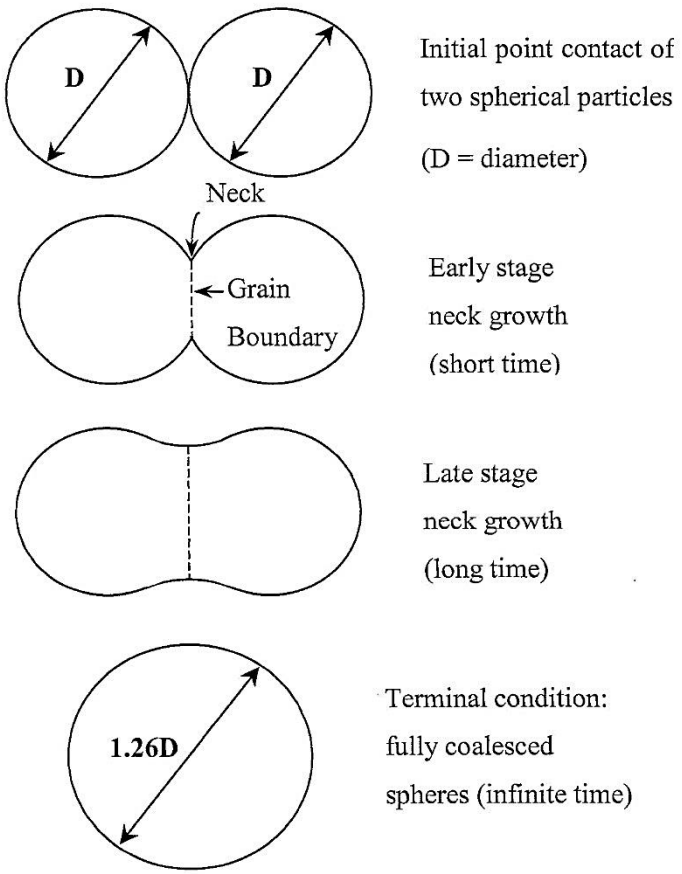

Figure 2.19 Classical sintering model of two adjacent particles (German, 1996)

In solid-state sintering, the mass transportation can occur as surface diffusion or volume diffusion. The differentiation between surface diffusion and volume diffusion lies in the transport mechanism. For surface diffusion, the mechanism of mass surface transport involved motion of atoms between defects of crystalline solid. Surface diffusion initiates at lower temperature than other mass transport processes, thus contributing to the initial sintering of many materials. This is important for producing high open pores with good mechanical strength without densification and loosening the open pore structure (German, 1996). As for volume diffusion, the main mechanism involves motion of vacancies (the sites where an atom is missing from a crystallographic structure) through a crystalline structure. As described by German (German, 1996) there are three main diffusion pathways that contribute to volume diffusion sintering. The pathways started with diffusion adhesion and followed by diffusion densification then dislocation climb. Diffusion adhesion allows vacancies to flow from the neck surface to particle the surface through the particle interior. This results in mass deposition at the neck surface. In densification, the vacancies move from neck surface to the

inter-particle grain boundary resulting in densification and shrinkage. The final pathway allows vacancies dislocation by secretion or annihilation, which also results in densification. This process is common for compacted powder. Volume diffusion is dominantly common for many ceramics and crystalline materials. Figure 2.20 illustrates the volume diffusion pathways.

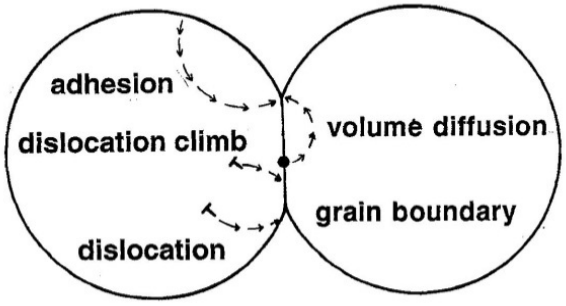

Figure 2.20 Diffusion pathways (German, 1996).

In liquid state sintering, the sintering process occurs in the presence of liquid phase. The formation of liquid during sintering improves the mass transport rates which results in better sintering rate in comparison to solid state sintering (German, 1996).

In sintering process, parameters that influence the quality of the sintered parts are:

- temperature
- time
- pressure

Unlike other processing technologies, various processing steps and variables need to be considered for the production of sintered parts. For example, in the shaping step, simple die compaction, isostatic pressing, slip casting, injection moulding, may be selected according to the shape and properties of required end product (Kang, 2005).

2.14 Materials Characterisations and Analysis

In this section, the experimental analysis techniques that were used in this research will be introduced. These analysis techniques include methods for materials characterisation; such as pycnometer, differential scanning calorimetry (DSC), X-Ray diffraction (XRD), and scanning electron microscopy (SEM), and mechanical properties analysis.

2.14.1 *Density Measurement using Pycnometer*

Pycnometers are flasks with accurate volumes which can be used to determine the density of the material by measuring the liquid volume displaced by a solid material (in powder, granular or bulk form). The method of determining the density is based on Archimedes Principle of buoyant force. The buoyant force on a submerged object is equal to the weight of the fluid that is displaced by the object.

The most common pycnometer being the specific gravity (SG) bottle is often used for measuring SG of finely milled powders. It is also used for measuring the relative density of liquids whereby a liquid weight is divided by the weight of an equal volume (using the same vessel) of water. Liquids other than water can be used in these pycnometers when water is a problem, the most common being xylene. The pycnometer (Figure 2. 21a) is a flask with a close-fitting ground glass stopper with a fine capillary hole through it. This fine hole releases a spare liquid after closing a top-filled pycnometer, thus enabling the density to be measured accurately, by referencing to an appropriate working fluid such as water or mercury, using an analytical balance. Figure 2.19a shows SG bottles on the right and a large Bulk Pycnometer in Figure 2. 21b. The Bulk Pycnometer can be used for measuring bulk density (BD), apparent specific gravity (ASG) or SG of larger pieces or chips using a similar procedure to that of the SG bottle (Berger, 2010). The testing method is as given in BS EN 1389:2003 (BSI, 2003).

(a) (b)

Figure 2. 21 Density bottle (Impact-test, 2013, Jaytecglass, 2012).

2.14.2 *DSC*

Differential scanning calorimetry (DSC) is used to monitor heat effects associated with phase transitions and chemical reactions as a function of temperature. According to the classification, calorimetry is a technique for determining the quantity of heat that is either absorbed or released by a substance undergoing a physical or a chemical change which alter the internal energy of the substance (Kubyshkina, 2014). The internal energy at constant pressure is known as enthalpy, H. Since the DSC is at constant pressure, heat flow is equivalent to enthalpy changes and can be either positive or negative. The equation of heat flow is as shown in equation 2.1.

$$\frac{\Delta dH}{dt} = \left(\frac{dH}{dt}_{sample}\right) - \left(\frac{dH}{dt}_{reference}\right) \tag{2.1}$$

Where H = enthalpy

t = time

In an endothermic process, heat is absorbed and, therefore, heat flow to the sample is higher than that to the reference. Hence, ΔdH/dt is positive. In an exothermic process, such as crystallization, some cross-linking processes, oxidation reactions, and some decomposition reactions, the opposite is true, and ΔdH/dt is negative.

In a DSC, the difference in heat flow to the sample and a reference at the same temperature is recorded as a function of temperature. The reference is an inert material such as alumina or an empty aluminium pan. The temperature of both the sample and reference are increased at a constant rate (Figure 2.22).

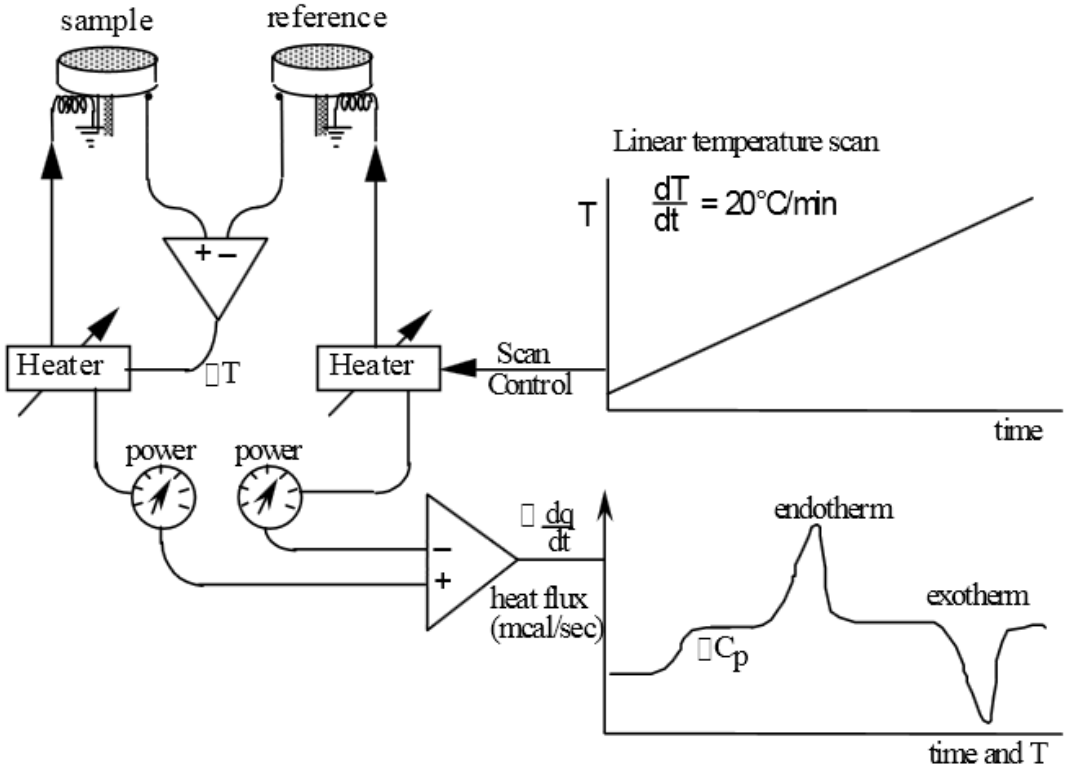

Figure 2.22 Schematic of a DSC (Colby, 2007).

In DSC analyses of polymer samples, the occurring thermal transitions are when they are cooled down or heated up under inert atmosphere. DSC is use to determine the melting and glass transition temperatures, as well as various transitions in liquid crystalline mesophases as shown in figure 2.23 (Braun et al., 2012).

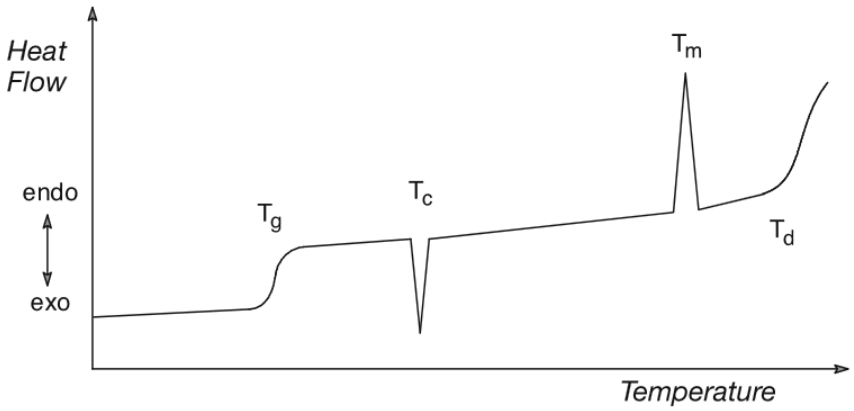

Figure 2.23 Schematic DSC thermogram of semi-crystalline polymer which denote the point of glass transition temperature T_g, crystallisation temperature T_c, melting temperature T_m and decomposition temperature T_d (Braun et al., 2012).

2.14.3 *SEM*

The scanning electron microscope (SEM) uses a stream of focused electrons over a small specimen surface to create an image at extremely small scale. The electrons in the beam interact with the sample, producing various signals by electron-sample interactions when the incident electrons are decelerated in the solid sample. These signals include secondary electrons (that produce SEM images), backscattered electrons (BSE images), diffracted backscattered electrons (EBSD that are used to determine crystal structures and orientations of minerals), photons (characteristic X-rays that are used for elemental analysis and continuum X-rays), visible light (cathodoluminescence–CL), and heat (Figure 2.24). SEM is used to reveal information about the sample that include information about external morphology (texture), chemical composition, and crystalline structure and orientation of materials making up the sample (Swapp, 2007).When the specimen is irradiated with a fine electron beam, secondary electrons are emitted from the specimen surface which are received by a detector that interprets the stream of electrons by observing the two-dimensional scanning of the electron probes over the surface into an image from the detected secondary electrons. This process requires the examined samples observed under SEM to be grounded by attaching the samples SEM stubs before being painted with conductive material and coated with gold. Most modern light microscope has a maximum magnification of about 1000x.

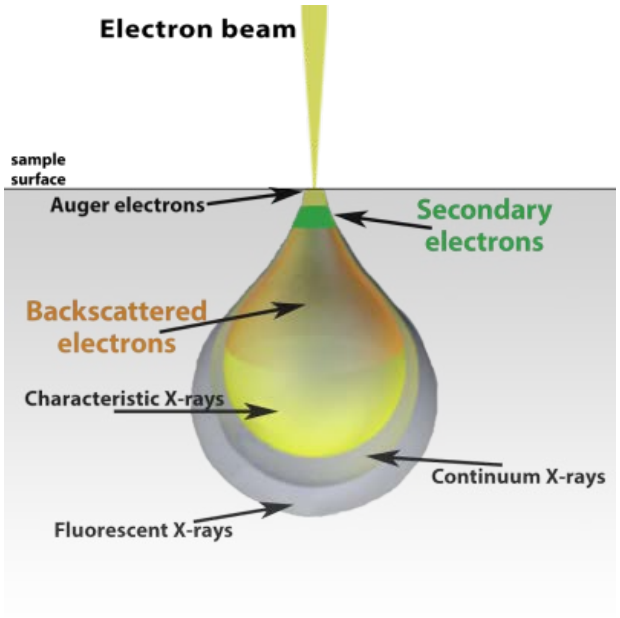

Figure 2. 24 Various signal from electron-sample interactions when the incident electrons are decelerated in the solid sample (Nanoscience, 2014).

Normally, the assembly of a SEM system consists of three main sub-assembly; the electron optical column (electron source/gun, magnetic lenses, magnetic coils, and apertures), vacuum systems (chamber, valves) and signal detection and display (detectors, electronics and display unit) (Figure 2.25).The resolving power of the microscope was not only limited by the number and quality of the lenses but also by the wavelength of the light used for illumination. White light has wavelengths from 400 to 700 nanometres (nm). The average wavelength is 550 nm that results in a theoretical limit of resolution (not visibility) of the light microscope in white light of about 200 – 250nm. The maximum resolution obtained in an SEM depends on multiple factors, like the electron spot size and interaction volume of the electron beam with the sample. While it cannot provide atomic resolution, some SEMs can achieve a resolution below 1 nm. Typically, modern full-sized SEMs provide resolution between 1-20 nanometres whereas desktop systems can provide a resolution of 20 nm or more.

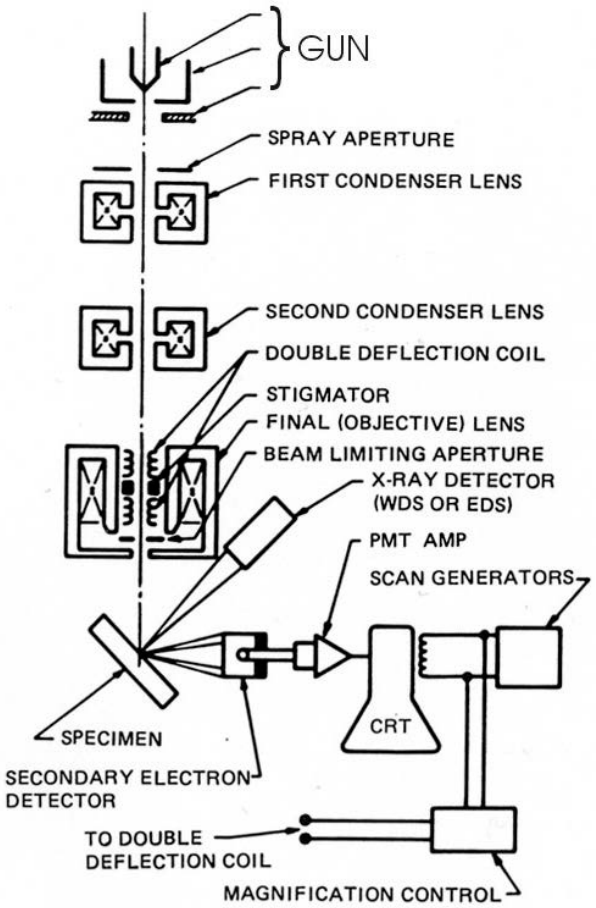

Figure 2.25 schematic of SEM and x-ray optics (Swapp, 2007).

SEM is widely used in a number of industries and laboratories to investigate the microstructure and chemistry of a range of organic and inorganic materials such in characterisation the surface topology of bioceramic (Cannillo et al., 2009, Szucs and Brabazon, 2009).

2.14.4 *XRD*

X-Ray Diffraction (XRD) technique is used to identify different crystal phases present in crystalline materials. When crystalline materials are exposed to X-rays, the lattice of the crystal diffracts the ray. As X-rays have wavelengths on the order of a few angstroms (1 Angstrom = 0.1 nm), this make X-rays suitable for diffraction of atoms in crystalline materials as the typical inter atomic distance in crystalline solids are at this range. When incident X-Ray interacts with the crystal, X-Ray diffraction spectra will be observed that is unique to that particular crystal type. Crystal phases are determined from the comparison of known samples. The relationship describing the angle at which a beam of X-rays of a particular wavelength diffracts as Bragg's Law (Figure 2.26) is given in equation 2.2

$$2d\sin\theta = n\lambda \qquad (2.2)$$

where λ= wavelength of the X-Ray

θ = scattering angle

n = integer representing the order of the diffraction peak.

d = inter-plane distance (of either atom, ions or molecules)

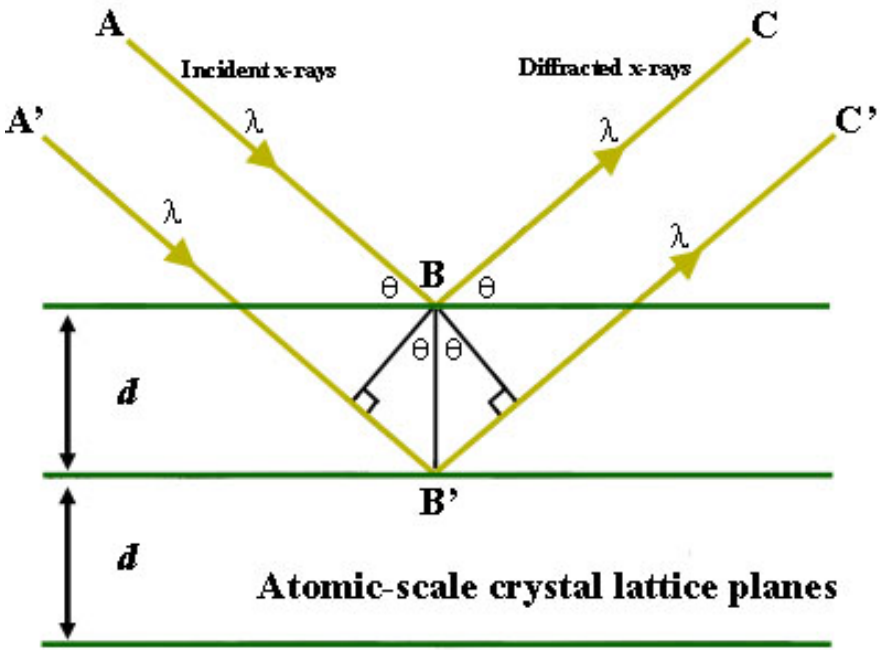

Figure 2. 26 Bragg's Law reflection. The diffracted X-rays exhibit constructive interference when the distance between paths ABC and A'B'C' differs by an integer number of wavelengths (λ) (Henry et al., 2007).

2.14.5 *Mechanical Testing*

Simple mechanical tests such as tensile, compressive, impact and bending test are used to evaluate the mechanical strength of materials. Most often tensile tests, for example, are conducted on ductile materials to measure the stiffness, ductility and strength of the materials. Figure 2.27 shows the stress-strain curve in which related nomenclatures are used to describe the general deformation behaviour of the ductile materials. The stiffness of materials is defined by the elastic modulus or Young's modulus (E), a fundamental property of the material. The value of E can be obtained from the slope of the linear range in the stress-strain curve. The region indicating a linear relationship between stress and strain is known as elastic region. The upper value A as shown in figure 2.26 of this linear relationship is called the proportional limit σ_{pl}. The tensile strength σ_u is the maximum strength before fracture while the yield strength σ_y is the strength which the behaviour of the material changes from elastic to plastic deformation (BSI, 2009a). A graphical 0.2% strain offset is normally used for aluminium as it does not have a well-defined yield point.

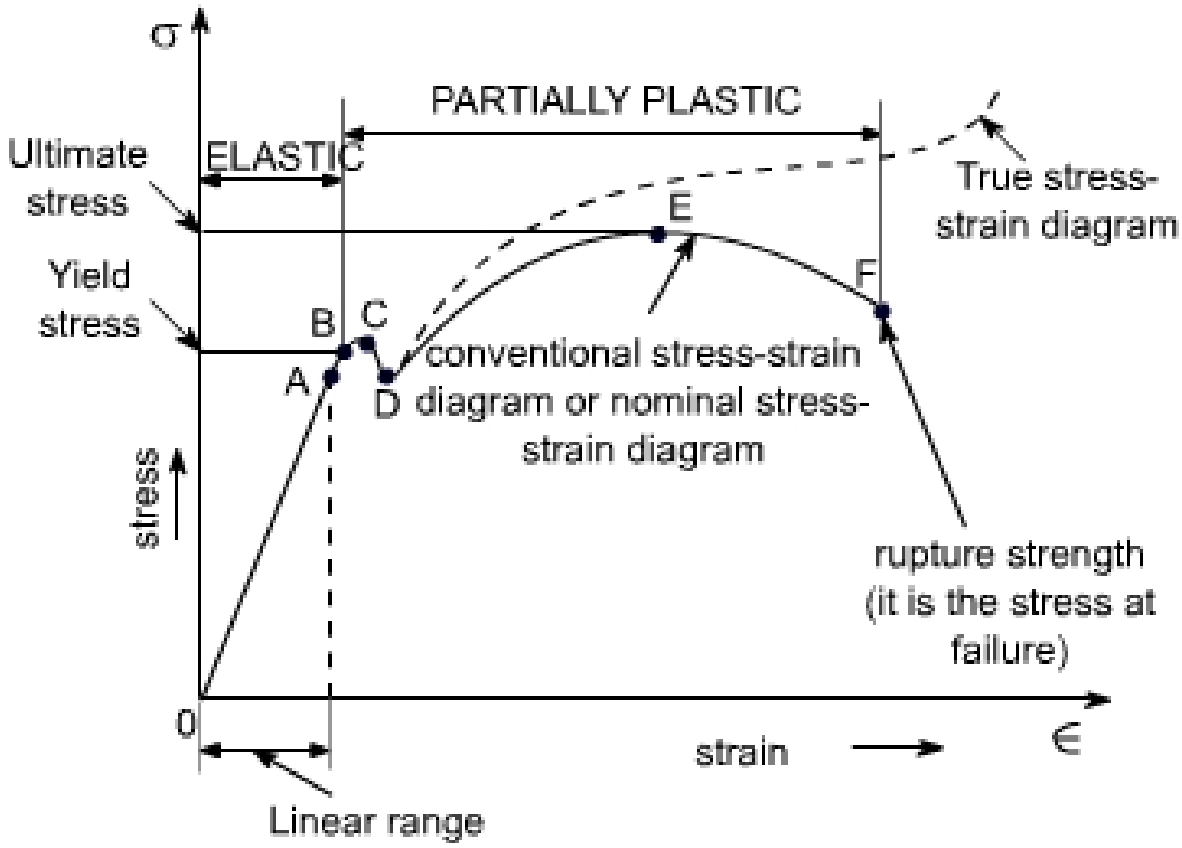

Figure 2.27 Typical stress-strain diagram for ductile materials.

Materials that do not have distinguishable yield point are referred to as brittle materials. The stress-strain curve of brittle materials is near linear before fracture failure. Testing of brittle materials is usually conducted using flexural test. This test can be conducted by either 3-point bending (Figure 2.28) or 4-point bending. For medical grade ceramics materials, the testing method is as outlined in BS EN ISO 6872:2008 (BSI, 2008) while for brittle biopolymer it is as stipulated in BS EN ISO 20795:2010 (BSI, 2010). Both these standards defined the aspects of material purity, sample preparation, test method and analysis of the results.

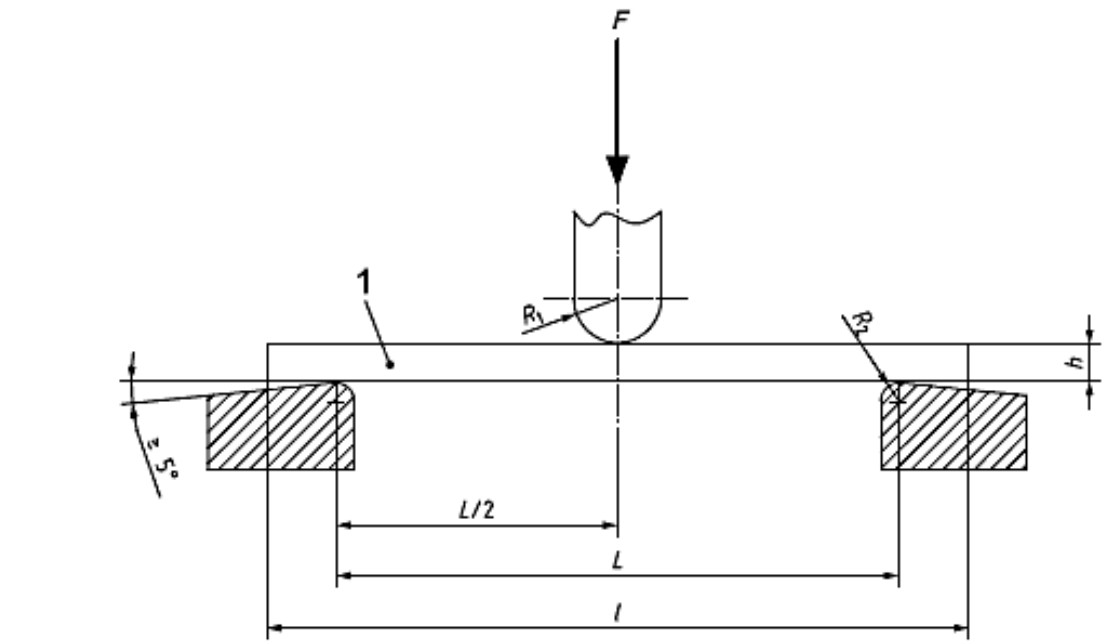

Key

1	test specimen	h	thickness of specimen
F	applied force	l	length of specimen
R_1	radius of loading edge	L	length of span between supports
R_2	radius of supports		

Figure 2.28 Specimen's initial position at start of test (BSI, 2011).

2.15 Methodology

The following flow-chart (Figure 2.29) depicts the general methodology used in this research. The initial step in this methodology is to identify and establish suitable AM systems which can be used to fabricated biomaterials in particular AWGC and PLGA. It then further identifies conventional processes that can be integrated with suitable AM system to produce low cost complex artefacts. Materials are then prepare to suit the processing route and tested for conformity to the process. When this is completed, the outputs are analysed for mechanical properties and material characteristics. This is to verify that the processing route does not change the characteristics of the materials and mechanical properties are identified. The successful process is then tested on case studies to produce complex artefacts.

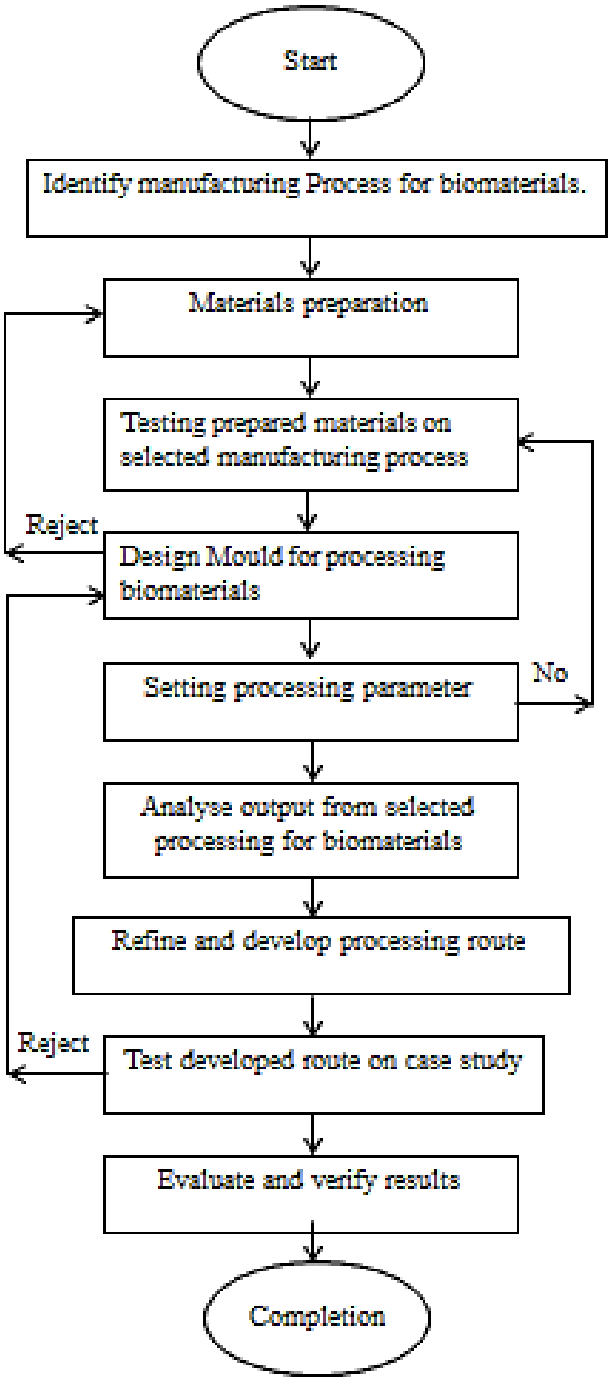

Figure 2.29 Methodology flow chart used in the proposed study.

Chapter 3: 3D Printed Moulds for Lost Wax Casting of Apatite Wollastonite Powder

3.1 Introduction

The study described in this chapter was conducted in two core parts together with a specific case study. In the first part, materials characteristics were determined to establish appropriate process parameters. It is then followed by the fabrication of test specimens for the analysis of mechanical properties as well as material characterisation after sintering. Finally, in the last stage, a medical device in the form of mandible implant was designed and fabricated. In this stage, the mandibular geometry created using the proposed route was assessed for ability to create physiologically shaped parts and ability to maintain shape definition throughout the process. Integrated design (using CAD software) and manufacturing of mould (using AM technologies) was explored in order to establish a new route for producing patient specific bioceramic medical devices.

3.2 Material Characterisations and Methods

The materials used in this research are AW and PMMA, both in powder form. The particles size for AW powder ranges from 53 to 90µm and were obtained from Glass Technology Services, Sheffield, UK which is assumed to be matching with the AW nominal chemical composition of MgO 4.6, CaO 44.7, SiO_2 34.0, P_2O_5 16.2, CaF_2 0.5 by wt.% (Kokubo, 1991b). The PMMA (Ganzpearl GM-0600, GM0800) powder were manufactured by Ganz Chemical Co. Ltd. Japan with particles size ranges from 4-8µm. PMMA belongs to the acrylic resins family and in general is an ester of methacrylic acid (CH_2=C[CH_3]CO_2H). It is a hard plastics, rigid, but brittle material, with a glass transition temperature ranging from 85°C to 145°C; dependant on the molecular weight (M_w) or grade of the PMMA. Normally it is classified at 105°C with density of 1.17 to 1.20g/cm^3. PMMA has good mechanical strength, acceptable chemical resistance, and extremely good weather resistance. PMMA was selected as binder since it is biocompatible with low melting temperature and can be completely eliminated during the heat treatment process thus avoiding toxicity posed by acrylic binder (Goodridge et al., 2006a).

The experimental setup in preparing the test samples for the research work involved the use of equipment as listed in Table 3.1.

Table 3.1 List of equipment used in the study.

Item	Equipment	Purpose
1.	Aluminium V-Mixer	Powder mixing chamber
2.	Lathe machine	Rotate mixing chamber
3.	Oven, Binder Oven	Drying PMMA powder
4.	DSC, Mettler Toledo	Thermal analysis of PMMA, in particular to Tg
5.	XRD, PANalytical X'Pert Pro MPD with Philips PW3040/60 X-ray generator and fitted with an X'Celerator	Chemical composition analysis of sintered AW
6.	SEM, Hitachi S2400 SEM with an Oxford Instruments Isis 200 ultra-thin window X-ray detector.	Morphological analysis
7.	Furnace, Carbolite	Sintering of AW
8.	Hot Plate, Fisher Scientific	Use as part of density determination
9.	Digital Balance, Mettler AE100 and Fisher Scientific	Use as part of density determination
10.	Motic microscopes with Motic Images Plus 2.0 software	Measurement and surface observation of sintered specimens
11.	Tensile machine Instron 4505 with controller interface model 4500.	Mechanical properties testing of sintered AW

3.2.1 *Materials*

Figure 3.1 shows the constitution of AW particles used in this study as obtained from the same supplier in two different batches. The first batch (b1) was obtained in particle size of 75microns while the second batch (b2) was obtained in particle size of 120microns. Both batches were sieved using stack arrangement of sieve in 120μm, 90μm, 53μm, and 25μm. After sieving most of the particle obtained are in the range of 53-90μm. As can be seen from figure 3.1a (200μm and 100 μm images) the amount of area filled with 53-90μm is less than in figure 3.1b with a high amount of particles in the 25μm range. While in figure 3.1b (200μm and 100 μm images) the amount area filled with particles in the range of 53micron makes up the main distribution of the image area. This can be attributed to the first batch which was

produced in 75µm. The form of AW particles as shown is in the shape of highly irregular frits with varying aspect ratios and sizes. The distribution of any given particles size was random with a high percentage of the particles were in the range of 53-90µm though there are a few particles which are slightly bigger than 90µm. This can be attributed to the fact that some of the particles have high aspect ratios that allowed them to pass through the sieve. This can also be presumably due to particle agglomeration. In addition, some smaller particles were observed which had not been removed by sieving, because of agglomeration.

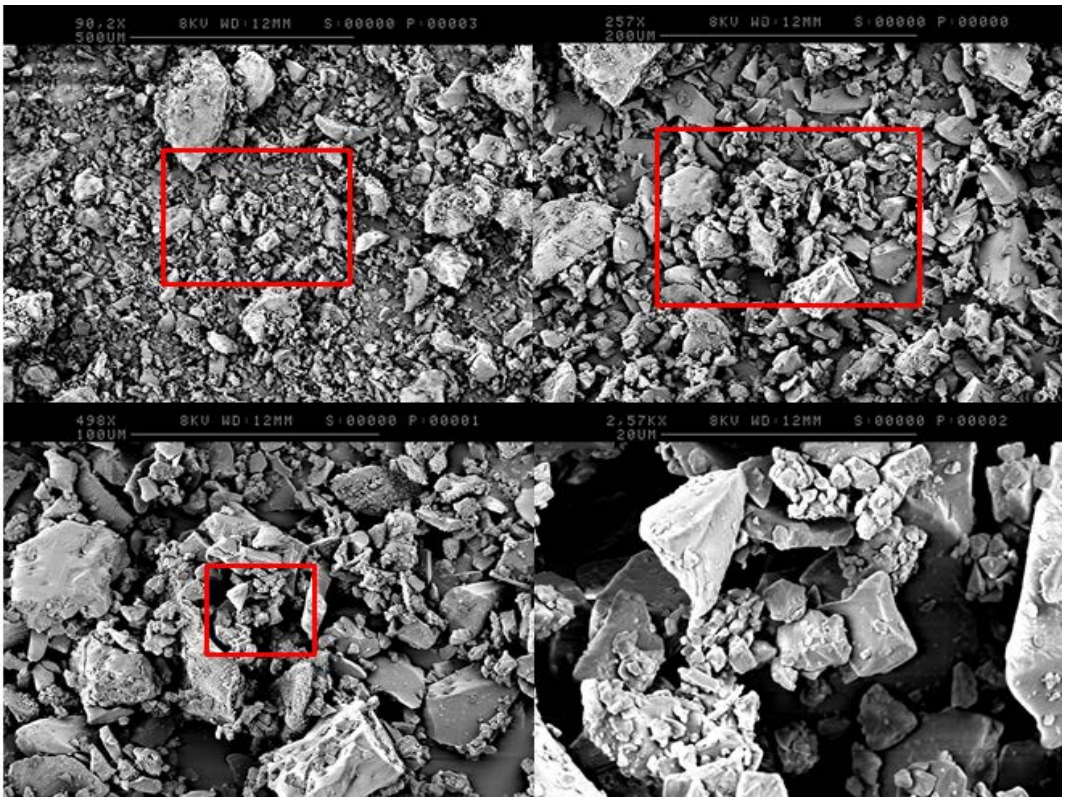

(a)

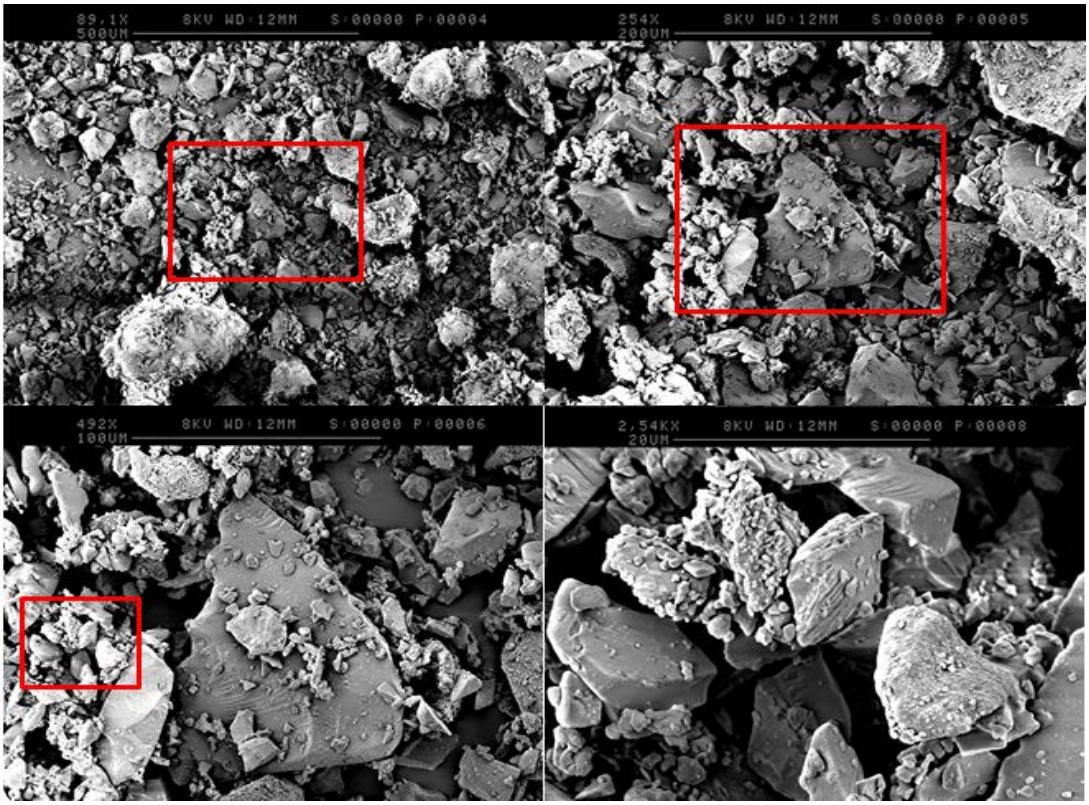

(b)

Figure 3.1 AW frits as obtained (a)batch1 and (b)batch2, mostly in the range of 53-90µm with few larger than 90µm; scale bar at top left, top right, bottom left and bottom right are 500µm, 200µm, 100µm and 20µm respectively.

Two different types of PMMA were initially used in the study. Both PMMA Ganzpearl GM-0600 and GM0800 of same particle sizes were investigated for the powder distribution characteristic. As shown in figure 3.2, most of the PMMA particles size ranges from 4-8µm is in the shape of spheres. Ganzpearl GM-0600 was distributed more evenly as compare to GM-0800, which tended to be held together.

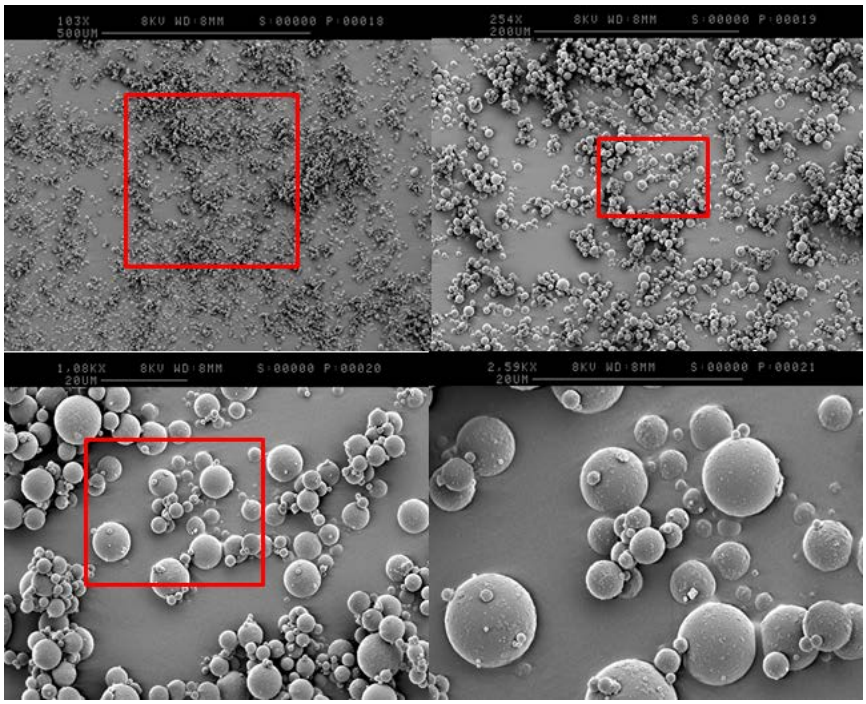

(a)

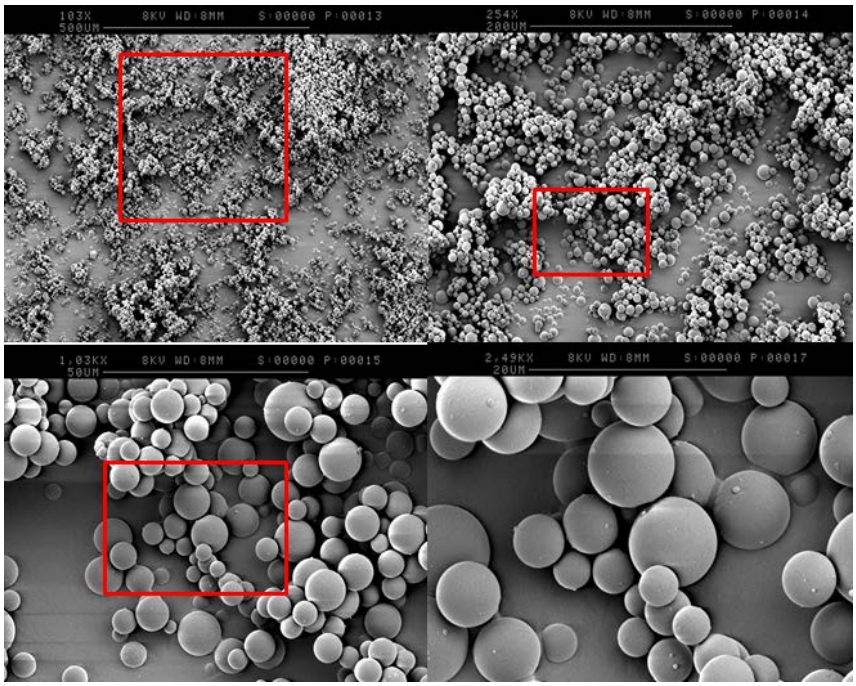

(b)

Figure 3.2 PMMA particles of mostly below the size 4um as obtained (a) GM0600 fairly dispersed and (b) GM0800 closely lumped; scale bar at top left, top right, bottom left and bottom right are 500μm, 200μm, 50μm and 20μm respectively.

3.2.2 *Powder Mixing*

The powder mixture was prepared by firstly placing the PMMA powder in an electric drier oven (Binder, GmbH) prior to blending with AW powder for half an hour. This is to eliminate any moisture absorbed by PMMA as it is known to absorb moisture due to a long time in storage. An aluminium 'V' mixer was used for mixing the PMMA and AW powder. The 'V' mixer used was cleaned thoroughly off any residue using alcohol-based solvent before any mixing was performed. The powders were mixed in the aluminium 'V' mixer placed on a lathe machine. The mixing speed on the lathe was set at 65 rpm for 105 minutes. The mixture composition of AW and PMMA powder were measured by weight ratio. The ratios of AW to PMMA used were 95:5, 85:15, and 75:25. The weights of these powders were measured using a digital balance (Fisher Scientific, UK) with accuracy of ±0.01g.

Differential scanning calorimeter (DSC) and scanning electron microscopy (SEM) were used to examine the materials and parts. The examination provided an understanding on the working principle during the fabrication process. Material characterisation for PMMA was conducted using a Mettler Toledo DSC for thermal analysis; T_g in particular. An SEM analyser was used to examine the unmixed and mixed AW to PMMA particles as well as the morphology of the sintered specimens, which shows how particles were being connected together. Density measurements of sintered specimens were performed using the Archimedes principle from the BS EN ISO standard for porous ceramic (BSI, 1995) while the geometry measurement were taken using Motic Microscopy with accompanying software. Based on BS EN ISO standard of mechanical testing for dental ceramic (BSI, 2009b), three point bending tests were carried out using an Instron 4505 with controller interface model 4500, UK.

The distribution of AW to PMMA particles powder mixtures were determined by observation of SEM images. In figure 3.3a, after the blending period as described in section 3.2.1, PMMA GM0600 particles adhered to the frits of AW. The particles were uniformly distributed and blended. Minimal agglomerations were observed of GM0600 as compared to GM0800 (Figure 3.3b) in both the mixture components.

AW frits were clearly clustered with GM0600 particles as compared to GM0800 particles that were more detached from AW. Hence, PMMA GM0600 was used as the binding powder with A-W in preparing the green parts.

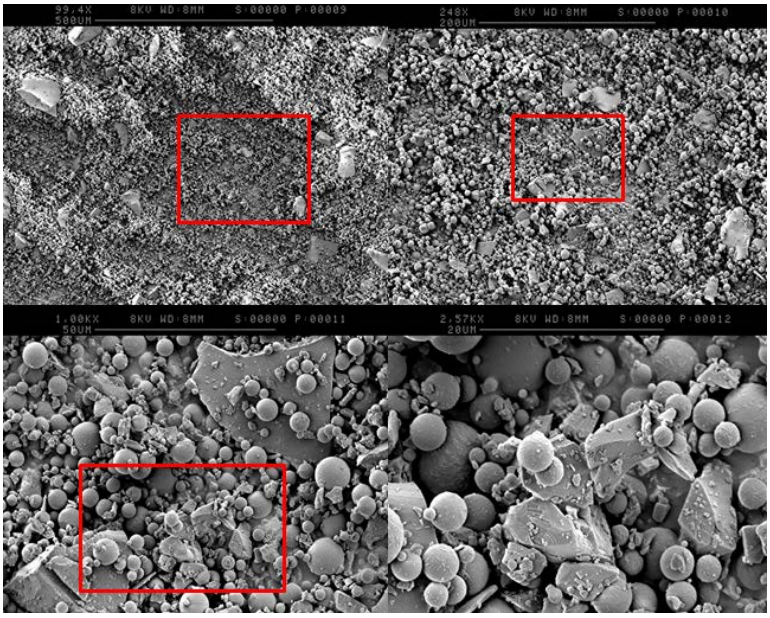

(a)

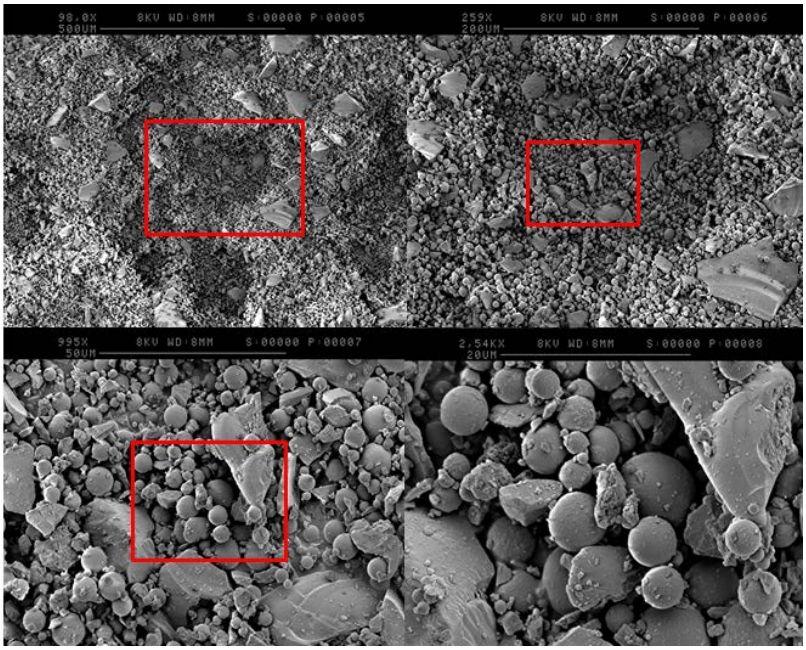

(b)

Figure 3.3 AW-PMMA powder mixtures (a) PMMA GM0600 adheres well to A-W and (b) PMMA GM0800 did not blend well with A-W. The scale bar at top left, top right, bottom right and bottom right are 500μm, 200μm, 50μm and 20μm respectively.

3.2.3 *DSC Analysis*

PMMA test samples inside 49mg aluminium crucibles were preheated for 5minutes at 30°C and then continued to be heated up until 200°C. Nitrogen flow rate of 5ml/min and heating rate of 10°C/min was set during the DSC analysis. Four test samples of PMMA as shown in figure 3.4 indicated that the range of T_g (glass transition temperature) is from 124°C to 128°C. Additional two more test samples were as shown in appendix B6.

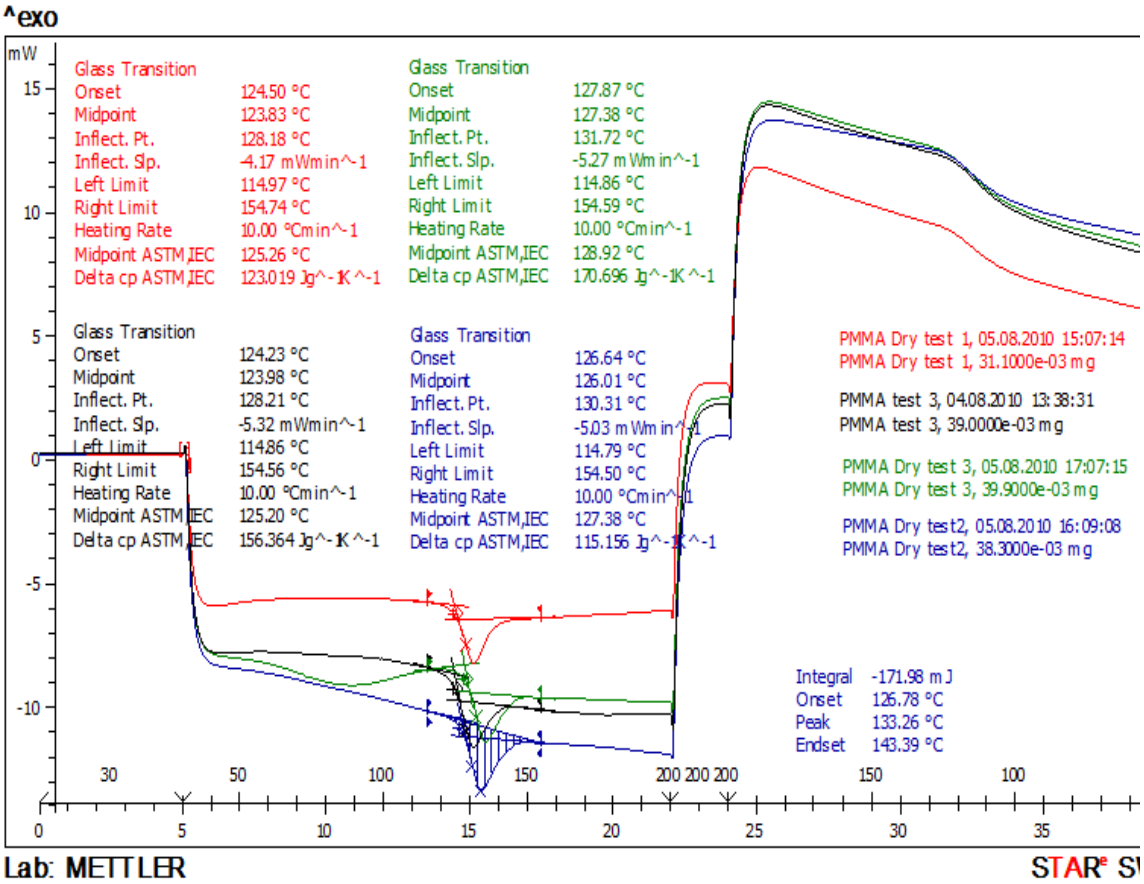

Figure 3.4 DSC tests of four out of six PMMA powder samples.

The T_g of PMMA is 125.19°C ± 1.43°C. The interval estimate on Tg for all the test samples of PMMA used in this study lies between 123.83°C and 127.38°C (Table 3.2) with a 95% confident level. The nominal value for T_g of PMMA as described in most literature varies between 85°C to 145°C; dependant on the grade of PMMA, with most at slightly over 100°C (Chow et al., 2008, Frazer et al., 2005). The T_g of PMMA used in this study fall within this range. Hence, this temperature was used as the reference temperature for temperature setting in the process of producing green part test specimens.

Table 3.2 Average T_g of PMMA at midpoint.

	n	Min. T_g	Max. T_g	Average T_g	SD	CL	CI	
							High	Low
PMMA	6	123.83	127.38	125.19	1.43	1.50	126.69	123.69

3.2.4 *Fabrication of AW glass ceramic specimens*

Figure 3.5 show the process of producing A-W glass ceramic specimens. This procedure of fabricating the A-W glass ceramic rods is as described in the following steps: -

1. Aluminium foil of thickness between 0.1 mm to 0.2 mm was wrapped tightly between four to eight times around a 3.2 mm diameter mandrel. Copper wire was then wound around the foil to create a mould. This is to strengthen the mould and distribute heat. The mould was then slid off the mandrel, and the foil at one end folded over to close one end of the cylinder.

2. Powder mixture; by percentage weight ratio, of 53-90μm AW (from Glass Technology Services, Sheffield) and 4-8 μm PMMA (Ganzpearl GM-0600) was made by mixing the composition in a 'V' mixer on a lathe machine. The powder was mixed at a speed of 65 rpm for 105 min.

3. The powder mixture was then heated in an oven at 120°C for 60min to dry the PMMA powder as it cans easily absorbed moisture. Then the heated powder mixture was poured into the foil mould through a small funnel with a tapered end and diameter of 2.0mm. During filling care was taken to ensure that the temperature of the powder remained above 110°C for easy flow of powder mixture, and that no air pockets were formed in the mould by poking and compression the filled mixture with pin and rod.

4. Once the mould had been filled, it was placed in an oven and heated to 145°C to consolidate the PMMA powder. The filled mould was maintained at 145°C for 2 hours, before the heater was switched off, and the oven allowed cooling at its normal rate.

5. Once the filled mould was at room temperature, carefully removing the copper wire and then unwinding the aluminium foil will expose the “green part”, (a cylindrical rod of ceramic powder held together by PMMA binder).

6. The green part was then placed into a sintering boat before been placed into a furnace. The heating profile in the furnace was predefine where the temperature in the furnace was raised from room temperature to 779°C at a rate of 10°C per minute, and then held at that temperature for one hour, before increased to 1150°C, again at a rate of 10°C per minute, and again held at that temperature for one hour(Xiao et al., 2007) (see Figure 3.6).

7. The furnace was allowed to cool a rate of 10°C per minute before heating was then switched off and, the sintered rods could be removed from the furnace.

3.2.5 *Characterisation of sintered specimens*

In order to obtain sintered testing specimens, the produced green parts were sintered according the heating profile in Figure 3.6. This heating profile creates an optimum nucleation and propagation of glass-ceramic crystal growth, which benefits the increase of strength (Xiao et al., 2007). During the heating process, burned out of PMMA binder occurred, leaving pure sintered AW glass ceramic as PMMA does not leave any residue (Goodridge et al., 2006a). XRD and EDX analysis were performed on the sintered specimens such as to ensure the presence of wollastonite and hydroxyl/apatite and the chemical composition is similar to Kokubo’s formulation. In addition, besides 3-point bending test; physical properties measurements were conducted to evaluate the outcome of the process flow (Figure 3.5).

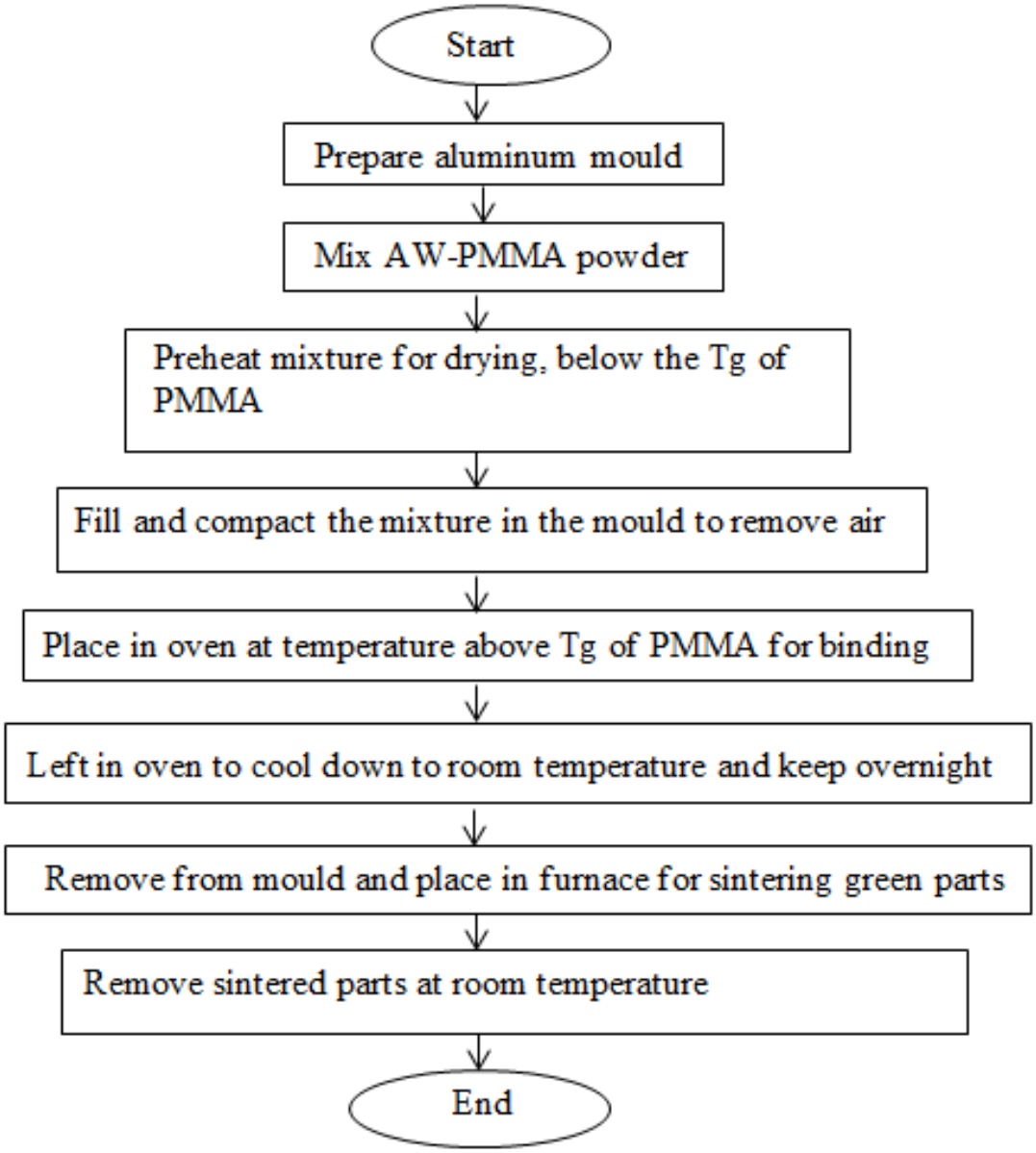

Figure 3.5 Process flow in preparing sintered test specimens.

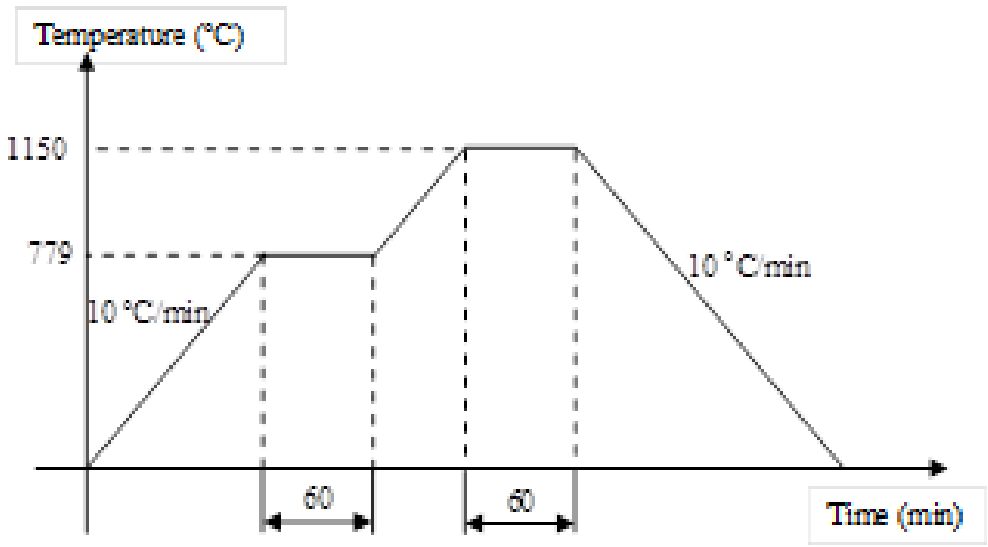

Figure 3.6 Heating Profile for sintering AW green parts.

3.2.5.1 **Dimensional Measurement**

As the green parts are fragile and the closing of the Vernier callipers jaws during measurement could break the specimens, Vernier callipers was not used. Instead, Motic microscope with Motic Images Plus 2.0 software was used to measure the diameter of both the green parts and sintered parts. Calibration was performed before each set of measurements, and each specimen measurement was taken three times and averaged (Figure 3.7). As observed from the measurements taken, no significant variation was observed in repeated measurements in which the green parts and the sintered parts diameters are 3.110mm ±0.132 and 2.412mm±0.073, respectively (Table 3.3).

Twenty-two samples of green parts and sintered parts were measured. Eleven green parts in total were measured with an average diameter of 3.113 mm as compare to the 3mm diameter of the mandrel, a 4% deviation. The range of green parts produced is between 2.853 mm and 3.319 mm. While, the eleven sintered rods parts had an average diameter of 2.412 mm, with a range of between 2.314 and 2.528 mm. The margin of errors for both green parts and sintered were 0.08mm and 0.048mm respectively. The average shrinkage was 22.5% (Table 3.3) as calculated from equation 3.1,

$$\text{Percentage of shrinkage} = \frac{d_0 - d_1}{d_0} \times 100\% \qquad (3.1)$$

where d_0= diameter of green part

d_1= diameter of sintered part

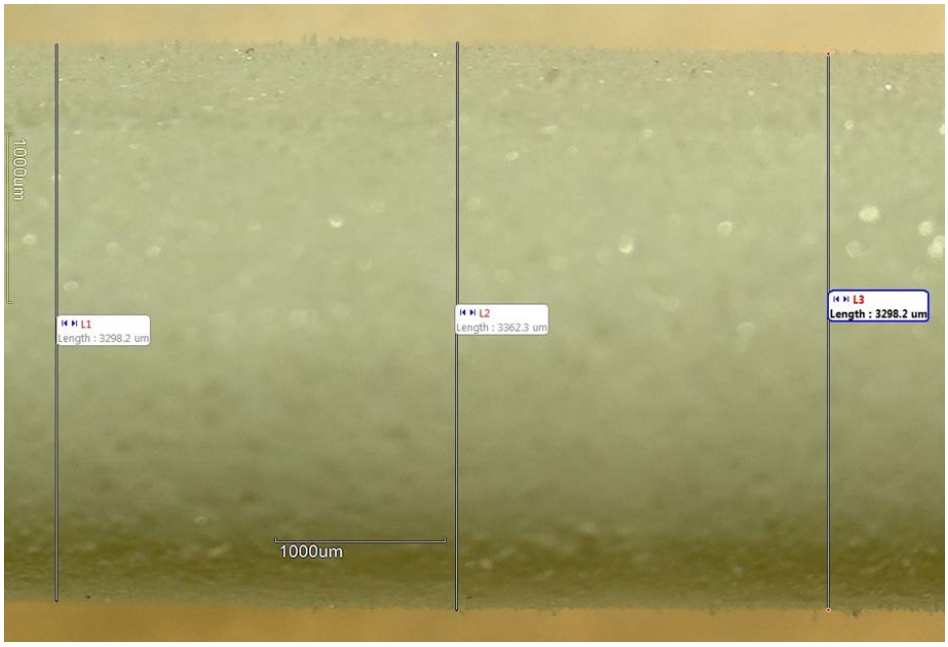

(a)

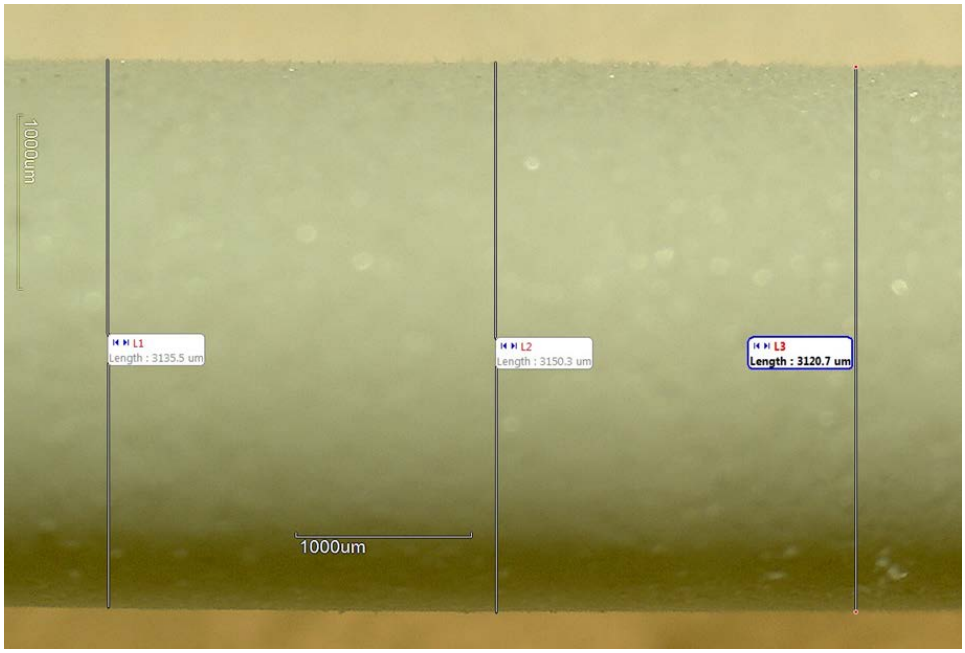

(b)

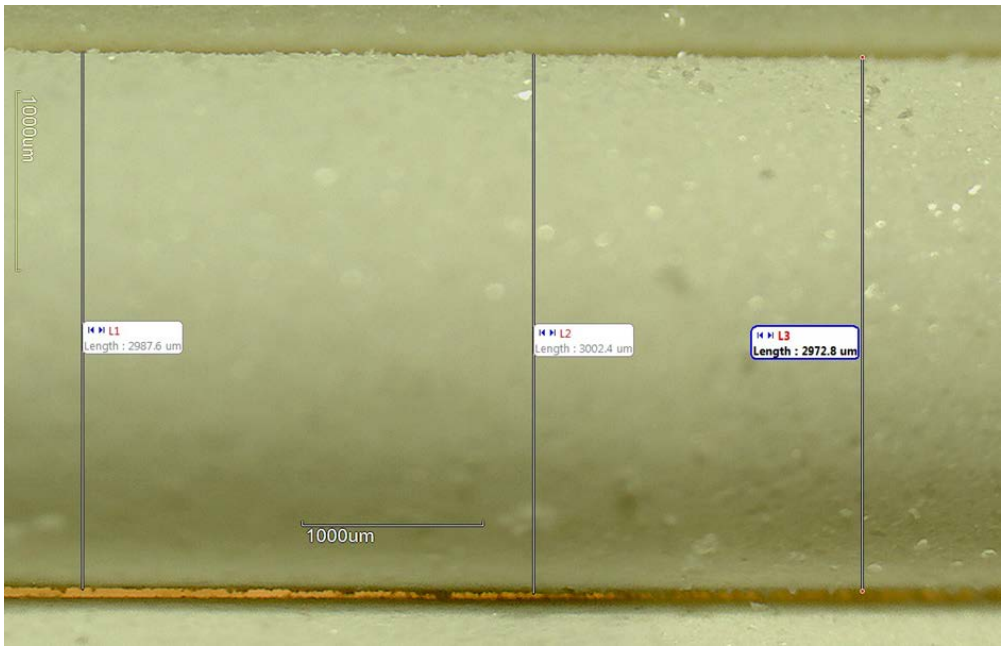

(c)

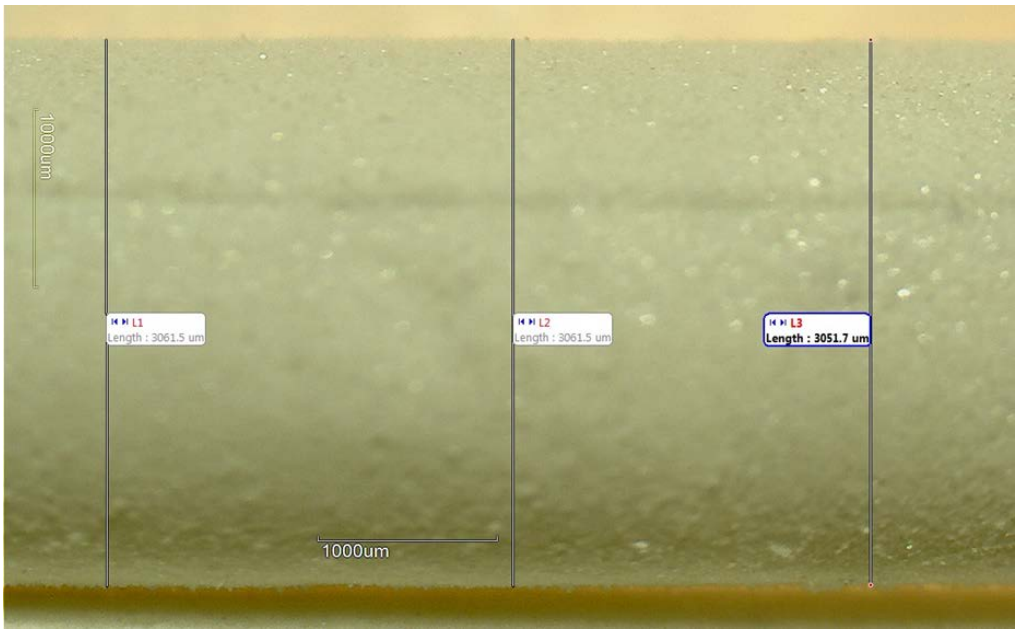

Figure 3.7 Three Measurements were taken on sintered specimens (a), (b), (c) and (d) where variation is not significant; scale bar on images is 1000μm.

Table 3.3 Samples average geometrical measurements.

Diameter	n	Ave. variation on three-repeated measurements. (mm)	Min. (mm)	Max (mm)	Ave. (mm)	SD	CL %	CI (mm)	Percent of Average Shrinkage %
Green parts	11	3.110 ±0.132	2.853	3.319	3.113	0.131	95	3.113 ±0.088	22.5
Sintered parts	11	2.412 ±0.073	2.314	2.528	2.412	0.071	95	2.412 ±0.048	

The amount of shrinkage corresponds to the amount of binder used and some residue of air or moisture during filling of the mould at room environment. The shrinkage occurred as the particles attempt to achieve a denser packing under the influence of surface tension from the polymer melt during thermal debinding(Rahaman, 2008). Furthermore, decomposition of the binder, residue of air or moisture trapped in the green parts can result in bubble formation and caused flaw formation as well as geometry deformation (Dong and Bowen, 1989).

3.2.5.2 **Density and porosity**

Pycnometer was used to determine the density and open porosity of the AW samples, with thirteen samples being measured. A 25ml density bottle was used with distilled water as the liquid medium. Dry sintered sample and empty density bottle were weighted separately before been weighted together. Density bottle was then filled with distilled water and weighted before dry sample was placed inside it to determine the suspended weight of the sample. The density of the samples were determined from the known density of the distilled water, the weight of the sample, the weight of density bottle filled with water and the weight of density bottle with both the sample and water (BSI, 2003).

In order to determine the porosity of the sample, the sample then was boiled in a volume of 50 to 75 ml of water using a Fisher Scientific hotplate for 15minutes in order to fill out open pores. The sample was immediately dried upon taken out with paper towel of excess water. Sample was then put in an empty density bottle and weighted. Again, the suspended weight of the boiled sample was weighted.

The calculation performed in order to obtain the apparent and relative densities are as outline in equation 3.3 and equation 3.5. Calculations of samples were based on a true density for the AW at 3.07 g/cm³, PMMA at 1.19g/cm^3 and distilled water temperature taken at 22°C, 0.9978g/cm^3. The samples were on average 26.9% porous (porosity ranges from 19.6% to 36.7%), with on average 51.0% of the pores being open (Table 3.4 and Figure 3.8).

The related equations used for determining the physical properties of the fabricated AW specimens; such as apparent density, relative density and true porosity, are as given:

Volume of solid $V_s = \frac{(m_3 - m_0) - (m_2 - m_1)}{\rho_w}$ (3.2)

Apparent Density of solid $\rho_s = \frac{m_s}{V_s} = \frac{m_s}{(m_3 - m_0) - (m_2 - m_1)} \times \rho_{water}$ (3.3)

Bulk Density $\rho_b = \frac{(m_1 - m_0)}{(m_{1w} - m_0) - (m_2 - m_3)} \times \rho_{water}$ (3.4)

Relative Density $\rho_r = \frac{\rho_s}{\rho_{AW}} = \frac{m_s}{(m_3 - m_0) - (m_2 - m_1)} \times \frac{\rho_{water}}{\rho_{AW}}$ (3.5)

Apparent Porosity $= \frac{soaked\ body - dry\ body}{soaked\ body - suspended\ body} = \frac{(m_{1w} - m_0) - (m_1 - m_0)}{(m_{1w} - m_0) - (m_2 - m_3)}$ (3.6)

Total Porosity $\phi = 1 - \rho_r$ (3.7)

True Porosity $= \frac{\rho_{AW} - \rho_b}{\rho_{AW}} \times 100\%$ (3.8)

Weight of dry body sample $W_1 = (m_1 - m_0)$ (3.9)

Weight of suspended body in water $W_2 = (m_2 - m_3)$ (3.10)

Soaked body weight $W_3 = (m_{1w} - m_0)$ (3.11)

The values of all measured variables for $m_0, m_1, m_{1w}, m_2, and\ m_3$ are given in appendix B1.

Table 3.4 Density and porosity measurements of AW as determine using pycnometer.

Item	weight of dry sample W_1 (g)	suspended in water weight W2 (g)	soaked body weight W3 (g)	bulk density g/cm3	apparent solid density g/cm3	relative density	apparent porosity %	true porosity	Percentage of open porosity %
n	13	13	13	13	13	13	13	13	13
Min	0.2675	0.1640	0.2834	1.94	2.32	0.63	9.63	19.60	41.02
Max	0.3175	0.1992	0.3353	2.47	2.77	0.80	16.44	36.66	64.30
Ave	0.2867	0.1764	0.3042	2.25	2.60	0.73	13.60	26.86	50.97
SD	0.0169	0.0123	0.0171	0.14	0.12	0.04	2.20	4.49	6.06
Std Error	0.0047	0.0034	0.0047	0.04	0.01	0.03	0.61	1.24	1.68
CI	0.0101	0.0074	0.0103	0.08	0.03	0.07	1.33	2.71	3.66

As seen from table 3.4 and equation 3.3 and equation 3.4, the apparent solid density and bulk density are differentiated by the amount of water that occupied the open porosity. Figure 3.8 shows the internal surface for the sintered region of the AW particles and the pores created from the sintering process. The squared region indicates the pores in the sintered sample while the circled region indicated the sintering of the particle, where the region of necking between particles created pores of varying sizes below 100μm. As shown from the squared region which indicates the breaking surface of the sintered particle, open and close pores were

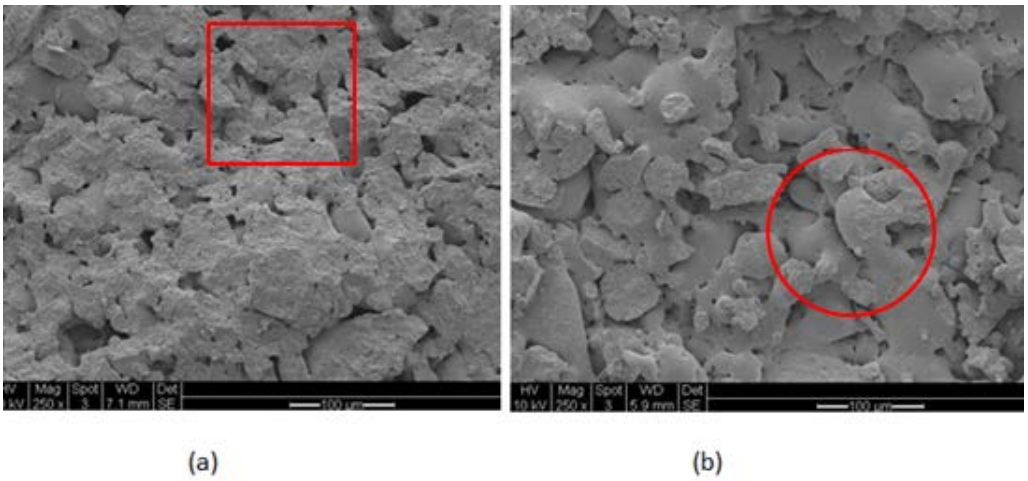

Figure 3. 8 Image (a) and (b) of the cross section of sintered AW samples.

clearly visible for particles of AW joined in accordance with sintering phenomena.

Figure 3.9 shows the open and close micropores and sub-micropores (indicated by circled region) on the native surface. SEM images of the outer surface and cross sectional surface, indicating that the model was porous, with pore sizes of the order of 20 μm and a few micropores. Porosity in structure is influencing feature that affect osteoconductivity in addition to the chemical composition, and surface topography (Kokubo, 2008).

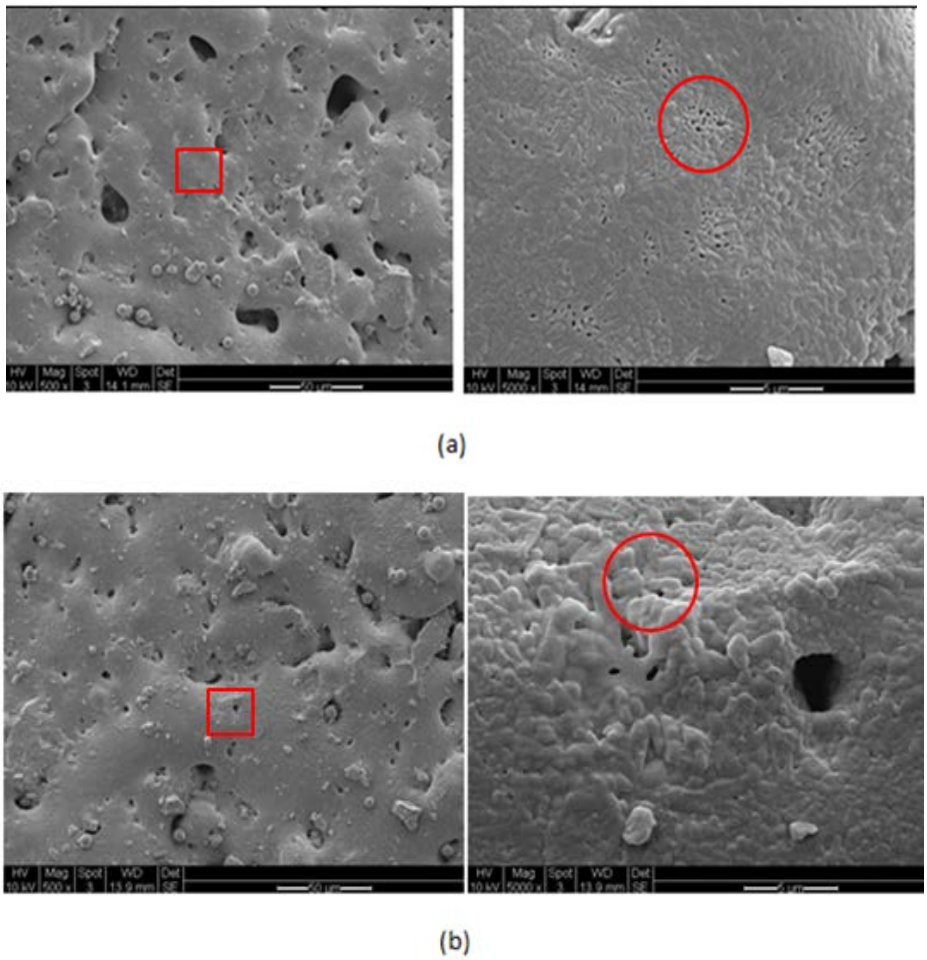

Figure 3.9 SEM images (a) and (b) of sintered porous A-W glass ceramic 80%wt on the external surface of two samples at 500X and 5000X magnification indicating micro-porosity; scale for left image and right image are 50μm and 5μm respectively.

The porosity level achieved in this study is adaptable for mimicking cortical bone structure, but increased macroporosity would need to be designed into the structure in order to optimise the quality of porosity for bone ingrowth. The amounts of porosity from the SEM images indicate that an estimate of 20% to 30% pores in the samples that include some micro porosity.

Comparing to the SEM images (Figure 3.10) of A-W specimens produced using SLS; no distinguishable differences were prevalent in the external surface of the sample that was fabricated using aluminium sheet mould. However, for internal surface, there appeared more pores in the sample produced by the method proposed in this study. As porosity and interconnected channel encourage cell propagation, the feature that is generated by this fabrication method is considered to serve the purpose of TE applications (Figure 3.10).

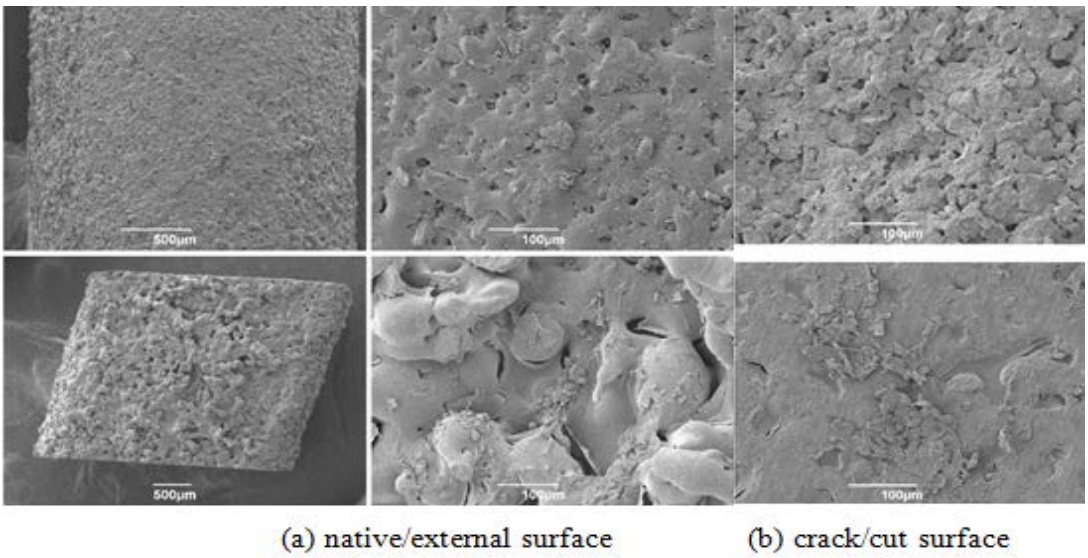

Figure 3.10 Scaffolds as produced by the proposed method (top) and scaffolds produced by SLS.

3.2.5.3 **Flexural Strength from Three Point Bend test**

The samples were tested on a universal testing machine (Instron 4505 with controller interface model 4500) at a crosshead speed of 0.5 mm/min. The setup for the bending test as shown (Figure 3.11) was based on BS EN ISO 6872:2008 (BSI, 2008). The spans between supports for both sets of tests were 20mm. The tests were carried out at room temperature of 24°C with humidity of 38% R.H.

The modulus of rupture (flexural strength) and flexural modulus was calculated using the equations 3.12 and 3.13 as follows:

$$\sigma = \frac{8FL}{\pi D^3} \tag{3.12}$$

$$E = \frac{4FL^3}{3\pi D^4 \delta} \tag{3.13}$$

Where E = flexural modulus GPa

σ = strength in MPa

F = break force, N

δ = deflection, mm

L = support (outer) span, mm

D = specimen diameter, mm

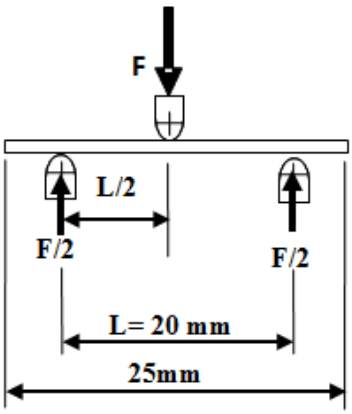

Figure 3.11 Bending test diagram as based on BS (BSI, 2008).

Two batches of samples were used in the test. Batch 1 samples used in the tests were ranging from 2.35mm to 2.65mm in diameter while, for Batch 2 diameter, the range is from 2.56mm to 3.06mm and 25.2mm to 28.4mm in length; respectively. Figure 3.12(a) shows the samples load versus deflection diagrams exhibit a linear relation for load and deflection between the deflection range from 0.015mm to 0.05mm for batch 1 and 0.035mm to 0.065mm for batch 2. Figure 3.12 (b) diagrams were obtained using fewer data point by setting the sampling rate to one data point/second. The average flexural strength for batch 1 was 63.83 MPa, with the range observed over 11 tests to be from 53.14 to 82.80 MPa. While for batch 2, the average flexural strength was 76.45 MPa, with the range observed over 11 tests to be from 60.71 to 92.62 MPa. The average flexural modulus for batch 1 is 26.65GPa and 23.51GPa for batch 2(Table 3.5). Using a 2tails t-test with confidence level of 95% ($p<0.05$), the p-value and t-statistic value obtained for the diameter, flexural modulus and flexural strength are p=0.00007, t-stat=6.532; p=0.1425, t-stat=1.592; and p=0.0048, t-stat=3.609; respectively.

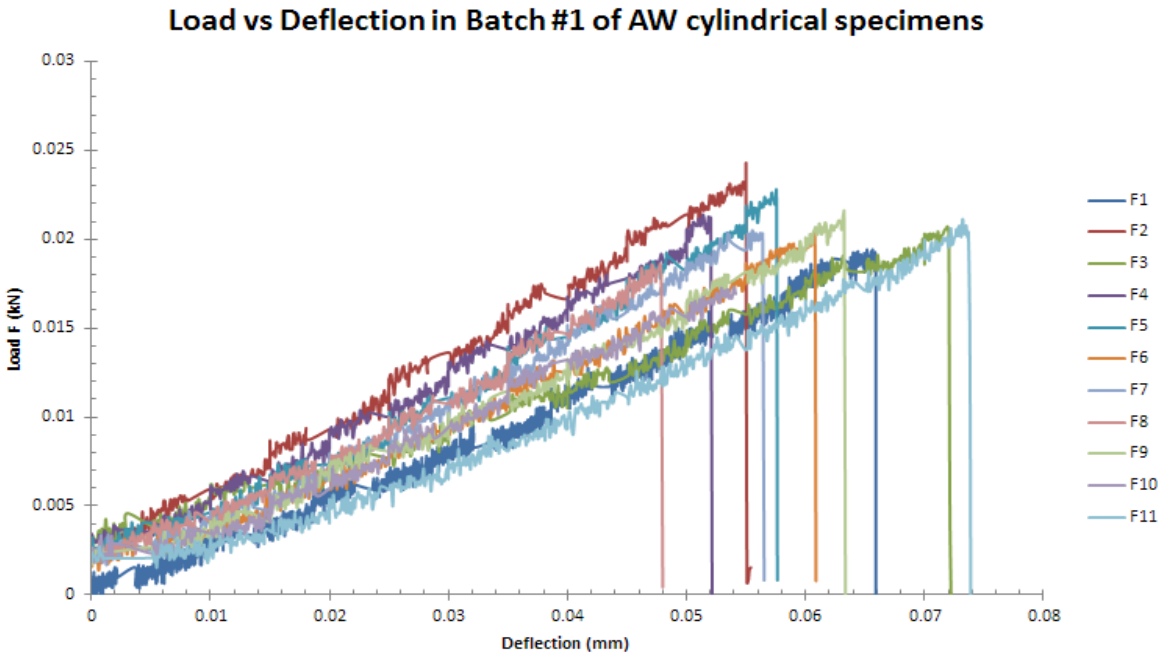

(a)

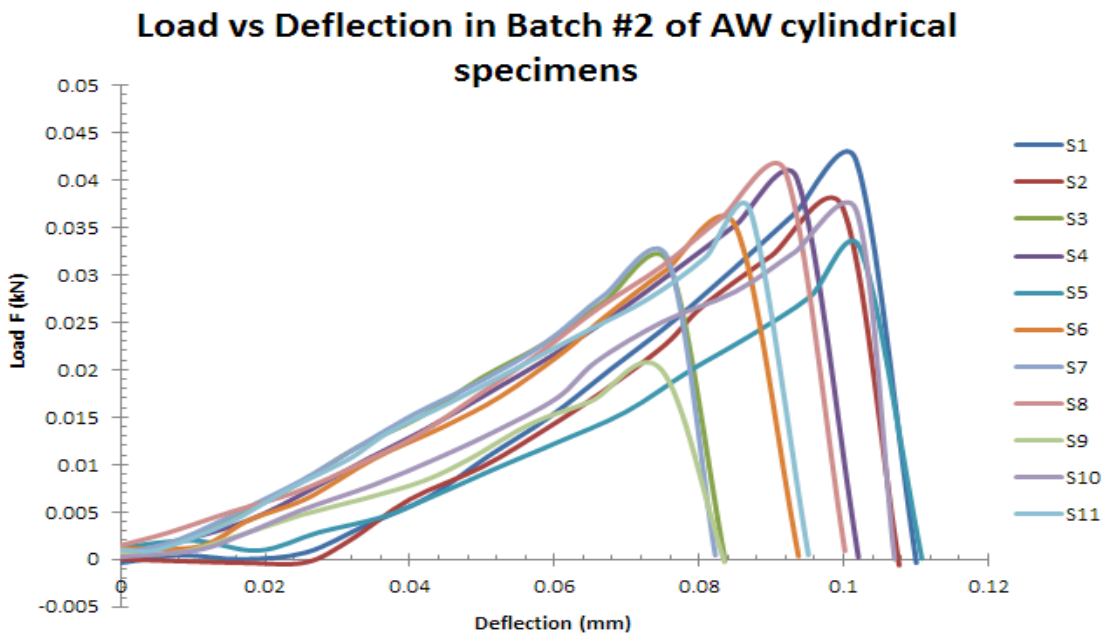

(b)

Figure 3.12 Load versus Deflection for 2 batches of AW cylindrical specimens from 3 Point bending test.

Table 3.5 Flexural Modulus and Modulus of Rupture (Flexural Strength).

		Diameter (mm)	Break Force (N)	Displacement at break force δ_{break} (mm)	Flexural Modulus E (GPa)	Modulus of Rupture (Flexural Strength) σ (MPa)
Batch 1	n	11	11	11	11	11
	Minimum	2.35	17.3	0.048	21.74	53.14
	Maximum	2.65	24.29	0.102	32.53	82.80
	Median	2.55	20.7	0.058	25.24	62.75
	Mean	2.55	20.82	0.06	26.65	63.83
	SD	0.082	1.854	0.015	4.055	7.400
	Standard Error	0.025	0.559	0.005	1.22	2.231
	CL 95%	0.055	1.245	0.010	2.72	4.971
	High	2.605	22.065	0.07	29.37	68.801
	Low	2.495	19.575	0.05	23.93	58.859
Batch 2	n	11	11	11	11	11
	Minimum	2.56	20	0.08	17.18	60.71
	Maximum	3.06	42.1	0.10	28.67	92.62
	Median	2.85	36.7	0.09	23.56	74.81
	Mean	2.85	35.0	0.09	23.51	76.45
	SD	0.121	6.13	0.01	3.77	9.03
	Standard Error	0.036	1.85	0.003	1.14	2.72
	CL 95%	0.081	4.12	0.007	2.53	6.07
	High	2.931	39.12	0.097	26.04	82.52
	Low	2.769	30.88	0.083	20.98	70.38
	t Stat	6.532			1.592	3.609
	P(T<=t) two-tail	0.00007			0.1425	0.0048
	t Critical two-tail	2.228			2.228	2.228

3.2.6 *XRD and EDX evaluation of material after fabrication process*

The chemical composition of the sintered specimens was analysed using a PANalytical X'Pert Pro MPD, powered by a Philips PW3040/60 X-ray generator and fitted with an X'Celerator. Diffraction data was acquired by exposing powder samples to Cu-Kα X-ray radiation, which has a characteristic wavelength (λ) of 1.541874 Å. X-rays were generated from a Cu anode supplied with 40 kV and a current of 40 mA.

The data was collected over a range of 5-100 2θ with a step size of 0.0334 2θ and nominal time per step of 150 seconds. Fixed anti-scatter and divergence slits of ¼ were used together with a beam mask of 10mm. All scans were carried out in ‘continuous’ mode using the X’Celerator RTMS detector.

Phase identification was carried out by means of the X'Pert accompanying software program PANalytical High Score Plus in conjunction with the International Centre for Diffraction Data (ICDD) Powder Diffraction File 2(PDF-2) database (2003 and 2009).

As shown in table 3.6 and figure 3.13 for AW glass-ceramics the crystalline phases are generally apatite/fluorapatite, wollastonite, diopside and whitlockite. From the PDF2 (2009), the compounds are diopside (01-073-6374), hydroxylapatite (01-080-6260), wollastonite (04-010-0710) and whitlockite (04-015-8362). For the older PDF (2003), the compounds are wollastonite 1A (01-072-2284), hydroxylapatite (01-073-1731), fluorapatite (01-071-0880) and calcium magnesium phosphate (01-070-0682). Hence from both XRD analyses, there are evidence of apatite and wollastonite in the glass ceramics used in this research. Although different PDF2 database that were used yielded different results, the peaks patterns are consistent. The XRD results show comparable pattern to other researchers (Cannillo et al., 2009, Podporska et al., 2008). The similarity in the diffraction peak list patterns for AW phase in the samples indicates that the processing route has not affected the composition in any way.

Table 3.6 Chemical compounds based on different ICDD PDF2 database.

2003		2009	
Ref. Code	Compound Name	Ref. Code	Compound Name
01-072-2284	Wollastonite 1A	04-010-0710	Wollastonite
01-073-1731	Hydroxylapatite	01-080-6260	Apatite
01-071-0880	Fluorapatite	04-015-8362	Whitlockite
01-083-1817	Diopside	01-073-6374	Diopside
01-070-0682	Calcium Magnesium Phosphate		

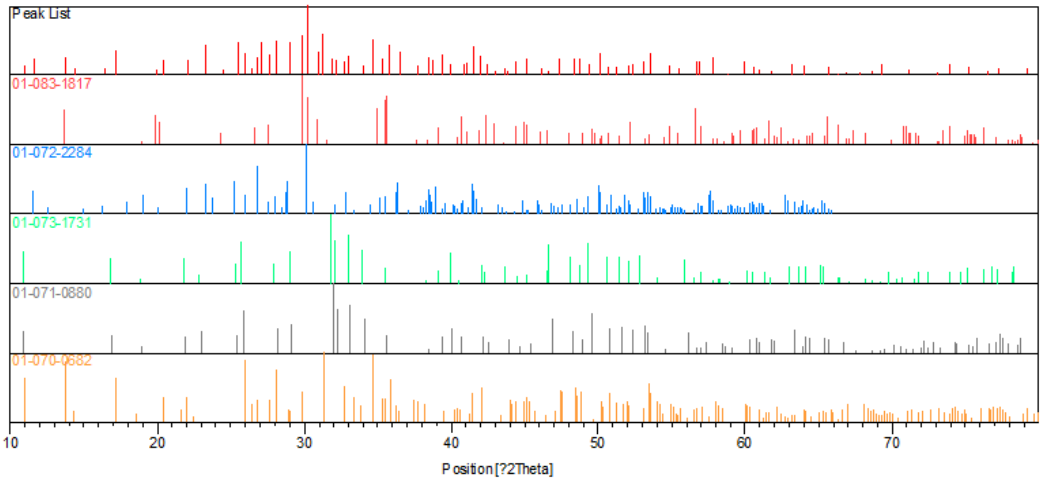

Ref. Code	Compound Name	Chemical Formula
01-083-1817	Diopside	Ca Mg Si2 O6
01-072-2284	Wollastonite 1A	Ca Si O3
01-073-1731	Hydroxylapatite	Ca5 (P O4)3 (O H)
01-071-0880	Fluorapatite	Ca5 (P O4)3 F
01-070-0682	Calcium Magnesium Pho:	Ca2.81 Mg0.19 (P O4)2

(a) AW1

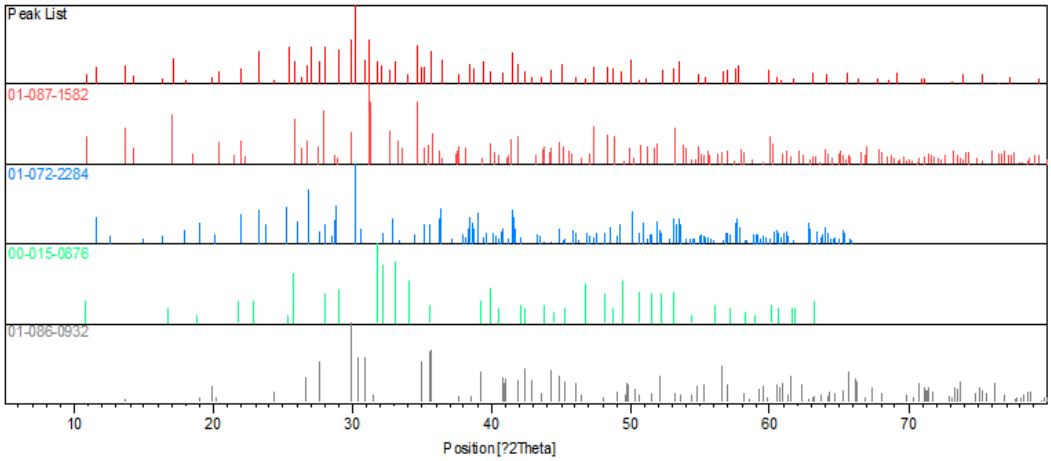

Ref. Code	Compound Name	Chemical Formula
01-087-1582	Calcium Magnesium Phosphate	(Ca2.589 Mg0.411) (P O4)2
01-072-2284	Wollastonite 1A	Ca Si O3
00-015-0876	Fluorapatite, syn	Ca5 (P O4)3 F
01-086-0932	Diopside	Ca Mg Si2 O6

(b) AW2

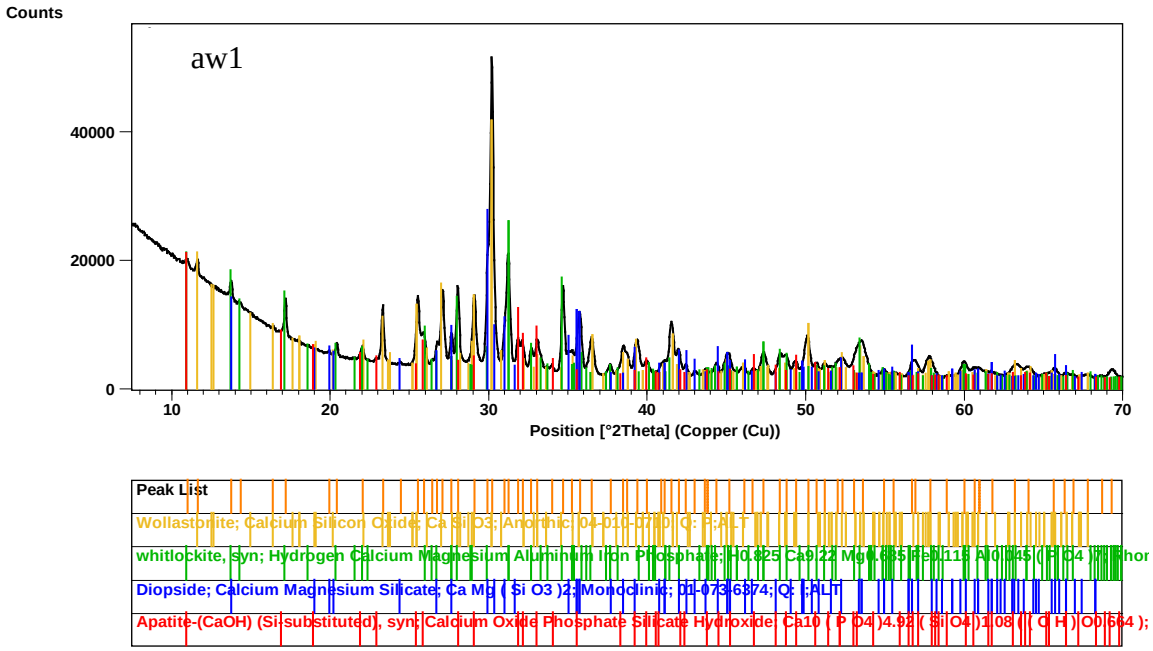

(c) AW1

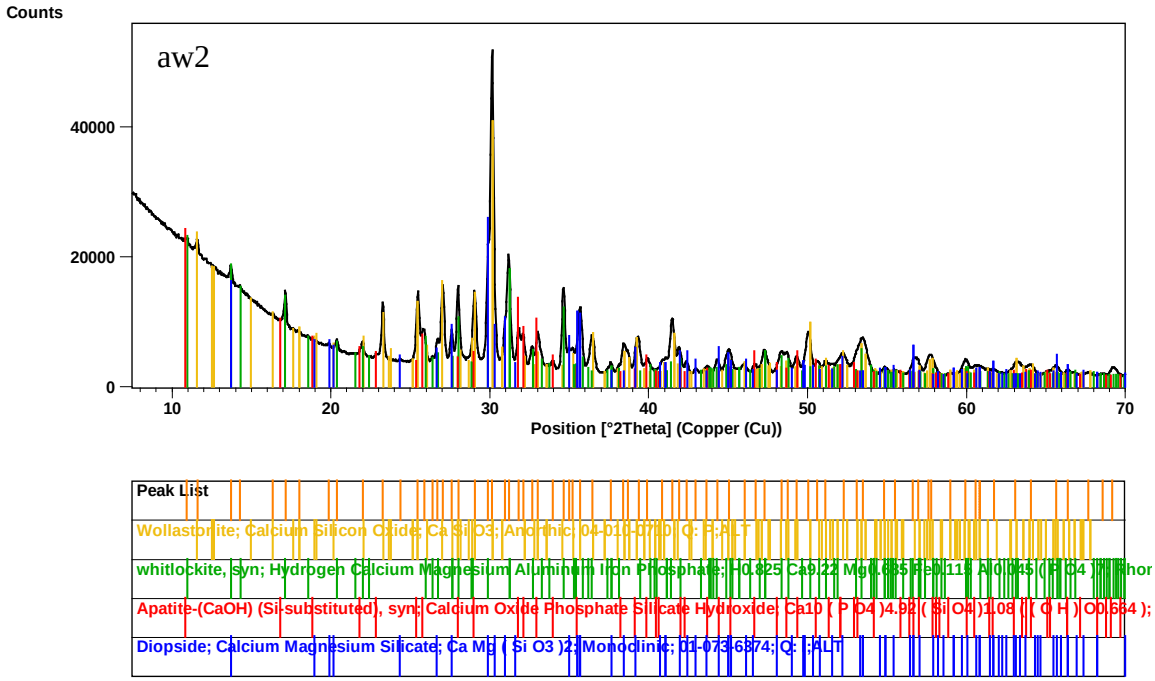

(d) AW2

Figure 3.13 XRD analysis of the sintered AW cylindrical specimens indicating the consistent peaks pattern using newer ICDD database (a-b) 2003 and (c-d) 2009.

EDX analyses were conducted on the sintered samples in order to ensure that the chemical composition is comparable to Kokubo's formulation (Table 3.7). As shown in table 3.7 ,

besides the main chemical composition of silicon, phosphorus, calcium and magnesium; there are traces of carbon residue which might be resulted from the burnout of the PMMA binder used.

Table 3.7 The EDX results of the sintered AW cylindrical specimens' chemical composition as compared to Kokubo's formulation.

	norm wt %		
Element	AW1	AW2	Kokubo's formulation
Silicon	14.13	12.67	15.88
Phosphorus	5.08	4.03	7.06
Calcium	29.92	25.12	31.96
Magnesium	2.75	2.32	2.76
Carbon	2.44	7.06	
Oxygen	45.68	48.80	42.10
Aluminium			
Fluorine			0.25
	100	100	100.01

Table 3.7 and figure 3.15, show the different between Kokubo's formulation and the AW used for this research. From the EDX results there is a small percentage of carbon elements presence in the sintered parts. No further analysis was performed to identify the source of carbon element, as it is assumed to be caused by the burned out of the PMMA binder used during the green part fabrication. Furthermore, a small amount of carbon residue can normally be found in particle surfaces binders (Masia et al., 1989) during normal pure state burn out in thermal debinding and is difficult to be removed.

By assuming the relative proportions of each element to be based on 100%, the different between the chemical compositions of AW used in this research for all elements with Kokubo's formulation is 1.5% for silicon, 22% for phosphorus, 3.4% for calcium and 10% for magnesium while from XRD analysis, compound peak list of the sintered specimens showed clear evidence of apatite/fluorapatite, wollastonite, diopside and whitlockite.

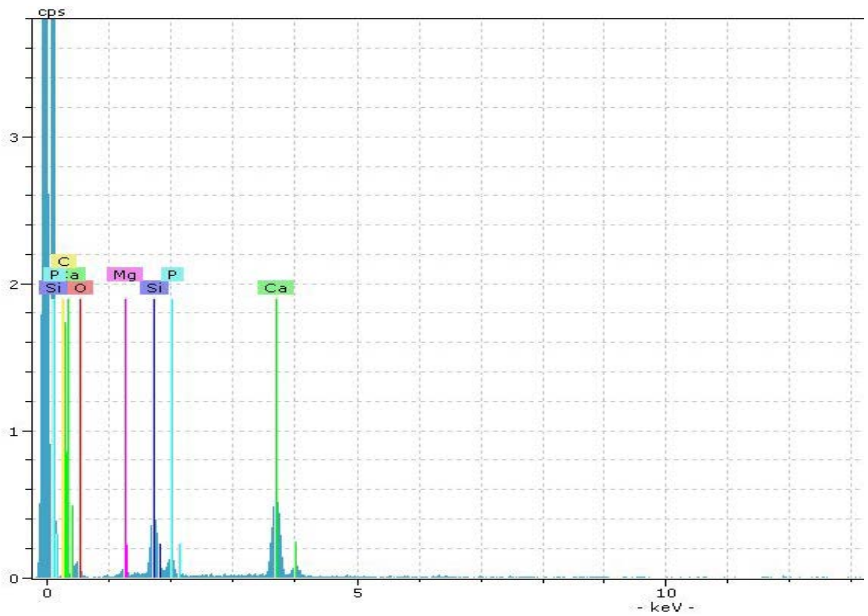

(a) AW1

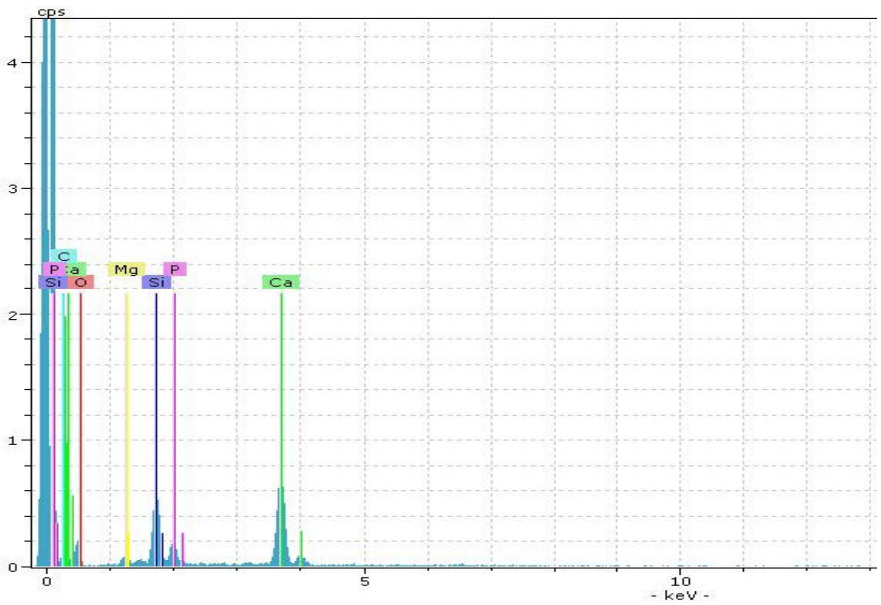

(b) AW2

Figure 3.14 EDX results for sintered two samples specimen fabricated using aluminium sheet mould using the same batch of AW-PMMA powder mixture.

3.3 Assessment of moulding process

The proposed fabrication of AW glass ceramic round specimens was via moulding. At a later stage of this study, the intention was for fabricating patient specific medical devices using personalised moulds. Therefore, the requirement was that the moulding system be producible using AM technologies. Initial moulding systems were created to assess the viability of

different moulds for use with different mixing ratio of AW-to-PMMA. Figure 3.16 shows some of the different mould designs for used in this study.

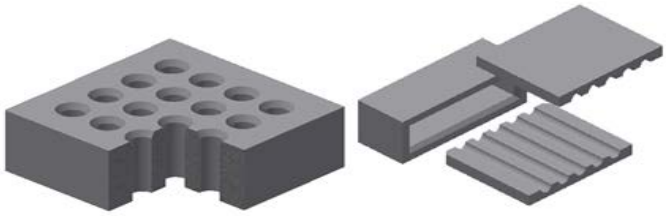

(a)

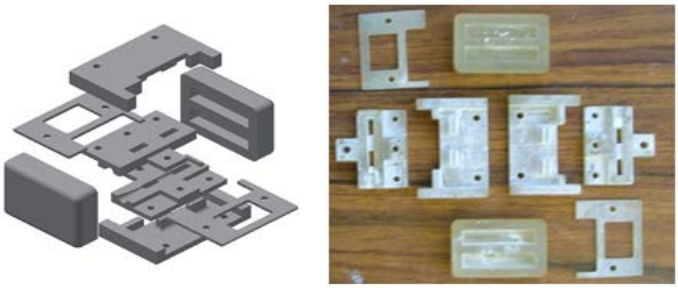

(b)

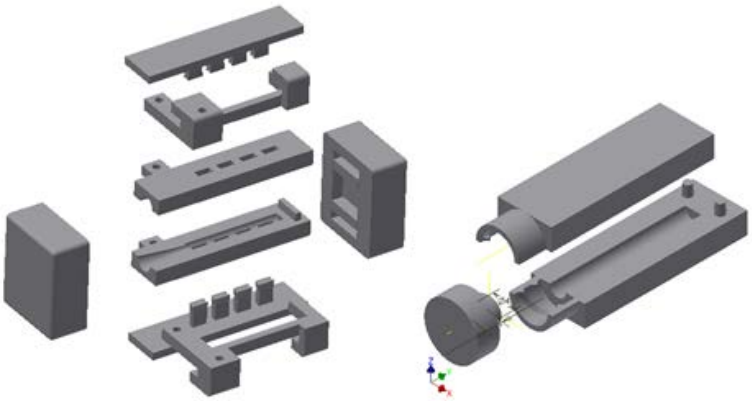

(c)

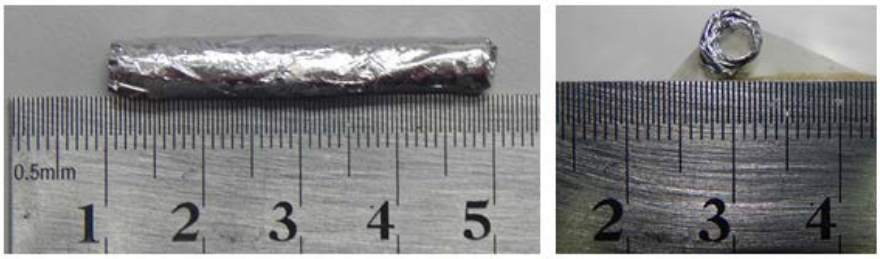

(d)

Figure 3.15 Different moulds designed to assess the viability for used in AW scaffold round specimens fabrication; (a) two different designs for aluminium block mould without ejector, (b) CAD design (left) and SLA mould (right)for moulding system with ejector, (c) alternative CAD designs and (d) simple Al sheet mould.

In total eight different moulding systems were proposed to produce samples rod for 1mm and 3mm diameter of 20mm in length. 5%, 10%, 15%, 20%, 25% and 30% by weight of PMMA were blended with AW respectively. Green parts were prepared from the blended powder by different moulding methods.

3.3.1 *SLA mould*

A moulding system was design to produce 3mm diameter cylindrical specimen with length of 25mm. It was created using Inventor 2009 (Autodesk, USA) software (Figure 3.16a, b and c). Once the design was verified, stl files were generated for each of the subcomponents in the moulding system. A service bureau (Paragon Rapid Technologies Ltd., UK) was used to print the stl files. The files were printed with Watershed XC material using 3D Systems SLA 250 machine (Figure 3.17a). The mould was filled with AW-PMMA mixture and placed in the oven at a maintained temperature of 145°C for 2 hours, before the heater was switched off, and the oven allowed cooling at its normal rate. Specimens produced from SLA mould were powdery up to the ratio of 15% PMMA. The ratio was further increased to 20% PMMA where bonding started, and specimen began to form but were not strong enough to be ejected using the ejector (Figure 3.17b). The specimens are not handleable even the ratio was increased to 25% as the strength of the specimens are too fragile. Furthermore, some of the green parts split into two and stuck to the wall of the mould as the bond in the green parts are not strong enough. No further investigation was carried out as this is looking into producing load-bearing parts for bone replacement.

(a) (b)

Figure 3.16 Greenpart inside (a) SLA mould, and (b) greenpart as removed from mould.

3.3.2 *Aluminium (Al) block mould*

Since the material used in fabricating the SLA mould has a low thermal conductivity (DSMSOMOS®), a better thermal conductive material was selected instead for a new design of the moulding system. In order to test the feasibility of the idea in using better thermal conductive material, aluminium block and sheet moulds were designed and tested.

The design of the block mould was made simpler (Figure 3.16a) to be fabricated. Aluminium block was used to fabricate the design as shown. The cylindrical cavities were drilled and bored to create a smooth surface. Pushpins of 3mm diameter were cut to the required length. The mould was filled with AW-PMMA mixture and underwent the same heating process for creating the green parts as before. The powder mixture was not able to consolidate for a ratio of up to 15%. The ratio of PMMA was increased up to 25% where the powder mixture consolidated and the green part was able to form in a cylindrical shape. A pushpin was used to release the green part from the mould. However, when the green part is pushed out from the mould individually, it broke into two or more pieces. The green part was not strong enough where it broke under its own weight (gravitational force) and from the friction between the green part surface and the mould surface that cause the bonding to break. This happened for both the design. In order to avoid this, a supporting structure needs to be placed underneath the green part, and friction be reduced.

3.3.3 *Aluminium shell mould*

Based on the concept of shell moulding, the design of moulding system was to use a thin sheet of material that conforms to the shape of the part. A steel rod of 3.2mm diameter was uses as the pattern to form multiple shell moulds. Instead of sand-resin mixture, aluminium foil was wrapped around the metal mandrel steel rod since the objective was to create cylindrical shape parts. Figure 3.18 shows the completed mould of diameter 3.0mm and length 40mm. The thickness of the aluminium foil was about 0.8mm to maintain shape and just flexible enough when unrolled to expose the green parts. Copper wire was then wound helically around the aluminium sheet mould before the mandrel was pulled out to create a shell mould. The cooper wire acted to support and heating-cooling mechanism to the aluminium sheet shell mould. The same procedure was used to generate the green parts as described in section 3.2.4. Green parts were successfully produced using this method for PMMA ratio of 20% upward. The green parts were later sintered under the heating profile as shown in Figure 3.6. in sub-section 3.2.5.

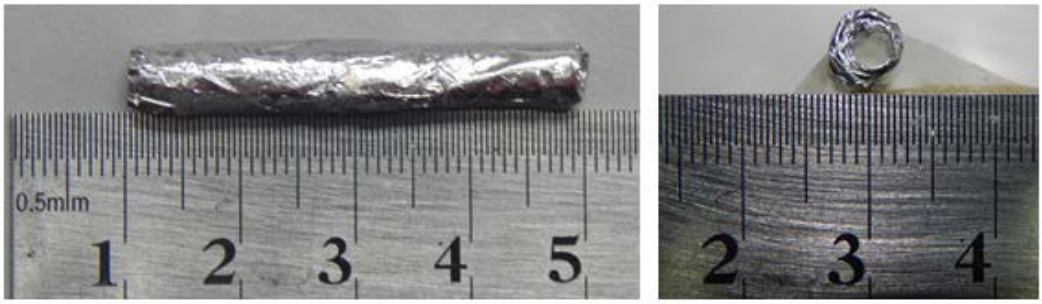

Figure 3.17 Simple rolled-up Aluminium sheet mould of diameter 3.0mm.

3.3.4 *FDM with aluminium sheet shell mould*

Based on the initial finding in section 3.2 and sub-section 3.3.3, development of a moulding system was started by designing the mould using CAD software. A simple design was created that used the concept of utilising aluminium foil that conforms to the shape of the cavity of the mould. Figure 3.19 show the CAD models of the moulds were designed using Autodesk Inventor2009.

The first design was a simple cavity mould, which produced cylindrical specimen. The mould was fabricated in ABS material using an FDM machine (BST Statrasys, USA). The designs of the mould were enlarged to compensate for the thickness of the aluminium foil used. The CAD model was later exported as an STL file for fused deposition fabrication. Design on the left (Figure 3.19(a)) was held together by end clamp while on the right (Figure 3.19(b)) was held by 4 M8 screws.

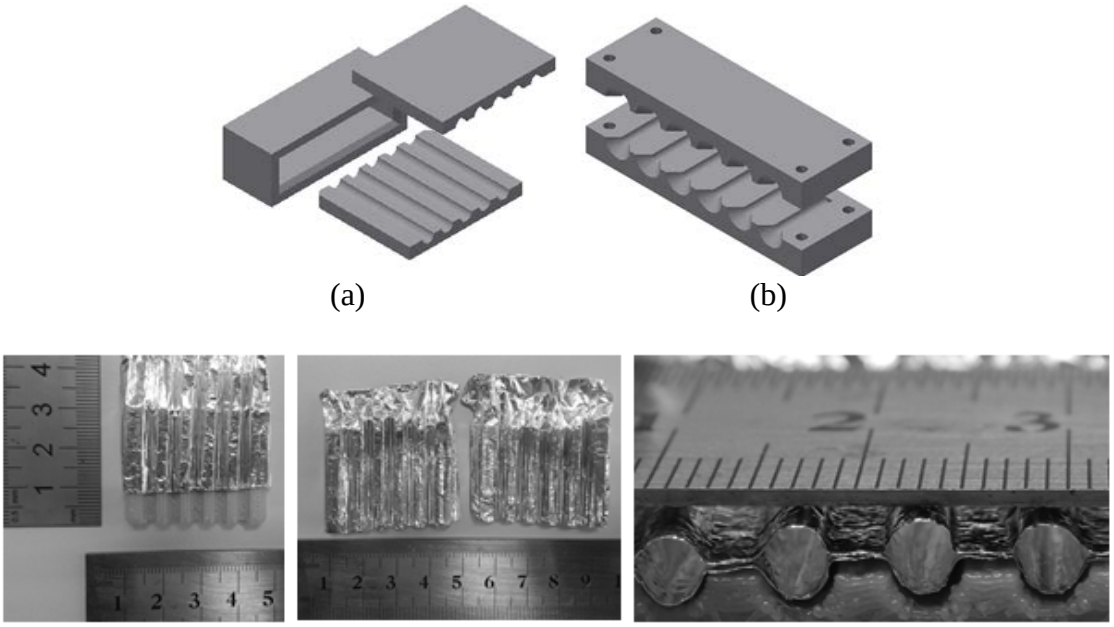

(a) (b)

(c)

Figure 3.18 Two designs of mould that use aluminium foil to ease removal of moulded part (a) 2-piece Al mould with end-cover (b) 2-piece mould incorporating end cover, and (c) Al sheet on the fabricated mould with top view and assembled front view.

3.3.4.1 **Fabrication Process**

The mould was prepared by placing aluminium foil across the mould cavity of 4.0mm in diameter with length of 30mm and rods of 3.2mm were used to indent the aluminium foil such that the foil will conformed to the mould cavity. Mould release agent was sprayed onto the foil. Once in place, the assembly was held together by clamping force. Preheated AW-PMMA mixture was gravity fed into the mould using a funnel of 2mm diameter opening. Light tapping was applied on the funnel to loosen up the powder mixture such that it flows into the mould. Then, a small rod of diameter 3mm was used to compact the mixture in the cavity. The completed assembly was later placed in the oven according to the setup as described in sub-section 3.2.4 to solidify the PMMA particles and bound the AW powder. The outcome from this setup was not as promising as using the setup where the aluminium foil was completely exposed to heating (refer sub-section 3.2.4 and 3.3.3). Therefore, the duration of heating time was increase substantially such that the heat can penetrate the mould assembly and reached the powder mixture. This produced favourable improvement to the green parts but at the expense of a longer time. Since ABS has low thermal conductivity, the ABS mould by FDM takes a longer heating time to penetrate the mould assembly. Therefore,

in order to reduce the time, different alternative of heating process are needed such as microwave heating. This is discussed as future work in section 7.2.

3.3.5 *Different moulding system outcome*

The outcome from the different moulding systems for the AW-PMMA powder mixture ratios was as shown in Table 3.10. In all three moulding system used, the mould made with aluminium sheet look the most promising, as it can produce green parts with the lowest percentage of PMMA.

A weight ratio of 80% AW to 20% PMMA was selected as this ratio provides handleable green parts without breaking when remove from aluminium sheet mould. However, cares are taken when handling the green parts as they broke easily.

Table 3.8 Samples of different AW-PMMA ratio tested on different mould.

Sample	Percentage by weight Ratio of AW-PMMA		Mould used			Result
	AW (%)	PMMA (%)	SLA Watershed XC Clear (X)	Aluminium Block (Y)	Aluminium Sheet (Z)	
APM1	95	5	Powdery	Not tested	Not tested	APM1 was not used as parts were not formed.
APM2	90	10	Powdery	Not tested	Not tested	APM2 was not used as parts were not formed.
APM3	85	15	Partially bond. Broke when removed from the mould	Partially bond. Broke when removed from the mould	Partially bond. Broke when removed from the mould	APM3 was not used as parts cannot be handled.

APM4	80	20	Broke when removed from the mould	Broke when removed from the mould	Handleable, with care, a few samples broke when transferring to sintering oven.	APM4-Z was able to produce handleable parts.
APM5	75	25	Broke when removed from the mould	Broke into two pieces when removed from the mould	Handleable, gently	APM5-Z was able to produce handleable parts.
APM6	70	30	Not tested	Not tested	Handleable, gently	APM6-Z was able to produce handleable parts.

Based on the outcome as shown in Table 3.9 and Figure 3.17, the route to create AW specimens was to use aluminium sheet mould with a powder mixture ratio of 80%wt. AW to 20% wt. PMMA even though it is not ideal. In this research, the need is to determine the lowest possible mixing ratio of AW-to-PMMA to be used in the fabrication where the required length to be cut from the possible length of 25mm of the sintered specimens is 3mm for used in TE study. However, for this research a powder mixture ratio of 70%wt. AW to 30% wt. PMMA was selected as this is more ideal and stable for fabrication of implants and implants by 3DP.

3.4 Case Study

A specific case study was developed to gauge the feasibility of using the FDM pattern with aluminium sheet to produce shell mould for the fabrication of a customised complex part.

3.4.1 *Specific Case Study Background*

Bone defects cause by congenital deficiencies, cancer resections, and traumas are often reconstructed using the autografts and allografts procedure. In the reconstruction in en bloc resection of mandible, it has always been a challenge for surgeons and patients. Although the procedures of bone grafting are used in bone repairs, there are concerns of invasive bone collection from healthy sites, discomfort and morbidity to donor site, limited material from donor site, the need of further surgery, the risk of transmitted disease, and social or religious

refusal in some regions in the world (Schlickewei and Schlickewei, 2007, Schmitz, 2005, Silber et al., 2003, St John, 2003). Furthermore, the process of grafting aesthetical and precise bone to fit the deformity is time-consuming and laborious. In addition, fixation fails are caused by a number of mechanisms that include insufficient amount of fixation, fracture of the plate, loosening of the screws, and devitalisation of bone around screws (Cienfuegos et al., 2008). It has been reported that with the use of rigid reconstruction plate to reconstruct a large mandibular defect in patients who do not have bone grafts following tumour excision, the frequency of a plate fracture to be 2.9% to 10.7% (Martola et al., 2007, Shibahara et al., 2002, Freitag et al., 1991). This couple with the fact of complications during surgical attachment of the reconstruction plate (Kim and Park, 2007). In order to overcome these limitations, artificial bone substitutes are seen as the logical choice since they are non-invasive and free from contamination. In this particular case study, the approach to the reconstruction of the whole resected mandible is by integrating DFMA methodology and AM technologies in the design and fabrication of the implants. In this section, the design and AM customised prosthesis for restoration of continuity and stability in the mandible were described.

3.4.2 *Design and AM manufacturing of Implant Moulding System*

In the design and fabrication of the implant, concerning factors that need to be overcome are to engineer anatomically correct pieces of viable and functional implant for bone reconstructions and to attach the implant with ease. Normally most of the fixation methods for mandibular reconstruction and fracture system consist of drill bits, plate bending forceps, plate holding forceps, plate cutters, cannulas, taps, countersinks, plate bending pliers, plate cutters, drill guides and screwdrivers to facilitate the placement of screws and modification of plates. The implant for reconstruction is secured in place by plate and screw (Figure 3.20a). Hence, by benefiting from the geometrical freedom allowed in AM and the DFMA methodology, the implant was design to integrates the fixation method into the implant such that it is able to be attach to the mandible without the need of plate and screw (Figure 3.20b).

A lower jaw bone model in STL format was imported to the CAD software for design of the implant. The lower jaw is non-defective and was obtained from a secondary source (3DSystems). A simulated defective section was created on the jaw by cutting a section of it using CAD software (Figure 3.18b).

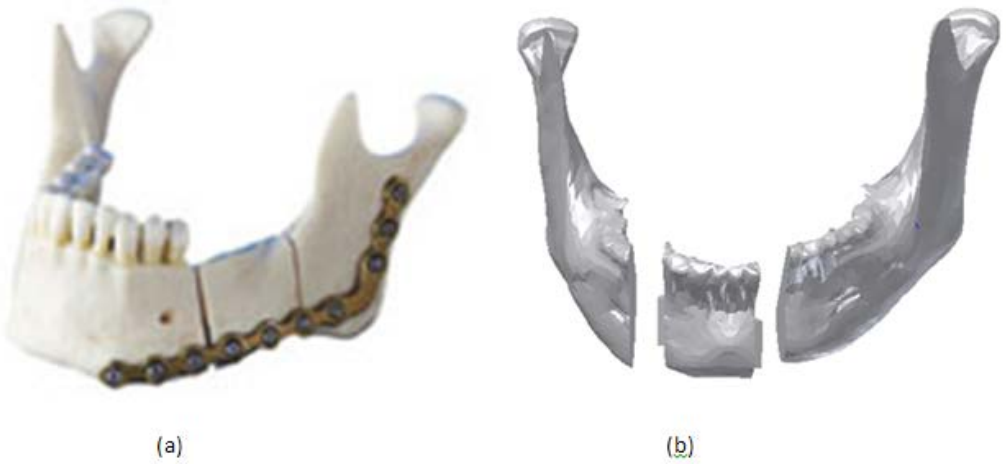

Figure 3.19 (a) Conventional implant fixation method. (b) A section cut-out for implant with slotted joint.

3.4.3 *DFMA methodology in design of mandible implant*

As has been mentioned earlier, the fixation of the implant to the resected mandible required considerable amount of parts, tools and assembly steps. By reducing the amount of parts, tools and assembly steps, the operational cost can be kept to minimal. The typical cost for ORIF mandibular fracture fixation management per person is £34,636 in UK (Schmidt et al., 2000) and increasing from USD26,089 to USD35,804 in USA (Pena et al., Shetty et al., 2008). Thus by incorporating AM technology in the design stage of fixation devices, the assembly steps can be reduced which can lead to overall cost reduction for fracture fixation management. The reduction of the part count and the possibility to even reduce the number of parts in an assembly to one is doable using AM as AM geometric freedom allows the designer to consolidate parts in ways that have previously been impossible (Mansour and Hague, 2003).By using the DFMA methodology, some of the parts and assembly steps can be reduced. The recommendations by Boothroyd (Boothroyd, 1994) are as outlined: -

a) Is it necessary for parts to have a relative movement between them?

b) Is it necessary to have different materials specification for physical or chemical reasons or both?

c) Must the component be dismountable to facilitate the maintenance?

Based on the consideration as set in the DFMA rules, the part count in attaching the implant was reduced to one as relative motion is not required between parts where only a single

material is used and is bioactive. Thereby eliminating the need to remove the implant fixators as the implant fixation can be achieved through biological and bioactive fixation methods.

3.4.4 *Design of Implants for mandible reconstruction*

A 3D computer model in stereolithography (stl) format of a mandible was obtained from 3D Systems. This model was imported to CAD modeller Autodesk Inventor2009 (using StlImport software add-on from Sycode). A section of the mandible was selected to be a representative geometry for a small implant. Based on the outcome from DFMA guidelines, some simple features were added to the model to illustrate how location and fixation could be achieved (see Figure 3.21a.) for the implant (Khan, 2010). The model was then used to generate a multipart mould model (see Figure 3.21b). The CAD model of the mould was translated into STL format and imported into Statrasys Dimension SST768 fused deposition machine. CatalystEX software was used to implement some corresponding preparations on the STL model such as checking the model water-tightness, build orientation and supports before the final file was sent to be processed into a CMB file that was sent to the Dimension printer for printing the part. A layer thickness of 0.33mm was selected, and commercial ABS plastic was used during the fabrication of the mould as shown in Figure 3.21c.

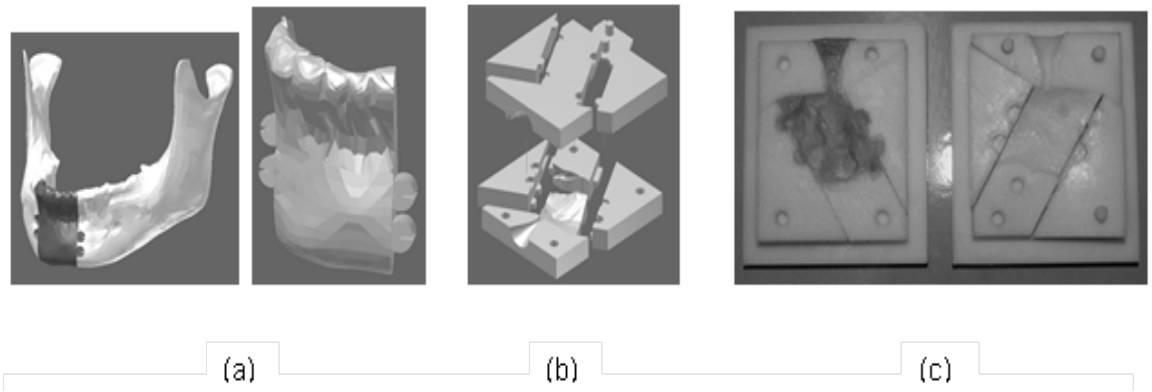

Figure 3.20 (a) CAD implants model, (b) CAD multiple parts mould of implants and (c) FDM fabricated mould with one-half of the mould filled with modelling wax as used in LWC.

3.4.5 *Fabrication and Attachment of Implants for mandible reconstruction*

Using the same procedure as described in sub-section 3.2.4 and sub- section 3.3.4, the FDM mould cavities were then layered with aluminium foil of 0.8mm thick. The foil was then pressed to conform to the shape of the cavity (Figure 3.22). When both halves of the mould

are prepared with aluminium foil, the mould is closed and clamped. Preheated AW-PMMA powders were poured into the mould and were pressed manually with rod. The prepared assembly was then placed in the oven to bind the mixture in producing the green part. The green part was removed from the oven and placed in a sintering furnace.

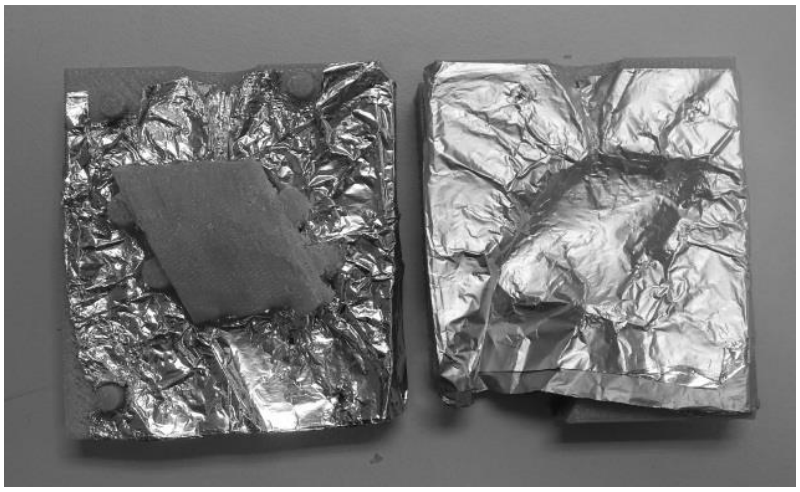

Figure 3.21 Aluminium foil as pressed into the cavity of the AM mould.

The result is not favourable as shown in Figure 3.23. This can be because the green parts of the AW-PMMA powder mixture were not fully compacted inside the mould, and air is still trapped in the mixture. When sintering is performed, this created crack in the implant. Furthermore, heat was not evenly distributed as the mould is of uneven thickness and undercuts. No further investigation was carried out using this moulding technique.

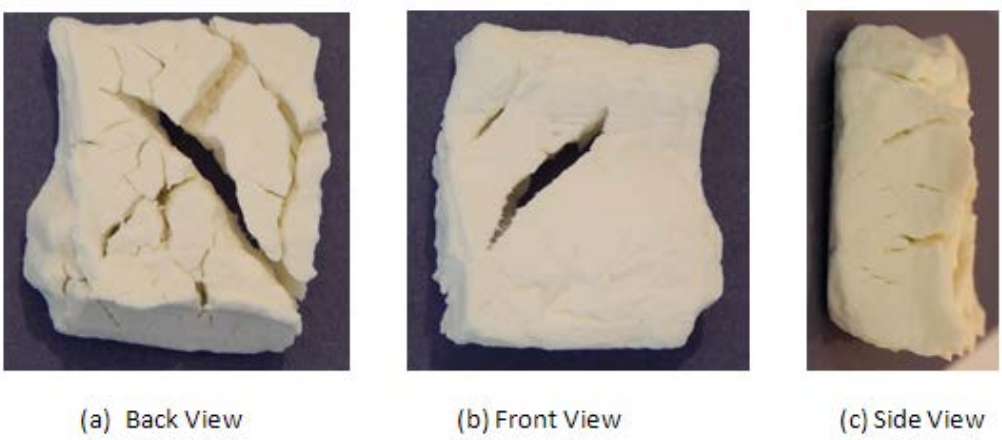

Figure 3.22 Sintered AW implant from green part of implant produced from FDM mould with Al sheet shell mould.

The mould was redesigned with multiple holes (Figure 3.24b) to allow heat to reach the AW-PMMA powder mixture and thus, reduce the heating time. However, the outcome is still the same. Cracks were still prevalent during sintering as the powder was not being compacted properly, and air is still trapped within the powder especially at the undercut and at the joint region. No further work was performed to ensure that the powder was compacted fully as this will increase the cost and processing time.

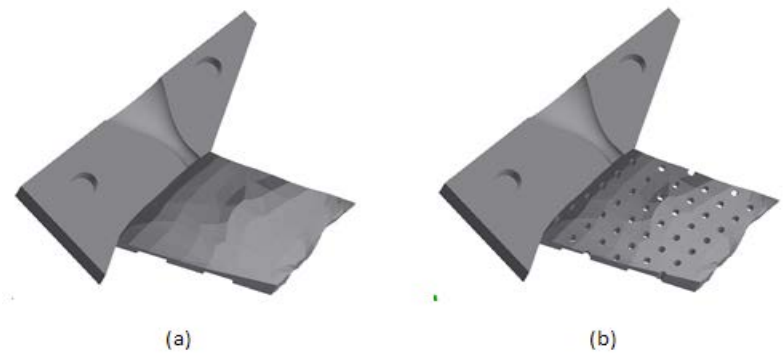

Figure 3.23 (a) Initial design and (b) redesign for better heat penetration.

3.4.6 *Integration Indirect AM and lost wax process.*

Another alternative to shell moulding technique is by lost wax casting (LWC). Lost wax process (investment casting) and shell moulding share some similarities in the mould design and process. In lost wax process, a refractory slurry flows around the wax pattern to create the mould whereas, in shell moulding; resin-bonded silica sand is placed onto a heated pattern, forming shell-like mould halves. In this approach, two methods of indirect AM were proposed. The first method is indirect tooling by creating a mould for generating wax model while the second method is by using AM part as a master pattern for creating soft tooling to produce wax models.

3.4.7 *AM Indirect tooling.*

Indirect tooling is an extension of AM technologies in producing a mould. Indirect tooling incorporates pattern-based methods in which the tool is cast from an AM artefact that represents the part to be moulded. By AM indirect tooling method, mould was fabricated using AM technologies in order to produce sacrificial models to be used in lost wax casting process. This is known as Rapid Tooling (RT). A 3D model of the mould was created using Autodesk Inventor2009 as described previously in sub-section 3.4.2. Since the design of the mould is the same, the FDM mould from sub-section 3.4.4 was reused to produce wax models

of the implant. The cavities of the mould were filled with modelling wax in which sacrificial pattern is generated. Scopas Yellow Modelling Wax Type B (Alec Tiranti Ltd., Berkshire, UK) was manually worked into the cavities of each half of the mould (see Figure 3.21c) as it softens during the moulding process. Petroleum jelly was applied to the mould cavities prior to filling the cavities with wax for ease of demoulding. A complete wax model of the implant was achieved by joining the two halves. The wax model with gating was then suspended in a container. Cerrostone plaster (Special Plasters Ltd., Birmingham) was prepared by mixing with water and was poured over the wax model pattern. This was left overnight to set. The wax pattern in the mould was then melted out by inverting the mould and heated to 90ºC in the oven. Powder mixture of 80wt% of 53-90μm AW (Glass Technology Services, Sheffield) and 20wt% of 4-8 μm PMMA (Ganzpearl GM-0600) was used to fill the cavity generated in the hardened plaster mould. The powder was preheated to 120ºC for 60 minute to dry it. This allowed it flow freely into the mould cavity. The powder was compacted using vibration and pressure (applied using an aluminium rod). This assembly was heated using the same heating profile used as for the cylindrical rods. At the end of the furnace cycle, the cast was soaked in water to soften the plaster, and a small hammer was used to crack the plaster and expose the fabricated implant. Figure 3.25 shows a comparison between the FDM, the wax model and the fabricated AW part and several of the implants as produced from this method. There is a slight variation on the AW part due to shrinkage as well as small cracks. With further fabrications by adjusting the powder packing, some improvements were noted on the parts in term of reducing crack, and the geometrical shape is near to the model geometry. This result is better than the outcome as describe in section 3.4.5.

A flow chart of the entire process flow in obtaining the customised AW implants is summarised Figure 3.26. With this method the cost is kept low as the total materials cost for the fabrication components; the FDM mould (£260.15, cost for material and 14hours printing time), modelling wax (£16/kg, 1 hours) and Cerrostone plaster (£11/25kg, overnight), amounted to less than £270.00 as the wax and plaster had only minimal cost contribution. The total hours spend in this process was 15hours and overnight for plaster to set. The cost of using this approach (Rapid Tooling approach) is as shown in Table 3.11.

FDM model Wax Model Sintered AW

(a)

(b)

Figure 3.24 (a) Show Comparison between FDM model (left) with a wax model (middle) and AW part, while (b) show the outcome of several AW parts that were produced. Some improvements were noted on the parts in term of reducing crack, and the geometrical shape is near to the model geometry.

Table 3.9 Materials cost for fabricating a unit of AM indirect tooling.

Component	Material Price/ unit	Time	Amount used
FDM Mould	£260.15	*14hours (cost of printing time is inclusive in the material price/unit)	£260.15
Modelling Wax	£16/kg (kit)	1 hours (preparation, and setting)	£4.00 (Less than a quarter of kit)
Cerrostone Plaster	£11/25kg	overnight	£0.50 (minimal)
	Total	15 hours + overnight	Less than £264.55

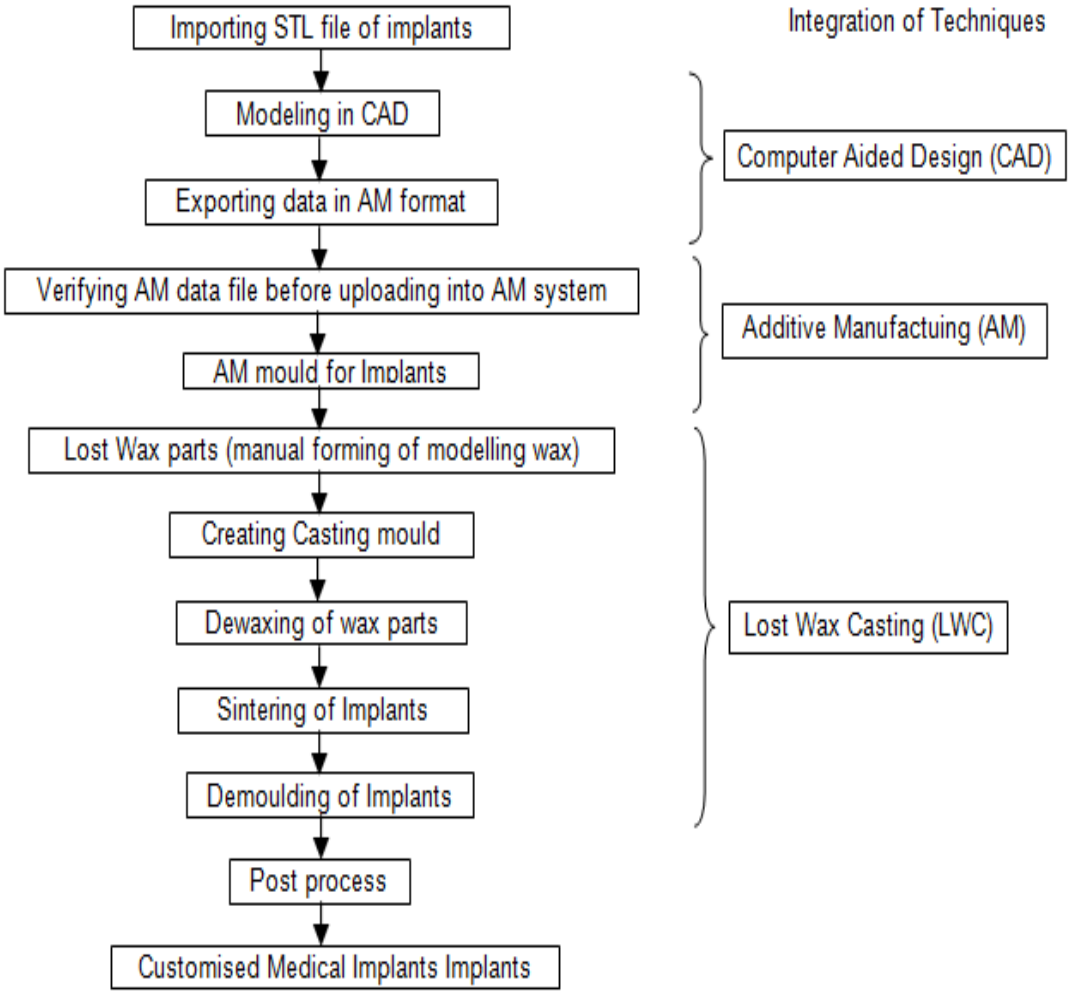

Figure 3.25 Processing flow in indirect fabrication of customised AW medical implants.

3.4.8 *AM in soft tooling*

In this second approach of indirect tooling, a master pattern of the implant was generated for used in creating the soft tooling. A master pattern was modelled using CAD software as describe in section 3.4.4. and the detailed steps as described in appendix C3. The implant's CAD model was 3D printed using FDM. Permanent dark coloured ink is used to create parting lines. The parting lines were drawn onto the master pattern as a guide when splitting the mould into two halves. The FDM master pattern was affixed with modelling wax gating. The assembly was then placed in the centre of the moulding box by attaching the end of the gating to the bottom of the box. A 1:1 by weight mixing ratio of a two parts translucent silicone RTV moulding compound was prepared (Addition Cure 33 Silicone Rubber, Alec Tiranti Ltd., Berkshire, UK). Mixing and degassing of the mixture need to be completed within a 20 minutes time frame. Vacuum was applied to remove air bubbles from the moulding compound prior to pouring and after pouring as air trapped will cause defects. The mixture was then poured over the pattern and filled the moulding box (Figure 3.27(a)). This was left to cure for 4 hours. The hardened soft RTV mould was split along the parting lines using scalpel knife. Figure 3.27(b) show the RTV mould. Based on the parting line, non-uniform corrugated splitting surface/plane was created to ease in the assembly of the mould. This will only allow a single mating plane, thus saving time when assembling the mould.

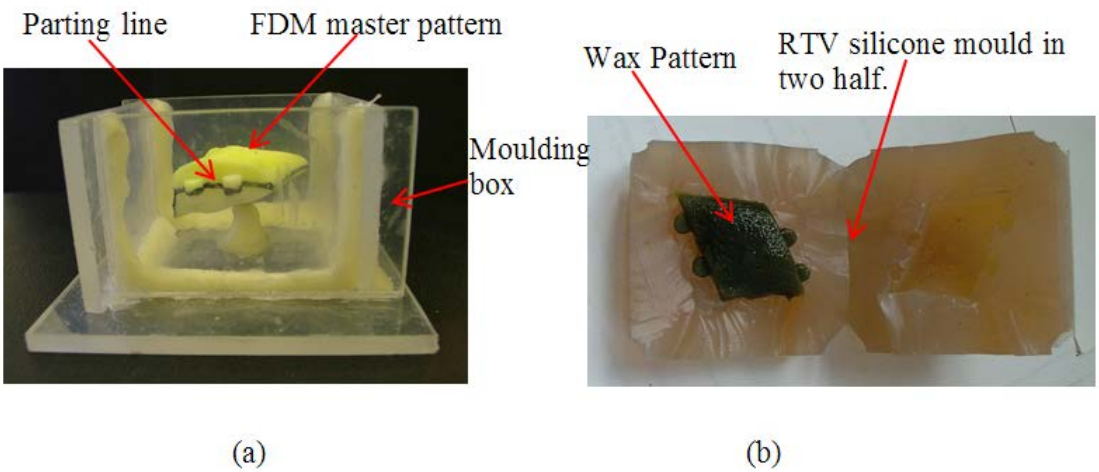

Figure 3.26 (a) Preparation for soft tooling moulding with FDM master pattern and (b) wax pattern as duplicated from RTV silicone mould of the FDM master pattern.

The RTV mould was then used to obtain the wax model (Figure 3.28a). The model produced was able to capture all the features of the master pattern with a slight deviation to the surface

near the inlet (Figure 3.28b). The investment casting or lost wax casting (LWC) process was the applied to obtain the AW implant. Figure 3.29 shows the process flow and sequence in obtaining the AW implant. The diagram depicted the integration of using both AM with LWC as an indirect method in fabricating bioceramic implants. The total cost of this approach amounted to £38 as shown in Table 3.12.

Table 3.10 Materials cost for fabricating a unit of AM soft tooling.

Component	Material Price/ unit	Time	Amount used
Master Pattern	£11.73	12hours (printing time)	£11.73
Translucent Silicone RTV mould	£32/kg (kit)	6 hours (preparation, setting time and post-process)	£15 (Less than half the kit amount)
Green Casting Wax (Paraffin Wax) pattern	£12/kg	1 hour (less than)	£0.35 (minimal)
Cerrostone Plaster	£11/25kg	overnight	(minimal)
	Total	19 hours + overnight	Less than £38

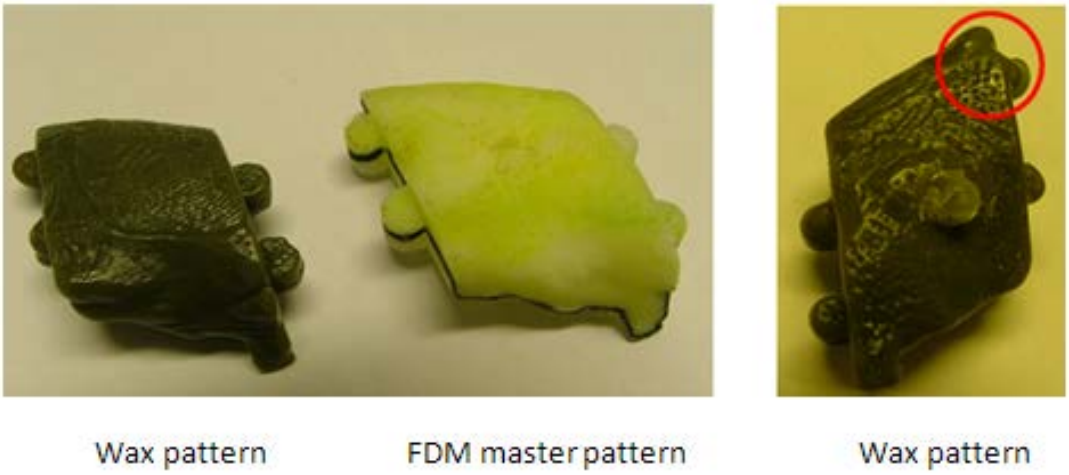

(a) (b)

Figure 3.27 (a) Wax model (left) obtained from RTV silicone moulding process comparing to the FDM master pattern (b) minor deviation of features.

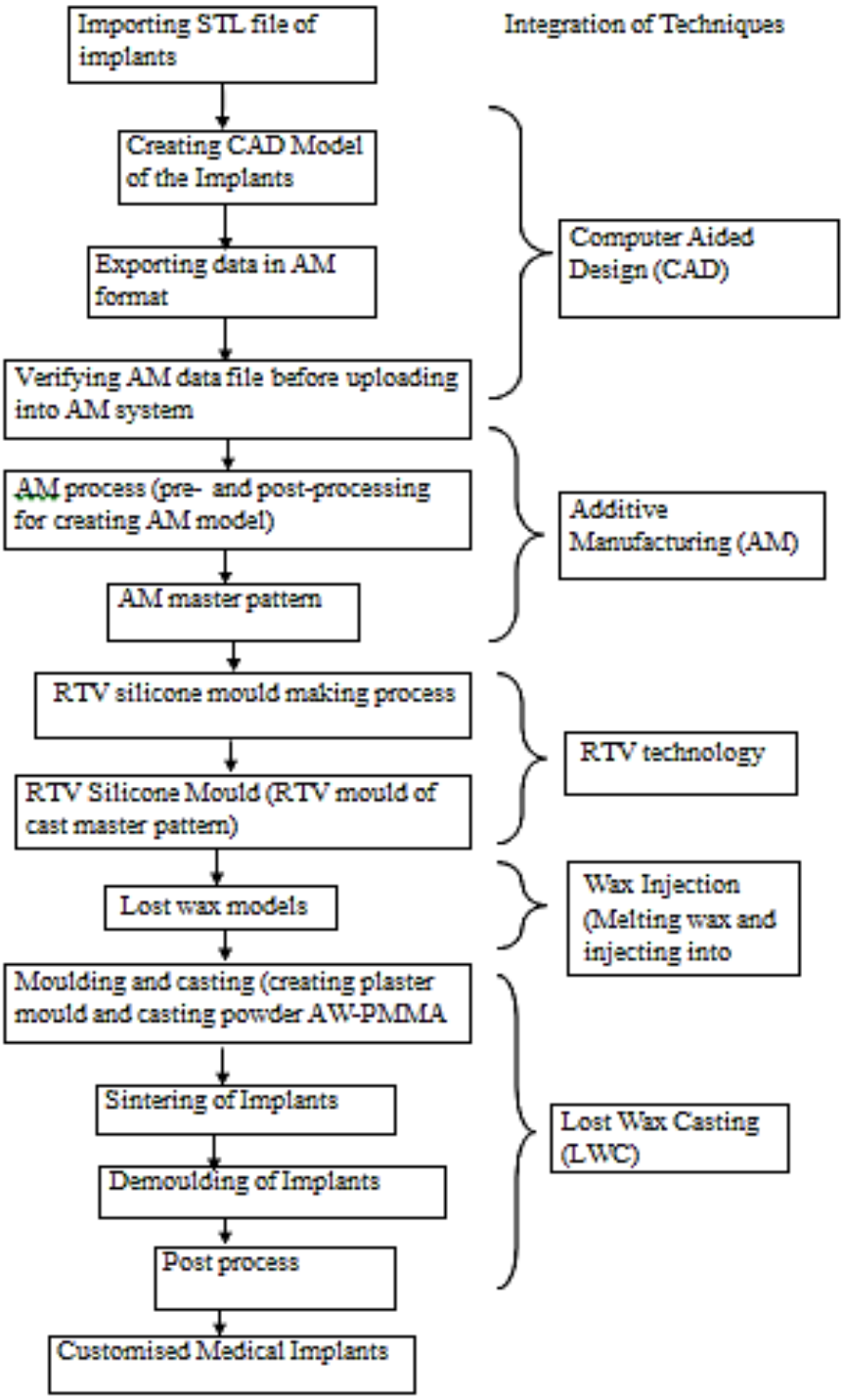

Figure 3.28 Processing flow in fabricating customised AW medical implants by indirect AM with the integration of RTV silicone mould and LWC process.

3.5 Discussion

The flexural strength obtained from both batches of sintered AWGC was compared with flexural strength of human bone. The average Young's modulus is 23.51GPa±4.06 for batch 1 and 26.65GPa±3.77 for batch 2 as fabricated using the Aluminium foil mould. Table 3.13 shows the value of AW-GC, cortical bone and cancellous bone. As evident from the table, AWGC can be used for BGS either as scaffolds or large bone defect replacement. In addition, the processing route of integrating AM with LWC in the fabrication of AWGC artefacts does not affect the compound composition in any way as this was shown from results of similar crystallisation diffraction patterns of AW phase in XRD analysis.

Table 3. 11 Mechanical Properties of Natural bone and bioceramics.

	Young' Modulus GPa	Flexural Strength MPa
Cortical bone	3.8 – 11.7	82 – 114 (tensile)
Cancellous bone	0.2 – 0.5	10 – 20 (tensile)
Cerabone AW	118	215 (bending)
Fabricated AW with 26.9% porosity	23.51 – 26.65	63.83 – 76.45 (bending)

3.5.1 *Comparison of AM in indirect tooling and soft tooling*

Based on the two methods in producing the AW implants, main differences can be attributed to the fabrication of the wax model and the CAD model. The overall cost and time in fabricating the implants are influenced by CAD modelling time, FDM parts cost and wax model fabrication time and cost. The total time and cost for producing the FDM indirect tooling was 15hours and £270 respectively as compared to RTV soft tooling of 19hours and £38. Figure 3.30 shows a comparison between the wax model from indirect tooling and soft tooling. The wax model produced by RTV silicone moulding was able to capture the geometrical feature of the master pattern as compared to indirect tooling. However, in the fabricated implants both have sign of defects in which was caused by uneven packing of the powder mixture inside the casting mould. In sintering ceramics, defects are shown to be

influenced by the powder compaction process (Shinohara et al., 1999) in which potential fracture origins were formed in green bodies through the dimple in the powder granules, inadequate cohesion of the granules and the large grains developed from large particles in the green body.

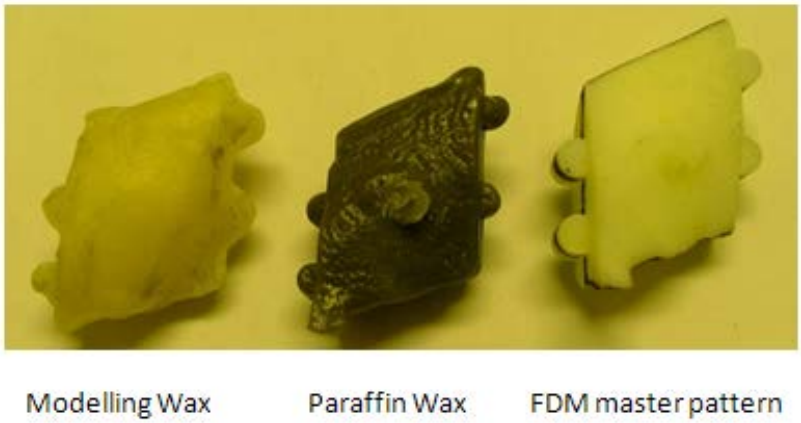

Figure 3.29 Comparison of the wax model with FDM model. Model from modelling wax showing higher loss definition of the feature as compared to the wax model from RTV soft tooling.

The RTV silicone mould method was able to produce implant close to the master FDM pattern as shown in figure 3.30.This approach can be adapted as a low cost method to fabricate patient specific implant as the use of RTV moulding had also been demonstrated to be favourable in other research for the fabrication of gas turbine blade (Vaezi et al., 2011) and femoral prosthesis (Ramos and Simoes, 2009). Furthermore, the accuracy of the wax patterns produced are high as reported by Rahmati et al. (Rahmati et al., 2007) and Yarlagadda et al. (Yarlagadda and Hock, 2003).

3.6 Conclusions

The integration of low cost conventional manufacturing with AM and CAD technologies can be approach as an alternative method to create bioceramic BGS Indirect AM tooling route, utilising lost wax casting and sintering techniques allowed AWGC medical implants to be fabricated. This approach can keep the fabrication cost low and yet still be able to capture the intended design geometry closely. The processing route did not change the composition of AWGC and porosity was evidence in the implants. The porosity level and bending strength of the parts produced was similar to that of cortical bone, but increased macroporosity and inter-

connected channels would need to be designed into the structure in order to optimise cell propagation and bone growth.

Table 3.12 Comparison between indirect tooling and soft tooling in indirect AM for processing bioceramic.

	Rapid tooling	Soft tooling
Number of CAD model	9	1
FDM parts fabrication	9	1
Additional process	No	RTV moulding process
Wax model fabrication	1	1
Time	15 hours+ overnight	19 hours + overnight
Cost	£270.00	Less than £38
Closeness to actual designed shape.	Medium	High

Comparing both indirect AM methods (using AM mould and master pattern, Table 3.13), the overall cost is significantly lower than using direct AM methods for fabricating large customised bone implants or BGS. However, there is a compromise of using indirect AM methods in term of time as the time will increase due to the additional steps taken and the use of manual labour. In addition, if simple shape scaffolds of small size are required, then the aluminium foil sheet moulding method will be more economical as the materials cost the mould amounted to less than £2.

Chapter 4: 3D Printing of bioceramics powder

4.1 Introduction

This chapter describes a process for fabricating implants using indirect three dimensional printing (3DP). An AW powder mixture is developed in this study of the printing process. Characterisation was performed on the powder mixture bondability prior to use in a commercial 3D Printer machine. Morphology analysis and mechanical testing were performed to study the characteristics of the printed artefacts. Artefacts were designed and manufactured to evaluate the capabilities of the process.

4.2 Materials and Methods

A list of materials and equipment used in this study is as shown Table 4.1.

Table 4.1 List of equipment used in the study.

Item	Description	Purpose
Materials		
AW, Sheffield Glass Ltd., UK	Powder in particle sizes of 120μm and below	Built material for Specimen and Implant
Maltodextrine, Sigma-Aldrich, UK.	53μm particles	Binding agent
Polyvinylpyrolidone (PVP);(Kollidon90), BASF	53μm particles	Binding agent
Fine sugar, Tate UK	On the shelf grade	Binding agent
Darvan C-N, Lake Chemicals and Minerals Ltd., UK.	Liquid	Surfactant
Alcohol (Ethanol), Fisher Scientific, UK.	Absolute (200 proof) and molecular biology grade	Reagent
Equipment		
Sieve shaker	Adjustable speed vibrating shaker with timer control.	Vibrate powder
Stainless steel sieve mesh, Fisher Scientific, UK.	Mesh sizes of 90μm, 53μm and 20μm.	Particles separation

Planetary ball mill with ceramic jar and balls, Pascall L9FS	Constant rotational speed ball mill.	Particles reduction of AW.
Aluminium 'V' mixer	In-house fabricated mixer.	Mixing of AW and binding agent powder mixture.
Carbolite furnace	Programmable furnace of up to 1600°C.	Sintering of AW
Motic microscopes with Motic Images Plus 2.0 software	Window XP compatible software	Measurement and surface images
Cambridge Stereoscan 240 SEM machine, UK	-	Morphological analysis of materials
Instron 5567 universal testing machine with Bluehill Software, Instron UK	Bench top Universal testing machine with low load cell.	Mechanical testing of specimens

4.2.1 *Process*

The raw materials used in this study were prepared according to the procedure as shown in figure 4.2. The AW powders obtained from the supplier were placed inside a ceramic jar to be milled to finer particles sizes using a planetary ball mill ball. Planetary dry ball mill (Pascall L9FS) was used to obtain different particles size of AW (Figure 4.1). Ceramic jar of 1000ml volume with a mixture of 6mm and 9mm diameter ceramic balls charge were used. The AW powders were ball milled for 4 hours at an operational jar speed of 85rpm. A sieve shaker with sieves of mesh 90μm, 53μm and 20μm was used to sieved the milled AW into four different sizes of above 90μm, 53μm to 90μm, 20μm to 53μm, and below 20μm. The milling was conducted under the setting conditions of the critical speed and time of milling. The calculation of critical milling speed and operational speed is calculated from equation 4.1 and 4.2 as shown below,

$$\nu = \frac{\pi}{2} * \sqrt{\frac{g}{R-r}} \qquad \text{rpm}$$

$$\nu = \frac{29.9}{\sqrt{R}} \quad \text{rpm} \qquad (4.1)$$

where

ν=critical speed (rpm),

R= radius of ball mill (i.e. jar inner diameter) (m), and

r= radius of ball (m)

g=9.81m/s^2.

Operational speed = 50% to 75% of critical speed (4.2)

For optimal efficiency in milling, the jar was filled with 50% volume of ball charge and 20% volume of AW powder. The amount of material charge and numbers of ceramic ball charge used were determined from the planetary ball mill manual using equation 4.3 and equation 4.4 in order to achieve maximum efficiency in the milling process.

$$\text{Material charge} = \frac{1}{2} norminal\ capacity\ of\ jar * density\ of\ material \qquad (4.3)$$

Figure 4.1 Ball mill machine that was used in the milling process of AW powders.

A ‘V’ mixer was used to prepare the powder mixture. The inside surface of the ‘V’ mixer was cleaned with alcohol-based solvent and purged with compress air. A lathe machine was used to rotate the ‘V’ mixer at a speed of 120rpm for 60minute for mixing of the powder mixture. The mixtures were evaluated against a set of different binder solutions. Based on the outcome, a Z-Corp 3DP was later used to 3D print artefacts using the selected combination of powder

binder and binder solution. Green parts produced were then sintered, and the material characteristics and mechanical properties were evaluated.

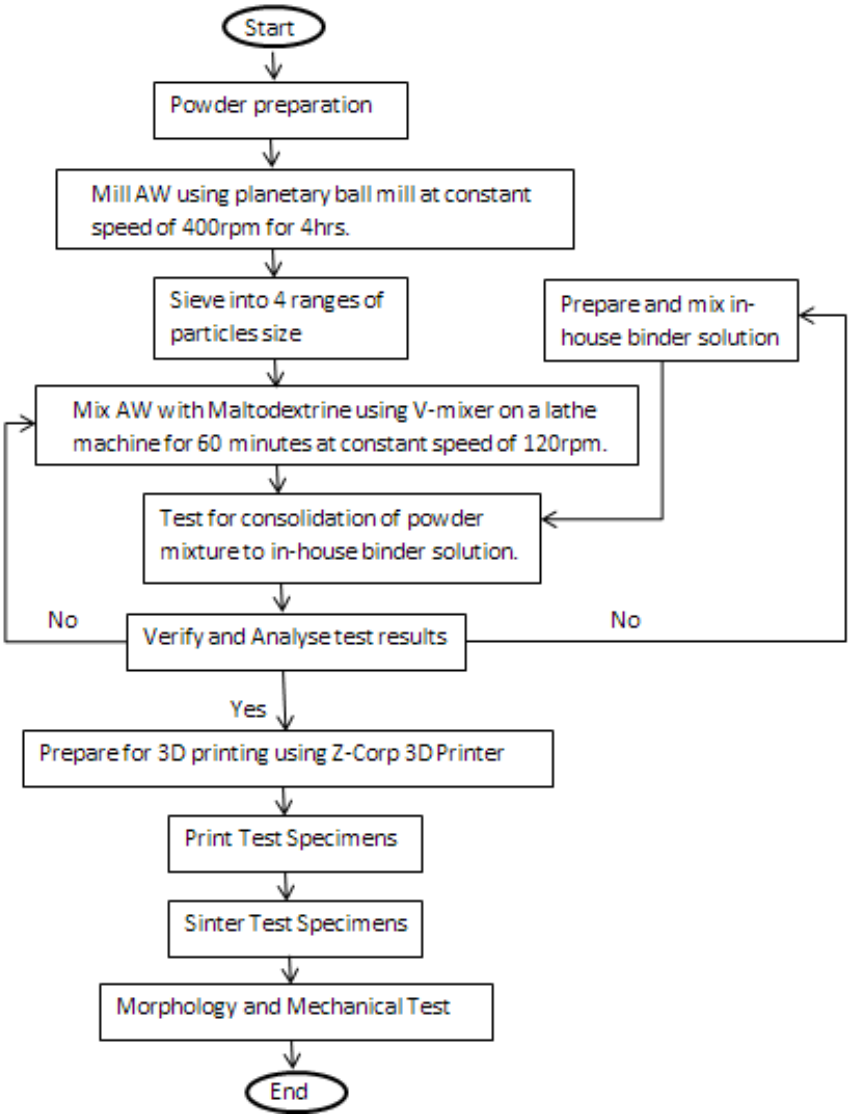

Figure 4.2 Process Flow and Characterisation of AW powder mixture.

4.2.2 *Materials*

The AW powders supplied by Sheffield Glass Ltd., UK in different batches were used as is. The chemical composition of AW powders supplied were assumed to be comparable to Kokubo's formula of 4.6% MgO, 44.7% CaO, 34.0% SiO_2, 16.2% P_2O_5, and 0.5% CaF_2, (Kokubo, 1991b). Figure 4.3a shows the particles of AW 53µm -90µm and maltodextrine below 53µm as received. Most of the particles in AW were 53µm and below with few in the

90μm range. In Figure 4.3b, particles were round and made up of mostly 20μm to 30μm size particles although some of the maltodextrine particles were melted during SEM analysis.

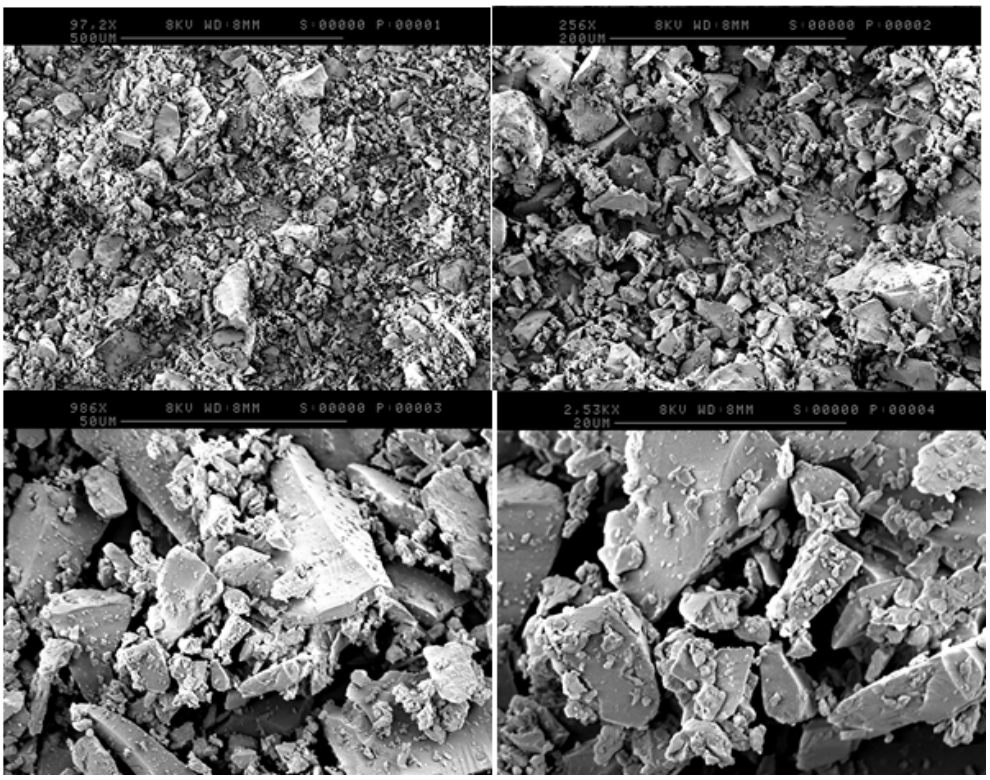

(a)

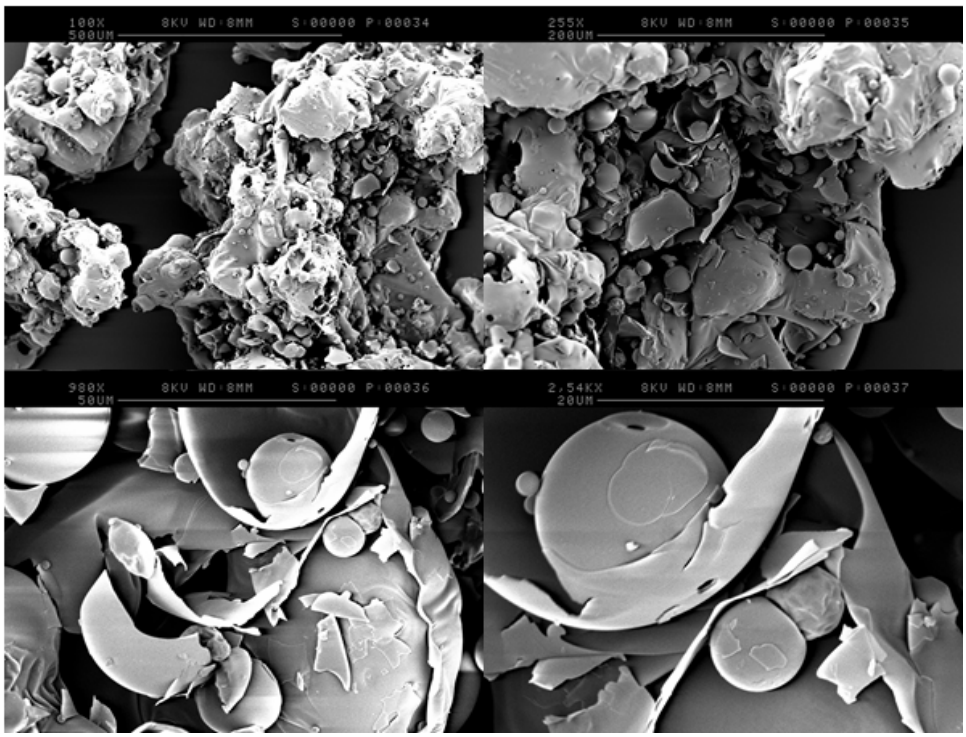

(b)

Figure 4.3 Particles of AW 53μm -90μm and maltodextrine below 53mm as received..

4.2.3 *Powder Blending*

Three different ranges of particles size were sieved for use in preparing different mixtures of AW powder ratio. Blending of the different mixtures was done using a 'V' mixer on a conventional lathe machine as described in Figure 4.2. AW and three different binders were mixed for testing of suitability of binder to binder solution compatibility. The four mixtures with varying ratio of AW particles range size were prepared. Table 4.2 shows the AW particles mix and the binding agent mixture ratio to AW.

Table 4.2 Ratio of AW mixture preparation.

Mixture preparation	Percentage of AW particles range ratio 70%		Percentage of Binding Agent Mixture ratio 30%	
M1	70%	53µm to 90µm	50%	Maltodextrine
	30%	20µm to 53µm	50%	Fine sugar
M2	10%	53µm to 90µm	50%	Maltodextrine
	82%	20µm to 53µm	50%	Fine sugar
	8%	below 20µm		
M3	100%	53µm to 90µm	100%	Maltodextrine
M4	100%	53µm to 90µm	100%	Polyvinylpyrolidone (PVP)

The mixtures of the preparations are as shown in figure 4.4. SEM images on the distribution of AW powder frits were uniform where binding agents were clearly attached to the AW frits. Maltodextrine powder shows a much better distribution as compared to PVP powder. Preparation M4 was not test on the Z-Corp 3DP as it seems not to give a good spread during powder spreading, and the binding outcome might not be even. Hence, only three mixture preparations were used on the Z-Corp 3DP; M1, M2 and M3.

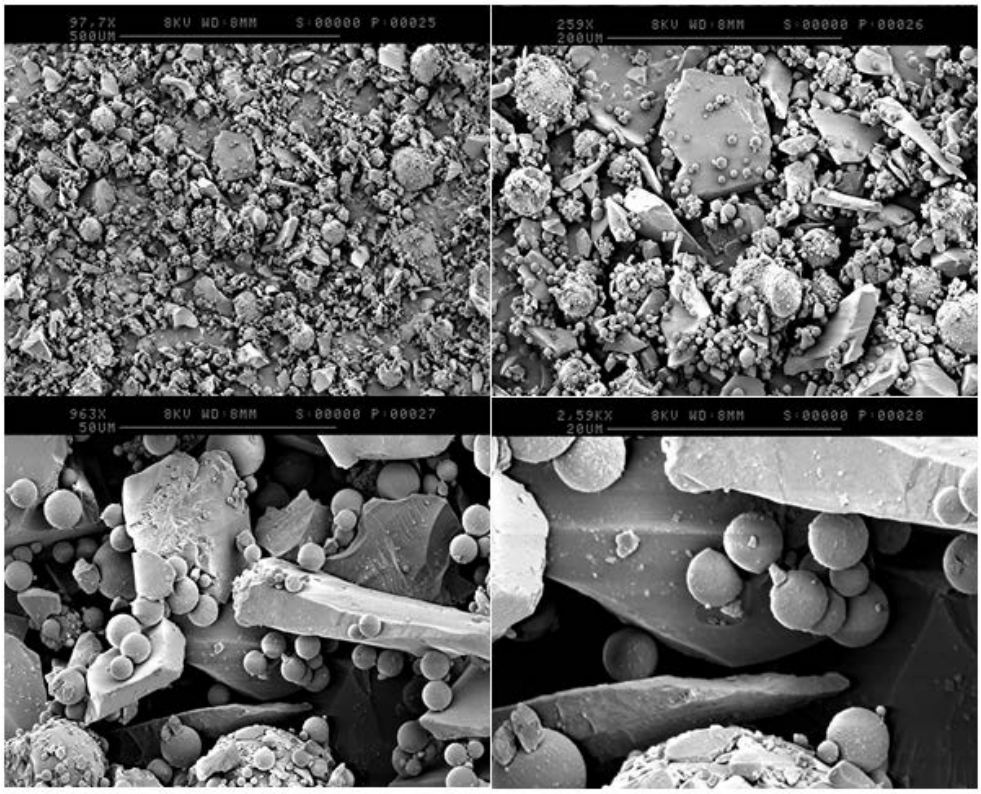

AW with maltodextrine

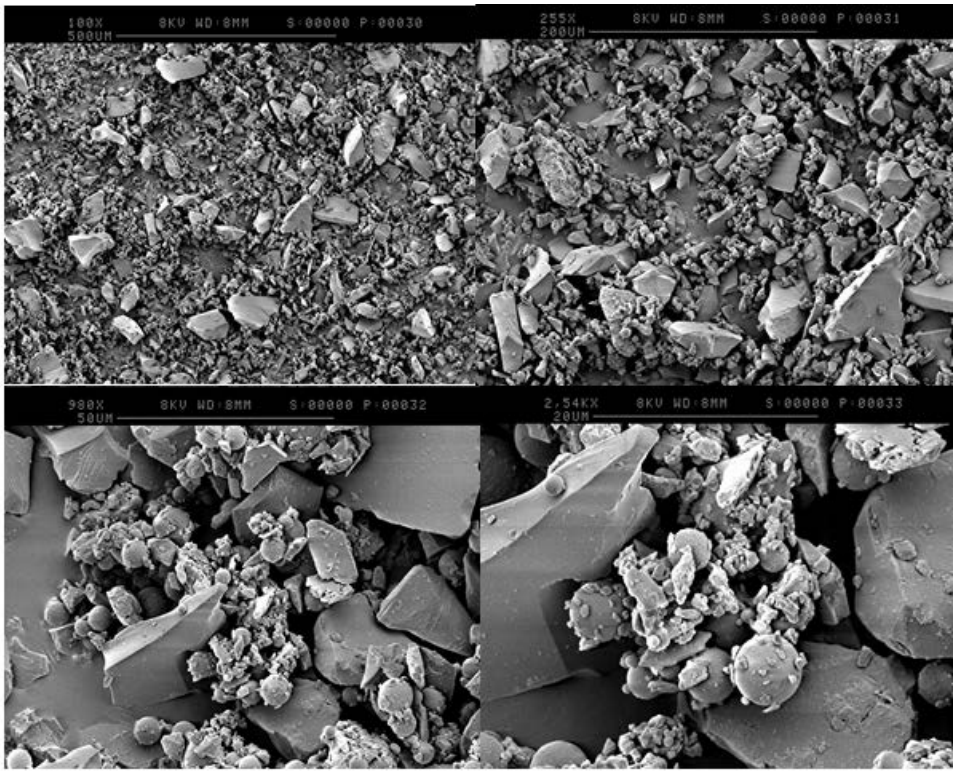

AW with Kollidon90 (Polyvinylpyrrolidone PVP)

Figure 4.4 SEM images of different preparations.

4.2.4 *Binder Preparation*

Four binder solutions were prepared as shown in Table 4.4. The compounds used in creating the binder solutions are distilled water, alcohol and surfactant. The ratio of water to alcohol is 80%BV: 20%BV (Seitz et al., 2009). Surfactant was added to reduce the surface tension. In the Z-Corps 3DP, the binder solution composition is as given in Table 4.3. The generic composition for binder solution consists of water, alcohol and surfactant.

Table 4.3 Components of ZP18 binder solution.

Components	**Approximate % by weight**	**C.A.S. No. & EINECS No.**	**UK/EU Classification**
Glycerol	1-10%	56-81-5200-289-5	Irritant XiS 23 24/25
Preservative (Sorbic acid salt)	0-2%	Trade Secret	Irritant XiR 36/37/38, S 26, S 36
Surfactant	<1%	Trade Secret	Irritant XiR 36, S 24, S 26
Pigment	<20%	Trade Secret	R 42/43
Water	85-95%	7732-18-5	NA

4.3 Process Development

4.3.1 *Binder Evaluation*

Each of the solutions prepared were tested onto different AW powder mixtures in open space at room temperature. An atomiser was used to deposit the binder solution on to the powder mixture. After two hours, observation was made to a certain the solidification of the powder mixture was completed. Observation and measurement were performed using Motic microscope with Motic Images plus 2.0 software. Analysis of the consolidation powder mixture to binding solution was performed (Table 4.4).

Table 4.4 Result of spraying different binder solution to AW maltodextrine powder mixture M3.

Binder Solution	Number of sprays	average Thickness (µm)	Sample images after 2hours 3 sprays	Sample images after 2hours 4 sprays
Distilled water	1	364.00	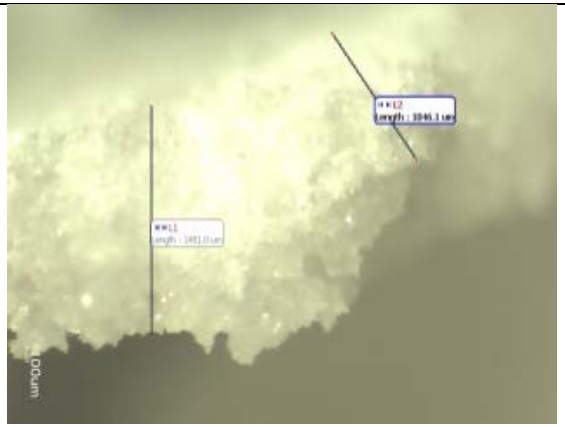	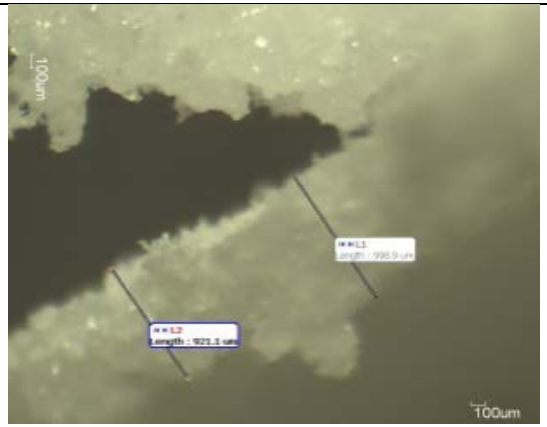
	2	818.63		
	3	624.28		
	4	480.00		
Distilled Water + 18%ABV Ethanol	1	758.53	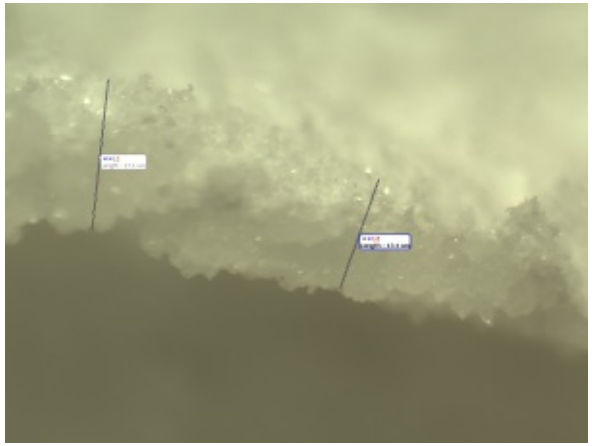	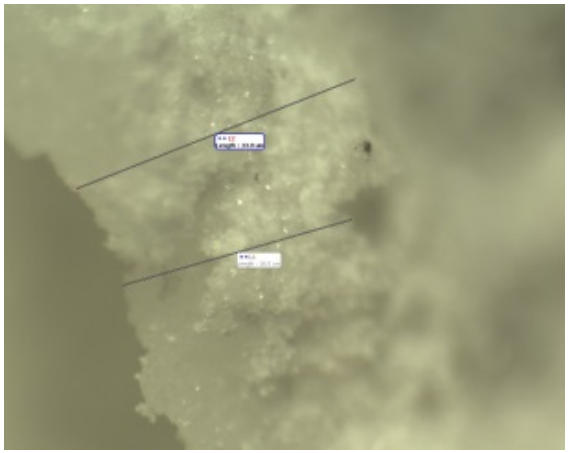
	2	1105.75		
	3	777.80		
	4	1542.58		

Distilled Water + 1% BV Darvan-C: 1mL of Darvan-C and 99mL of water	1	501.23		
	2	390.55		
	3	349.30		
	4	576.63		
Distilled Water + 18%ABV Ethanol +1% BV Darvan-C : 1mL of Darvan-C and 99mL of diluted ethanol	1	460.15	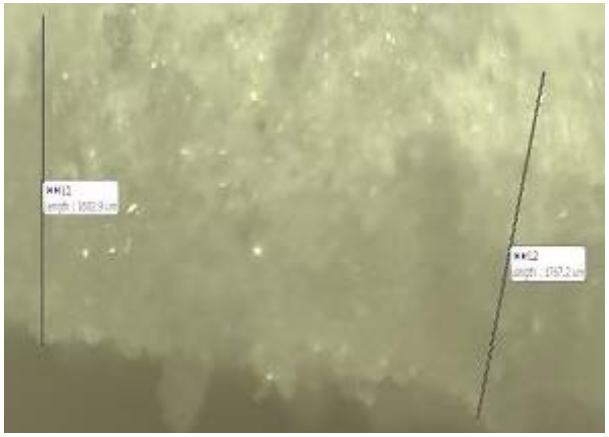	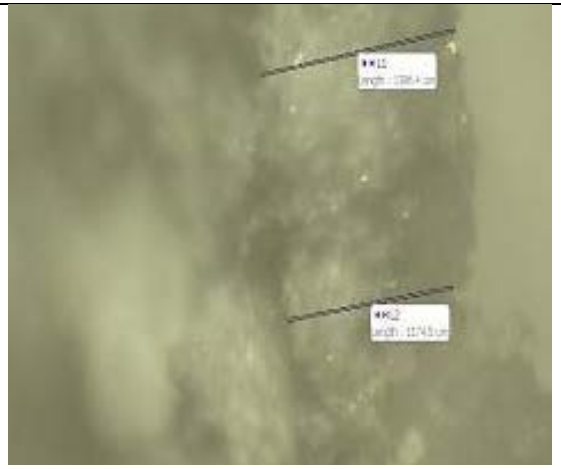
	2	981.23		
	3	842.53		
	4	640.23		

All the sample solution tested did indicate that there are consolidations of the power mixture. Maltodextrine reacted with all the solution but to a varying degree in thickness and the time taken to consolidate the powder mixture. Maltodextrine is known to bind with water to form a gel like substance (Visavarungroj and Remon, 1992, Nonaka, 1997). It is successfully used in 3D printing of ceramic research (Marchelli et al., 2011, Utela et al., Suwanprateeb et al., 2010). The role of Darvan C-N is to lower the interfacial tension between a liquid and a solid while ethanol is to accelerate the drying time of the print. This requirement is necessary to facilitate the working principle of inkjet printing. As observed, the thickness does not increase linearly with the amount of binder. The amounts of spraying tend to converge in the fourth spray (Figure 4.5). This indicated that a sufficient amount of binder solution used for the lowest layer thickness suitable for the 3D printer. The selected binder solution preparations were tested on a Z-Corp 310Plus 3D printer.

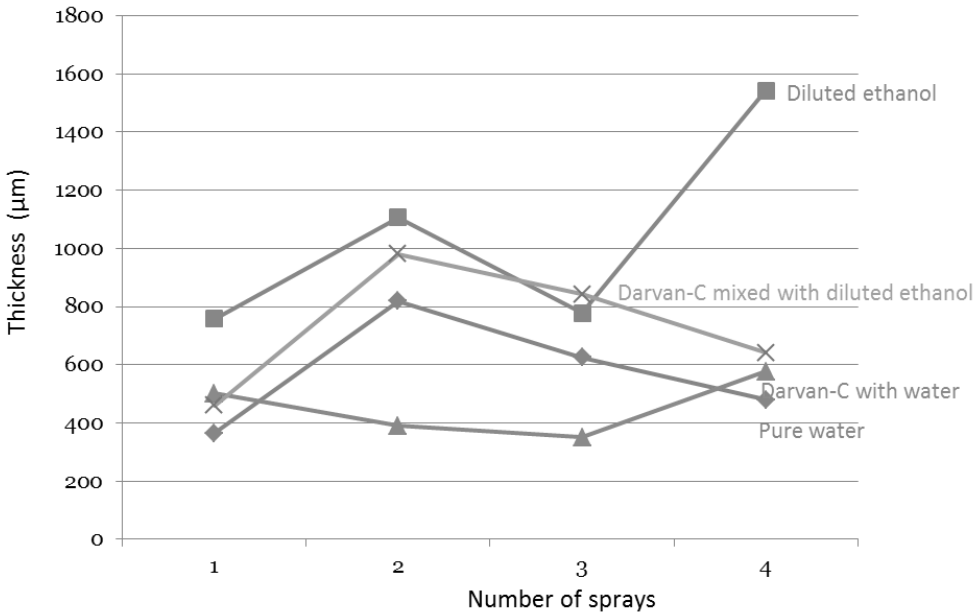

Figure 4.5 The influence of the amount of binder solution to the layer thickness.

4.3.2 *Powder Blend Evaluation*

During printing, preparation M1 and M2 were incompletely printed due to clogging of the HP11 print head used on the Z-Corp 3DP machine. No further investigation was performed on these two preparations as to the cause of clogging. It was suspected that the particles smaller than 53µm when air bound and clog up the print-head. With preparation M3 printing was completed for all the test specimens. Figure 4.6 shows the test specimens printed on a 3D printer and the specimens produced were with discrepancy. Even though the setup was able to print the 3D specimens completely, clogging of the printhead still occurred after a few runs.

Several specimens of the test parts were successfully manufactured. The printed parts were fragile after printing and were left to dry in the 3D printer chamber overnight before removal from the print platform. No further drying was necessary as the objects were to be taken for sintering using the same heating profile as described in section 3.2.5. The geometrical shape of the green-part specimens was distorted as compare to the CAD model. The degree of distortions was not the same for all the specimens as the build orientation, and surface shear caused some of the specimens to have more curling and distortions than others (Figure 4.7). The sintering process did not influence the specimens' distortion. These conditions were also observed in work by Farzadi (Farzadi et al., 2014).

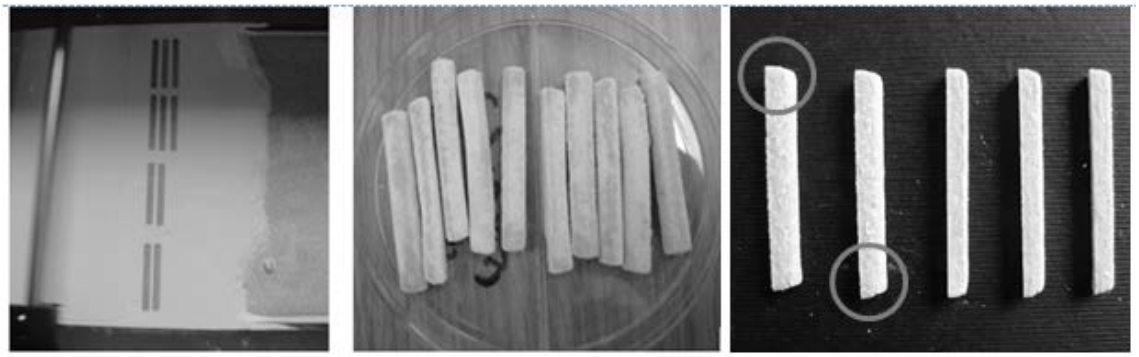

(a) (b) (c)

Figure 4. 6 (a)Printing orientation of AW test specimens on Z-Corp 310Plus 3D printer, (b) different distortion in green part specimens and (c)samples of sintered part where the bottom surface are straighter than the top surface. Circled areas showing the effect of curling.

Samples were also assessed for surface characteristics as shown in Figure 4.8.The surfaces were rough due to jetting of the binder solution on the powder bed. This phenomenon was also prevalent in Farzadi's and Seitz's work (Farzadi et al., 2014, Seitz et al., 2005) which influence the surface texture of the printed parts and the geometry. However; in the case of surface texture, this is an added advantage as cells propagate better in rough surfaces as it act positively in directing osteogenic responses of progenitor cells which stimulate both *in vitro* and *in vivo* bone formation (Marinucci et al., 2006, Lincks et al., 1998). The top surface is rougher with more peaks and valleys as compare to the bottom surface.

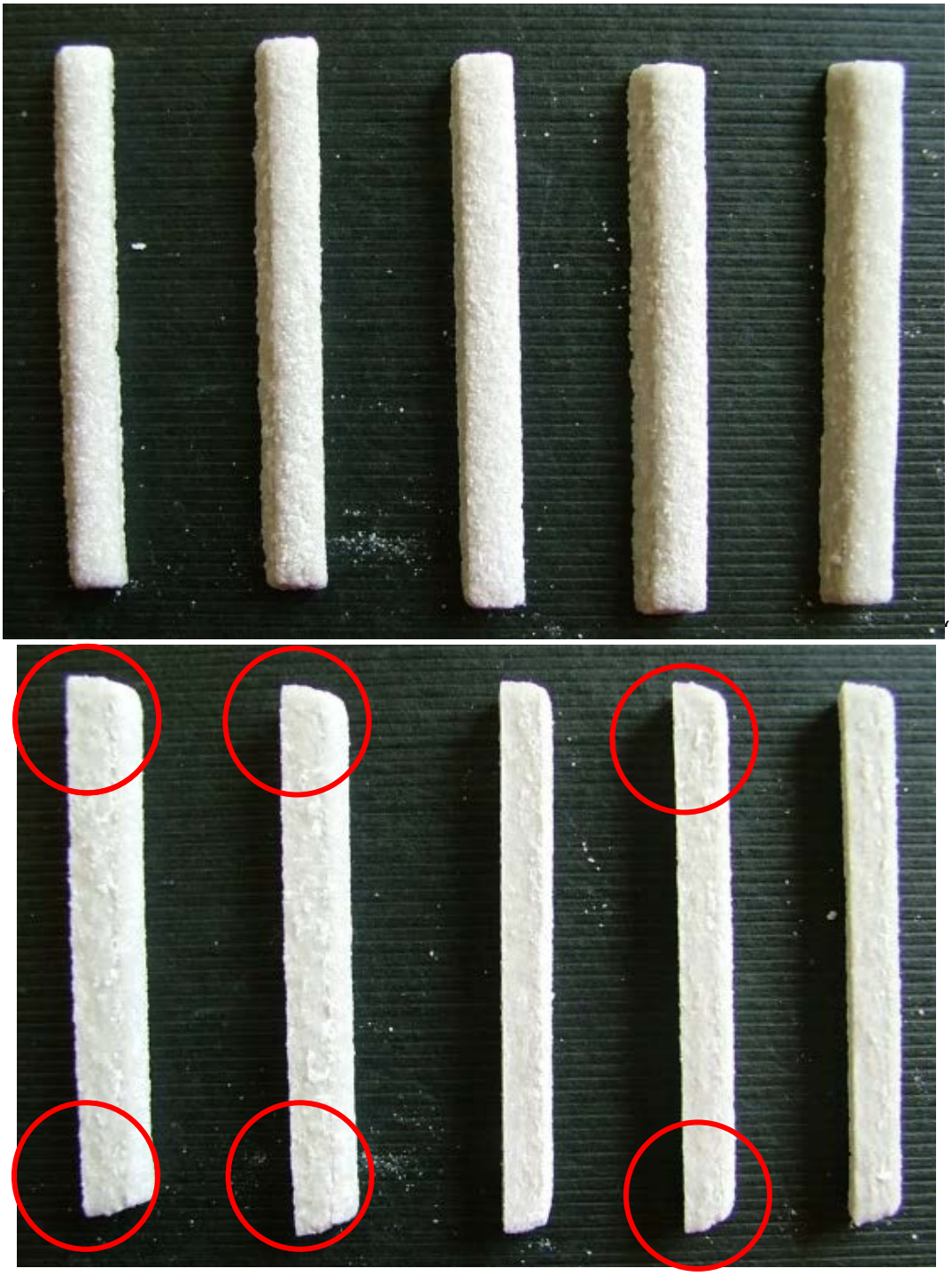

(a) surface tension between successive layer produce curling effect

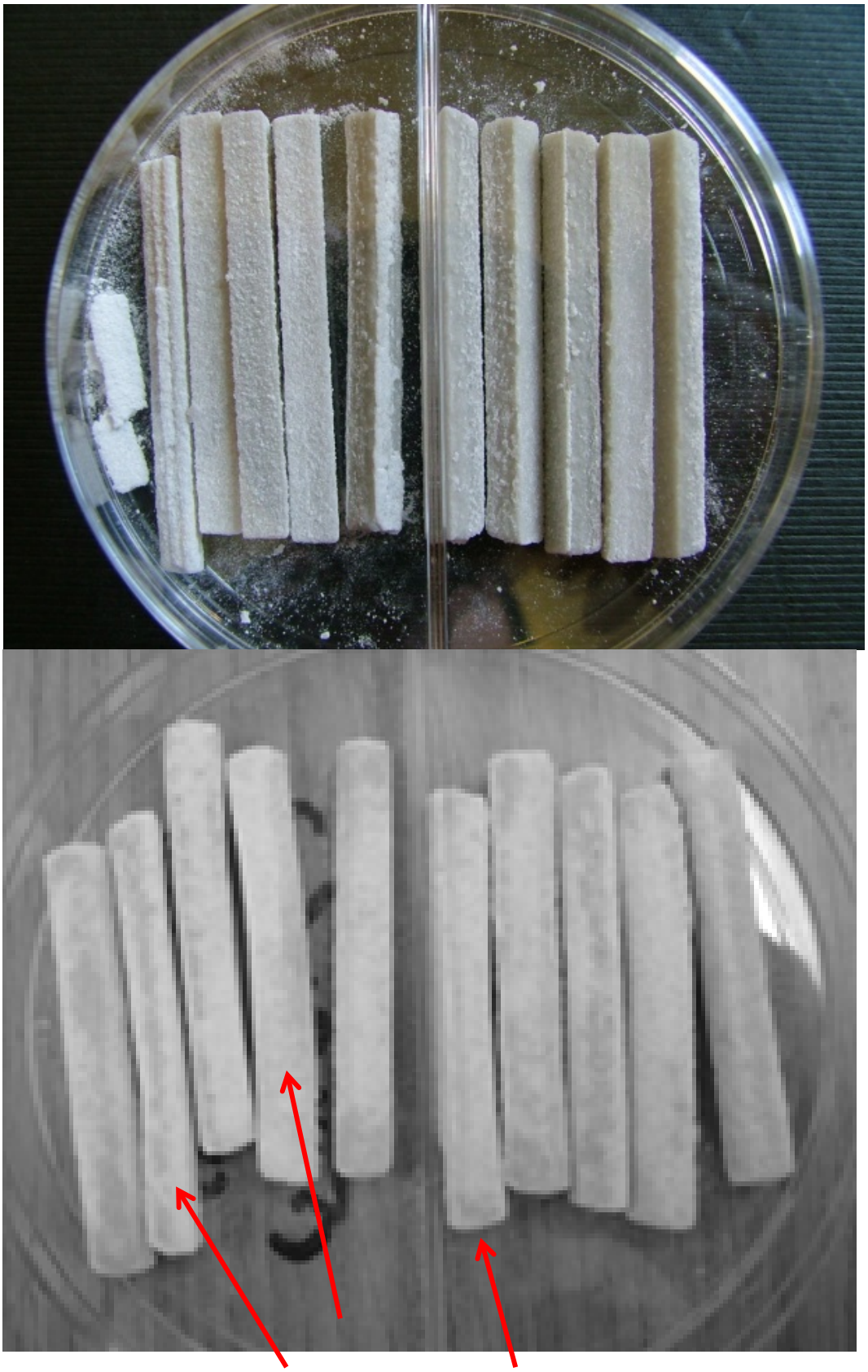

(b) different degree of distortion cause by uneven wettability

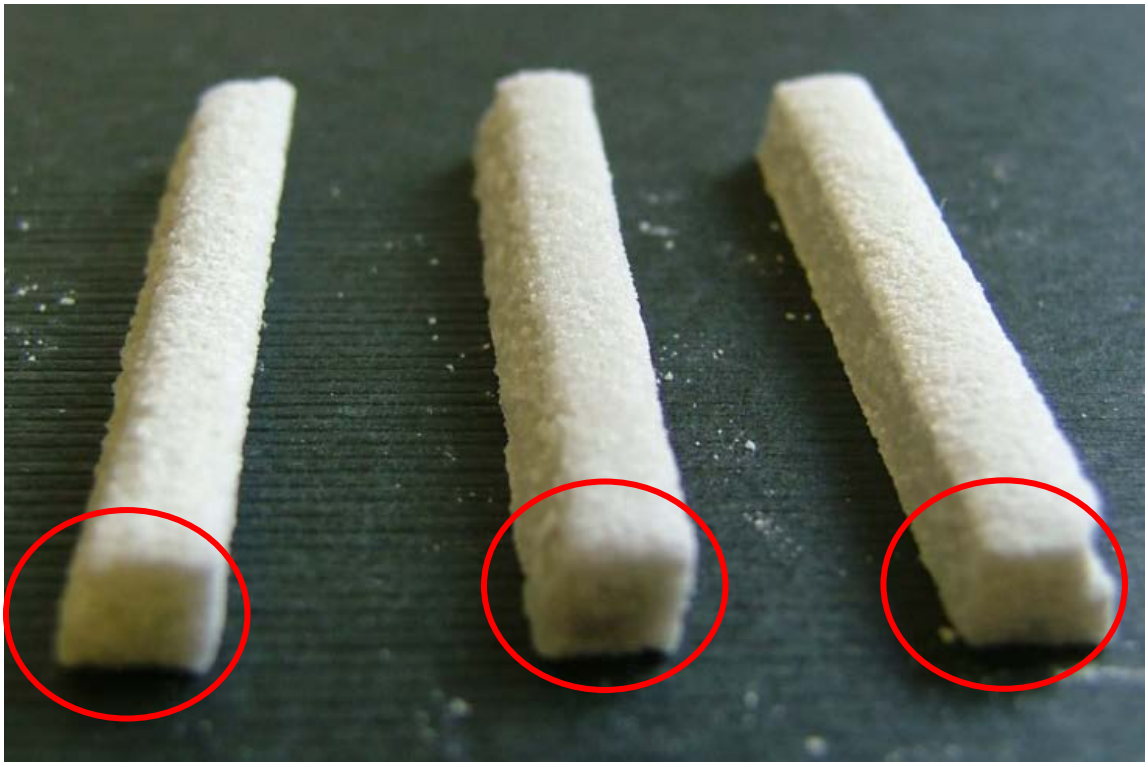

(c) Surface shearing as an effect of powder spreading.

Figure 4.7 Printing effects (a), (b) and (c) on the geometrical accuracy of 3D artefacts.

All the specimens' side view indicated there is a slight curling. This is due to structural curl and moisture curl; an effect cause by surface tension and wettability; as evidenced from figure 4.8a and figure 4.8b. While in figure 4.8c it is less obvious as it is printed along the Y-orientation which has shorter distance of print. The specimens that were printed along the width-based (shorter distance of print) rather than length-based (longer distance) displayed different physical and mechanical characteristics (Farzadi et al., 2014).

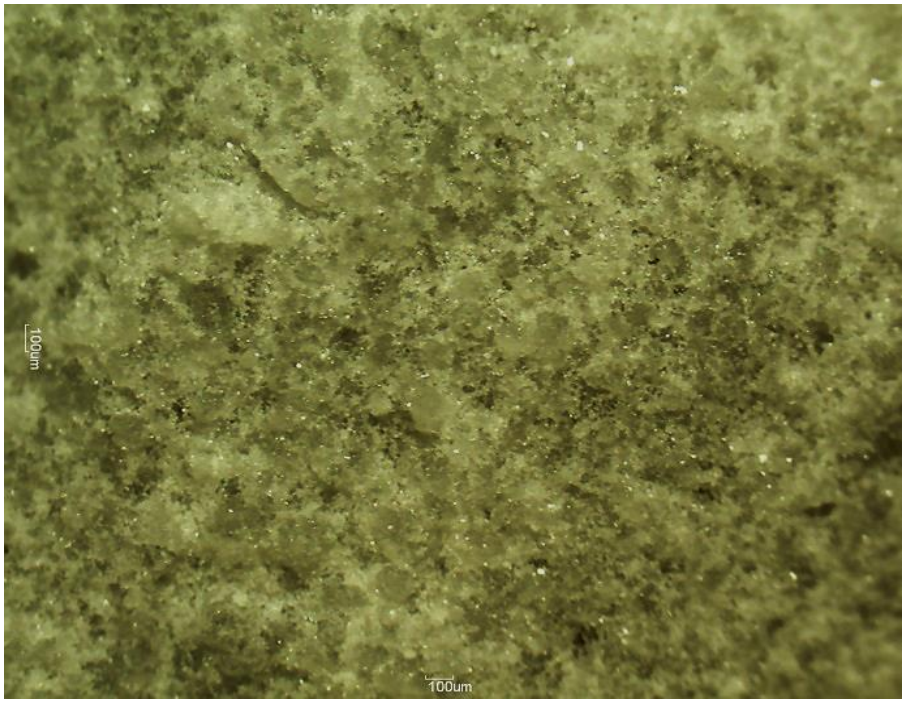

Surface at Top, closest to last build layer.

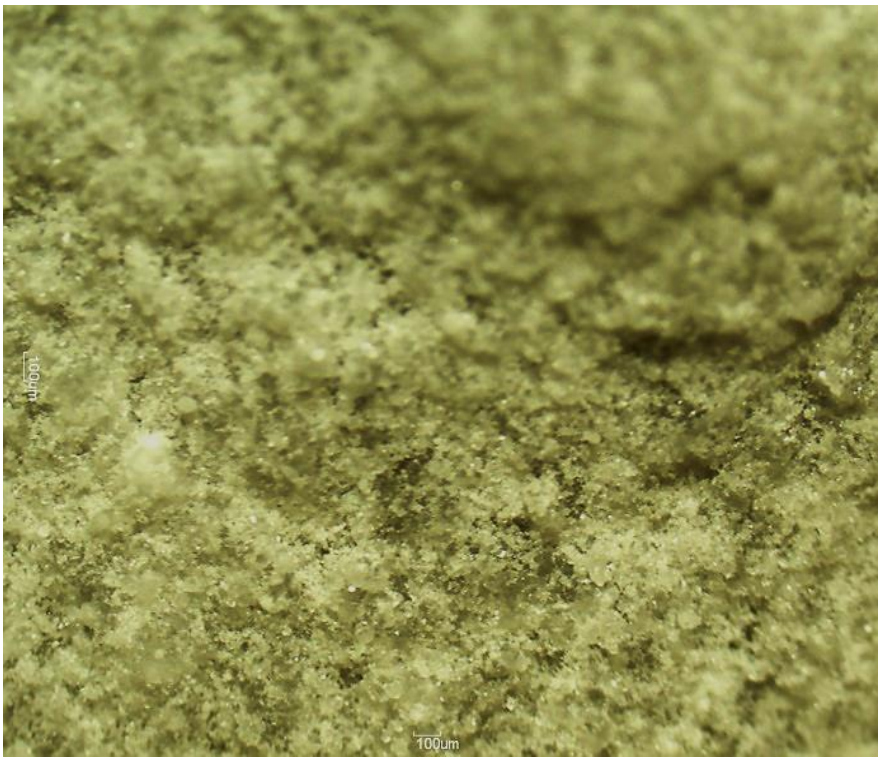

Surface at the bottom, closest to print platform.

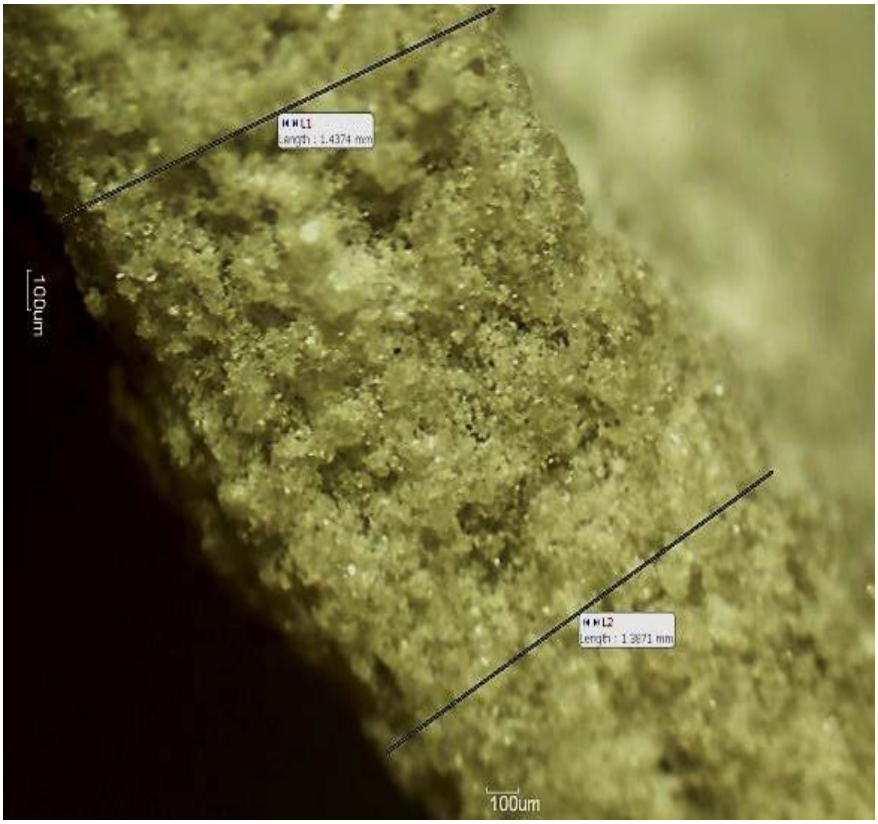

Side surface

(a) Specimen A

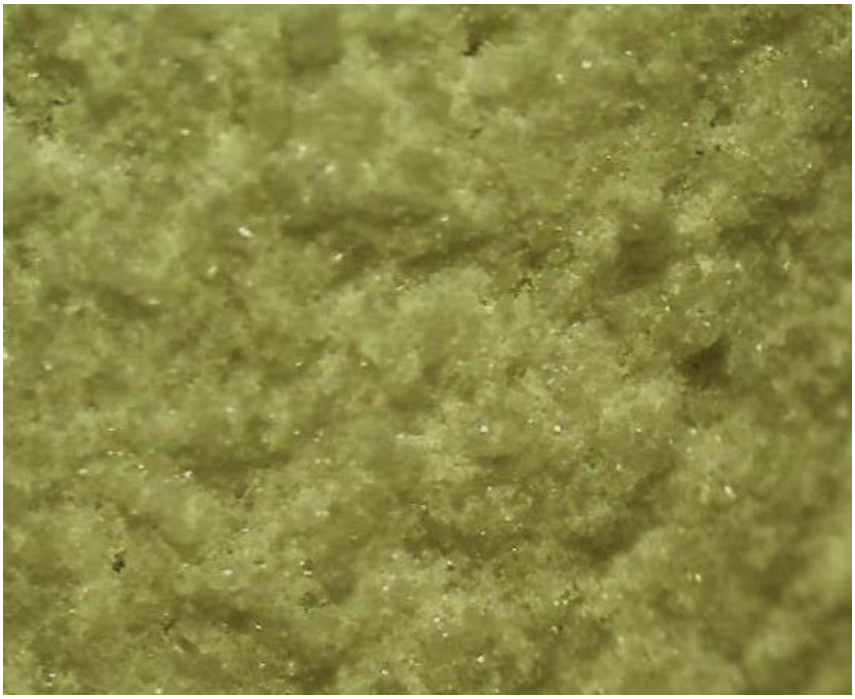

Surface at Top, closest to last build layer.

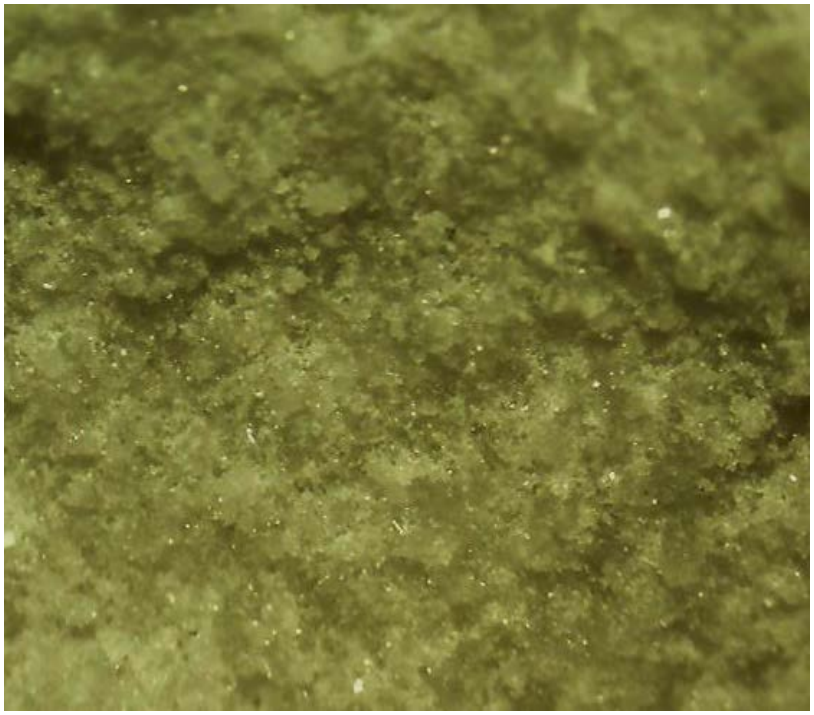

Surface at the bottom, closest to print platform.

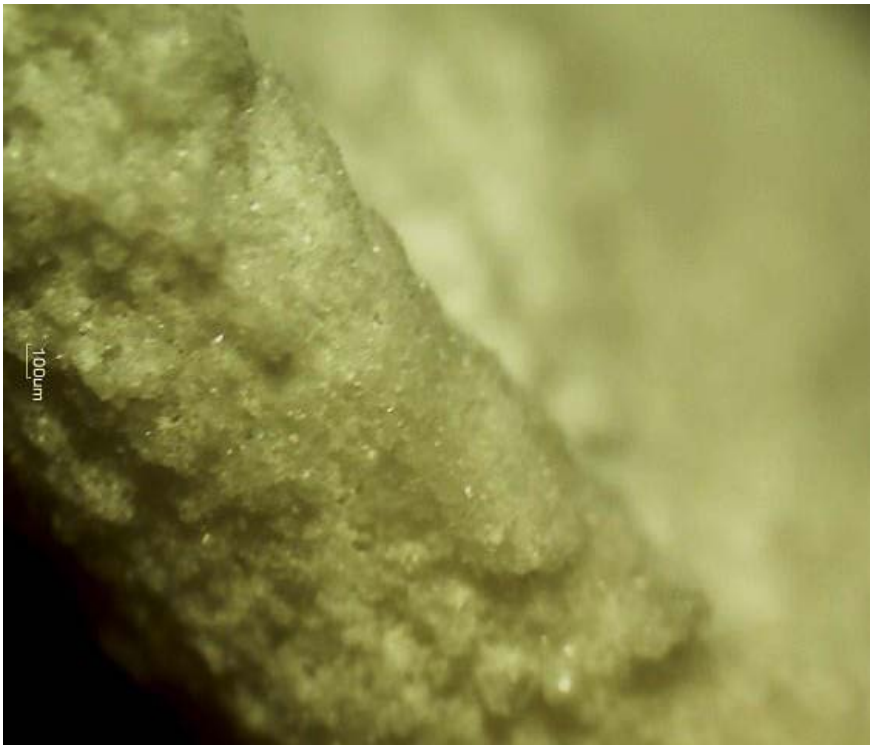

Side surface

(b) Specimen B

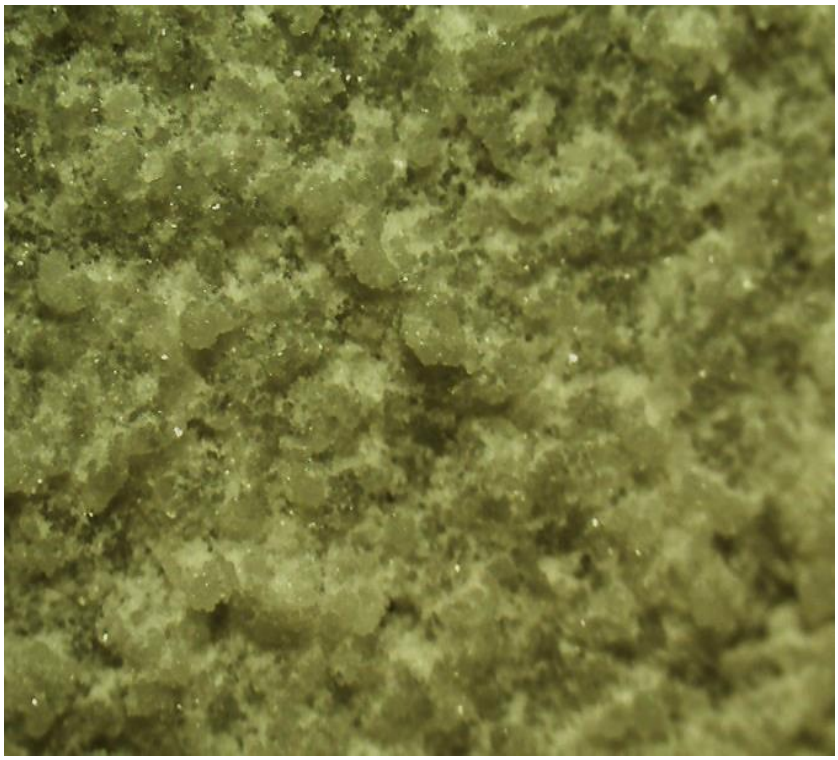

Surface at Top, closest to last build layer.

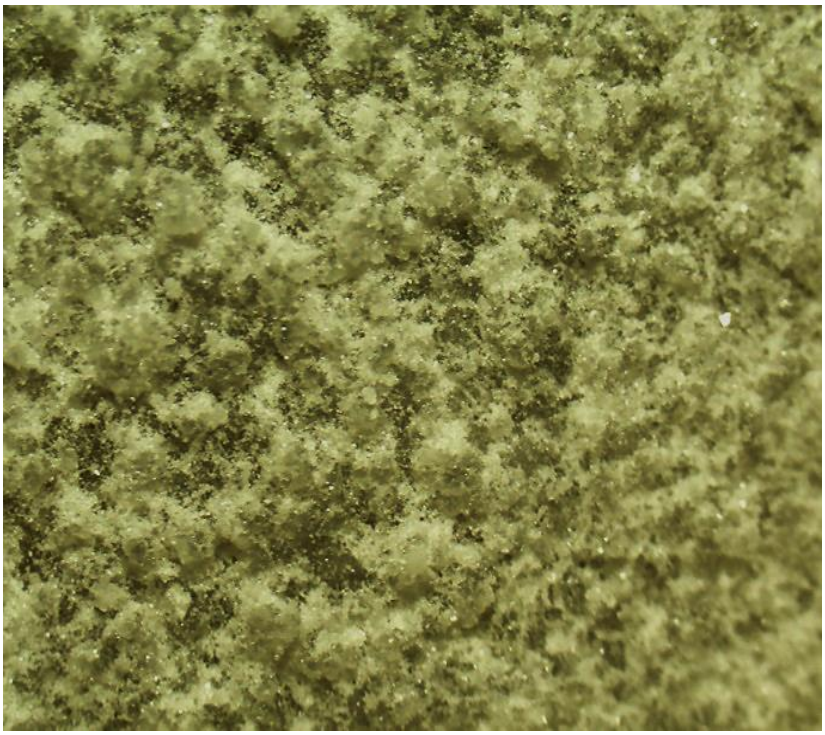

Surface at the bottom, closest to print platform.

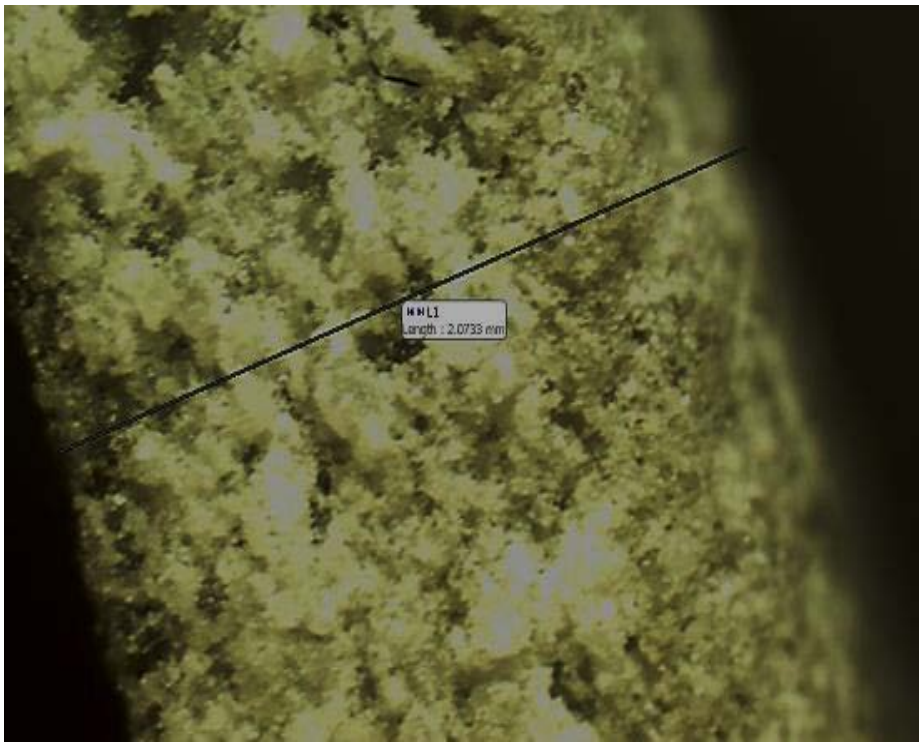

Side surface

Figure 4.8 Surface texture of top, bottom and side of printed samples (a), (b) and (c).

In addition, the geometrical shapes were also printed for geometry verification. Figure 4.9 shows the specimens and sample 3D objects that were printed using this setup. Specimen A is the printed object of a 3D rectangular slab, while specimen B and specimens C are patches for mandibular fracture repair. By observation, all the printed artefacts showed good geometry profile which matched the CAD model with minimal discrepancy. However, if an accurate comparison is needed, the printed artefacts can be 3D scanned and the scanned model can then be matched to the original CAD model. The scanned data is then used to generate a virtual model which will be superimposed onto the original CAD model. By establishing the same origin point for both models beforehand, the interference tools in the CAD software can be used to determine the percentage of discrepancy or similarity by knowing the amount of interference of the superimposed models. The volume and some overall dimensions such as maximum x-distance, y-distance and z-distance can be known for both models using the measurement tools in the CAD software.

Figure 4.9 Specimens printed using the prepared AW-maltodextrine mixture with ethanol-Darvan-C based binder solution.

4.3.3 *Sintering*

In order to study the characteristic of the 3D printed parts, morphology analysis and mechanical testing were performed. The test specimens were sintered using high-temperature furnace. The heating profile for sintering AW is as described in section 3.2.5. The test specimens were placed in ceramic boats for sintering inside the furnace (Figure 4.10). A total of 20 samples were produced to be sintered under the mentioned profile. The sintering process removed the binding agent maltodextrine and caused the AW particles to adhere and consolidate. The observed and measured sintering shrinkage of the sintered specimens ranges between 35% and 53%, in either the width or thickness, depending on the build orientation. Orientation of 3D printed objects will affect the characteristics and mechanical properties (Pilipovic et al., 2009, Kim and Oh, 2008, Pham and Dimov, 2003). In addition, in all powder sintering process the porosity is temperature and time dependence.

Figure 4.10 Equipment used in sintering AW green parts.

The microstructures of the sintered samples indicate that there are macro and micro pores (Figure 4.11). The porosity in the sample is observed to consist of open and close pores. The pores size as observed from the SEM images ranges from 20μm to 200μm. The internal structure of the specimens as shown in Figure 4.11b indicated that most of the pores size is in the region of 20μm with few at 100μm or higher as compare the outer region having pore of up to 500 μm. From the observation of the SEM images of the sintered samples morphology, the samples are highly porous (refer to Figure 4.11). In the sintering process, open pores began to form and elongated due to neck growth, grain growth, and pore shrinkage. Eventually, the pores were encapsulated inside the coalesced particles or remain as closed pores. The SEM images of the surface morphology in the sintered particles at the internal surface show the necking of AW particles and grain growth; which is in agreement with work performed by Marchelli et al. (Marchelli et al., 2011, Butscher et al., 2011a). In this sintering process that was performed, the setting of temperature and time were maintained to obtain optimum nucleation of AW-GC and not the strength nor the porosity. It is known that porosity is time and temperature dependence and thus the rate of densification had an effect pores elongation which influenced the degree of porosity (Rahaman, 2008).

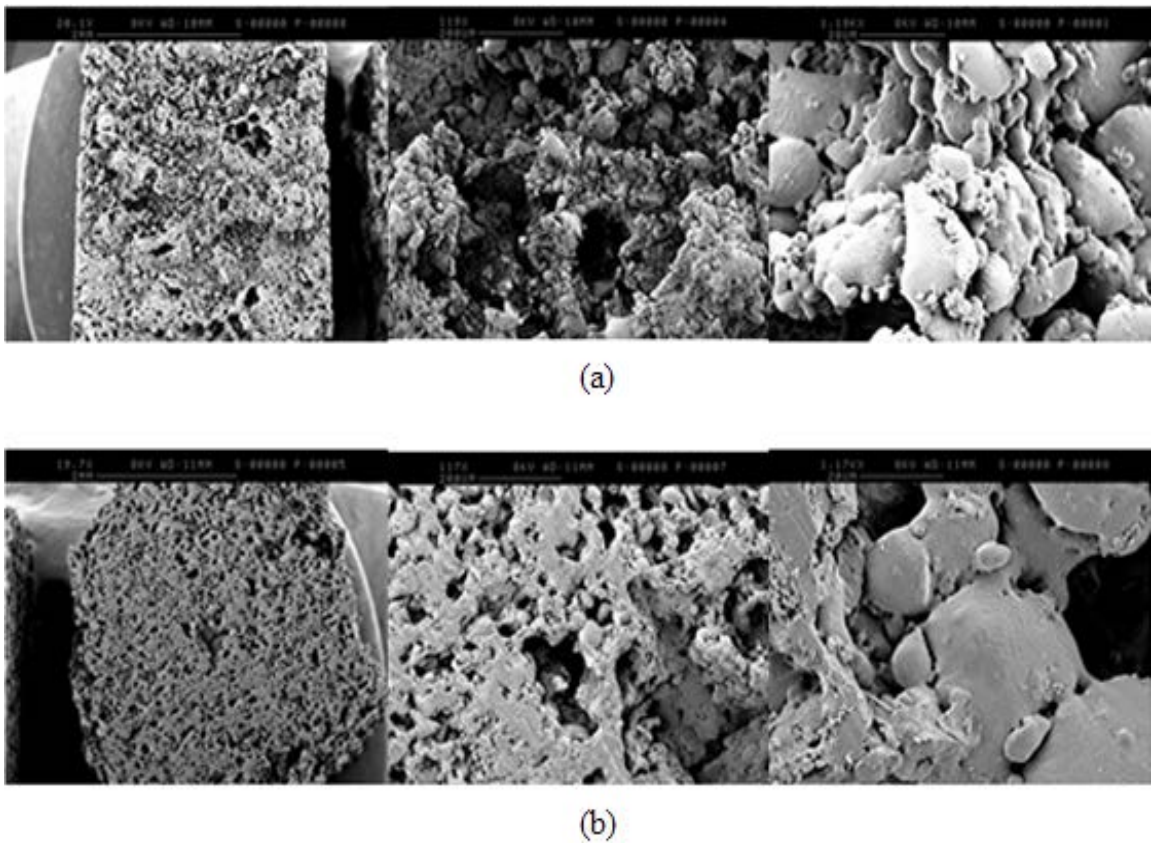

Figure 4.11 SEM images of sample at (a) outer surface and (b) at bending failure surface (from left to right) at 20X magnification (2mm scale bar), 117X (200μm scale bar), and 1170X (20μm scale bar) .

4.3.4 *Accuracy*

Test samples were measured for consistency and accuracy of print. Each dimension was measured four times, and the mean value of the measurement was used as the value for calculating the bending strength. A t-test with 95% confidence interval was conducted. In the greenpart (unsintered) specimens, CAD model of dimension 6mm by 6mm by 30mm was created for 3D print. While for sintered specimens, the CAD model is 10mm by 10mm by 50mm. Statistical tools were used to analyse the accuracy of the obtained AM artefacts.

In the unsintered specimens, the mean value for width and thickness is 5.448±0.206 mm and 5.017±0.1419 respectively. T-test was used as the median and mean are close which indicated that this is a normal distribution. The results from the t-test, $p<5\%$ using Microsoft Excel 2010 are as tabulated in Table 4.5. This is statistically significant as the value p is less than 0.05.

The percentage of deviation in width and length is not the same. Normally the shrinkage of printed artefacts is not the same in the X, Y, and Z-direction as it is influenced various factors such as powder particles size, powder flowability, layer thickness and binder saturation (Vaezi and Chua, 2011, Lozo et al., 2008, Farzadi et al., 2014).

Table 4.5 Accuracy of 3D printed green specimens.

Item	Unsintered Samples	
	Average width	Average thickness
n	5	5
min	5.1575	4.8275
max	5.695	5.1725
median	5.5025	5.065
Mean	5.448	5.017
Std. Deviation	0.205817	0.1419
Std. Error	0.092044	0.06346
hyp mean	6	6
alpha	0.05	0.05
tails	2	2
d.f.	4	4
t stat	5.997	15.490
p value	0.001945	0.000051
t critical	2.776	2.776
95% Confidence Interval(CI) for Mean High	5.7036	5.1932
95% Confidence Interval(CI) for Mean Low	5.1924	4.8408
significant	Yes	Yes

In the sintered specimens, the CAD model has a dimension of 10mm by 10mm by 50mm (in order to produce sintered specimens that do will have a dimension of roughly 6mm by 6mm cross section). After sintering, the thickness along the span of the samples those were not post-processed using sandpaper ranges from 5.74mm to 6.5275mm while the width ranges

from 5.2525mm to 6.0675mm. As for post-processed using sandpaper of sintered samples, it ranges from, 5.12mm to 6.11mm and 4.7875mm to 5.1975mm in width and thickness respectively (Table 4.6). Overall observation and calculated average of width and thickness dimensions in the sintered parts indicated that there was a 40% to 50% decrease in the corresponding dimensions of the 3D CAD models.

Table 4.6 Accuracy of sintered 3D printed specimens.

Item	Sintered Samples, Not sanded		Sintered Samples, Sanded	
	Average width	Average thickness	Average width	Average thickness
n	10	10	10	10
min.	5.74	5.2525	5.12	4.7875
max	6.5275	6.0675	6.11	5.1975
median	5.9253	5.54	5.255	5.01
Mean(Average)	6.0121	5.5105	5.4255	4.997
Standard Deviation	0.2289	0.2698	0.2760	0.1298
Standard Error	0.0724	0.0853	0.0873	0.0410
hyp mean	10	10	10	10
alpha	0.05	0.05	0.05	0.05
tails	2	2	2	2
d.f.	9	9	9	9
t stat	55.0943	52.6174	52.4091	121.905
p value	5.38E-13	8.13E-13	8.42E-13	4.27E-16
t critical	2.262157	2.262157	2.262157	2.262157
Confidence interval (CI) High	6.1758	5.7035	5.6230	5.0898
Confidence interval (CI) Low	5.8483	5.3175	5.2280	4.9042
Significant	Yes	Yes	Yes	Yes

As can be seen in figure 4.12a specimens was not completely rectangle as model from CAD software. The shape of it is slightly trapezoidal (indicated by circles) which show that there is some curling occurred when successive layers are deposited on to the recently built surface. This phenomenon happened because of structural curl and moisture curl. Structural curl is caused by the difference in the level of particles, fillers, fibre area density or fibre orientation

through the layer thickness while moisture curl developed when the layer picked up more moisture on one side than the other. Curling in 3D printed parts has been reported, and methods were suggested to overcome this (Farzadi et al., 2014, Suwanprateeb et al., 2010, Khalyfa et al., 2007). However, in this study no attempt was made toward rectifying this phenomenon.

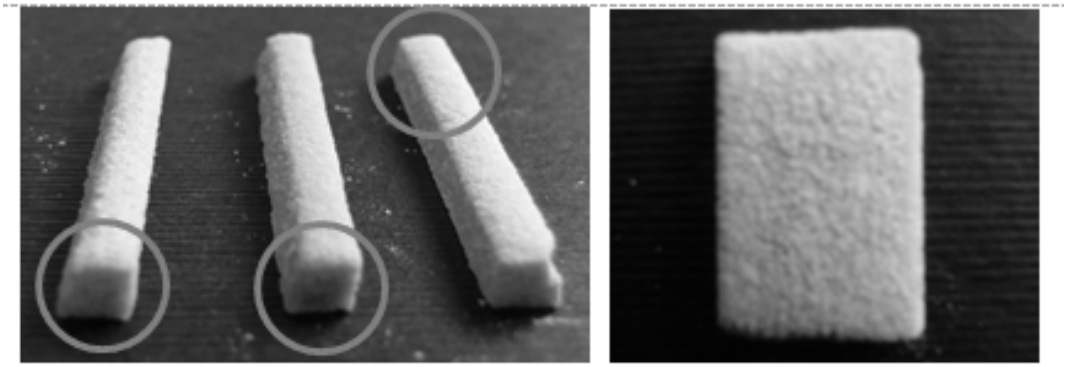

(a)

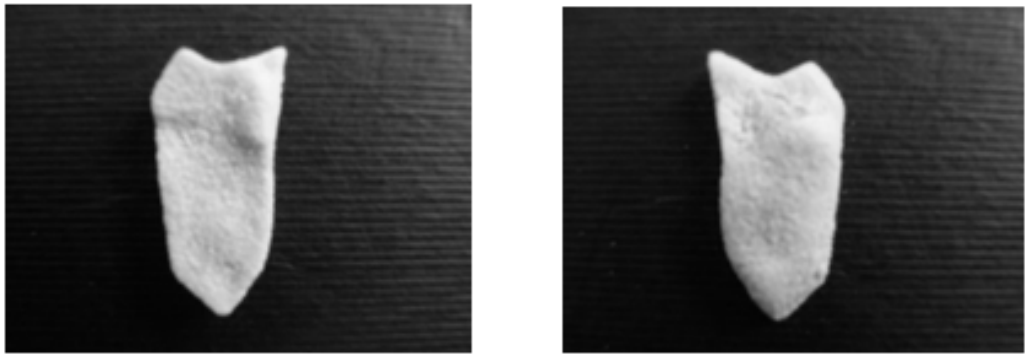

(b)

Figure 4.12 3D printed artefacts showing minor geometrical deviation from the CAD model, (a) curling of printed parts, and (b) different in surface profile in top and bottom surface of AW fracture patch.

For validity purposes, a mandible fracture fixation patch was printed and compare to the CAD model. This thickness of the part was 4mm, and the maximum length was 15mm. In the figure 4.12b the specimen from the CAD models created for the mandible fracture fixation patch was 3D printed. By observation, the geometry of the printed patches was similar to the CAD models. However, in order to quantify the similarity of the 3DP printed part to the CAD model in terms of the size and geometry, the printed part need to be 3D scanned. Scanned data of the printed part is then used to create a virtual model and compared to the original CAD

model. Both models will initially be position using the matching points in the CAD environment. Then, by superimposing the scanned model to the CAD model and using the interference tool in the CAD software, the volume of interference can be known.

Comparison was also performed on 3D printed mandible implant with the fabricated implant from indirect soft tooling. The features were more defined in the 3D printed implant, and fewer defects were seen on the implant (Figure 4.13). In addition, the texture of the 3DP printed implant has a grainy finish as compare to the surface finish of the implant produced from the indirect soft tooling. The reason for the grainy surface is during and after the building, the part is surrounded by un-agglomerated powder. The powder encases the artefacts in the printing process. Not only does the powder provide support for the artefacts but at the same time some of surrounding powder particles also adhered to the printed surface.

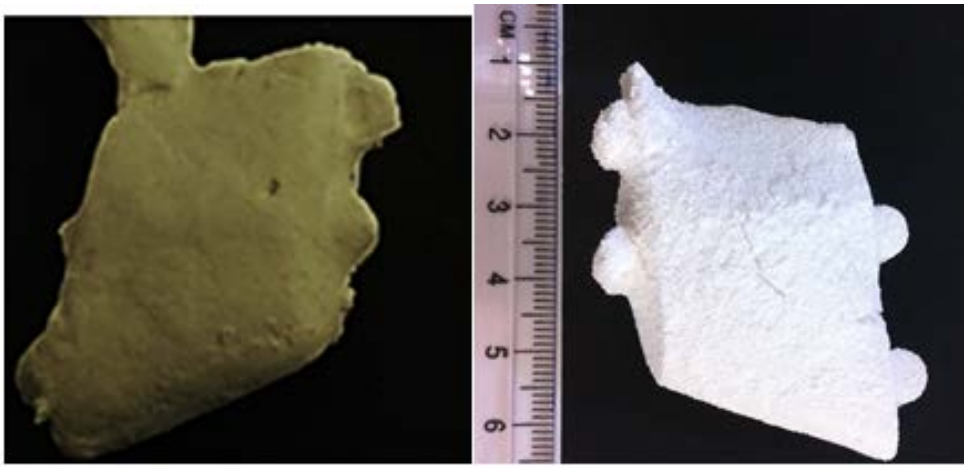

Figure 4. 13 Comparison of outcomes from two different approaches; indirect tooling and 3D printing.

4.3.5 *Mechanical Properties*

In order to determine the mechanical properties of the samples, the test samples were tested by 3 point bending test (BSI, 2008), using Instron 5565. The loading rate was set with a load cell of 1kN at rate of 0.5mm/min. Testing was conducted in room temperature environment. Three set of testing was conducted. Using Excel2010, statistical analysis with p-value, t-distribution was performed to determine the confidence interval of the Young's Modulus (Flexural modulus) and flexural strength (Modulus of Rupture).

Figure 4.14 shows the stress strain graph of unsintered AW test specimens. The curves show normal stress-strain behaviour of solid specimens, as the specimens still consist of all the composition of AW and maltodextrine with some moisture as maltodextrine retained water.

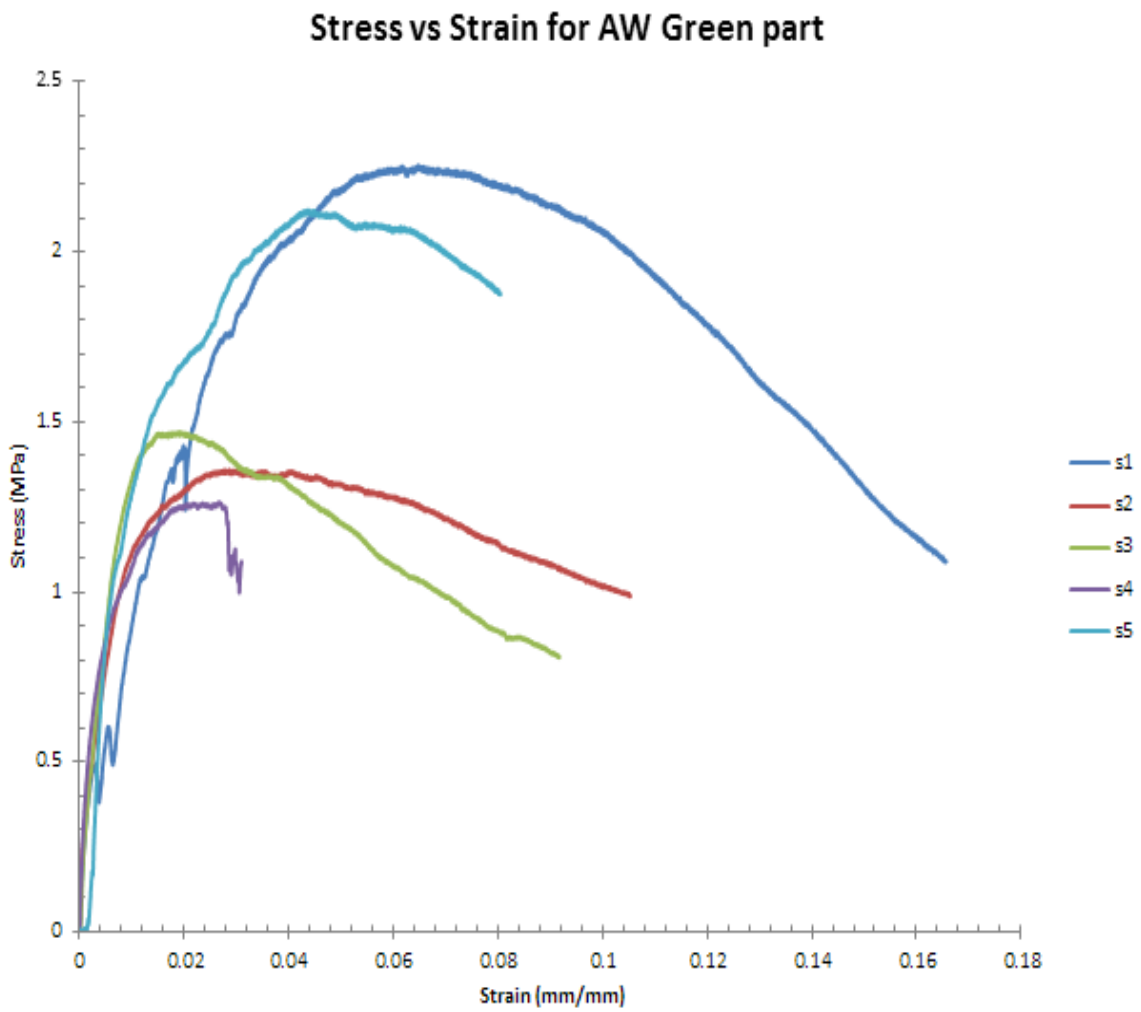

Figure 4.14 AW green parts stress-strain curve.

In the sintered test specimens, two conditions were set for the testing specimen. One set of specimen was post process by sanding to achieve smooth surface while the other set was left as is from sintering with rough surface. Figure 4.15 shows the post process sintered AW parts where the stress-strain curves displayed the behaviour of porous, brittle material under bending load. The curves show a lot of spike indicating transition of a solid region to porous region in the sintered specimens. This is also true for unsanded sintered parts. As shown in figure 4.16, the spikes were more dominant as the surface is rougher.

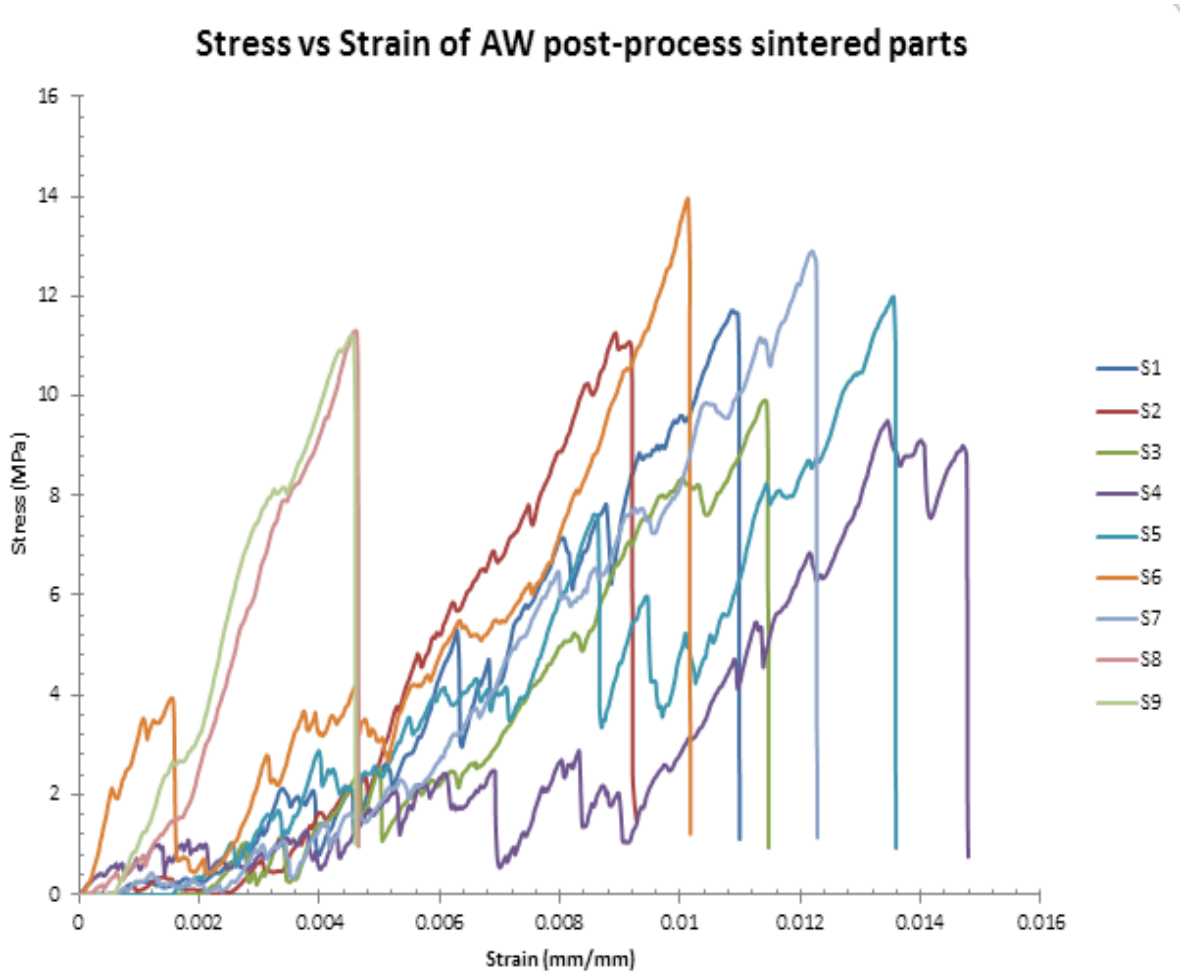

Figure 4.15 AW sanded sintered parts stress-strain curve.

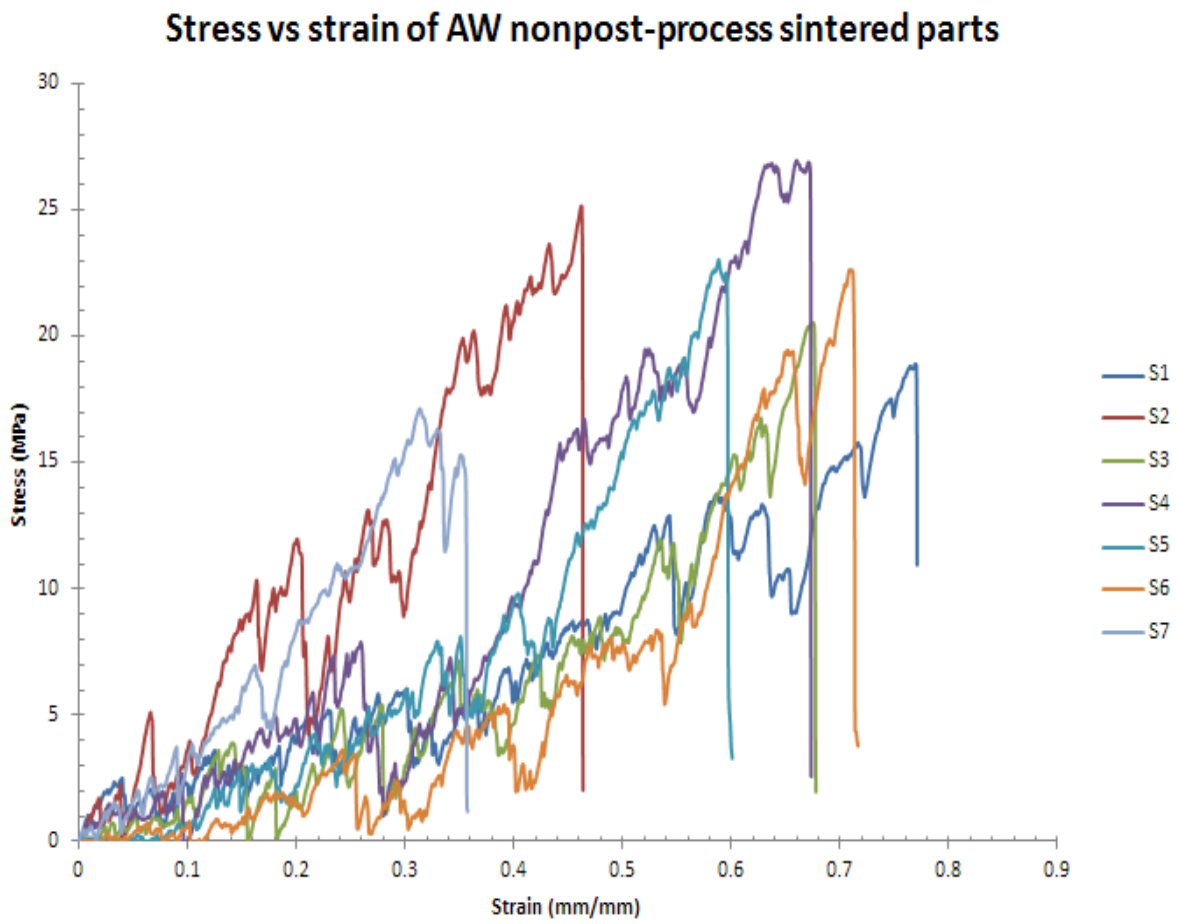

Figure 4. 16 AW unsanded sintered parts stress-strain curve.

The basic statistical analyses of the mechanical properties are as shown in table 4. Based on established value from previous works (Kokubo, 2008), dense AW-GC Young's Modulus is taken to be 118GPa.

The results obtained from the 3-point bending test are as shown in table 4-7. The flexural strength of green parts is about 15% - 35% of the sintered parts. While for post-process sintered parts, it is 2.4 times the flexural strength of the non-post processed parts. The differences in strength may be attributed to the stress concentration of the applied load due to the roughness of the surface texture. The post processed parts have larger flexural strength as it has less peaks and valleys than non-post processed parts. These peaks and valleys create stress concentration points that induced crack propagation which lead to lower load for failure. If the peak-to-valley height of the surface roughness is in the range of the critical defect size value, the roughness can affect the flexural strength (Fischer et al., 2003). Therefore, besides the natural microscopic defect, another parameter which affects the flexural strength of a ceramic component is surface roughness. Surface roughness and surface microstructure are two known factors that significantly influenced the failure of porcelain or

ceramics materials (Rashid, 2014, Whitehouse, 2002). As concluded from (de Jager et al., 2000, Fischer et al., 2003), surface roughness influences the strength of porcelain and ceramic material where the smoother the surface, the stronger the sample except when the inner structure of the material causes greater stress concentration than that caused by the combination of surface roughness and surface flaws. Therefore the results obtained demonstrated that post process parts with smoother surface than the non-post process sample will have higher value of flexural strength.

Table 4.7 Young's modulus and Flexural strength of printed 3D specimens from M3 mixture preparation.

		Unsintered samples (green parts)	Specimens not sanded, left overnight in 3DP chamber	Sanded, removed from 3DP after 3hrs, overnight in room environment
average Width *b (*mm)		5.45	6.01	5.43
average thickness (Height) *t (*mm)		5.02	5.51	5.00
n		5	10	9
Average Flexural Strength (Modulus of rupture) (MPA)		1.69	4.79	11.53
Confidence Level (95.0%)				
	High	2.261	5.87	12.58
	Low	1.119	3.17	10.48
Average Young's Modulus (Flexural Modulus) (GPA)		0.15	0.80	2.64
Confidence Level (95.0%)				
	High	0.211	1.46	3.70
	Low	0.081	0.14	1.58

4.3.6 *XRD analysis of sintered parts fabricated using 3DP*

XRD analysis was performed on the sintered 3DP parts. Two different PDF2 database were used as a measure to verify and compare with the result obtained in chapter 3 section 3.2. As shown from Figure 4.18, there is evidence of wollastonite and hydroxyl/apatite in all the

sintered artefacts produced by 3DP of the glass ceramics used in this research. Even though slightly different readings were obtained from the different PDF2 database, the peaks patterns are consistent. The XRD results show comparable pattern to other researchers (Cannillo et al., 2009, Podporska et al., 2008). The similarity in the diffraction peak list patterns for AW phase in the samples indicates that the processing route has not affected the composition in any way.

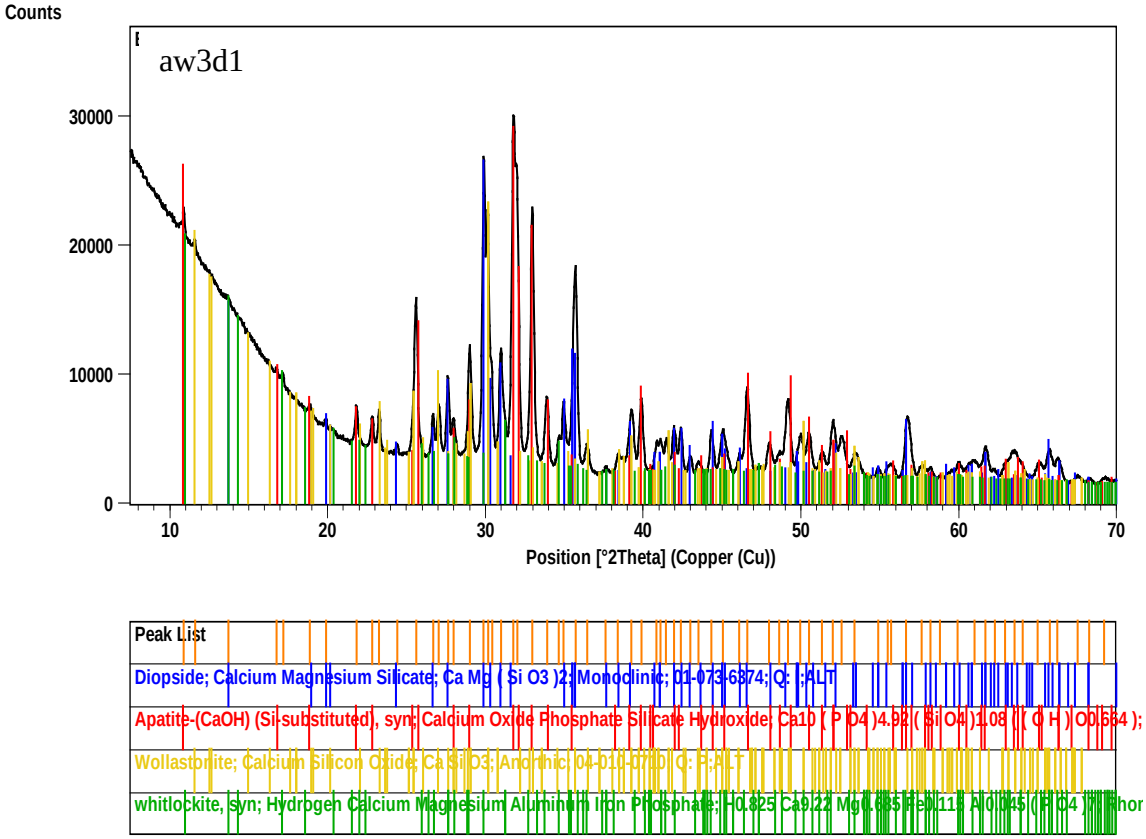

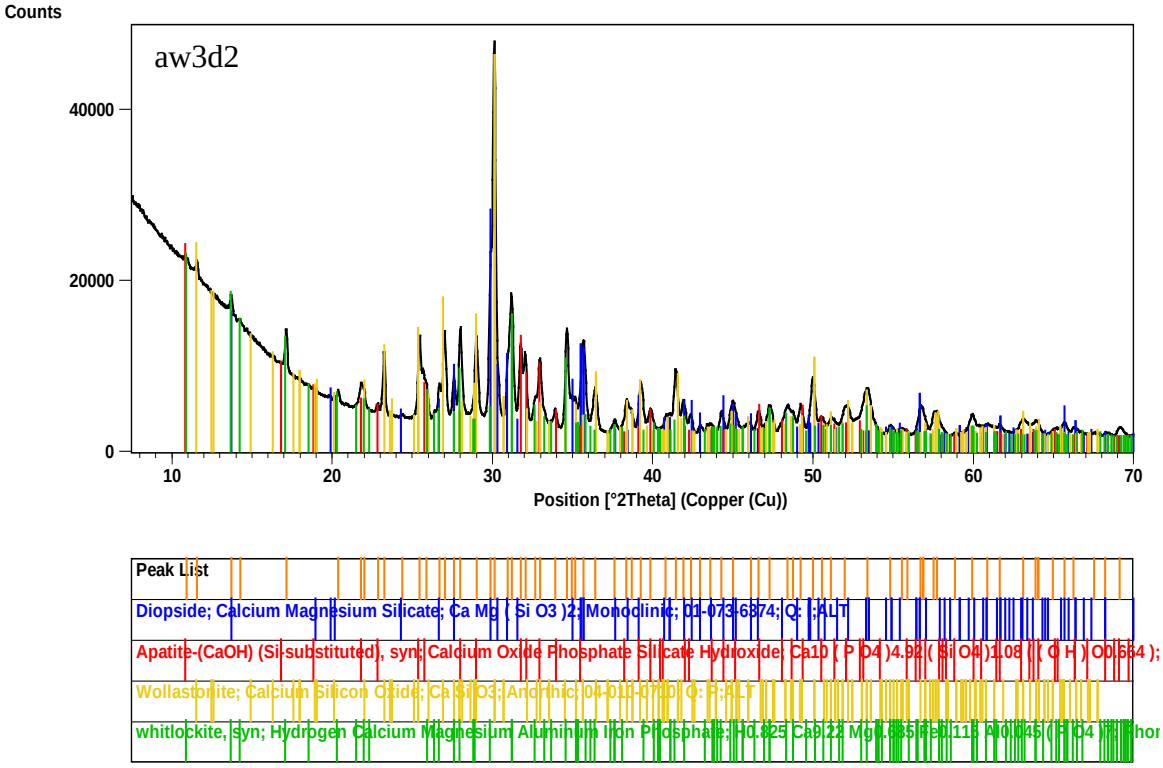

(a) XRD analysis using ICDD PDF2 (2009).

aw3d1

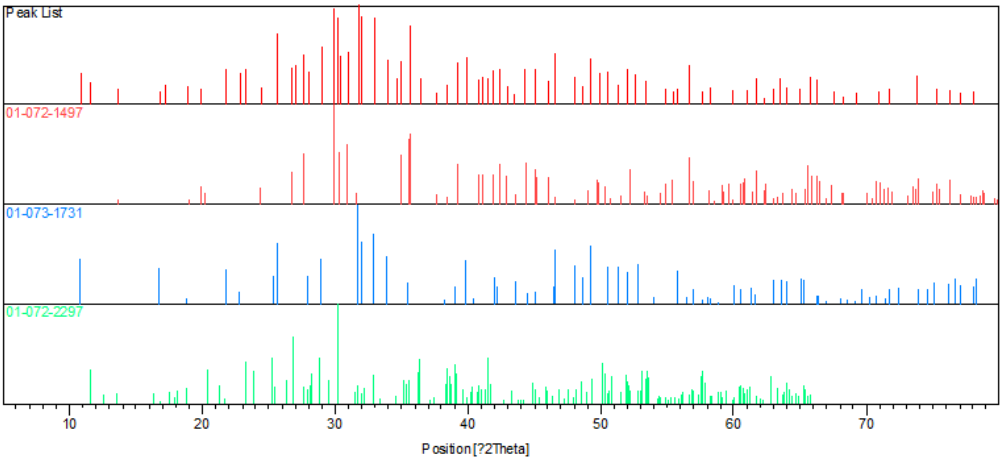

Ref. Code	Compound Name	Chemical Formula
01-072-1497	Diopside	Ca Mg Si2 O6
01-073-1731	Hydroxylapatite	Ca5 (P O4)3 (O H)
01-072-2297	Wollastonite 2\ITM\RG	Ca Si O3

Aw3d2

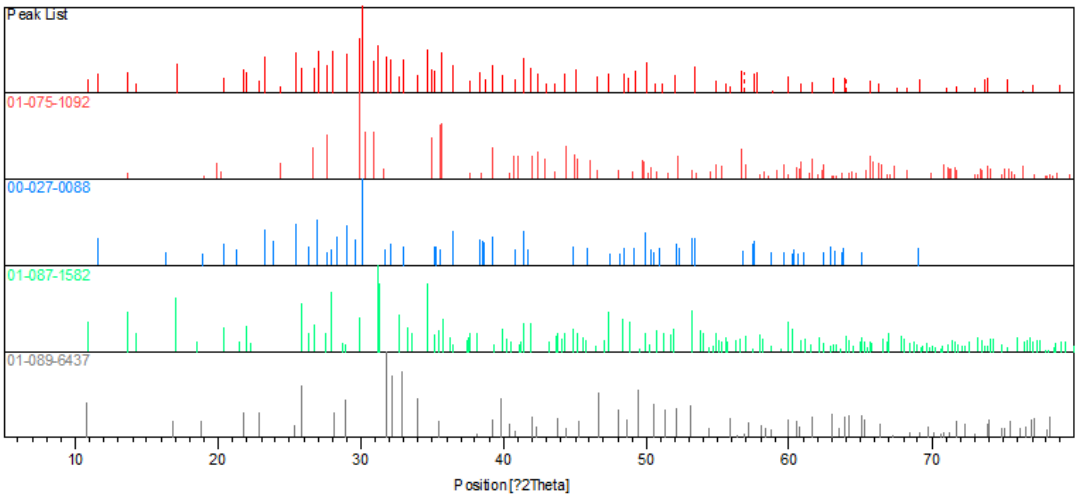

Ref. Code	Compound Name	Chemical Formula
01-075-1092	Diopside	Ca Mg Si2 O6
00-027-0088	Wollastonite-2\ITM\RG	Ca Si O3
01-087-1582	Calcium Magnesium Phosphate	(Ca2.589 Mg0.411) (P O4)2
01-089-6437	Hydroxylapatite, syn	Ca10.042 (P O4)5.952 (O H)2.292

(b) XRD analysis using ICDD PDF2 (2003)

Figure 4.17 XRD analysis using 2 different ICCD database for samples which used maltodextrine binder and PVA solution.

4.4 Discussion

To capture a more accurate reading of the printed specimens, four measurements of width and thickness along the span of each specimen were taken. Along the points of data captured, the dimensions for each point are different. The non-uniformity indicates that the range in AW particles size of up 53µm and binder saturation have a direct impact on the accuracy and surface morphology. Samples that were not sintered indicated that there were variations in the dimension as opposed to the CAD model. Shrinkage in the printed part geometry due to wetting in the powder materials, as well as the burnout of the maltodextrine compound, was observed. Furthermore, material shrinkage during printing led to a slight curling of the first few layers of the printed parts.

4.5 Conclusion

The indirect 3DP medium developed using AWGC-maltodextrine mixture with an in-house binder solution was successfully printed. With this medium, cost of printing 3D artefact for

patient specific implants can be reduced as the material used as binding agents were sourced from non-proprietary materials.

The accuracy of the obtained 3DP artefacts is statistically significant as the p-value is less than 0.05 (Table 4.6). Hence, this is a repeatable process for producing AW glass ceramic of 10x10mm (width by height) cross-section specimens with a standard deviation of less than ±0.2760mm in both width and thickness. Different shrinkage in the X, Y, and Z-direction normally are rectified by calibrating the AM machine with the prepared material and binder solution. This can be performed by 3D printing a benchmark artefact and compared it to the reference object.

The mechanical properties of AW glass ceramic produced by 3DP are lower than the result found in chapter 3. This different is attribute to the methods in preparation of the green parts for sintering in term of powder compaction as it can induce defect in the sintered parts (Shinohara et al., 1999). In addition, the rough surface texture produced from the binder jetting effect also decrease the strength of 3DP parts as rough surface induce micro cracks and flaws in the 3DP parts (de Jager et al., 2000, Fischer et al., 2003) .

.

Chapter 5: 3D Printed Moulds for Biopolymers

5.1 Introduction to Chapter

This chapter establishes a method for the creation of personalised polymer structures by sintering PLGA granules in a mould manufactured using the stereolithography process. The study of the fabrication route for a patient specific PLGA fixation plate has been performed in two parts. The initial part has been used to evaluate the manufacturing parameters, which was followed by rectangular specimen creation for assessing material and mechanical properties. In the final part, a mandibular geometry has been created in order to assess the ability to create physiologically shaped parts and the ability to maintain shape definition throughout the process.

Bioresorbable devices had been used in maxillofacial surgery to achieve the application of a biocompatible material. Studies have indicated that fractures of the mandible account for 36-70% of all maxillofacial fractures (Deogratius B.K et al., 2006, Lee, 2012). The fabricated fixation plate was customised to fit the geometry of the fractured mandible.

5.2 Material Characterisation

In order to establish operating conditions for the process, simple rectangular bars were made and their mechanical properties were measured. The rectangular bars were moulded using the mould manufactured by AM methods. Initial work focused on determining the temperature in selecting the mould material that would have to withstand the processing temperature and the AM methods for manufacturing it.

5.2.1 *Material and DSC Analysis*

This study used bioresorbable biopolymer PLGA materials obtained from Sigma-Aldrich in pellet form. The virgin pellets were in a range of sizes. Three different ratios of Lactide:Glycolide co-polymer were purchased and stored in the refrigerator before use as-is during the experiments. The three different ratios of PLGA used in this research have almost the same average molecular weight as shown in Table 5.1.

Table 5.1 Properties of Lactide:Glycolide co-polymer.

PLGA materials from Sigma-Aldrich	Co-polymer ratio	Average Molecular weight Mw	Inherent Viscosity dL/g
P2191	50:50	30,000-60,000	0.55 – 0.75
P2066	65:35	40,000-75,000	0.55 – 0.75
430471	85:15	50,000-75,000	0.55 – 0.75

A Mettler Toledo 823e differential scanning calorimeter was used to characterise the thermal properties; in particular T_g, of the biopolymers used in this study. The DSC test conducted used a 100µl Aluminium crucible that was placed in a heat flux cell. Nitrogen flow rate of 50ml/min as cooling medium was controlled with a Mettler FP90 controller connected to FP85 heat flux cell. A preheat run was performed to completely removed moisture before DSC analysis. The starting temperature was 25°C and ended at 125°C with 10°C increments. Data taken was synchronised to every 1 second. The DSC analysis was carried out with weights of approximately 5mg of PLGA, the weight of a single pellet. Analyses of the measured results indicate the biopolymer's glass transition temperature (Charles-Harris et al., 2007). The average glass transition temperatures obtained for the PLGA materials were from the DSC analysis.

Through DSC analysis, the main polymers glass transition temperatures T_g are evaluated as shown in figure 5.1. The T_g for PLGA 50:50, 65:35 and 85:15 range from 42°C to 65°C as shown in Table 5.2. This range matches with most PLGA glass transition temperatures (Armentano et al., 2010, Tai et al., 2010, Liu et al., 2002, Liu and Ma, 2004, Passerini and Craig, 2001).

Table 5. 2 Glass transition temperature of biopolymer PLGA.

PLGA	Range of Glass Transition Temperature, T_g (^{o}C)	Suggested Maximum Sintering Temperature (^{o}C)
50:50	42 to 50	60
65:35	44 to 60	70
85:15	48 to 65	75

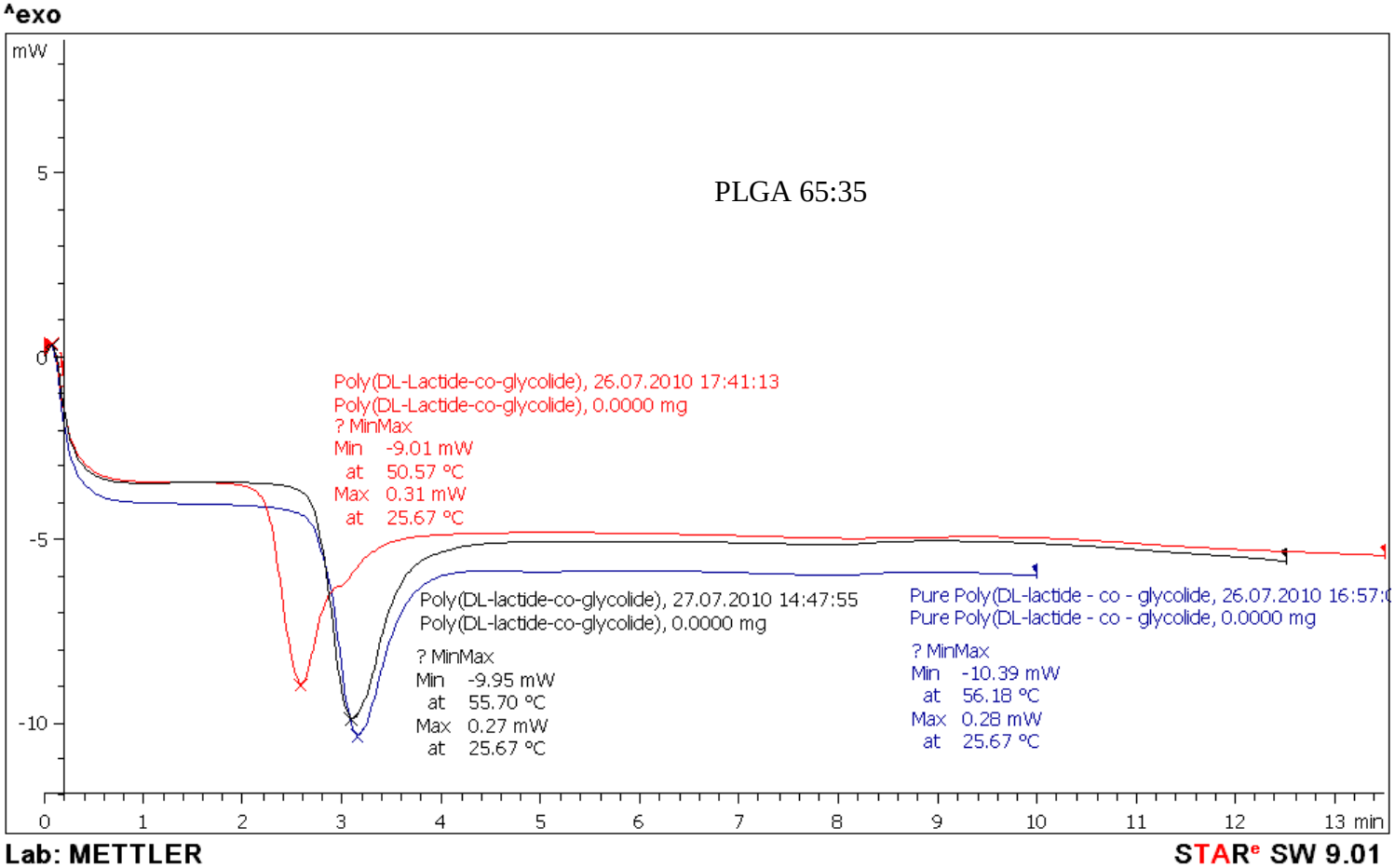
^exo
mW
5
0
-5
-10
PLGA 65:35
Poly(DL-Lactide-co-glycolide), 26.07.2010 17:41:13
Poly(DL-Lactide-co-glycolide), 0.0000 mg
? MinMax
Min -9.01 mW
at 50.57 °C
Max 0.31 mW
at 25.67 °C
Poly(DL-lactide-co-glycolide), 27.07.2010 14:47:55
Poly(DL-lactide-co-glycolide), 0.0000 mg
? MinMax
Min -9.95 mW
at 55.70 °C
Max 0.27 mW
at 25.67 °C
Pure Poly(DL-lactide - co - glycolide, 26.07.2010 16:57:
Pure Poly(DL-lactide - co - glycolide, 0.0000 mg
? MinMax
Min -10.39 mW
at 56.18 °C
Max 0.28 mW
at 25.67 °C
0
1
2
3
4
5
6
7
8
9
10
11
12
13 min
Lab: METTLER
STARe SW 9.01

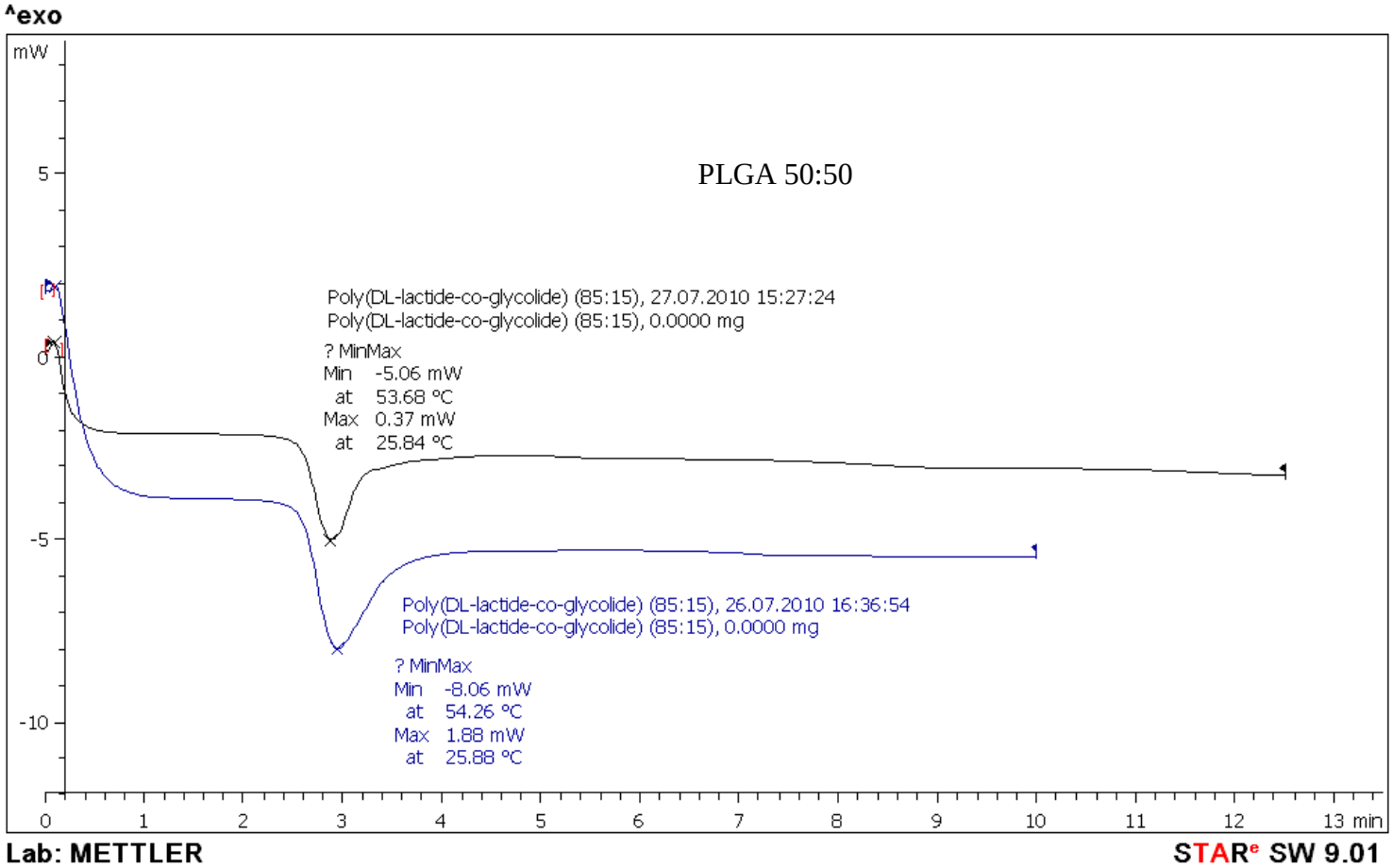
^exo
mW
PLGA 50:50
Poly(DL-lactide-co-glycolide) (85:15), 27.07.2010 15:27:24
Poly(DL-lactide-co-glycolide) (85:15), 0.0000 mg
? MinMax
Min -5.06 mW
at 53.68 °C
Max 0.37 mW
at 25.84 °C
Poly(DL-lactide-co-glycolide) (85:15), 26.07.2010 16:36:54
Poly(DL-lactide-co-glycolide) (85:15), 0.0000 mg
? MinMax
Min -8.06 mW
at 54.26 °C
Max 1.88 mW
at 25.88 °C
5
0
-5
-10
0 1 2 3 4 5 6 7 8 9 10 11 12 13 min
Lab: METTLER
STARe SW 9.01

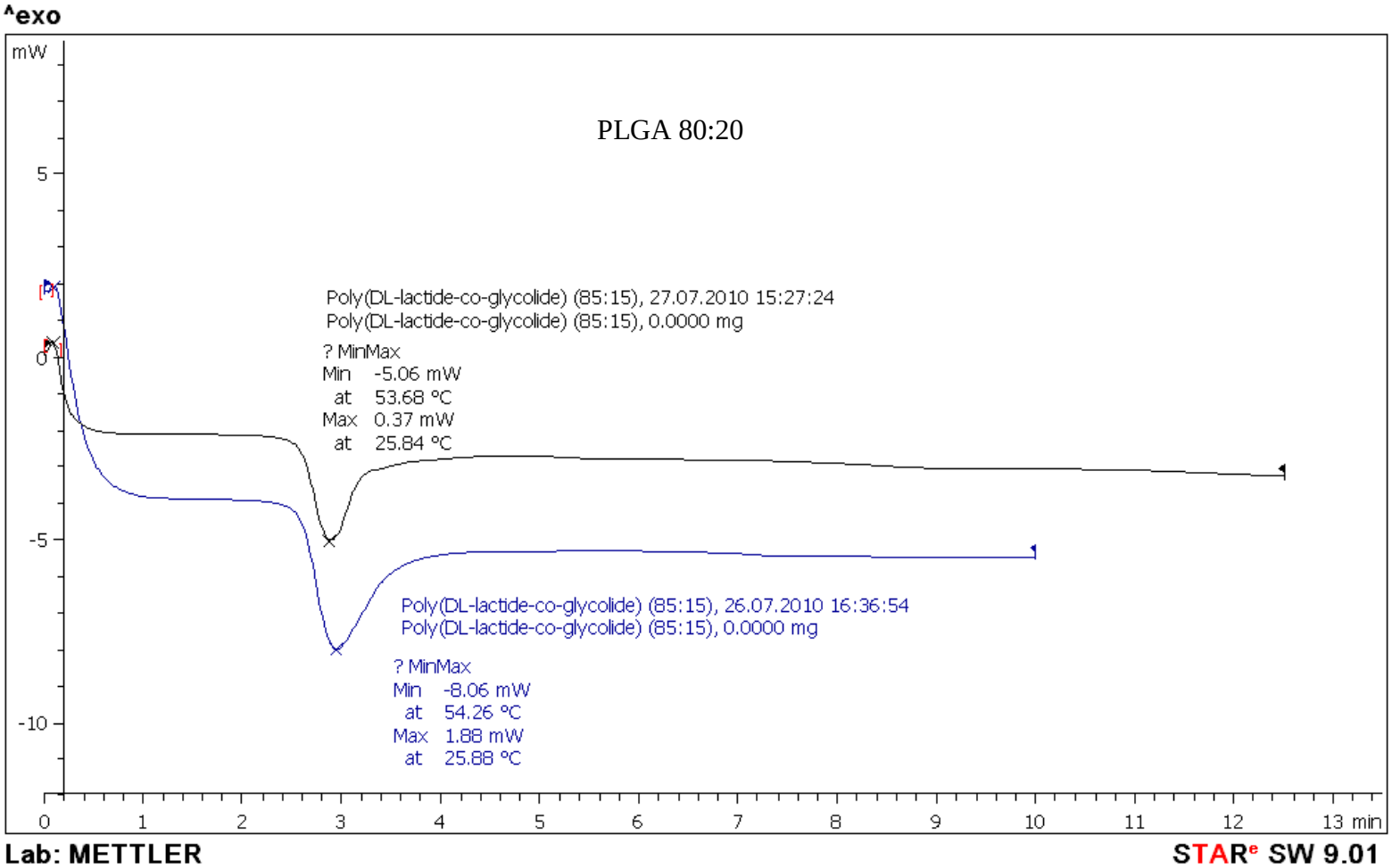
^exo
mW
PLGA 80:20
Poly(DL-lactide-co-glycolide) (85:15), 27.07.2010 15:27:24
Poly(DL-lactide-co-glycolide) (85:15), 0.0000 mg
? MinMax
Min -5.06 mW
at 53.68 °C
Max 0.37 mW
at 25.84 °C
Poly(DL-lactide-co-glycolide) (85:15), 26.07.2010 16:36:54
Poly(DL-lactide-co-glycolide) (85:15), 0.0000 mg
? MinMax
Min -8.06 mW
at 54.26 °C
Max 1.88 mW
at 25.88 °C
5
0
-5
-10
0
1
2
3
4
5
6
7
8
9
10
11
12
13 min
Lab: METTLER
STARe SW 9.01

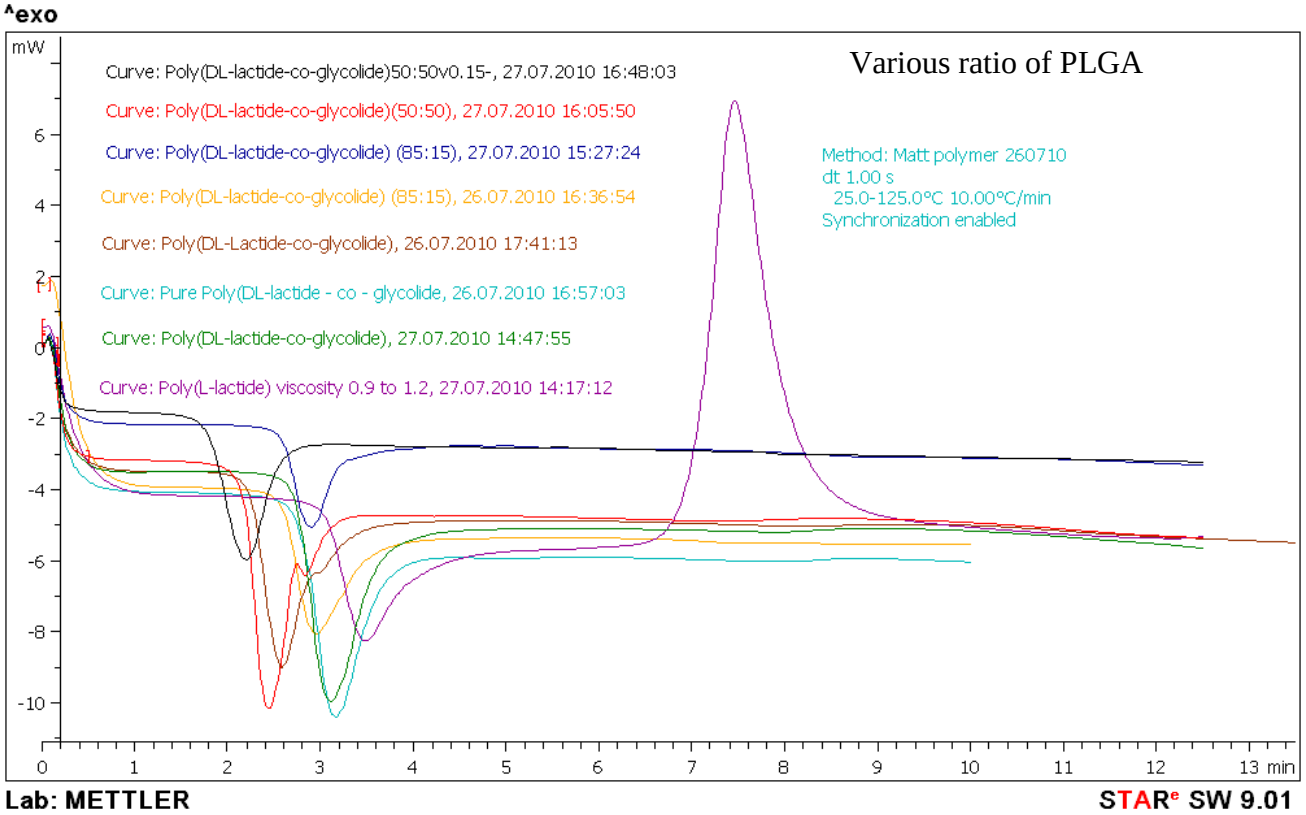

Figure 5.1 DSC analysis of various ratio of PLGA.

Based on this analysis, the SLA material selected for the mould was 18920 ProtoGen with UV and thermal post-cure as shown in Table 5.3. The selected material was used to produce a moulding assembly that can withstand temperature of up 97.5^{o}C. In the melt moulding process, the temperature that is suitable to use is between 5°C to 10°C above the T_g of biopolymer (Thomson et al., 1996). Hence, the fabrication temperature for PLGA 3D structure investigated was varied between 65°C-80°C (Table 5.2).

Table 5.3 Glass transition temperature of SLA material.

	WaterShed XC 11122	Somos 9420 UV	ProtoGen 18920 UV Post-cure	ProtoGen 18920 UV & Thermal Post-cure	Polypropylene
T_g	39-46°C	57-60°C	69°C	97.5^{o}C	41°C

5.3 Moulding Process Development

In order to determine the mechanical properties of the sintered PLGA, test specimens were produced using the modified melt moulding procedure. Instead of melting the PLGA granules inside the mould as carried out in melt moulding process, the granules are heated above the glass transition temperature by about 5%-10% which is below the melting temperature of PLGA. In this fabrication process, parameters for sintering temperature, holding time and load on moulding system were varied in order to achieve an optimum setting in the process. This setting would produce sintered structure with suitable mechanical strength and chemical consistency. Figure 5.2 list the steps used in processing the test specimens. Test specimens were moulded using SLA moulds produced by Paragon Rapid Technologies Limited UK. Mould release agent Ambersil; obtained from RS Components UK, was applied to the mould to ease the release of the moulded test specimens. The PLGA pellets were placed manually inside the SLA mould cavities (Figure 5.3). Each of the cavities measured 5mm by 2mm by 40mm in width, height and length. There are five cavities in total. The design of the mould is as shown in figure 5.3b.

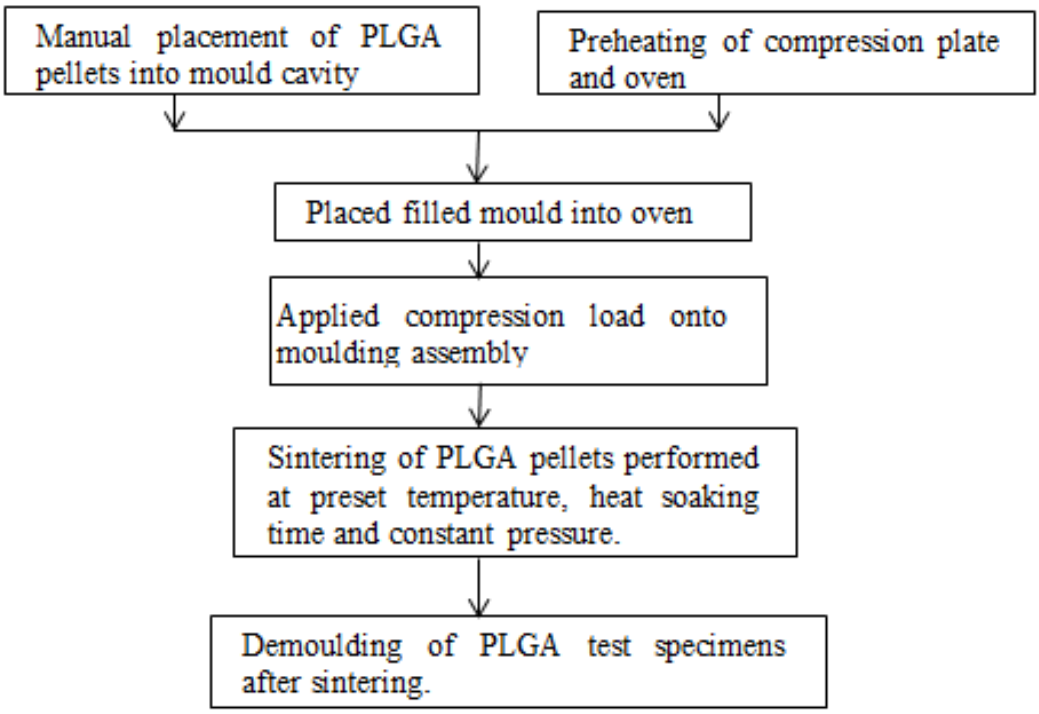

Figure 5.2 Processing of PLGA Specimens

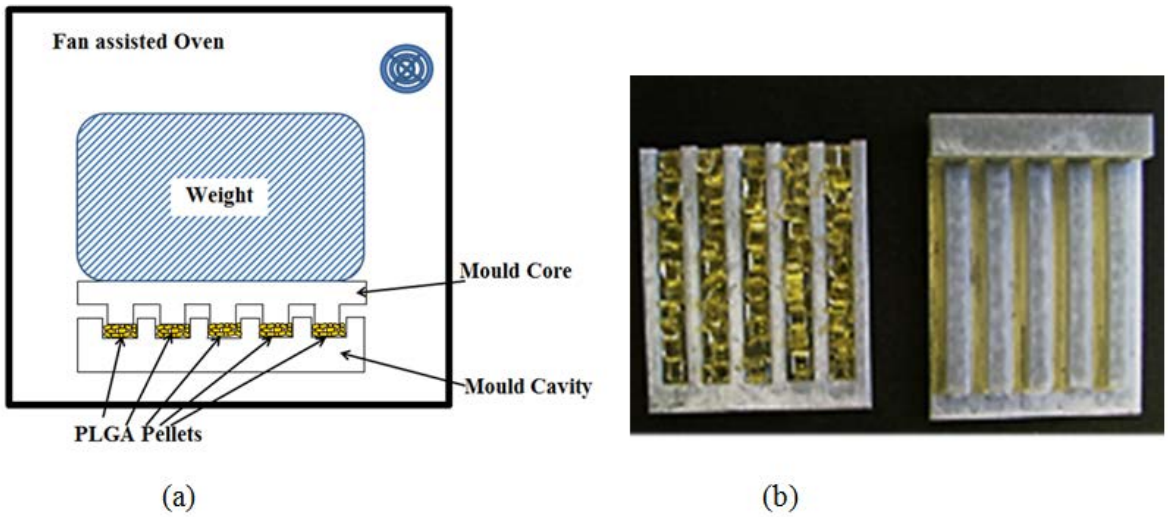

Figure 5.3 (a) SLA mould in the heating setup and (b) PLGA pellets in SLA mould.

5.3.1 *Load and Temperature Combination Optimum Process Setting*

A fan-assisted oven from BINDER GmbH was used to preheat the heating chamber together with the compression weight. Then the completely filled mould was placed inside the oven, and compression weight was applied onto the mould assembly. Heat was applied to the

moulding assembly to above the glass transition temperature of PLGA and the assembly heat soaked before the heater was switched off to allow the oven chamber to cool down at its natural rate to room temperature. The sintering process followed a predefined heating profile. Once the filled mould was at room temperature, the test specimens were de-moulded. The specimens were removed from the mould using tweezers.

Based on the result of T_g for PLGA used; as shown in Table 5.2, an initial value of 65°C was predefined as the sintering temperature for this investigation. The load used for all three different ratios PLGA was varied between 7lbs (3.2kg) to 15lbs (6.8kg) for the specimens. The result in Table 5.4 shows that in the 1st to the 4th columns, the process was unsuccessful. Picture in column (a) and (b) show the necking region of PLGA pellets while in columns (c) and (d) the sintering of PLGA pellets was without visible necking region on the specimen but with some incompleteness to the specimens. Subsequently the temperature was increased to between 70°C to 80°C. With a temperature of 73°C, PLGA specimen was successfully fabricated as shown in the last column in Table 5.4. Therefore, all following fabrication processes of PLGA pellets was sintered using the heating profile as shown in Figure 5.4. Sintering of PLGA pellets was performed by placing into a mould and heated at 73°C for 2 hours with an applied weight of 15lbs$_f$ to the moulding system, which is equivalent to 9.7psi or 0.7bar. The mould is left in the sintering oven to cool to room temperature before de-moulding.

Table 5.4 Results of different parameter settings in melt moulding of PLGA pellets.

PLGA	Load =7lbs Heat Soaked =1.5hrs	Load=7lbs Heat Soaked =2.5hrs	Load=10lbs Heat Soaked =2hrs	Load=12lbs Heat Soaked =2hrs	Load=15lbs Heat Soaked =2hrs
specimens					
	(a)	(b)	(c)	(d)	(e)

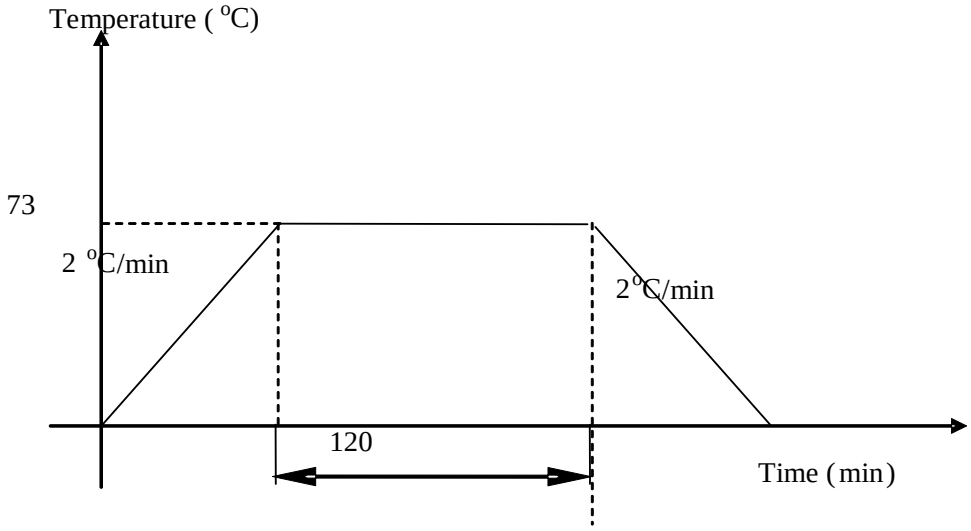

Figure 5.4 Heating profile for the sintering process of PLGA.

5.3.2 *Evaluation and Analysis*

Three point bending test of specimens were used to obtained the mechanical properties of PLGA. The three point bending test was conducted on an Instron 5567 universal testing machine with Bluehill® Software, Instron UK. The test was conducted using a load cell of 1kN with loading speed of 0.5mm/min. Testing was based on BS EN ISO 178:2010 (BSI, 2011). The layout of the test is as shown in figure 5.5.

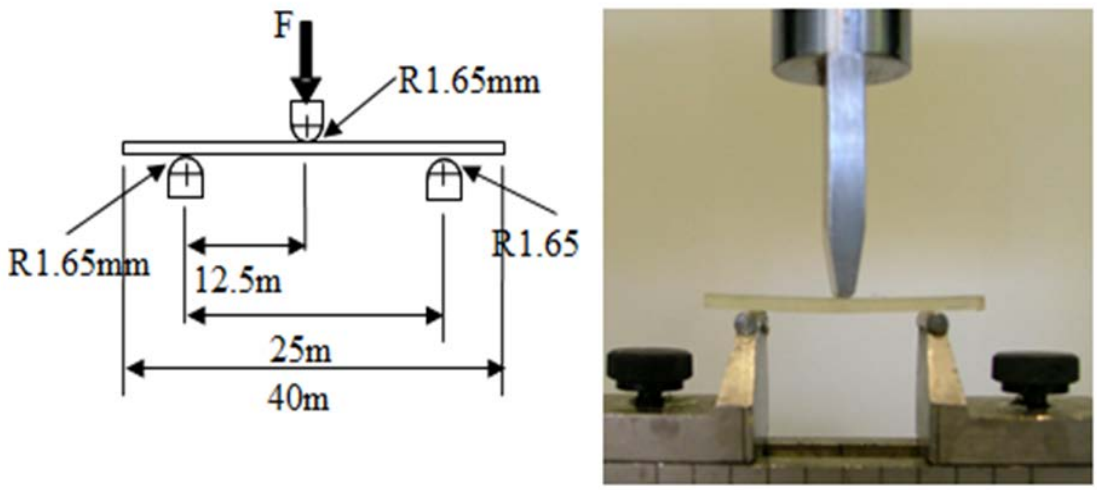

Figure 5.5 Bending test diagram and the actual test on a universal testing machine rig.

Motic microscopes with Motic Images Plus 2.0 software from Speed Fair Co. Ltd, Hong Kong and Cambridge Stereoscan 240 SEM machine were used to investigate the morphology of specimen surface and fracture surface at failure in bending test. Investigation on the type of bending failure in the sintered test specimens were based on images from both analysis methods; using microscopy and SEM analysis. In SEM analysis, specimens were gold coated prior to analysis. Further DSC analyses were performed to ensure that the fabrication route does not significantly alter the PLGA.

Statistical analysis was performed using t-test with values of $p<0.05$ to indicate statistical significance. All calculations were made using Microsoft Excel 2010 Data Analysis Tools.

5.3.3 *Results*

In total, ten rectangular test specimens for each different PLGA ratio of co-polymer are fabricated from the SLA mould that has five cavities measuring 5mm x 2mm x 40mm each. All measurements for each different PLGA ratio of co-polymer specimens were taken (refer appendix B5) and the range of thickness and width for the specimens are from 1.869mm to 2.924mm and 5.027mm to 5.267mm respectively.

The overall length is 40mm for all the specimens and the span length in the three points bending test is 25mm. The mechanical test is based on 3-point bending testing procedure of BS EN ISO178:2010 (BSI, 2011) and was conducted for all 30 specimens. The results are as shown in figure 5.6 and table 5.5.

The equations used are as follows: -

Flexural Strength is-

$$\sigma_f = \frac{3FL}{2bh^2}$$

where σ_f is flexural strength, in megapascals (MPa);

F is applied force, in newton (N);

L is the span, in millimetres (mm);

b is the width, in millimetres(mm);

h is the width, in millimetres(mm).

and

Flexural Modulus is: -

$$E_f = \frac{\sigma_{f2} - \sigma_{f1}}{\varepsilon_2 - \varepsilon_1}$$

where E_f is flexural modulus, in gigapascals(GPa);

σ_{fi} is flexural strength at point of deflection, in megapascals(MPa);

ε_i is strain at point of deflection.

From figure 5.6(a), (b) and (c), all PLGA ratios exhibited a linear relationship of stress-strain up to a strain value of 0.015. Specimens give a maximum yielding stress and then break before the conventional deflection. Since the maximum flexural stress and the breaking stress are far apart with a plateau stating at strain value of 0.03mm/mm in most specimens, the specimens' failure types of the three PLGA's ratio are considered to be plastic failure mode. The fracture images are as shown in figure 5.7.

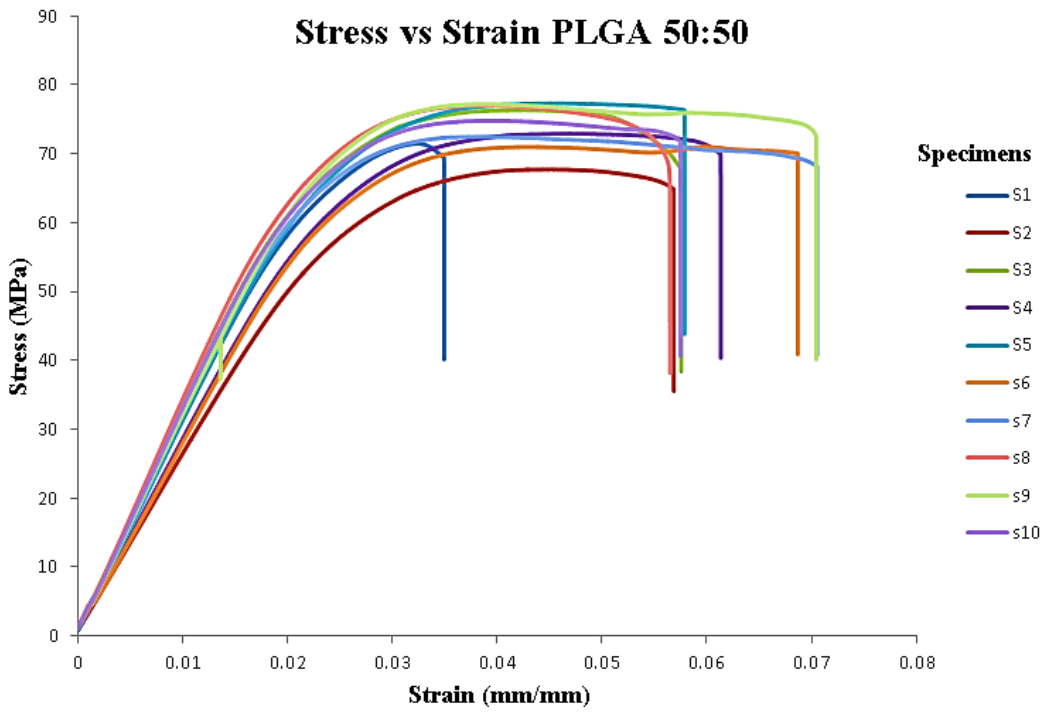

(a)

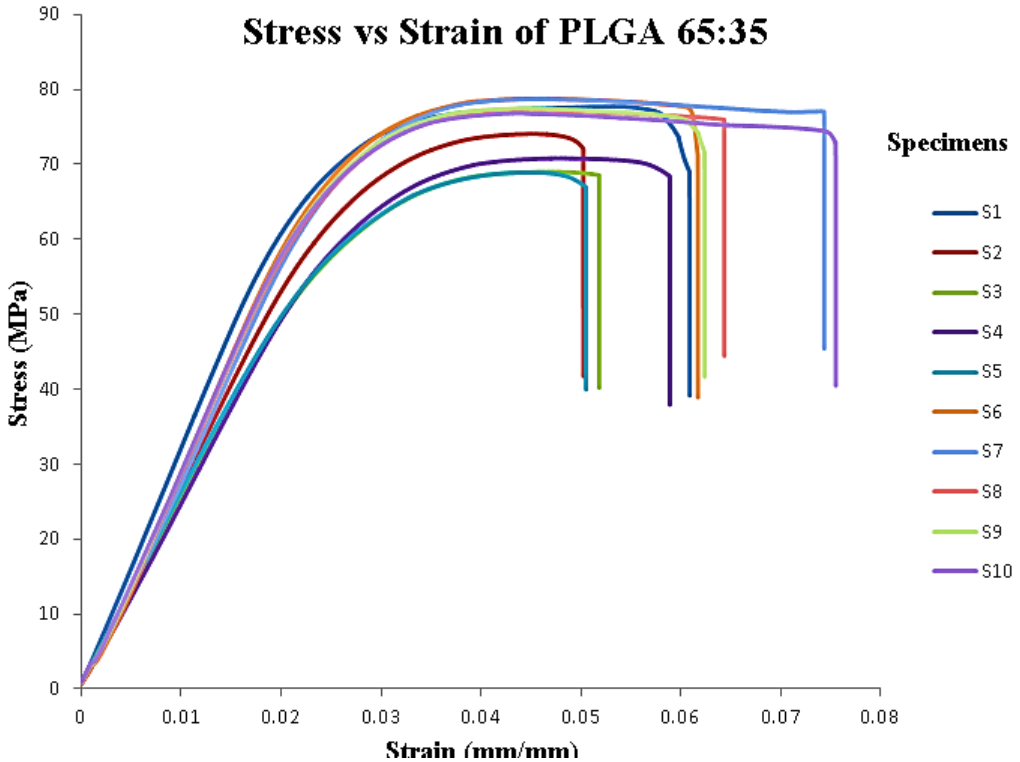

(b)

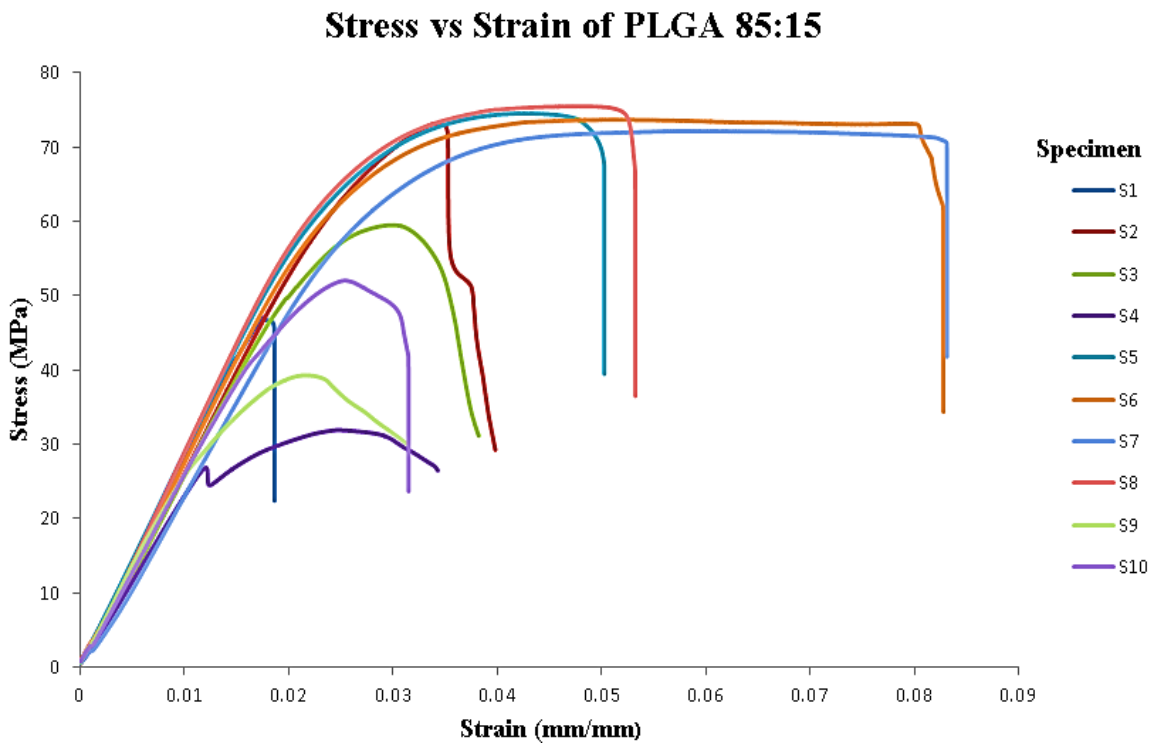

(c)

Figure 5.6 Stress-Strain curves of PLGA co-polymers.

Table 5.5 Statistical Analysis for Mechanical Properties of PLGA fabricated under heating profile and load of 15lbs (6.8kg) as described in 5.3.1.

PLGA		Thickness h (mm)	Width b (mm)	Max. Flexural Load F_{max} (N)	Deflection at Max. Flexural Load δ_{max} (mm)	Flexural Modulus E (GPa)	Flexural Strength σ (MPa)
50:50	Mean $\overline{x}$	1.9941	5.059	36.4799	2.74166	3.05642	73.8465
	Standard Error(SE)	0.032	0.010	1.9607	0.24193	0.08345	1.02495
	Median	1.96	5.046	33.3365	2.61964	3.12785	73.8709
	Standard deviation (SD)	0.1002	0.032	6.2003	0.7651	0.2639	3.2412
	Minimum	1.869	5.027	31.012	1.79839	2.54449	67.742
	Maximum	2.209	5.129	47.814	4.53176	3.40505	77.3431
	n	10	10	10	10	10	10
	DOF	9	9	9	9	9	9
	Critical value	2.26	2.26	2.26	2.26	2.26	2.26
	CL 95%	0.0717	0.023	4.435476	0.54728	0.18878	2.3186
65:35	Mean $\overline{x}$	2.1121	5.064	45.2063	2.40741	2.85153	74.97068
	Standard Error(SE)	0.0197	0.008	1.1351	0.11943	0.08139	1.250328
	Median	2.116	5.073	46.7375	2.25753	2.92338	77.0258
	Standard deviation (SD)	0.0622	0.027	3.5896	0.37767	0.25737	3.953883
	Minimum	2.026	5.027	38.004	2.15496	2.51046	68.9448
	Maximum	2.213	5.097	48.431	3.41576	3.19789	78.7849
	n	10	10	10	10	10	10
	DOF	9	9	9	9	9	9
	Critical value	2.26	2.26	2.26	2.26	2.26	2.26
	CL 95%	0.0445	0.019	2.5678	0.27017	0.18411	2.828437

85:15	Mean $\overline{x}$	2.5442	5.118	50.8887	1.5632	2.6498	59.8873
	Standard Error (SE)	0.0691	0.021	5.3214	0.1901	0.0638	5.1744
	Median	2.576	5.110	51.3885	1.4543	2.6747	65.8316
	Standard deviation (SD)	0.2185	0.067	15.4650	0.6018	0.2017	16.3628
	Minimum	2.159	5.036	31.097	0.7257	2.2604	31.9156
	Maximum	2.894	5.267	70.643	2.3758	2.9183	75.5009
	n	10	10	10	10	10	10
	DOF	9	9	9	9	9	9
	Critical value	2.26	2.26	2.26	2.26	2.26	2.26
	CL 95%	0.1563	0.048	12.0379	0.4304	0.1443	11.7053

The results of the basic statistical analysis with the confidence intervals are presented in Table 5.5 and the p-value<0.5, t-test results in Table 5.6.

The confidence interval in repeating the manufacturing of the specimen is as calculated using p-test with t-distribution. As shown in Table 5-5, there is no significant variation in terms of dimensions and mechanical properties of PLGA test specimens using the fabrication process. However, for PLGA 85:15 the interval estimate for dimension and flexural strength are higher than PLGA 50:50 and PLGA 65:35.

The average thickness and width are in a range of between 1.994 mm to 2.544 mm and 5.059mm to 5.125mm, respectively. The flexural modulus and flexural strength ranges from 2.650GPa to 3.056GPa and 59.887MPa to 73.847 MPa, respectively (Table 5.6). The result for fracture modulus is as comparable to PLGA parts produced using solvents (Armentano et al., 2010).

Table 5.6 Mean value for 95% confidence interval for sintered test samples of PLGA.

Ratio of PLGA co-polymer	Glass transition temperature T_g (^oC)	Dimension		Flexural Modulus (GPa)	Flexural Strength (MPa)
		Thickness (mm)	Width (mm)		
50:50	42-55	1.994±0.072	5.059±0.023	3.056±0.189	73.847±2.319
65:35	44-60	2.112±0.045	5.064±0.019	2.852±0.184	74.971±2.828
85:15	48-65	2.544±0.156	5.118±0.048	2.650±0.144	59.887±11.705

In order to understand further the behaviour of PLGA co-polymers during three points bending test, images are captured at bending fracture failure surface. The distance of tension from surface before failure is about 35μm (Figure 5.7). Images also showed the pellets region A (smooth surface) and material consolidation region B experiencing ductile failure (crystal-like surface) as indicated in figure 5.7.

SEM analysis of the test specimens at outer surface show that the specimens' are fully consolidated (Figure 5.8). The surface texture of the specimens consists of the negative impression of the mould surface as well as the overlapping cause by movement of the PLGA co-polymers relative to the mould walls. In figure 5.9, the fracture surface displays the cause of fracture failures that begin with craze having level brittle failures bands and splintering chips. Both PLGA 50:50 and 85:15 showed signs of micro-crack lines as indicated from images using 10000X magnification (Figure 5.9.)

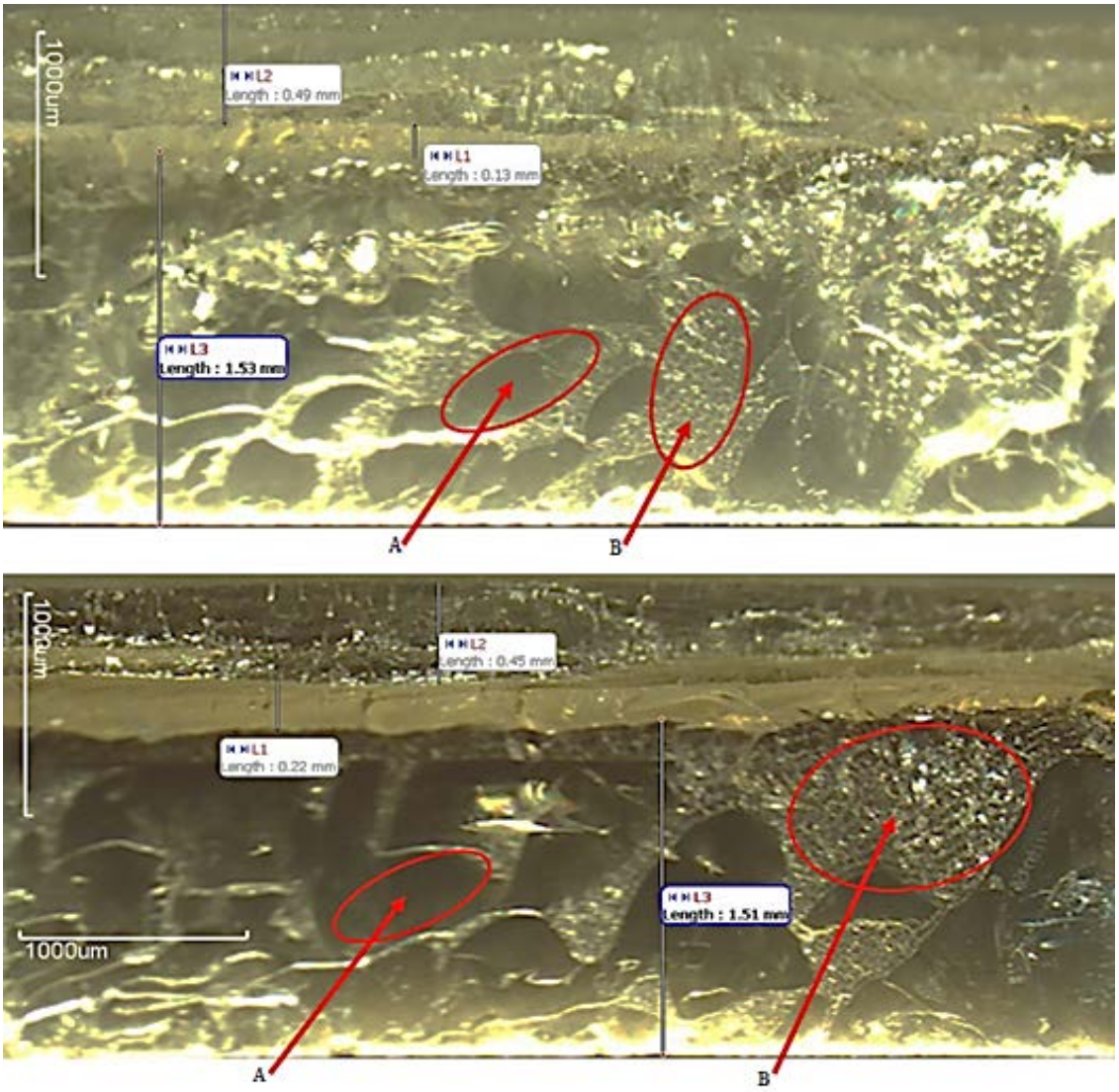

Figure 5.7 Fracture of PLGA 50:50(above) and PLGA 65:35 (below) obtained from bending test showing the region of tension at the top with craze.

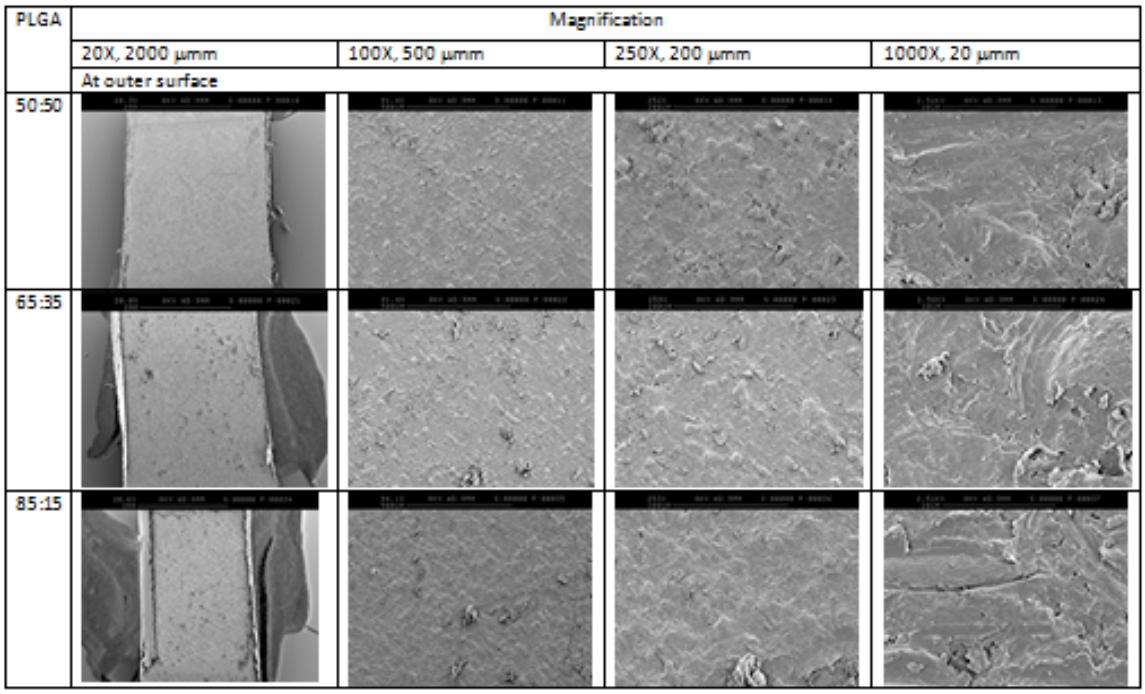

Figure 5.8 SEM images at outer surface of specimens.

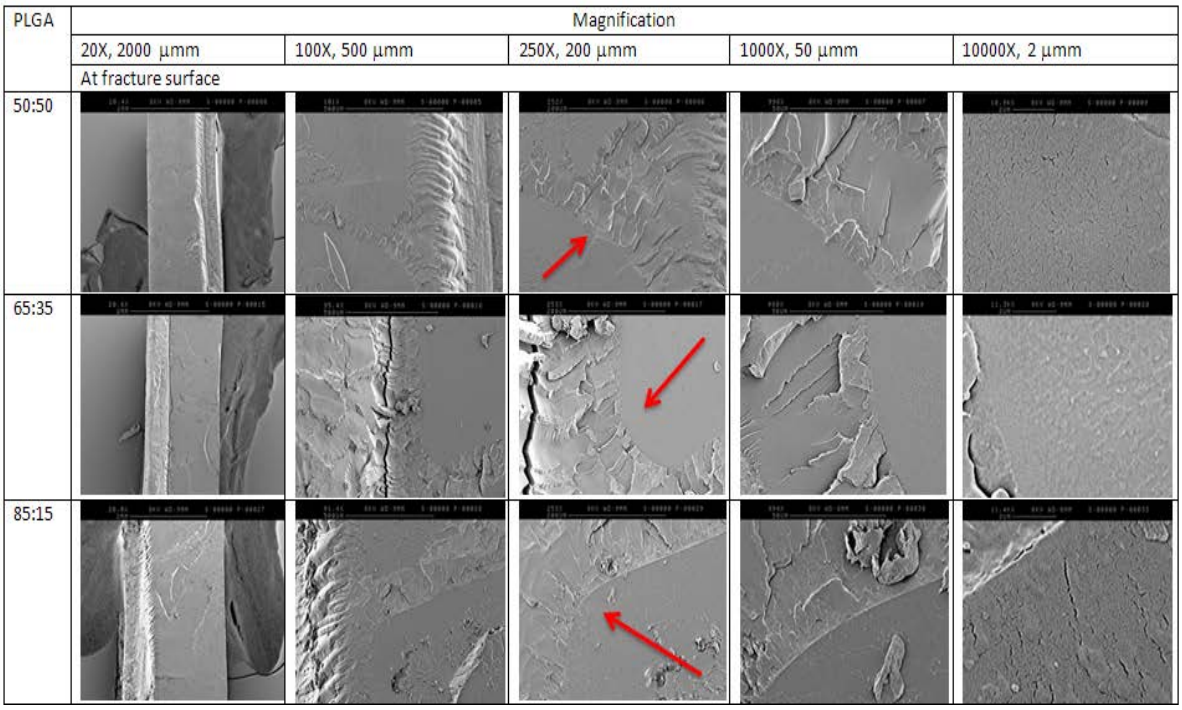

Figure 5.9 SEM images at fracture surface from 3 point bending test.

5.3.4 *DSC Evaluation of material after fabrication process*

Comparison of both virgin PLGA as received and sintered PLGA for all three different ratios were performed using DSC. Three cycle analysis were carried out in which the surface area under the curve of DSC thermograms for both the 1st and 2nd cycle does not show any significant variation in total energy between virgin and sintered PLGA. The integral of all the thermograms in sintered PLGA show a different of less than 10% (Figure 5.10). This indicated that the processing route does not alter the properties of PLGA. It can be concluded that the sintering temperature profile with applied pressure had not altered the biopolymer, similar with the findings of Rothen-Weinhold et al using melt-manufacturing by extrusion or injection (Rothen-Weinhold et al., 1999).

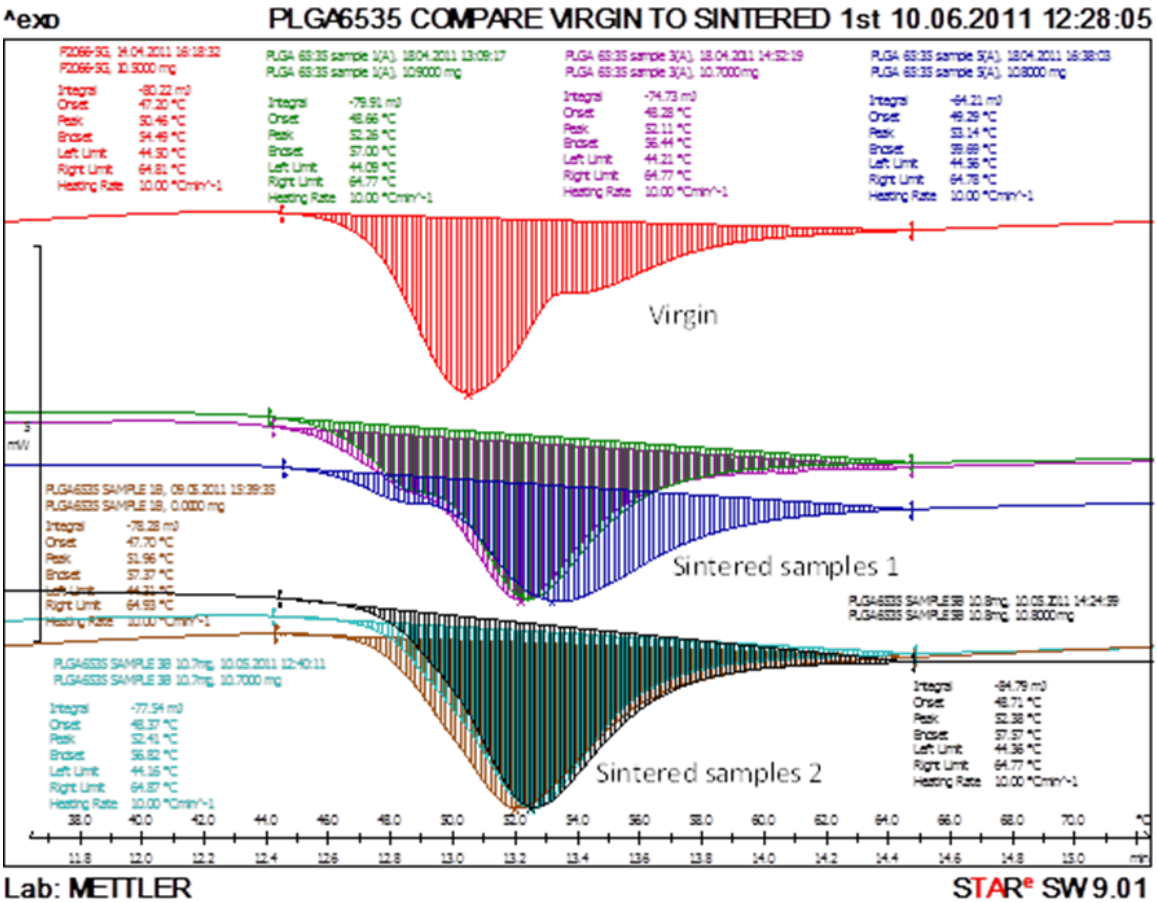

Figure 5.10 Comparison of virgin to sintered PLGA 65:35.

5.4 Case Study

In order to establish the feasibility of this proposed route of manufacturing 3D biopolymer structure using mould printed with stereolithography, a case study on the mandible fracture fixation method was proposed. The patch was designed as an alternative solution to the normal practice of fracture fixation using standard off the shelf plate.

5.4.1 *Specific Case Study Background*

Mandibular fracture is one of the most common injuries to patients who suffer facial trauma. 50% of patients admitted to hospital with facial trauma require surgery to repair fractured mandible (Kar and Mahavoi, 2012, Sakr et al., 2006, Iida et al., 2003, Iida et al., 2001, Ellis Iii et al., 1985). The most common site of most mandible fractures due to trauma is at the mandibular angle and mandibular body (Kostakis et al., 2012, Natu et al., 2012, Sakr et al., 2006, Navarro et al., 2004, Iida et al., 2001) although fractures can occur anywhere in the mandible as shown in figure 5.11. Rectification of defective bone structures due to trauma has benefited from the introduction of mostly rigid metal prostheses. However, the high stiffness of metal implants can cause stress shielding in bone restoration due to mismatch of material properties.

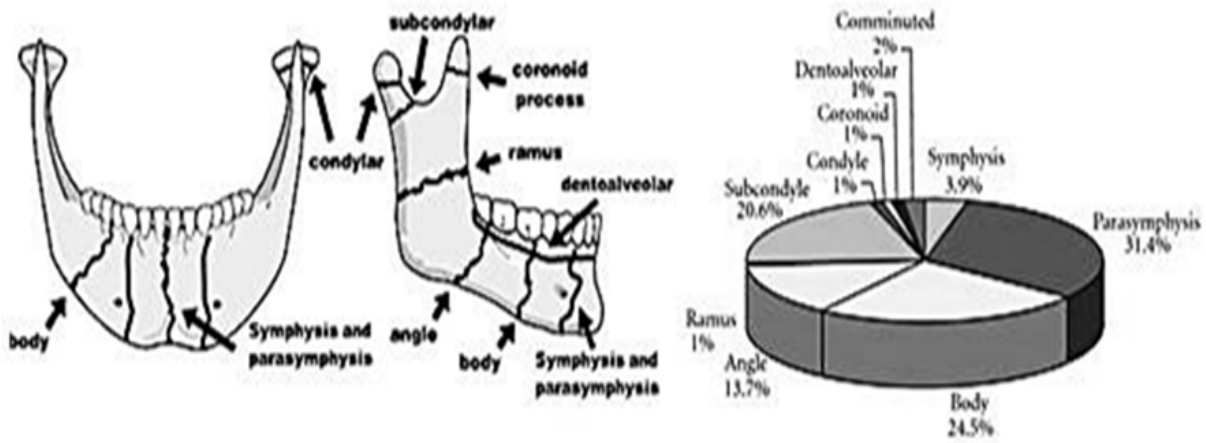

Figure 5.11 Fracture Occurrence for Regions of the Mandible (Natu et al., 2012).

In the management of mandibular fractures, general treatment strategies depend on the age and anatomical site. Adults and children require a different approach in the treatment of

mandibular fractures. Similarly, fractures at different anatomical sites in the mandible need different treatment since they differ in their biomechanics and complications.

Surgical repair of mandibular fractures is the most effective method of restoring normal anatomy. The goals of a mandibular fracture repair include the recovery of pre-injury jaw structure and restoration of normal function through a solid bony union at the fracture site. This bony union can be achieved by preventing infection and by a suitable period of immobilization (Fedok et al., 1998). Open Reduction with Internal Fixation (ORIF) is currently the preferred method for mandibular fractures treatment (Bouloux et al., 2014, Bhagol et al., 2013, Chrcanovic, 2012, Lovald et al., 2010, Alkan et al., 2007, Ellis Iii, 1999). ORIF refers to the fracture site been surgically exposed for access and metal plates are affixed directly to the bones by way of metal bone screws. These metal plates align the fracture site and provide fixation during the healing process. Figure 5.12 shows a bone plate after placement in an ORIF procedure.

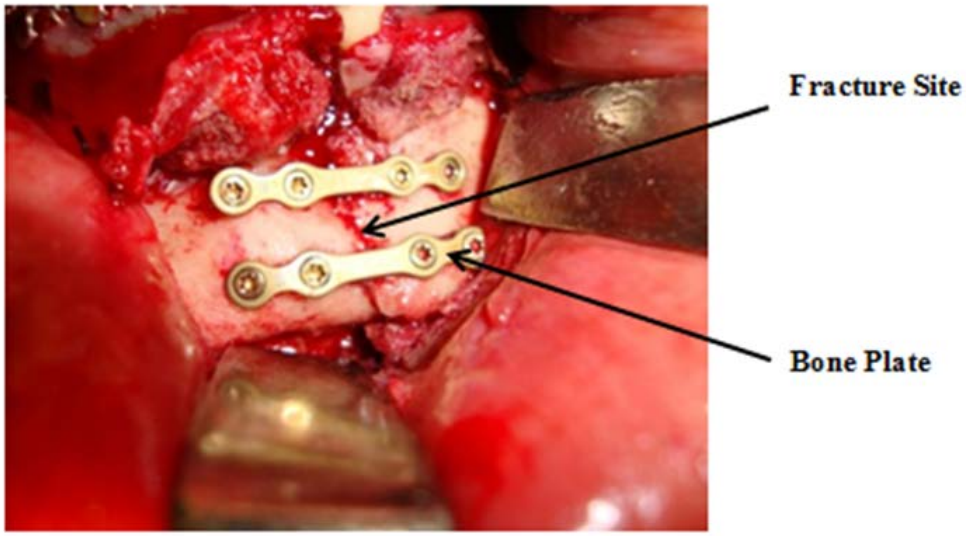

Figure 5.12 Bone Plate Used in an Open Reduction Internal Fixation Procedure(ORIF) (Bhagol et al., 2013).

Complications associated with mandibular fracture treatment include perioperative complications and postoperative complications. These include plate breakage during bending, drill breakage during drilling, screw head stripping and breaking during insertion, screw failure and the need to use emergency screws, dropping of micro-material in the operative field, inappropriate insertion of screws in anatomic structures such as tooth roots or nerves,

infection at the fracture site, exposed hardware, improper location of screws and plates, dislocation of bone parts fixed using micro-plates and palpability of the implanted material (Duygu et al., 2007, McDermott et al., 2004, Zhang, 2004, Goodacre et al., 2003, Goodacre et al., 1999) . In addition; once the bone has healed, difficulties can occur during the second operation to remove the metal implants, screws, plates, and rods where screw head stripping and screw or plate breakage can happen. All these drawbacks have driven the development of bioresorbable materials as a possible replacement for metallic devices. Bioresorbable bone plate must be mechanically functional in order for the fracture to heal before the plate resorbs. The degradation time of biopolymers ranges between 1 month to greater than 24 months depending upon the formulation and composition of the biopolymers (Sabir et al., 2009). Polylactide and polyglycolide, as well as copolymers polyglycolide-co-polylactide and poly(L-lactide-co-D,L-lactide) (P[L/DL]LA) are most often used in the manufacturing of bioresorbable plates and screws which follow the conventional method of fracture fixation, which still retain some of the integral complications of ORIF. This case study tried to address the complication in attaching fracture plate to the fracture site and propose fracture plate fixation by adhesive bonding.

5.4.2 *Design and AM manufacturing of Patch Moulding System*

The steps in the modelling start with the acquisition of a 3D computer model in stereolithography (STL) format of a mandible. This file was obtained from 3DSystems, USA; a supplier of AM system. A fixation patch was design for a simulated fracture on the body region of the mandible as this is indicated to be the most likely region of fracture in the mandible (Kostakis et al., 2012, Natu et al., 2012, Fridrich et al., 1992). Figure 5.13 shows the process flow in designing the moulding system.

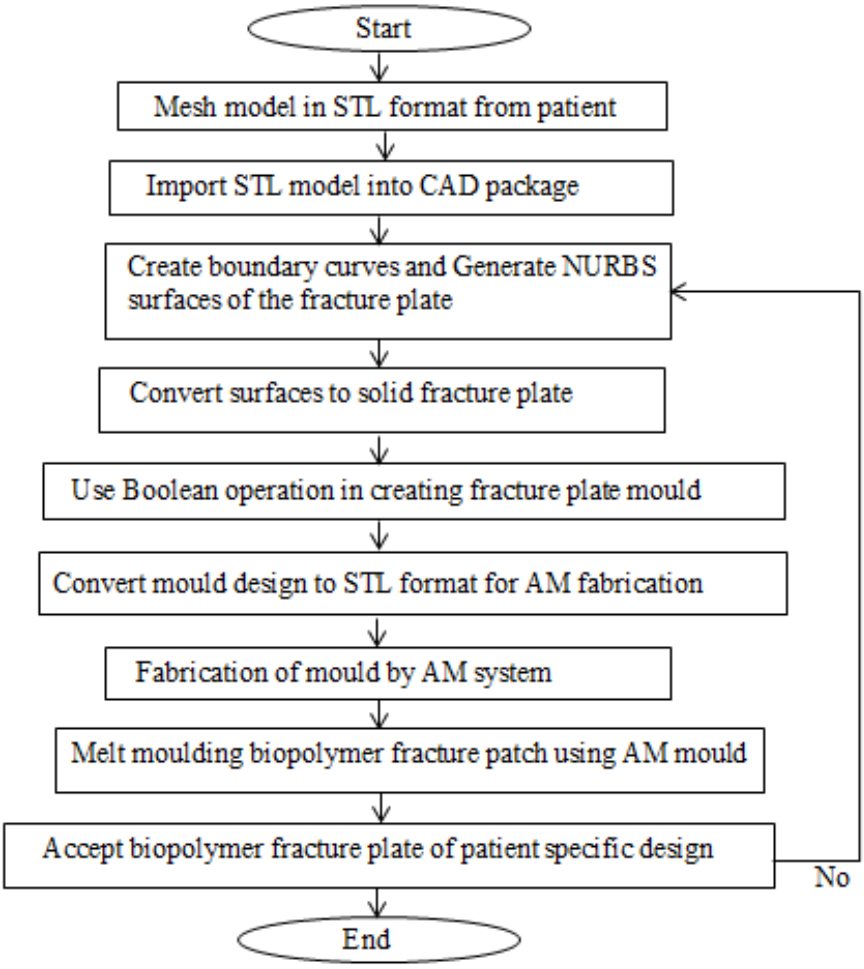

Figure 5.13 Process flow in design and manufacture of moulding for customised fracture patch.

CAD modeller Rhino 4 with RhinoReverse was used in designing the fixation patch. The surface geometry of the site was reverse engineered using RhinoReverse (Figure 5.14) from the STL model of the mandible. The STL file was imported into Rhino 4 as a mesh model. In order to reduce the design time for the surface patch, RhinoReverse was used to generate NURBS curves. Using the RhinoReverse RRLoadMesh and RRCommit, Rhino mesh object was imported, and the closed curve polylines were converted to a surface patch. The surface geometry of the fracture site was then used to generate solid CAD model of the patch using Rhino SolidExtrude (Figure 5.14).

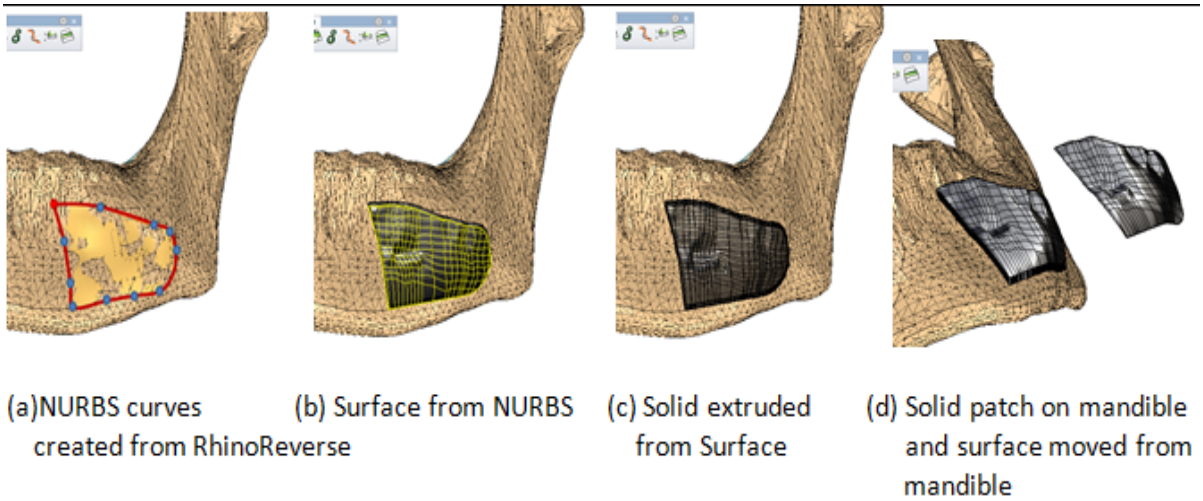

Figure 5.14 Step in reverse engineered the fracture patch.

The geometry of the patches (Figure 5.15); which was customised to the shape of high occurrence fractured site, was then fabricated using FDM method. The CAD model of the patch was translated into STL format. In order to produce a watertight STL file for AM, several sequence of Rhino command was performed. The sequence involved mesh reduction as well as mesh repairs involving holes and gaps repair, mesh welding, and mesh unify which can be accomplished by manually selecting the mesh or by using features of mesh repair in the software. The validity of a watertight mesh was performed using Rhino SelNakedMeshEdgePt. When the mesh was verified to be watertight, the patch was translated in an STL format file using the option of binary translation to produce smaller file size as compare to using ASCII option for STL translation.

The file is later imported into Stratasys Dimension SST768 fused deposition machine. CatalystEX software verified and processed the STL file into a CMB file. The Dimension SST768 printer used the file for 3D printing. A layer thickness of 0.33mm was selected, and commercial ABS plastic was used during the fabrication. The printed patches were used for form fitting purpose (Figure 5.16).

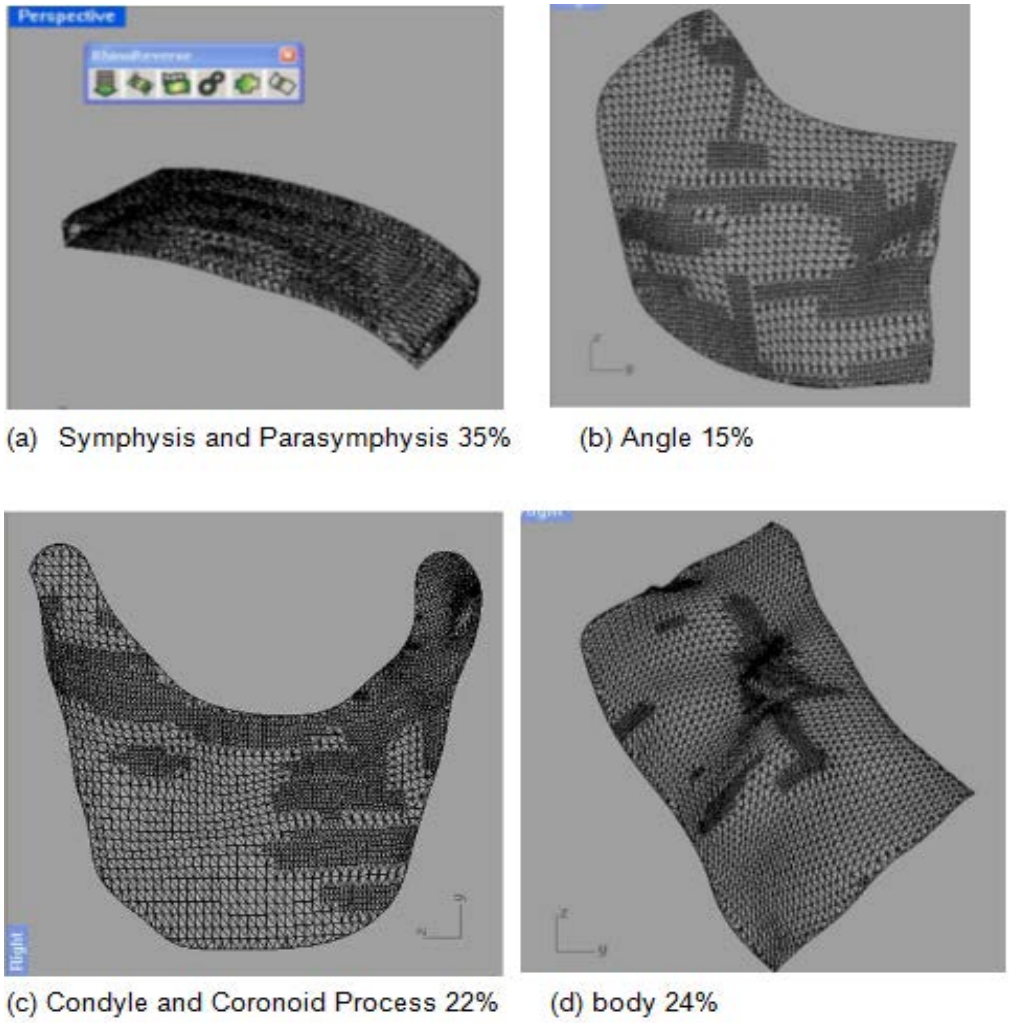

Figure 5.15 Various fixation plates were created for high occurrence sites of fracture.

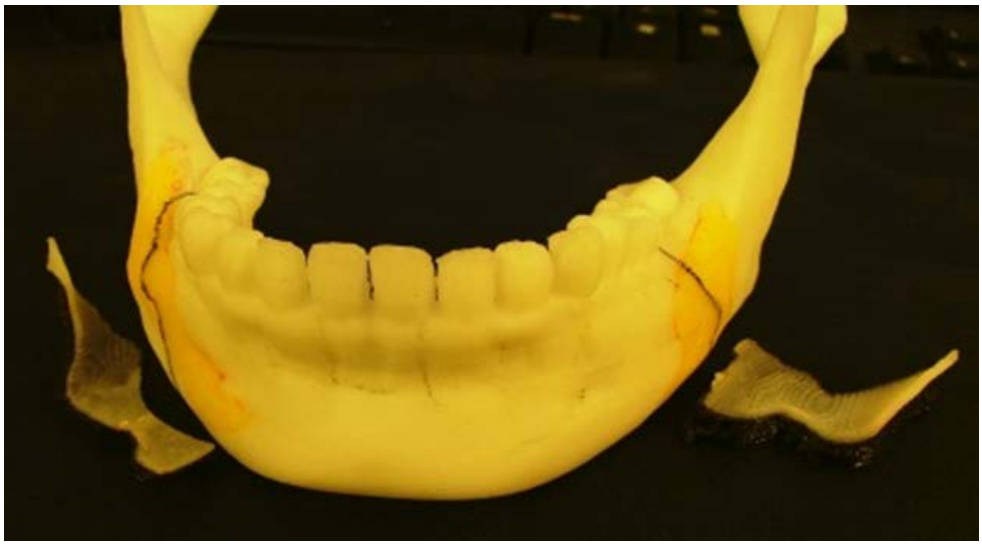

Figure 5.16 FDM model of the fixation plate for form fitting test.

5.4.3 *Mould Design and Manufacture*

Once the designed plate was satisfied to fit on the fracture site, CAD model of the patch that was converted to STL format was then imported into Autodesk Inventor2009 for use in the mould design stage. The steps taken to design the mould are as shown from the Inventor Browser Panel (Figure 5.17). The mould was designed to take advantages provided by AM technologies. A multi-piece mould was created to ease removal of fabricated products (Figure 5.18). Material usages were reduced by creating pockets on the back of the mould pieces. These pockets also act in assisting the heating process. The 3D model of the moulding assembly was later translated into STL format and upload to an SL system for fabrication. Paragon Rapid Technologies Limited UK used the stereolithography process and materials from DSM Somos® ProtoGen™ 18920 liquid photopolymer to perform the fabrication.

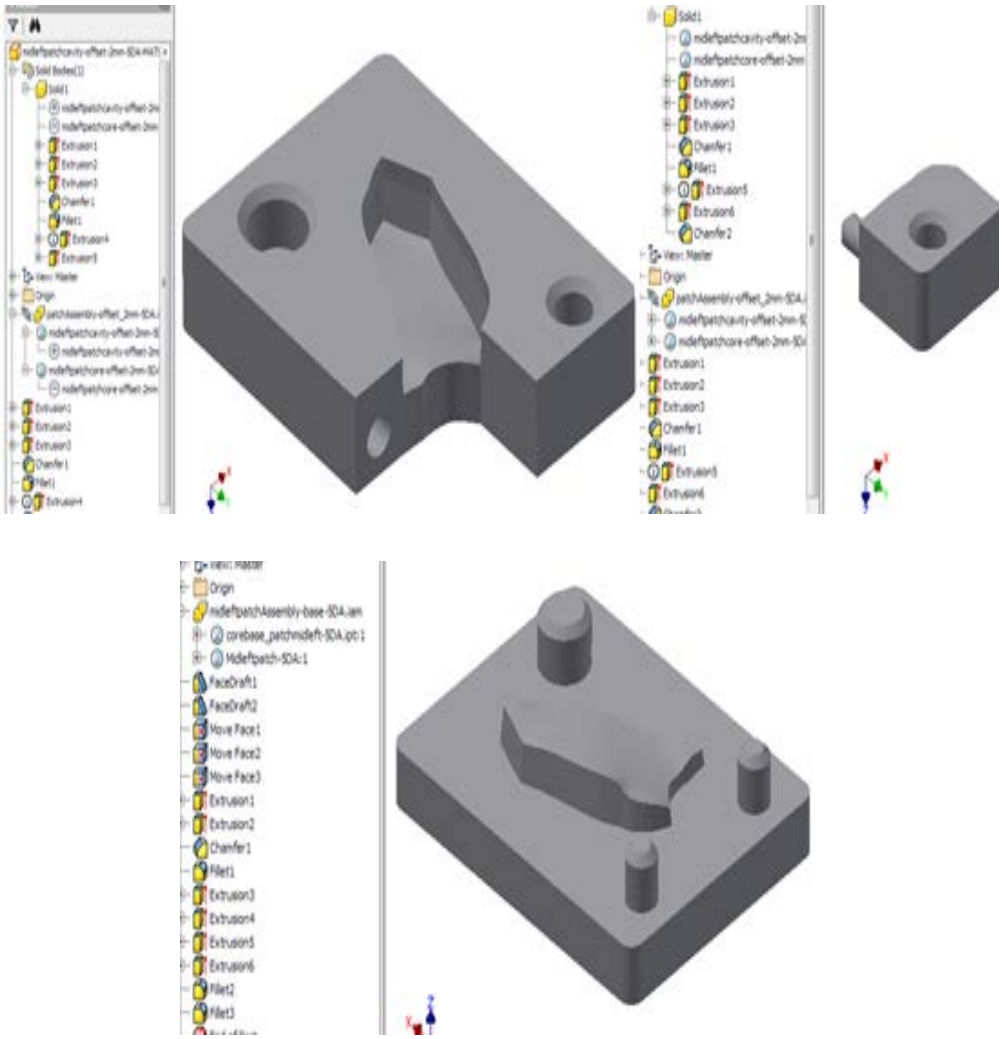

Figure 5.17 Individual part of the mould assembly as design from Autodesk Inventor. Design steps are as displayed in Browser Panel.

Figure 5.18 CAD model of the moulding assembly and exploded view.

5.4.4 *Attachment of a personalised fixation patch*

Bioresorbable material PLGA was used to fabricate the fixation plate. The proposed manner in which the plate is to be attached the fracture site is by the use of adhesive bonding. Morita et al. and Heiss et al. indicated one of the potential usages of medical bone adhesive in traumatology and operative orthopaedics is in the area of joining fractures with a joint bridging fixation (Heiss et al., 2010, Morita et al., 1998).

5.5 Results

Figure 5.19(a) shows the PLGA pellets that were placed inside the mould cavity. Since there are voids between the pellets when placed inside the cavity, the amount of PLGA pellets needed is calculated based on the volume of the cavity. A slightly higher amount of PLGA pellets is used because of the shape of the pellets. This extra amount translated in flash mark when moulded (Figure 5.20) and can be removed by breaking it using long-nose plier. Figure 5.19(b) show the moulded plate as fabricated using the proposed fabrication route. The 2mm

fracture fixation plates have no loss of definition but were slightly thick (Figure 5.20), as compare to normal fixation plate of between 1.5mm to 2mm. This is to account for the strength required for load bearing at the fracture site. However, the patches were easily fitted to fracture jaw.

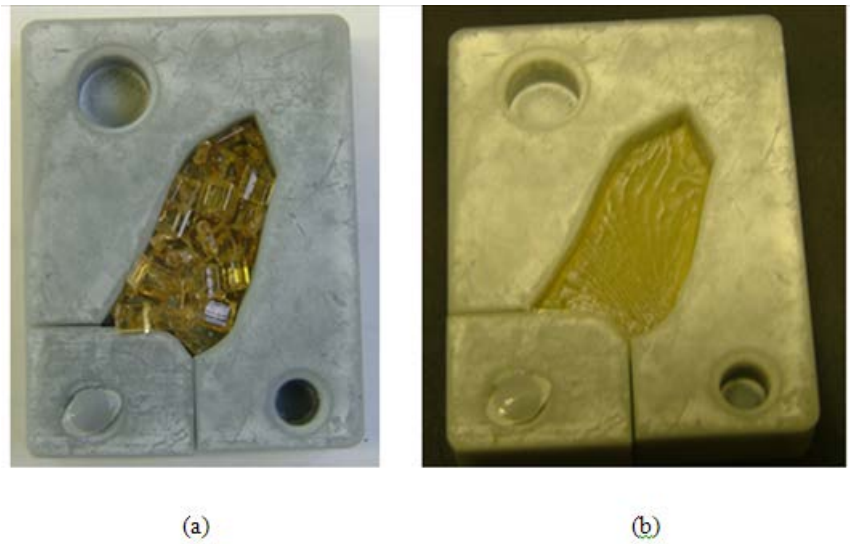

Figure 5.19 PLGA before and after sintering in SLA mould

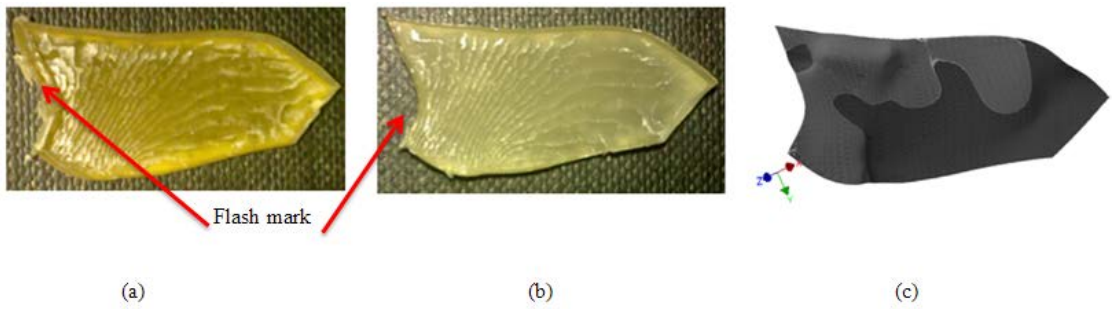

Figure 5.20 (a) PLGA 50:50, (b) PLGA 65:35 and (c) CAD model of the fracture plate.

As shown in figure 5.20, the geometry of the printed parts did not have significant variation from the model CAD object. Details of the mandible surface texture were imprinted clearly onto the patches. This surface texture and the step-effect of layers in AM can possibly provide added benefits to adhesion and cell attachment as adhesion strength of rough surfaces is better than smooth surfaces (da Silva et al., 2011) and the cell propagation are better with uneven

and rough surfaces (Kim et al., 2013, Wong et al., 1995) as rougher surfaces stimulates differentiation, growth and attachment of bone cells, and increases mineralization

5.6 Discussion

The integration of an AM tooling to assist in the fabrication of customised PLGA 3D structure for orthopaedic surgery proved to be feasible. A method to fabricate bioresorble devices using a combined AM tooling, sintering and applying pressure to pellets of PLGA for three different ratios of PLGA was developed. As with most of the research using melt moulding of PLGA microspheres to produce 3D porous PLGA scaffolds, the processing time taken was too long (Borden et al., 2002). Pellets of biopolymers are usually needed to be ground into fine powder (Leung et al., 2008, Thomson et al., 1996). However, in this study the pellets were not grounded as part of the objective is to reduce the time taken for the fabrication process. In this study, the sintering time for PLGA pellets investigated using different heating profiles, and compression loads had reduced the fabrication processing time. All the PLGA co-polymer ratios were sintered into fracture fixation plates with no loss of definition in geometry. The properties were not altered as indicated by the DSC analysis on the fabricated test samples. The mechanical properties were comparable to standard bioresorble device. However, this is the same as if getting from off-the-shelf in biometal fixation plate except that the PLGA fixation patch fabricated using AM produced exact anatomically shaped fracture plate that fit the patient fracture site. Before that patch can be used it needs post-processing to clear off the flash material as well as sterilisation. The method of sterilisation that should not change the PLGA characteristics was not conducted as the investigation it only confined into the manufacturability of personalised PLGA patch for fracture fixation.

The hardware involved in the fabrication of the fixation plate is fairly fundamental and readily available in most dental hospital except for the fixation plate mould which can be outsourced. This route can be feasibly implemented in a clinical setting of a dental hospital for fabrication of customised fixation plate.

Fracture fixation using adhesion indicated that the suggested method is viable although clinically no research has been conducted as of this investigation end (Heiss et al., 2010, Gosain, 2002, Gosain and Lyon, 2001, Gosain et al., 1998, Ahn et al., 1997). Ahn et al. concluded that using biodegradable plates and butyl-2-cyanoacrylate for rigid internal fixation

of osteotomiesed cranial bone fragments is as effective as using metal plate and screw fixation in the animal model. Furthermore, the strength of fixation by biopolymers is as comparable to metal. This has been shown to be achievable from investigation of bio-absorbable P(L/DL)LA bone plate (Kandalam et al., 2013). Gaball had demonstrated that plates that were designed to be less than half the volume of a titanium strut-style plate is as strong when fixating fractures of the mandible body despite the polymer material having only 6% of the stiffness of the titanium (Gaball et al., 2011). Therefore, in this study it is suggested that in order to hold the fractured mandible, the patch would be fixed to the fractured site using bio-adhesive and were presumed to be able fit tightly. In order to produce an equivalent force needed to hold the fracture together; as in conventional biometal plate and screw fixation, either a stronger bio-adhesive is used or a larger area of surface contact between the PLGA plate and the patience mandible bone be created. This can be verified by simulation using finite element analysis (FEA), which can be a future work in this study. Thus, by using the method of adhesive fixation of custom-fit fracture plate, the complications encountered from using standard metal plates and screw in fracture fixation can be eliminated.

Furthermore, as this investigation is to reduce the overall cost in fabricating personalized medical devices, mid-range CAD software were used in tandem with mid-range AM system to model. The design and fabrication of patient specific medical devices has been documented using high-end CAD software such as Pro/E, CATIA and Unigraphics NX (Wei, 2009, Sun et al., 2009, Richard et al., 2009, Williams et al., 2008, Liulan et al., 2007, Klein and Glatzer, 2006, Séquin, 2005). As described in this chapter, custom-fit fracture fixation plates were successfully design and fabricated using mid-range equipment.

Further cost reduction can be accomplished by using open source software and open source AM system based on material extrusion and Fused Filament Fabrication (FFF) such as Fab@home or RepRap machines. However, in using open source software and open source AM systems most of the support will only be available in the forum on the internet as compare to commercially available products with full supports, if required. With the movement of open source AM system, cost of printing 3D artefacts can be reduced with more choices of materials. This selection includes polymer filaments, wood-based and ceramic.

Chapter 6: General Discussion

6.1 Introduction

Defects in the oral and maxillofacial system can interrupt the normal functionality of patients especially functional problems associated with their occlusion and aesthetic concerns. Repair and regeneration of defectives bone tissues in the cases of tumour, trauma, osteoarthritis and decrease in bone density are normally addressed through tissue engineering. In this approach; biomimetic scaffolds are used, with a well-defined architecture that imitate and replicate living bone in terms of strength, morphology, porosity, bioactivity and load-bearing ability. These scaffolds guide and promote cells proliferation and differentiation into regenerated bone tissue.

Manufacturing approaches to the fabrication of ideal synthetics bone scaffolds can be divided into Additive Manufacturing (AM) approach and conventional approach. With the advancement of digital technology and material developments in AM, more industrial players are adopting the AM approach for bone tissue engineering (Bose et al., 2013). This can further be seen from the increase in usage of AM for medical application (Wohlers, 2013). The flexibility of AM to fabricate the complex 3D geometry of scaffolds with a controlled external and internal structure holds great promise for future scaffolds tissue engineering strategies. However, the high cost of acquiring an AM system that is capable of creating end-user scaffolds make this approach prohibitive for low income group. Hence, the aim of this work was to develop and evaluate novel biomaterial processing by indirect additive manufacturing methods using low cost AM system. In order to establish the processing approach, the research works were separated into a different section as described in chapter 3, chapter 4 and chapter 5.

6.2 Discussion

The results obtained in processing AW-GC in both the indirect methods yield different Young's modulus values. The average Young's modulus is between 23.51GPa to 26.65GPa and 0.8GPa to 2.64GPa for Aluminium foil mould and 3D printing, respectively. Even though the AW-GC-binding agent powder mixture used was 70:30 by weight, the sacrificial materials used as binding agents is different; which is PMMA and maltodextrine. This will influence the porosity as more maltodextrine will occupy the same volume as compare to PMMA because of the difference in density. Less AW-GC is used in building the same artefact when

using the AW-GC-maltodextrine as compared to using AW-GC-PMMA mixture. Hence, this produced a more porous artefact when maltodextrine is used as a binding agent. Furthermore during 3D printing maltodextrine absorbed the binder solution. The average porosity obtained is 26.86%±4.49% for Aluminium foil mould while, in indirect 3DP the porosity ranged from 45% to 55%. In addition to the different binding agent used, the different processes also contribute to the differences in Young's modulus. In the indirect method using Aluminium foil mould, compression was directly applied on to the AW-GC PMMA mixture. While for the indirect 3D printing method, pressure was indirectly applied to the AW-GC maltodextrine mixture from the roller during spreading of the powder mixture in 3DP process. Both these conditions had impact on the Young's modulus and was in agreement with others research work (Marchelli et al., 2011, Suwanprateeb et al., 2010, Chang et al., 2000). The calculated values and the Young's modulus values reported is thought to be the result of different processes as uniaxial pressing process produces a preferential pore alignment and result in a smaller Young's modulus in the pressing direction (Chang et al., 2000).

6.2.1 *Moulding of AW scaffolds by aluminium sheet mould*

In the initial stage of this research work, the objective is to produce scaffolds of 1mm and 3mm in diameter scaffolds for use in tissue engineering research. The AW-GC scaffolds were to vary from dense (5% porosity) to 50% porosity. Based on this various ratios of AW-GC and PMMA requirement, different strategies of removing the moulded scaffolds from the mould were incorporated in the design of the mould. As AM technologies have the advantages of geometrical design freedom (Parthasarathy et al., 2011, Kamrani and Nasr, 2006, Hague et al., 2004, Hague et al., 2003), various multiple parts mould were designed and fabricated. However, because of the force and the friction of the AW-GC scaffolds are relatively high as compare to the fragile scaffolds, most of the scaffolds were not able to be removed or ejected from the mould. Rather than having to eject the moulded parts, a new concept of fabrication was adapted from conventional manufacturing in the form of shell moulding. However, since the fabricated parts are fragile, flexible shell mould was concept was developed in which the can be unfolded/unrolled, and the fabricated part are removed by gravity feed. This method proved to be a success with mixing AW-GC to 20% or more by weight of PMMA. The ratio that was used to fabricate cylindrical scaffolds samples of 3mm diameter is 70%AW-GC to 30% PMMA. It was compared with scaffolds produced from SLS machine and found to be comparable by another group of researchers. The material cost

involved in making this flexible shell mould is £2, which is extremely low compare to using SLS.

Therefore, for low-cost manufacturing of simple bioceramics scaffolds this method can be an alternative approach. The making of the flexible aluminium shell mould does not require sophisticated tools.

6.2.2 *Shell moulding Process of AW 3D artefacts by mean of Rapid Tooling (RT)*

In extending the concept of flexible shell moulding using aluminium foil, RT was used to develop shell moulding process for the fabrication of complex organic shape artefacts. In the case study that followed, a resection of the mandible was fabricated to emulate the BGS for a large section of the mandible. The artefact fabricated was not good enough to be used as it had a lot of imperfection such as crack and non-completed features. These defects were attributed the difficulty in compacting the powder mixture as properly and uniformly compacted powder will encounter less deformation during sintering (Cocks, 2001).

6.2.3 *Lost wax casting (LWC) process of bioceramic 3D artefacts by mean of Rapid Tooling (RT)*

The total time and cost for producing the FDM indirect tooling was 15hours and £270 respectively as compared to RTV soft tooling of 19hours and £38. Figure 3-25 shows a comparison between the wax model from indirect tooling and soft tooling. The wax model produced by RTV silicone moulding was able to capture the geometrical feature of the master pattern as compared to indirect tooling. The RTV moulding is a labour driven process as preparation time is done manually. There is a difference of 4 hours between FDM indirect moulding techniques. Hence, the soft tooling method is more suited in low labour cost region. Therefore, this is a feasible method to be used in order to keep the cost of treatment low in developing countries.

6.2.4 *3D printing process of bioceramic 3D artefacts by indirect AM*

The printed artefacts were of non-uniformity when different measurements were taken along the length of the artefacts. This indicates that the range in AW particles size of up 53μm and binder saturation have a direct impact on the accuracy and surface morphology. Furthermore, material shrinkage during printing led to a slight curling of the first few layers of the printed

parts All Samples that were printed have an average dimension of less than the dimension from the CAD model even though the repeatability of the printing process is statistically significant. Shrinkage in the printed part geometry due to wetting in the powder materials, as well as the burnout of the maltodextrine compound, was observed. This created 50% porosity in the artefacts/samples even though the initial powder mixer was 70%:30%, the same in both RT process and 3DP process. The only different is the binding agent which in the later process maltodextrine is used.

6.2.5 *Crystallography Phase Comparison of Sintered AW parts from Moulding and 3D Printing.*

As three different methods were used in the fabrication of AW glass ceramic, a comparison was performed to verify that all these methods were able to produce AW glass ceramic that are comparable to Kokubo's AW glass ceramics. To complement the XRD analysis presented in chapter 3 and 4, EDX analysis (shown in Table 6.1) was performed on 5 samples, all of which were powders ground from the specimens that had been sintered (in chapter 3 and chapter 4) and not from original powder. These are labelled as aw1, aw2, aw3d1, aw3d2, and awfdm, where aw1, aw2, and awfdm are materials processed as described in chapter 3 (the original powder was mixed with PMMA powder, and then the composite powder was moulded in aluminium foil moulds and fused deposition moulds to produce green parts which were then sintered). Aw3d1 and aw3d2 came from a different batch of powder, but from the same supplier, and both were processed as described in chapter 4 (by 3D printing on the Z Corp machine, with maltodextrine used as part of the binder solution). The sintering of all specimens used the same heating profile as described in section 3.2.5. Table 6.1 shows the summary of the EDX results.

Table 6.1 EDX result of 5 sintered samples as compared to Kokubo's formulation.

	norm wt %						
	Shell Moulding		3D Printing		FDM moulding	Range	
Element	aw1	aw2	aw3d1	aw3d2	awfdm		Kokubo's formulation
Silicon	14.13	12.67	13.84	16.37	13.28	12.67-16.37	15.88
Phosphorus	5.08	4.03	4.86	5.82	4.46	4.03-5.82	7.06

Calcium	29.92	25.12	32.57	39.13	29.76	25.12-39.13	31.96
Magnesium	2.75	2.32	2.04	2.17	2.48	2.04-2.75	2.76
Carbon	2.44	7.06			10.78		
Oxygen	45.68	48.80	45.76	34.70	39.25	34.70-48.80	42.1
Aluminium			0.93	1.81			
Fluorine							0.25
	100	100	100	100	100		100.01

As indicated from Table 6.1, all of the sintered materials are similar to Kokubo's formulation. The aw3d1 and aw3d2 materials are very similar, as are the aw1 and aw2 materials. Overall the elemental content is consistent with them being two batches of material: one for aw1/aw2/awfdm and one for aw3d1/aw3d2. However, different type of binders were used for each batch, and it seems that for aw1, aw2 and awfdm that used the PMMA binder there were was some indication of residual carbon, while for aw3d1 and aw3d2, there were traces of aluminium. Based on the results of the EDX and XRD analysis (refer appendix B4), it can be recognized that the final composition of the structures is close to AW, but has been affected by contamination:

- The PMMA or other mechanism of contamination has led to there being a small but significant carbon content in aw1/aw2/awfdm, which has affected the phases produced in sintering.
- Contamination has also resulted in the low aluminium content in aw3d1/aw3d2.

Therefore, further tests would be necessary to establish the biocompatibility of the processed materials.

6.2.6 *Melt moulding processing of biopolymer 3D artefacts by mean of Rapid Tooling (RT)*

Various techniques for the fabrication of PLGA such as the solvent-casting separation and particulate leaching method or the phase separation method, face some forms of disadvantage

in particular where solvents are used in the process as large amounts of organic solvent are needed to dissolve PLGA. This requires a very long time to completely remove solvents from the resulting material (Makadia and Siegel 2011) and any residual solvents in the scaffolds may be harmful to transplanted cells or host tissues (Mooney et al., 1996). Various methods were used to fabricate PLGA such as emulsion techniques which require precise control of processing parameters for higher encapsulation efficiency, and phase separation techniques which tend to produce agglomerated particles and also require removal of large quantities of the organic phase from the microspheres. The main disadvantage in both processes is the adhesion of the microparticles to the inner walls of the spray-dryer (Makadia and Siegel 2011, Jain, 2000b). The proposed method does not employ the use of solvent. This method was able to produce 3D artefacts of PLGA without changing the physical and chemical characteristics of the PLGA.

With reference to earlier works by Thomson using melt-moulding method (Thomson et al., 1996, Thomson et al., 1998), the new methods proposed clearly indicated that this is a viable solution for producing patients' specific implantable devices at an affordable cost. Furthermore, the mould required can be fabricated from external service bureau or within the organisation itself as to produce the implants only required simple set up as outlined in Chapter 5.

Chapter 7: Conclusion and Future Work.

7.1 Conclusion

The XRD analysis that was performed on all samples from the different approaches used in fabricating glass ceramics yield similar peak list of wollastonite, diopside, whitlockite, fluorapatite, hydroxylapatite, and calcium magnesium phosphate. This suggested that some form of hydroxyl/apatite or calcium-magnesium-phosphate and wollastonite content in all the samples, even though the readings of each element in the microscopy spectrum were different for aw1, aw2 and awfdm with aw3d1 and aw3d2.

The experimental values of Young's Modulus obtained for AW-GC in both the different processing route of shell moulding (Chapter 3) and indirect 3D printing(chapter 4) yield different results. The difference between them is attributed to pressing process, and the porosity obtained. Calculated values and the Young's modulus values reported is thought to be the result of different processes as uniaxial pressing process produces a preferential pore alignment and result in a smaller Young's modulus in the pressing direction (Chang et al., 2000).

Depending on the application required, all three methods of processing AW glass ceramics into 3D artefacts are relatively low cost if compared to RM methods. The best approach to produce cheapest simple scaffolds is by using the flexible aluminium sheet mould method while both indirect AM methods give an acceptable account at producing complex artefacts. In both rapid tooling and soft tooling approach the surface finish and the mechanical strength are better than the 3DP approach. However, geometrical features of artefacts are clearly defined when 3DP approach is used. In order for these approaches to be acceptable, additional research to improve the output need to be performed and is listed as future work in section 7.2.

The wax patterns produced from the novel indirect AM method for processing biomaterials in both the medical case study illustrate that this approach can be deployed in the health sectors, in particular health sectors in low income country as the production cost is relatively low as compared to direct AM methods or the conventional methods. In the conventional wax patterns of investment casting, usually cost of mould is very high and the fabrication is time-consuming; the more complex the mould is, the higher the cost will be (Cheah et al., 2005, Pattnaik et al., 2014). By using mould created from FDM or FFF, the cost of mould can be

reduced as AM fabrication cost is not exponentially related to part complexity (I. Gibson et al., 2010, Atzeni et al., 2010, Hopkinson et al., 2006, Hague et al., 2004). The complex three-dimensional pattern mould can be easily manufactured directly from CAD data by employing the FDM process.

The use of AM processes to produce moulds for PLGA sintering, and the 3D printing of bioceramic powders formed the best overall results in terms of geometry definition and properties of the manufactured parts. Parts produced were observed to be accurate to within acceptable value of the as designed dimensions for both the PLGA sintering and the bioceramic powders 3D printing. The indirect AM methods are considered to be promising processing routes for customised medical devices.

7.2 Future Work

Whilst this research has achieved the research aim and objectives, there are several recommendations that could be implemented to take the research further. The possible future work includes the followings:-

- Based on the flexible aluminium sheet shell moulding concept, research can be conducted to develop a new procedure to improve powder compaction for complex geometrical in flexible aluminium sheet shell moulding.
- Use finite element methods on new implant design and approach to implant fixation through biological and bioactive mechanism.
- Explore indirect AM in producing mimicry bone structure from biocomposite of PLGA and AW as a new approach for implant fixation.
- An in-depth study on processing variables as stipulated in sintering mechanism that can improve the quality of the artefacts.
- Additional study in powder mixture particles size, saturation and compaction effect on 3DP artefacts.
- As FDM mould is made of ABS which has low heat transfer coefficient, the heating method by conduction can be replace with microwave heating in sintering of AWGC powder mixture as microwave energy can penetrated polymer mould.
- The volume fraction of porosity was not determined as the part of the objectives in chapter 4. The concern in this chapter is to estimate the proximity of the empirical Young’s Modulus E value to the value of cortical bone. In order to compare the

empirical Young's Modulus with the predicted theoretical E, the volume fraction of porosity of the specimens need to be determined beforehand according to Nielsen's equation. Volume fraction of porosity can be determined by intrusion methods such as mercury intrusion and microscopic image analysis or by Archimedes method. Hence, it is suggested that an additional work in determining the porosity of sintered AWGC using micro-CT is needed as this will provide better analysis regarding the percentage of closed and opened pores. Therefore the volume fraction of porosity will be included in the future work for 3DP artefacts.Thus the value of volume fraction of porosity and the shape factor can be determined.

Additional work will include the calculation for the estimate of the theoretical value for Young's Modulus in a porous body and comparison with the experimental results.

The theoretical value can be calculated from Nielsen equation that is given as: -

$$E = (E_0 * (1 - P) \wedge 2) / (1 + P / (f - 1)) \qquad (7.1)$$

Where E = Young's modulus

E_0 = Young's modulus for dense sample,

P = volume fraction of porosity, and

f = shape factor

As suggested by Nielsen, materials with porosity characteristic of joined particles be assigned a shape factor value of 0.4 or less, a shape factor between 0.3-0.7 is appropriate for porosity that resembles ribbons or dendrites and a shape factor of 0.6-1.0 is characteristic of pores enveloped by a solid phase (Nielsen, 1982, Nielsen, 1984).

References

3DPARTS (2011) How it work (http://www.3dparts.co.uk/how-it-works/ access date: May-2012).

3DSYSTEM (2014) Projet Series Printer (http://www.3dsystems.com/projet5500x, access date: July 2014).

AHN, D. K., SIMS, C. D., RANDOLPH, M. A., O'CONNOR, D., BUTLER, P. E. M., AMARANTE, M. T. J. & YAREMCHUK, M. J. (1997) Craniofacial skeletal fixation using biodegradable plates and cyanoacrylate glue. *Plastic and Reconstructive Surgery,* 99**,** 1508-1517.

ALEXIS, F. (2005) Factors affecting the degradation and drug-release mechanism of poly(lactic acid) and poly[(lactic acid)-co-(glycolic acid)]. *Polymer International,* 54**,** 36-46.

ALKAN, A., CELEBI, N., OZDEN, B., BAS, B. & INAL, S. (2007) Biomechanical comparison of different plating techniques in repair of mandibular angle fractures. *Oral Surgery, Oral Medicine, Oral Pathology, Oral Radiology, and Endodontology,* 104**,** 752-756.

ANIWAA (2014) Compare 3D Printers (http://www.aniwaa.com/3d-printers/compare-3d-printers/ access date: July-2014).

ARCAM (2013) Electron beam melting- Hardware (http://www.arcam.com/technolog y /electron-beam-melting/hardware/ access date: October 2013).

ARCOS, D., IZQUIERDO-BARBA, I. & VALLET-REGÍ, M. (2009) Promising trends of bioceramics in the biomaterials field. *Journal of Materials Science: Materials in Medicine,* 20**,** 447-455.

ARMENTANO, I., DOTTORI, M., FORTUNATI, E., MATTIOLI, S. & KENNY, J. M. (2010) Biodegradable polymer matrix nanocomposites for tissue engineering: A review. *Polymer Degradation and Stability,* 95**,** 2126-2146.

ASTM (2012) F2792 − 12a: Standard Terminology for Additive Manufacturing Technologies[1,2]. IN INTERNATIONAL, A. (Ed.) March 2012 ed., ASTM International, 100 Barr Harbor Drive, PO Box C700, West Conshohocken, PA 19428-2959. United States.

ATHANASIOU, K. A., ZHU, C. & LANCTOT, D. R. (2000) Fundamentals of biomechanics in tissue engineering of bone. *Tissue Engineering,* 6**,** 361-381.

ATZENI, E., IULIANO, L., MINETOLA, P. & SALMI, A. (2010) Redesign and cost estimation of rapid manufactured plastic parts. *Rapid Prototyping Journal,* Vol. 16 pp. 308 - 317.

BARTOLO, P. & BIDANDA, B. (2008) *Bio-materials and prototyping applications in medicine.*

BEN-NISSAN, B. & PEZZOTTI, G. (2004) Bioceramics: An Introduction. IN TEOH, S. H. (Ed.) *Engineering Materials for Biomedical Applications.* Singapore, WorldScientific.

BERCE, P., CHEZAN, H. & BALC, N. (2005) The application of Rapid Prototyping Technologies for manufacturing the custom implants. *ESAFORM 2005 Conference.* Cluj-Napoca, Romania.

BERGER, M. B. (2010) The importance and testing of density/ porosity/ permeability/ pore size for refractories *The Southern African Institute of Mining and Metallurgy Refractories 2010 Conference.* Southern Africa.

BERGSMA, J. E., ROZEMA, F. R., BOS, R. R., BOERING, G., DE BRUIJN, W. C. & PENNINGS, A. J. (1995) In vivo degradation and biocompatibility study of in vitro pre-degraded as-polymerized polyactide particles. *Biomaterials,* 16 pp. 267-274.

BERNARD, A. & FISCHER, A. (2002) New Trends in Rapid Product Development. *CIRP Annals - Manufacturing Technology,* 51**,** 635-652.

BERTRAND, P., BAYLE, F., COMBE, C., GOEURIOT, P. & SMUROV, I. (2007) Ceramic components manufacturing by selective laser sintering. *Applied Surface Science,* 254**,** 989-992.

BEST, S. M., PORTER, A. E., THIAN, E. S. & HUANG, J. (2008) Bioceramics: Past, present and for the future. *Journal of the European Ceramic Society,* 28**,** 1319-1327.

BHAGOL, A., SINGH, V. & SINGHAL, R. (2013) Management of Mandibular Fractures. IN (ED.), P. M. H. K. M. (Ed.) *A Textbook of Advanced Oral and Maxillofacial Surgery.* InTech.

BIBB, R., FREEMAN, P., BROWN, R., SUGAR, A., EVANS, P. & BOCCA, A. (2000) An investigation of three-dimensional scanning of human body surfaces and its use in the design and manufacture of prostheses. *Proceedings of the Institution of Mechanical Engineers, Part H: Journal of Engineering in Medicine,* 214**,** 589-594.

BOOTHROYD, G. (1994) Product design for manufacture and assembly. *Computer-Aided Design,* 26**,** 505-520.

BORDEN, M., ATTAWIA, M., KHAN, Y. & LAURENCIN, C. T. (2002) Tissue engineered microsphere-based matrices for bone repair: : design and evaluation. *Biomaterials,* 23**,** 551-559.

BORRILLE, A. V. & GOMES, J. D. O. (2011) Selection of additive manufacturing technologies using desicion methods. IN HOQUE, M. (Ed.) *Rapid prototyping technology - Principles and Functional requirements.* Shanghai, InTech.

BOSE, S., VAHABZADEH, S. & BANDYOPADHYAY, A. (2013) Bone tissue engineering using 3D printing. *Materials Today,* 16**,** 496-504.

BOULOUX, G. F., DEMO, M., MOE, J. & EASLEY, K. A. (2014) Mandibular fractures treated with small plates and screws reduce treatment cost. *Journal of Oral and Maxillofacial Surgery,* 72**,** 362-369.

BRACKETT, D., ASHCROFT, I. & HAGUE, R. (2011) TOPOLOGY OPTIMIZATION FOR ADDITIVE MANUFACTURING. *UTwired LFF symposium proceeding.* Texas.

BRASILEIRO, B. F. & PASSERI, L. A. (2006) Epidemiological analysis of maxillofacial fractures in Brazil: A 5-year prospective study. *Oral Surgery, Oral Medicine, Oral Pathology, Oral Radiology, and Endodontology,* 102**,** 28-34.

BRAUN, D., CHERDRON, H., REHAHN, M., RITTER, H. & VOIT, B. (2012) Methods and Techniques for Synthesis, Characterization, Processing, and Modification of Polymers. *Polymer Synthesis: Theory and Practice.* Springer Berlin Heidelberg.

BSI (1995) BS EN 993-1:1995 BS 1902-3.8:1995-Methods of test for dense shaped refractory products. Determination of bulk density, apparent porosity and true porosity. IN INSTITUTE, B. S. (Ed.), BSI.

BSI (2003) BS EN 1389:2003 Advanced technical ceramics. Ceramic composites. Physical properties. Determination of density and apparent porosity. IN INSTITUTE, B. S. (Ed.), Bristish Standard Institute, London.

BSI (2008) BS EN ISO 6872:2008-Dentistry. Ceramic materials. IN INSTITUTE, B. S. (Ed.), British Standards Institute, London.

BSI (2009a) BS EN ISO 6892 - 1:2009 Metallic Materials Tensile Testing. Part 1 Method of Test at Room Temperatures. IN BSI (Ed.), British Standards Institute, London.

BSI (2009b) BS ISO 22794:2009 Dentistry — Implantable materials for bone filling and augmentation in oral and maxillofacial surgery — Contents of a technical file (ISO 22794:2007, corrected version 2009-01-15). IN INSTITUTE, B. S. (Ed.), British Standards Institute, London.

BSI (2010) BS EN ISO 20795:2010 Dentistry — Base polymers Part 2: Orthodontic base polymers (ISO 20795-2:2010). IN INSTITUTE, B. S. (Ed.), British Standards Institute, London.

BSI (2011) BS EN ISO 178:2010 Plastics — Determination of flexural properties (ISO 178:2010). IN INSTITUTE, B. S. (Ed.), British Standard Institute, London.

BUTSCHER, A., BOHNER, M., HOFFMANN, S., GAUCKLER, L. & MÜLLER, R. (2011a) Structural and material approaches for bone tissue engineering in powder based 3D printing. *Acta Biomaterialia,* In Press, Accepted Manuscript.

BUTSCHER, A., BOHNER, M., HOFMANN, S., GAUCKLER, L. & MÜLLER, R. (2011b) Structural and material approaches to bone tissue engineering in powder-based three-dimensional printing. *Acta Biomaterialia,* 7**,** 907-920.

CALLAGHAN, J. T., TANG, Z. G. & HUNT, J. A. (2004) The in-vitro evaluation of PCL / PLGA copolymers as bone replacement materials. *Transactions - 7th World Biomaterials Congress.*

CANNILLO, V., PIERLI, F., SAMPATH, S. & SILIGARDI, C. (2009) Thermal and physical characterisation of apatite/wollastonite bioactive glass-ceramics. *Journal of the European Ceramic Society,* 29**,** 611-619.

CHANG, L. S., CHUANG, T. H. & WEI, W. J. (2000) Characterization of alumina ceramics by ultrasonic testing. *Materials Characterization* 45 pp. 221-226.

CHARLES-HARRIS, M., DEL VALLE, S., HENTGES, E., BLEUET, P., LACROIX, D. & PLANELL, J. A. (2007) Mechanical and structural characterisation of completely degradable polylactic acid/calcium phosphate glass scaffolds. *Biomaterials,* 28**,** 4429-4438.

CHARTIER, T., BADEV, A., ABOULIATIM, Y., LEBUADY, P. AND LECAMP, L. (2012) Stereolithography process: influence of the rheology of silica suspensions and the medium on polymerization kinetics-cured depth and width. *Journal of the European Ceramic Society,* Vol.32**,** pp. 1625-1634.

CHEAH, C. M., CHUA, C. K., LEE, C. W., FENG, C. & TOTONG, K. (2005) Rapid prototyping and tooling techniques: a review of applications for rapid investment casting. *The International Journal of Advanced Manufacturing Technology,* 25**,** 308-320.

CHEN, P.-Y. & MCKITTRICK, J. (2011) Compressive mechanical properties of demineralized and deproteinized cancellous bone. *J Mech Behav Biomed Mater* 4(7)**,** 961-973.

CHEUNG, H.-Y., LAU, K.-T., LU, T.-P. & HUI, D. (2007) A critical review on polymer-based bio-engineered materials for scaffold development. *Composites Part B: Engineering,* 38**,** 291-300.

CHEVALIER, J. & GREMILLARD, L. (2009) Ceramics for medical applications: A picture for the next 20 years. *Journal of the European Ceramic Society,* 29**,** 1245-1255.

CHIANG, W. M., C.S. LIM, C.K. CHUA, P.L. LO & ENG, C. T. (2005) Application of rapid prototyping and tooling in customised airway management. *Rapid Prototyping Journal* 11/2**,** pp 106-112.

CHOI, S. H. & SAMAVEDAM, S. (2002) Modelling and optimisation of Rapid Prototyping. *Computers in Industry,* 47**,** 39-53.

CHOW, W. S., TAY, H. K., AZLAN, A. & MOHD ISHAK, Z. A. (2008) MECHANICAL AND THERMAL PROPERTIES OF HYDROXYAPATITE FILLED POLY(METHYL METHACRYLATE) COMPOSITES *Proceedings of the Polymer Processing Society 24th Annual Meeting ~ PPS-24 ~ June 15-19, 2008* Salerno (Italy).

CHRCANOVIC, B. (2012) Fixation of mandibular angle fractures: clinical studies. *Oral and Maxillofacial Surgery,* 18**,** 123-152.

CHRISCHILLES, E., SHIREMAN, T. & WALLACE, R. (1994) Costs and health effects of osteoporotic fractures. *Bone* 15.

CHUA, C. K., LEONG, K. F. & LIM, C. S. (2010) *Rapid Prototyping: Principles and Applications,* Singapore, World Scientific Publishing.

CHUNG, T. W., TSAI, Y. L., HSIEH, J. H. & TSAI, W. J. (2006) Different ratios of lactide and glycolide in PLGA affect the surface property and protein delivery characteristics

of the PLGA microspheres with hydrophobic additives. *Journal of Microencapsulation,* 23**,** 15-27.

CIENFUEGOS, R., CORNELIUS, C.-P., ELLIS III, E. & KUSHNER, G. (2008) Mandible - Special considerations. IN FIGARI, M., ANICETO, G. S. & BUCHBINDER, D. (Eds.) *AO Surgery Reference -Online reference in clinical life.* v1.0 2008-12-01 ed., AO Foundation.

COCKS, A. C. F. (2001) Constitutive modelling of powder compaction and sintering. *Progress in Materials Science,* 46**,** 201-229.

COHEN, A., LAVIV, A., BERMAN, P., NASHEF, R. & ABU-TAIR, J. (2009) Mandibular reconstruction using stereolithographic 3-dimensional printing modeling technology. *Oral Surgery Oral Medicine Oral Pathology Oral Radiology and Endodontology,* 108**,** 661-666.

COLBY, C. (2007) Differential Scanning Calorimetry (http://www.colby.edu /chemistry/PChem/lab/DiffScanningCal.pdf access date: Jan 2014).

CRONSKAR, M., BACKSTROM, M. & RANNAR, L.-E. (2013) Production of customized hip stem prostheses - a comparison between conventional machining and electron beam melting (EBM). *Rapid Prototyping Journal,* 19**,** 365-372.

CUSTOMPARTNET (2012) Laminated object manufacturing (http://www.custompartnet.com/wu/laminated-object-manufacturing access date: November 2012).

CUT-CRPM (2014) CRPM's Additive Manufacturing Technologies (http://www.cut.ac.za/crpm-am-technologies/ access date: Febuary 2014).

DA SILVA, L. F. M., OCHSNER, A. & ADAMS, R. D. (Eds.) (2011) *Handbook of adhesion technology,* Berlin Heidelberg, Verlag-Springer.

DE BEER, N., DIMITROV, D. & VAN DER MERWE, A. (2008) Manufacturing of custom-made medical implants for cranio / maxillofacial and orthopaedic surgery - an overview of the current state of the industry. *Journal for New Generation Sciences,* 6**,** 1-15.

DE JAGER, N., FEILZER, A. J. & DAVIDSON, C. L. (2000) The influence of surface roughness on porcelain strength. *Dental Materials,* 16**,** 381-388.

DECKERS, J., SHAHZAD, K., VLEUGELS, J. & KRUTH, J. P. (2012) Isostatic pressing assisted indirect selective laser sintering of alumina components. *Rapid Prototyping Journal,* 18**,** 409-419.

DEOGRATIUS B.K, ISAAC M.M & S., F. (2006) Epidemiology and management of maxillofacial fractures treated at Muhimbili National Hospital in Dar es Salaam, Tanzania, 1998-2003. *J Int Dent,* 56**,** 4.

DERBY, B. (2005) 3D ink jet printing of ceramics and biomaterials. *21st International Conference on Digital Printing Technologies (NIP21)/International Conference on Digital Fabrication Technologies.* Baltimore, MD.

DICKENS, P., HAGUE, R. & WOHLERS, T. (2000) Methods of rapid tooling worldwide (http://wohlersassociates.com/Oct00MMT.htm access date: January 2008).

DIEGEL, O., SINGAMNENI, S., REAY, S. & WITHELL, A. (2011) Sustainable product design through additive manufacturing. *Asian International Journal of Science and Technology in Production and Manufacturing Engineering (AIJSTPME),* Vol.4 No.1**,** pp. 39 -45.

DOMB, A. J., KUMAR, N., SHESKIN, T., BENTOLILA, A., SLAGER, J. & EOMIM, D. T. (2001) Polymeric drug carriers IN DUMITRIU, S. (Ed.) *Polymeric biomaterials Revised and Expanded.* New York, Marcel Dekker Inc. .

DONG, C. & BOWEN, H. K. (1989) Hot-Stage Study of Bubble Formation During Binder Burnout. *Journal of the American Ceramic Society,* 72**,** 1082-1087.

DOTCHEV, K. & SOE, S. (2006) Rapid manufacturing of patterns for investment casting: Improvement of quality and success rate. *Rapid Prototyping Journal,* 12**,** 156-164.

DOUGLAS, T. S. (2014) Additive manufacturing : from implants to organs : forum - advances in medicine. *South African Medical Journal,* 104**,** 408-409.

DOWSON, D. (2006) Tribological principles in metal-on-metal hip joint design. *Proceedings of the Institution of Mechanical Engineers, Part H: Journal of Engineering in Medicine,* 220**,** 161-171.

DREAMS.ME.VT.EDU (2009) 3D Printing (http://www.me.vt.edu/dreams/binder-jetting/ access date: September 2013).

DUYGU, G., GULER, N., TORE, G. & SENCIFT, K. (2007) Dental implant complications. *International Journal of Oral and Maxillofacial Surgery,* 36**,** 1092-1093.

EBERT, J., OZKOL, E., ZEICHNER, A., UIBEL, K., WEISS, O., KOOPS, U., TELLE, R. & FISCHER, H. (2009) Direct Inkjet Printing of dental Prostheses Made of Zirconia. *Journal of Dental Research,* 88**,** 673-676.

EGGBEER, D., BIBB, R., EVANS, P. & JI, L. (2012) Evaluation of direct and indirect additive manufacture of maxillofacial prostheses. *Proceedings of the Institution of Mechanical Engineers, Part H: Journal of Engineering in Medicine,* 226**,** 718-728.

EL-MELIEGY, E. & VAN NOORT, R. (2012) Design of Medical Glass-Ceramics. *Glasses and Glass Ceramics for Medical Applications.* New York, Springer New York.

ELLIS III, E. (1999) Treatment methods for fractures of the mandibular angle. *International Journal of Oral and Maxillofacial Surgery,* 28**,** 243-252.

ELLIS III, E., MOOS, K. F. & EL-ATTAR, A. (1985) Ten years of mandibular fractures: An analysis of 2,137 cases. *Oral Surgery, Oral Medicine, Oral Pathology,* 59**,** 120-129.

EOS, G. (2011) Medical: Customer Case Study (http://www.eos.info/press/customer_case_studies/bego access date : November 2012).

ESSES, S. J., BERMAN, P., BLOOM, A. I. & SOSNA, J. (2011) Clinical Applications of Physical 3D Models Derived From MDCT Data and Created by Rapid Prototyping. *American Journal of Roentgenology,* 196**,** W683-W688.

FABRISONIC (2012) How it works (http://www.fabrisonic.com/how_it_works.html access date: November 2012).

FARZADI, A., SOLATI-HASHJIN, M., ASADI-EYDIVAND, M. & ABU OSMAN, N. A. (2014) Effect of Layer Thickness and Printing Orientation on Mechanical Properties and Dimensional Accuracy of 3D Printed Porous Samples for Bone Tissue Engineering. *PLoS ONE,* 9**,** 18.

FEDOK, F. G., VAN KOOTEN, D. W., DEJOSEPH, L. M., MCGINN, J. D., SOBOTA, B., LEVIN, R. J. & JACOBS, C. R. (1998) Plating techniques and plate orientation in repair of mandibular angle fractures: An in vitro study. *Laryngoscope,* 108**,** 1218-1224.

FISCHER, H., SCHAFER, M. & MARX, R. (2003) Effect of Surface Roughness on Flexural Strength of Veneer Ceramics. *Journal of Dental Research,* 82**,** 972-975.

FRAZER, R. Q., BYRON, R. T., OSBORNE, P. B. & WEST, K. P. (2005) PMMA: An essential material in medicine and dentistry. *Journal of Long-Term Effects of Medical Implants,* 15**,** 629-639.

FREITAG, V., HELL, B. & FISCHER, H. (1991) Experience with AO reconstruction plates after mandibular resection involving its continuity. *Journal of Cranio-Maxillo-Facial Surgery,* 19**,** 191-198.

FRIDRICH, K. L., PENA-VELASCO, G. & OLSON, R. A. J. (1992) Changing trends with mandibular fractures: A review of 1,067 cases. *Journal of Oral and Maxillofacial Surgery,* 50**,** 586-589.

FUJITA, H., IIDA, H., IDO, K., MATSUDA, Y., OKA, M. & NAKAMURA, T. (2000) Porous apatite-wollastonite glass-ceramic as an intramedullary plug. *J Bone Joint Surg [Br],* 82-B**,** 614-618.

GABALL, C., LOVALD, S., BAACK, B. & OLSON, G. (2011) Minimally Invasive Bioabsorbable Bone Plates for Rigid Internal Fixation of Mandible Fractures. *Archives of Facial Plastic Surgery,* 13**,** 31-35.

GARDAN, N. (2014) Knowledge Management for Topological Optimization Integration in Additive Manufacturing. *International Journal of Manufacturing Engineering,* 2014**,** 9.

GENTILE, P., CHIONO , V., CARMAGNOLA , I. & HATTON , P. V. (2014) An Overview of Poly(lactic-co-glycolic) Acid (PLGA)-Based Biomaterials for Bone Tissue Engineering *Int. J. Mol. Sci. ,* 15**,** pp 3640-3659.

GEORGIOU, G., MATHIEU, L., PIOLETTI, D. P., BOURBAN, P. E., MÃ¥NSON, J. A. E., KNOWLES, J. C. & NAZHAT, S. N. (2007a) Polylactic acid-phosphate glass composite foams as scaffolds for bone tissue engineering. *Journal of Biomedical Materials Research - Part B Applied Biomaterials,* 80**,** 322-331.

GEORGIOU, G., MATHIEU, L., PIOLETTI, D. P., BOURBAN, P. E., MANSON, J. A. E., KNOWLES, J. C. & NAZHAT, S. N. (2007b) Polylactic acid-phosphate glass composite foams as scaffolds for bone tissue engineering. *Journal of Biomedical Materials Research - Part B Applied Biomaterials,* 80**,** 322-331.

GERMAN, R. M. (1996) Sintering Theory and Practice. *Sintering Theory and Practice, by Randall M. German, pp. 568. ISBN 0-471-05786-X. Wiley-VCH, January 1996.,* 1.

GETTY, P. J. & PEABODY, T. D. (1999) *Complications and Functional Outcomes of Reconstruction with an Osteoarticular Allograft After Intra-Articular Resection of the Proximal Aspect of the Humerus*.*

GHAZY, M. M. S. A. (2012) Development of an additive manufacturing decision support system (AMDSS). *School of Mechanical and System Engineering.* Newcastle upon Tyne, Newcastle University.

GIBSON, I., ROSEN, D. W. & STUCKER, B. (2010) Additive Manufacturing Technologies. *Rapid Prototyping to Direct Digital Manufacturing.* Springer Science+Business Media LLC 2010.

GOLDBERG, V. M., AKHAVAN, S., (2005) Biology of bone grafts. IN LIEBERMAN, J. R., FRIEDLAENDER G.E. (Ed.) *Bone regeneration and repair biology and clinical applications.* Totowa, N.J., Humana Press.

GOODACRE, C. J., BERNAL, G., RUNGCHARASSAENG, K. & KAN, J. Y. K. (2003) Clinical complications with implants and implant prostheses. *The Journal of Prosthetic Dentistry,* 90**,** 121-132.

GOODACRE, C. J., KAN, J. Y. K. & RUNGCHARASSAENG, K. (1999) Clinical complications of osseointegrated implants. *The Journal of Prosthetic Dentistry,* 81**,** 537-552.

GOODRIDGE, R., DALGARNO, K. & WOOD, D. (2006a) Indirect selective laser sintering of an apatite-mullite glass-ceramic for potential use in bone replacement applications. *Proceedings of the Institution of Mechanical Engineers, Part H: Journal of Engineering in Medicine,* 220**,** 57-68.

GOODRIDGE, R. D., DALGARNO, K. W. & WOOD, D. J. (2006b) Indirect selective laser sintering of an apatite-mullite glass-ceramic for potential use in bone replacement applications. *Proceedings of the Institution of Mechanical Engineers Part H-Journal of Engineering in Medicine,* 220**,** 57-68.

GOSAIN, A. K. (2002) The current status of tissue glues: I. For bone fixation. *Plastic and Reconstructive Surgery,* 109**,** 2581-2583.

GOSAIN, A. K. & LYON, V. B. (2001) Use of tissue glue: Current status. *Perspect. Plast. Surg.,* 15**,** 129-145.

GOSAIN, A. K., SONG, L., CORRAO, M. A. & PINTAR, F. A. (1998) Biomechanical evaluation of titanium, biodegradable plate and screw, and cyanoacrylate glue fixation systems in craniofacial surgery. *Plastic and Reconstructive Surgery,* 101**,** 582-591.

HAGUE, R., CAMPBELL, I. & DICKENS, P. (2003) Implications on design of rapid manufacturing. *Proceedings of the Institution of Mechanical Engineers, Part C: Journal of Mechanical Engineering Science,* 217**,** 25-30.

HAGUE, R., MANSOUR, S. & SALEH, N. (2004) Material and design considerations for rapid manufacturing. *International Journal of Production Research,* 42**,** 4691-4708.

HEISS, C., SCHETTLER, N., WENISCH, S., CORDS, S., SCHILKE, F., LIPS, K. S., ALT, V. & SCHNETTLER, R. (2010) Bond strength of an alkylene bis(dilactoyl)-methacrylate bone adhesive: A biomechanical evaluation in sheep. *Journal of Biomaterials Science, Polymer Edition,* 21**,** 1345-1358.

HENCH, L. L. (1991) Bioceramics: From Concept to Clinic. *Journal of the American Ceramic Society Bulletin,* Vol. 74**,** pp: 1487-1510.

HENCH, L. L. (1998) Bioceramics. *Journal of the American Ceramic Society,* 81**,** 1705-1728.

HENCH, L. L. & ANDERSSON, O. (1993) "Bioactive Glasses" IN HENCH, L. L. & WILSON, J. (Eds.) *An Introduction to Bioceramics.* Singapore, World Scientific.

HENCH, L. L. & KOKUBO, T. (1998) Properties of bioactive glasses and glass-ceramics. IN BLACK, J. & HASTINGS, G. (Eds.) *Handbook of Biomaterial Properties.* London, Chapman & Hill.

HENCH, L. L. & POLAK, J. M. (2002) Third-Generation Biomedical Materials. *Science,* 295**,** 1014-1017.

HENCH, L. L. & WILSON, J. (1995) Bioactive Glasses and Glass-Ceramics: A 25-Year Restrospective. IN FISCHMAN, G., CLARE, A. & HENCH, L. L. (Eds.) *Bioceramics: Materials and Applications.* Ohio, The American Ceramic Society.

HENCH, L. L. & WILSON, J. (2013) Introduction. IN HENCH, L. L. (Ed.) *An Introduction to Bioceramics, Second Edition.* London, Imperial College Press.

HENRY, D., GOODGE, L. J. & MOGK, D. (2007) X-ray reflection in accordance with Bragg's Law (http://serc.carleton.edu /research_education/ geochemsheets/BraggsLaw.html access date Jan 2014).

HILL, P. A. (1998) Bone Remodelling. *British Journal of Orthodontics,* 25**,** pp. 101 - 107.

HOLAND, W. & BEALL, G. H. (2012) *Glass-ceramic technology,* Hoboken, New Jersey, John Wiley & Sons,.

HOLLISTER, S. J., LEVY, R. A., CHU, T. M., HALLORAN, J. W. & FEINBERG, S. E. (2002) An image-based approach for designing and manufacturing craniofacial scaffolds. *Int. J. Oral Maxillofac. Surg.,* 29**,** 67-71.

HON, K. K. B. (2007) Digital Additive Manufacturing: From Rapid Prototyping to Rapid Manufacturing IN HINDUJA, S. & FAN, K.-C. (Eds.) *Proceedings of the 35th International MATADOR Conference.* London, Springer

HON, K. K. B. & GILL, T. J. (2003) Selective Laser Sintering of SiC/Polyamide Composites. *CIRP Annals - Manufacturing Technology,* 52**,** 173-176.

HOPKINSON, N. (2006) Rapid Manufacturing: Benefits to Your Business and the Technologies to Consider. (http://www.timecompress.com/ magazine/archives.cfm retrieved on 23 Feb 2008). *TCT2006 RM Conference.*

HOPKINSON, N. & DICKNES, P. (2003) Analysis of rapid manufacturing—using layer manufacturing processes for production. *Proceedings of the Institution of Mechanical Engineers, Part C: Journal of Mechanical Engineering Science,* 217**,** 31-39.

HOPKINSON, N., GAO, Y. & MCAFEE, D. (2006) Design for environment analyses applied to rapid manufacturing. *Proceedings of the Institution of Mechanical Engineers, Part D: Journal of Automobile Engineering,* 220**,** 1363-1372.

HOPKINSON, N., HAGUE, R. & DICKENS, P. (2005) *Rapid manufacturing: An industrial revolution for the digital age,* West Sussex, England, John Wiley and Sons.

HOQUE, A. S. M., HALDER, P. K., PARVEZ, M. S. & SZECSI, T. (2012) Integrated manufacturing features and Design-for-manufacture guidelines for reducing product

cost under CAD/CAM environment. *Computers & Industrial Engineering,* 66**,** 988-1003.

HULBERT, S. F., HENCH, L. L., FORBERS, D. & BOWMAN, L. S. (1982) History of bioceramics. *Ceramics International,* Vol. 8**,** pp: 131-140.

I. GIBSON, D.W. ROSEN & STUCKER, B. (2010) Additive Manufacturing Technologies. Springer ScienceþBusiness Media, LLC.

IGNJATOVIC, N., SULJOVRUJIC, E., BUDINSKI-SIMENDIC, J., KRAKOVSKY, I. & USKOKOVIC, D. (2004) Evaluation of hot-pressed hydroxyapatite/poly-L-lactide composite biomaterial characteristics. *Journal of Biomedical Materials Research - Part B Applied Biomaterials,* 71**,** 284-294.

IIDA, S., HASSFELD, S., REUTHER, T., SCHWEIGERT, H.-G., HAAG, C., KLEIN, J. & MÜHLING, J. (2003) Maxillofacial fractures resulting from falls. *Journal of Cranio-Maxillofacial Surgery,* 31**,** 278-283.

IIDA, S., KOGO, M., SUGIURA, T., MIMA, T. & MATSUYA, T. (2001) Retrospective analysis of 1502 patients with facial fractures. *International Journal of Oral and Maxillofacial Surgery,* 30**,** 286-290.

IMPACT-TEST, U. K. (2013) 1000ml Pycnometer (http://impact-test.co.uk/ access date: July 2014).

JAIN, R. (2000a) The manufacturing techniques of various drug loaded biodegradable poly(lactide-co-glycolide) (PLGA) devices. *Biomaterials* 21(23)**,** pp 2475-2490.

JAIN, R. A. (2000b) The manufacturing techniques of various drug loaded biodegradable poly(lactide-co-glycolide) (PLGA) devices. *Biomaterials,* 21**,** 2475-2490.

JAMSHIDINIA, M., WANG, L., TONG, W. & KOVACEVIC, R. (2014) The bio-compatible dental implant designed by using non-stochastic porosity produced by Electron Beam Melting® (EBM). *Journal of Materials Processing Technology,* 214**,** 1728-1739.

JAYTECGLASS (2012) Density bottle.(http://www.jaytecglass.co.uk/laboratory-glassware/oil-test-glassware/density-bottlespyknometers/ access date: September 2013).

JONES, A. C., ARNS, C. H., SHEPPARD, A. P., HUTMACHER, D. W., MILTHORPE, B. K. & KNACKSTEDT, M. A. (2007) Assessment of bone ingrowth into porous biomaterials using MICRO-CT. *Biomaterials,* 28**,** 2491-2504.

JONES, J. R. & HENCH, L. L. (2001) Biomedical materials for new millennium: Perspective on the future. *Materials Science and Technology,* 17**,** 891-900.

KAMRANI, A. K. & NASR, E. A. (2006) *Rapid Prototyping: Theory and Practice.,* London, Springer.

KANDALAM, U., BOUVIER, A. J., CASAS, S. B., SMITH, R. L., GALLEGO, A. M., ROTHROCK, J. K., THOMPSON, J. Y., HUANG, C. Y. C. & STELNICKI, E. J. (2013) Novel bone adhesives: a comparison of bond strengths in vitro. *International Journal of Oral and Maxillofacial Surgery,* 42**,** 1054-1059.

KANG, S. L. (2005) Sintering : Densification, Grain Growth and Microstructure Jordan Hill, GBR, Butterworth-Heinemann (Available from: ProQuest ebrary access date October 2013).

KAR, I. & MAHAVOI, B. (2012) Retrospective Analysis of 503 Maxillo-Facial Trauma Cases in Odisha During the Period of Decâ€™04â€“Novâ€™09. *Journal of Maxillofacial and Oral Surgery,* 11**,** 177-181.

KARAGEORGIOU, V. & KAPLAN, D. (2005) Porosity of 3D biomaterial scaffolds and osteogenesis. *Biomaterials,* 26**,** 5474-5491.

KATTI, D. S., LAKSHMI, S., LANGER R. & LAURENCIN, C. T. (2002) Toxicity,biodegradation and elimination of polyanhydrides. *Adv. Drug Deliv Rev,* 54**,** pp 933-961.

KESHAW, H., GEORGIOU, G., BLAKER, J. J., FORBES, A., KNOWLES, J. C. & DAY, R. M. (2009) Assessment of polymer/bioactive glass-composite microporous spheres for tissue regeneration applications. *Tissue Engineering - Part A,* 15**,** 1451-1461.

KHALYFA, A., VOGT, S., WEISSER, J., GRIMM, G., RECHTENBACH, A., MEYER, W. & SCHNABELRAUCH, M. (2007) Development of a new calcium phosphate powder-binder system for the 3D printing of patient specific implants. *Journal of Materials Science-Materials in Medicine,* 18**,** 909-916.

KHAN, S. F., DALGARNO, KENNETH W. (2010) Design of customised bioceramic medical implants by layered manufacturing. IN BARTOLO, P. J. E. A. (Ed.) *Innovative Developments in Design and Manufacturing.* London, Taylor & Francis Group.

KIM, G. D. & OH, Y. T. (2008) A benchmark study on rapid prototyping processes and machines: quantitative comparisons of mechanical properties, accuracy, roughness, speed, and material cost. *Proceedings of the Institution of Mechanical Engineers, Part B: Journal of Engineering Manufacture,* 222**,** 201-215.

KIM, S.-G. & PARK, S.-S. (2007) Incidence of Complications and Problems Related to Orthognathic Surgery. *Journal of Oral and Maxillofacial Surgery,* 65**,** 2438-2444.

KIM, Y.-R., SEO, S.-H., LEE, E., PYO, M., KIM, H., PARK, S., LEE, D.-W., PIE, J.-E., RYU, J.-J. & KIM, M.-K. (2013) Effect of dental implant materials on the extracellular matrix formation and cellular adhesion in MG-63 cells. *Molecular & Cellular Toxicology,* 9**,** 327-334.

KITSUGI, T., YAMAMURO, T. & KOKUBO, T. (1989) Bonding behavior of a glassceramic containing apatite and wollastonite in segmental replacement of the rabbit tibia under load-bearing conditions. *The Journal of Bone and Joint Surgery,* Vol. 71**,** pp: 264-272.

KLAMMERT, U., VORNDRAN, E., REUTHER, T., MULLER, F. A., ZORN, K. & GBURECK, U. (2010) Low temperature fabrication of magnesium phosphate cement scaffolds by 3D powder printing. *Journal of Materials Science-Materials in Medicine,* 21**,** 2947-2953.

KLEIN, M. & GLATZER, C. (2006) Individual CAD/CAM fabricated glass-bioceramic implants in reconstructive surgery of the bony orbital floor. *Plastic and Reconstructive Surgery,* 117**,** 565-570.

KOBAYASHI, M., NAKAMURA, T., OKADA, Y., FUKUMOTO, A., FURUKAWA, T., KATO, H., KOKUBO, T. & KIKUTANI, T. (1998) Bioactive bone cement: Comparison of apatite and wollastonite containing glass-ceramic, hydroxyapatite, and β-tricalcium phosphate fillers on bone-bonding strength. *Journal of Biomedical Materials Research,* 42**,** 223-237.

KOKUBO, T. (1991a) Bioactive Glass-Ceramics: Properties and Applications. *Biomaterials,* Vol. 12**,** pp: 155-163.

KOKUBO, T. (1991b) Bioactive glass ceramics: properties and applications. *Biomaterials,* 12**,** 155-163.

KOKUBO, T. (2008) Bioactive glass-ceramics. IN KOKUBO, T. (Ed.) *Bioceramics and their clinical applications.* Cambridge, Woodhead Publishing.

KOKUBO, T., ITO, S., SAKKA, S. & YAMAMURO, T. (1986) Formation of a High-Strength Bioactive Glass-Ceramic in the System $MgO-CaO-SiO_2-P_2O_5$. *Journal of Material Science,* Vol. 21**,** pp: 536-540.

KOKUBO, T., KIM, H.-M. & KAWASHITA, M. (2003) Novel bioactive materials with different mechanical properties. *Biomaterials,* 24**,** 2161-2175.

KOKUBO, T., SHIGEMATSU, M., NAGASHIMA, Y., TASHIRO, M., NAKAMURA, T. & HIGASHI, S. (1982) Apatite and wollastonite containing glass-ceramics for prosthetic application. *Bulletin of Institute for Chemical Research, Kyoto University,* Vol. 60**,** pp: 260-268.

KOSTAKIS, G., STATHOPOULOS, P., DAIS, P., GKINIS, G., IGOUMENAKIS, D., MEZITIS, M. & RALLIS, G. (2012) An epidemiologic analysis of 1,142 maxillofacial fractures and concomitant injuries. *Oral Surgery, Oral Medicine, Oral Pathology, Oral Radiology,* 114**,** S69-S73.

KRUTH, J. P., LEU, M. C. & NAKAGAWA, T. (1998) Progress in Additive Manufacturing and Rapid Prototyping. *CIRP Annals - Manufacturing Technology,* 47**,** 525-540.

KUBYSHKINA, G. (2014) Differential Scanning Calorimetry theoretical background (http://www.fs.uni-lj.si/mma_bin.php?id=2010111100484104 access date Feb 2014).

LAM, C. X. F., MO, X. M., TEOH, S. H. & HUTMACHER, D. W. (2002) Scaffold development using 3D printing with a starch-based polymer. *Materials Science and Engineering: C,* 20**,** 49-56.

LANDES, C. A., BALLON, A. & ROTH, C. (2006) In-patient versus in vitro degradation of P(L/DL)LA and PLGA. *Journal of Biomedical Materials Research - Part B Applied Biomaterials,* 76**,** 403-411.

LAURENCIN, C., KHAN, Y. & EL-AMIN, S. F. (2006) Bone graft substitutes. *Expert Rev Med Devices,* 3**,** 49-57.

LEE, K. (2012) Global trends in maxillofacial fractures. *Craniomaxillofac Trauma Reconstr.,* 5**,** 22.

LEUNG, L., CHAN, C., BAEK, S. & NAGUIB, H. (2008) Comparison of morphology and mechanical properties of PLGA bioscaffolds. *Biomedical Materials,* 3.

LEVY, G. N., SCHINDEL, R. & KRUTH, J. P. (2003) RAPID MANUFACTURING AND RAPID TOOLING WITH LAYER MANUFACTURING (LM) TECHNOLOGIES, STATE OF THE ART AND FUTURE PERSPECTIVES. *CIRP Annals - Manufacturing Technology,* 52**,** 589-609.

LEWANDROWSKI, K.-U. (2002) Tissue Engineering and Biodegradable Equivalents : Scientific and Clinical Applications. IN LEWANDROWSKI, K.-U., WISE, D. L., YASZEMSKI, M. J., GRESSER, J. D., TRANTOLO, D. J. & E., A. (Eds.) New York, NY, USA, Marcel Dekker Incorporated.

LIN, A. C. & LIANG, S.-R. (2002) Rapid prototyping through scanned point data. *International Journal of Production Research,* 40**,** 293-310.

LINCKS, J., BOYAN, B. D. & BLANCHARD, C. R., ET AL. (1998) Response of MG63 osteoblastlike cells to titanium and titanium alloy is dependent on surface roughness and composition. *Biomaterials,* 19**,** pp 2219-2232.

LIU, F., JIA, D., WU, X., HOU, T., WU, C., YOU, C. & WANG, Y. (2002) [Effect of moulding and extruding conditions on mechanical properties of poly(D,L-lactide) and MDI chain-extending poly(D,L-lactide)/hydroxyapatite composite]. *Sheng Wu Yi Xue Gong Cheng Xue Za Zhi,* 19**,** 624-7.

LIU, X. & MA, P. X. (2004) Polymeric Scaffolds for Bone Tissue Engineering. *Annals of Biomedical Engineering,* 32**,** 477-486.

LIU, Y., LIAO, W., JIN, G., YANG, Q. & PENG, W. (2014) Additive manufacturing and digital design assisted precise apicoectomy: a case study. *Rapid Prototyping Journal,* 20**,** 33-40.

LIULAN, L., QINGXI, H., XIANXU, H. & GAOCHUN, X. (2007) Design and Fabrication of Bone Tissue Engineering Scaffolds via Rapid Prototyping and CAD. *Journal of Rare Earths,* 25, Supplement 2**,** 379-383.

LLOYD, A. W. (2002) Interfacial bioengineering to enhance surface biocompatibility. *Med .Device Technol.,* 13**,** 18-21.

LORENSEN, W. E. & CLINE, H. E. (1987) Marching cubes: A high resolution 3D surface construction algorithm. *SIGGRAPH Comput. Graph.,* 21**,** 163-169.

LOVALD, S., BAACK, B., GABALL, C., OLSON, G. & HOARD, A. (2010) Biomechanical Optimization of Bone Plates Used in Rigid Fixation of Mandibular Symphysis

Fractures. *Journal of oral and maxillofacial surgery : official journal of the American Association of Oral and Maxillofacial Surgeons,* 68**,** 1833-1841.

LOZO, B., STANIC, M., JAMNICKI, S., POLJACEK, S. M. & MUCK, T. (2008) Three-Dimensional Ink Jet Prints-Impact of Infiltrants. *Journal of Imaging Science and Technology,* 52.

LU, L., GARCIA, C. A. & MIKOS, A. G. (1999) In vitro degradation of thin poly(DL-lactic-co-glycolic acid) films. *Journal of Biomedical Materials Research,* 46**,** 236-244.

MAJI, P., BANERJEE, P. & SINHA, A. (2008) Application of rapid prototyping and rapid tooling for development of patient-specific craniofacial implant: an investigative study. *The International Journal of Advanced Manufacturing Technology,* 36**,** 510-515.

MAKADIA, H. K. & SIEGEL , S. J. (2011) Poly Lactic-co-Glycolic Acid (PLGA) as Biodegradable Controlled Drug Delivery Carrier. *Polymers,* 3**,** pp 1377-1397.

MALEKSAEEDI, S., ENG, H., WIRIA, F. E., HA, T. M. H. & HE, Z. (2014) Property enhancement of 3D-printed alumina ceramics using vacuum infiltration. *Journal of Materials Processing Technology,* 214**,** 1301-1306.

MANSOUR, S. & HAGUE, R. (2003) Impact of rapid manufacturing on design for manufacture for injection moulding. *Proceedings of the Institution of Mechanical Engineers, Part B: Journal of Engineering Manufacture,* 217**,** 453-461.

MARCHELLI, G., PRABHAKAR, R., STORTI, D. & GANTER, M. (2011) The guide to glass 3D printing: developments, methods, diagnostics and results. *Rapid Prototyping Journal,* 17**,** 187-194.

MARINUCCI, L., BALLONI, S. & BECCHETTI, E., ET AL. (2006) Effect of titanium surface roughness on human osteoblast proliferation and gene expression in vitro. *Int J Oral Maxillofac Implants.,* 21**,** pp 719-725.

MARTOLA, M., LINDQVIST, C., HÄNNINEN, H. & AL-SUKHUN, J. (2007) Fracture of titanium plates used for mandibular reconstruction following ablative tumor surgery. *Journal of Biomedical Materials Research Part B: Applied Biomaterials,* 80B**,** 345-352.

MASIA, S., CALVERT, P., RHINE, W. & BOWEN, H. K. (1989) Effect of oxides on binder burnout during ceramics processing. *Journal of Materials Science,* 24**,** 1907-1912.

MATTHEW, H. W. T. (2002) Polymers for tissue engineering scaffold. IN DUMITRIU, S. (Ed.) *Polymeric Biomaterials.* New York, Marcel Dekker.

MAVILI, M. E., CANTER, H. I., SAGLAM-AYDINATAY, B., KAMACI, S. & KOCADERELI, I. (2007) Use of three-dimensional medical modeling methods for precise planning of orthognathic surgery. *Journal of Craniofacial Surgery,* 18**,** 740-747.

MCDERMOTT, N. E., CHUANG, S. K., WOO, V. V. & DODSON, T. B. (2004) Complications of dental implants: identification, frequency, and associated risk factors. *The Journal of Prosthetic Dentistry,* 92**,** 78.

MCDONALD, P. F., LYONS, J. G., GEEVER, L. M. & HIGGINBOTHAM, C. L. (2009) In vitro degradation and drug release from polymer blends based on poly(dl-lactide), poly(l-lactide-glycolide) and poly(Îµ-caprolactone). *Journal of Materials Science,* 45**,** 1284-1292.

MECHANICALENGINEERINGBLOG (2012) What is rapid prototyping.

MELCHELS, F. P. W., FEIJEN, J. & GRIJPMA, D. W. (2010) A review on stereolithography and its applications in biomedical engineering. *Biomaterials,* 31**,** 6121-6130.

MELGOZA, E. L., VALLICROSA, G., SERENA, L., CIURANA, J. & RODRÃGUEZ, C. A. (2014) Rapid tooling using 3D printing system for manufacturing of customized tracheal stent. *Rapid Prototyping Journal,* 20 Iss 1**,** pp 2-12.

MELLOR, S., HAO, L. & ZHANG, D. (2014) Additive manufacturing: A framework for implementation. *International Journal of Production Economics,* 149**,** 194-201.

MIAO, X., TAN, L. P., TAN, L. S. & HUANG, X. (2007) Porous calcium phosphate ceramics modified with PLGA-bioactive glass. *Materials Science and Engineering: C,* 27**,** 274-279.

MIDDLETON, J. C. & TIPTON, A. J. (2000) Synthetic biodegradable polymers as orthopedic devices. *Biomaterials,* 21 pp. 2335-2346.

MOONEY, D. J., BALDWIN, D. F., SUH, N. P., VACANTI, J. P. & LANGER, R. (1996) Novel approach to fabricate porous sponges of poly(d,l-lactic-co-glycolic acid) without the use of organic solvents. *Biomaterials,* 17**,** 1417-1422.

MORITA, S., FURUYA, K., ISHIHARA, K. & NAKABAYASHI, N. (1998) Performance of adhesive bone cement containing hydroxyapatite particles. *Biomaterials,* 19**,** 1601-1606.

NAGAHANUMAIAH, SUBBURAJ, K. & RAVI, B. (2008) Computer aided rapid tooling process selection and manufacturability evaluation for injection mold development. *Computers in Industry,* 59**,** 262-276.

NAIR, L. S. & LAURENCIN, C. T. (2007) Biodegradable polymers as biomaterials. *Progress in Polymer Science,* 32**,** 762-798.

NAMII, O. (2013) Additive Fabrication for MetalFormers (http://namii.org/wp-content/uploads/2013/07/Additive-Fabrication-for-MetalFormers-Webinar-2013-06-25-rev-c.pdf access on 09/2013).

NANOSCIENCE (2014) SEM technology overview(http://www.nanoscience.com/ products/sem/technology-overview/ access date: Jan 2014).

NATU, S. S., PRADHAN, H., GUPTA, H., ALAM, S., GUPTA, S., PRADHAN, R., MOHAMMAD, S., KOHLI, M., SINHA, V. P., SHANKAR, R. & AGARWAL, A. (2012) An Epidemiological Study on Pattern and Incidence of Mandibular Fractures. *Plastic Surgery International,* 2012**,** 7.

NAVARRO, M., MICHIARDI, A., CASTAÃ±O, O. & PLANELL, J. A. (2008) Biomaterials in orthopaedics. *Journal of The Royal Society Interface,* 5**,** 1137-1158.

NAVARRO, M., VALLE, S. D., MARTÍNEZ, S., ZEPPETELLI, S., AMBROSIO, L., PLANELL, J. A. & GINEBRA, M. P. (2004) New macroporous calcium phosphate glass ceramic for guided bone regeneration. *Biomaterials,* 25**,** 4233-4241.

NIELSEN, L. F. (1982) Elastic Properties of Two-Phase Materials. *Mat. Sci. Eng.,* 52**,** 39-62.

NIELSEN, L. F. (1984) Elasticity and damping of porous and impregnated materials. *Journ. Am. Ceramic Soc.***,** 93-98.

NONAKA, H. H. (1997) Plant carbohydrate-derived products as fat replacers and calorie reducers. *Cereal Food World,* Vol. 42**,** 376-8.

NOORANI, R. (2006) *Rapid Prototyping: Principles and Applications,* New York, John Wiley and Sons.

NORDIN, R., RAHMAN, N. A., RASHDI, M. F., YUSOFF, A., RAHMAN, R. A., SULONG, S., NUR, A. M., RAZAK, N. A., JABAR, M. N. A., IBRAHIM, M. I., MOHAMED, N., AHMAD, S. H. R. & RAMLI, R. (2014) Oral and maxillofacial trauma caused by road traffic accident in two university hospitals in Malaysia: A cross-sectional study. *Journal of Oral and Maxillofacial Surgery, Medicine, and Pathology*.

NOVAKOVA-MARCINCINOVA, L. & KURIC, I. (2012) Basic and Advanced Materials for Fused Deposition Modeling Rapid Prototyping Technology *Manuf. and Ind. Eng* 11(1)**,** pp 22-27.

NOVITSKAYA, E. E., CHEN, P.-Y., HAMED, E., LI, J., LUBARDA, V. A., JASIUK, I. & MCKITTRICK, J. (2011) Recent advances on the measurement and calculation of the elastic moduli of cortical and trabecular bone: a review. *Journal Of Theoretical And Applied Mechanics,* 38**,** 209-297.

NYEMBWE, K. D., DE BEER, D., VAN DER WALT, J. G. & BHERO, S. (2013) A case study of tool manufacturing by metal casting in rapid prototyping sand moulds. *Interim : Interdisciplinary Journal,* 12**,** 210-218.

OBIELODAN, J. O., CEYLAN, A., MURR, L. E. & STUCKER, B. E. (2010) Multi-material bonding in ultrasonic consolidation. *Rapid Prototyping Journal,* Vol. 16 Iss: 3**,** pp.180 - 188.

OBJECT (2014) http://www.stratasys.com/ 3d-printers/design-series/ precision/objet500-connex3.

OBJET (2008) Polyjet Technology.

OGILVIE, C., CRAWFORD, E., HOSALKAR, H., KING, J. & LACKMAN, R. (2009) Long-term Results for Limb Salvage with Osteoarticular Allograft Reconstruction. *Clinical Orthopaedics and Related ResearchÂ®,* 467**,** 2685-2690.

ONO, K., YAMAMURO, T., NAKAMURA, T., KAKUTANI, Y., KITSUGI, T., HYAKUNA, K., KOKUBO, T., OKA, M. & KOTOURA, Y. (1988) Apatite-wollastonite containing glass ceramic-fibrin mixture as a bone defect filler. *Journal of Biomedical Materials Research,* Vol. 22**,** pp: 869-885.

OPTOMEC (2013) LENS Technology (http://www.optomec.com/3d-printed-metals/lens-technology/ access date : July 2014).

PARK, J. H., JUNG, J. W., KANG, H.-W. & DONG-WOO, C. (2014) Indirect three-dimensional printing of synthetic polymer scaffold based on thermal molding process. *Biofabrication,* 6**,** 025003.

PARTHASARATHY, J., STARLY, B. & RAMAN, S. (2009) Computer Aided Biomodeling and Analysis of Patient Specific Porous Titanium Mandibular Implants. *Journal of Medical Devices-Transactions of the Asme,* 3.

PARTHASARATHY, J., STARLY, B. & RAMAN, S. (2011) A design for the additive manufacture of functionally graded porous structures with tailored mechanical properties for biomedical applications. *Journal of Manufacturing Processes,* 13**,** 160-170.

PASSERINI, N. & CRAIG, D. Q. M. (2001) An investigation into the effects of residual water on the glass transition temperature of polylactide microspheres using modulated temperature DSC. *Journal of Controlled Release,* 73**,** 111-115.

PATTNAIK, S., JHA, P. K. & KARUNAKAR, D. B. (2014) A review of rapid prototyping integrated investment casting processes. *Proceedings of the Institution of Mechanical Engineers, Part L: Journal of Materials Design and Applications,* 228**,** 249-277.

PELTONIEMI, H., ASHAMMAKHI, N., KONTIO, R., WARIS, T., SALO, A., LINDQVIST, C., GRÄTZ, K. & SUURONEN, R. (2002) The use of bioabsorbable osteofixation devices in craniomaxillofacial surgery. *Oral Surgery, Oral Medicine, Oral Pathology, Oral Radiology, and Endodontology,* 94**,** 5-14.

PENA, I., ROBERTS, L. E., GUY, W. M. & ZEVALLOS, J. P. (2014) The Cost and Inpatient Burden of Treating Mandible Fractures: A Nationwide Inpatient Sample Database Analysis. *Otolaryngology -- Head and Neck Surgery,* 151**,** 591-598.

PHAM, D. & DIMOV, S. (2003) Rapid prototyping and rapid tooling—the key enablers for rapid manufacturing. *Proceedings of the Institution of Mechanical Engineers, Part C: Journal of Mechanical Engineering Science,* 217**,** 1-23.

PHAM, D. T. & DIMOV, S. S. (2001) *Rapid manufacturing: The technologies and applications of rapid prototyping and rapid tooling*.

PHAM, D. T. & GAULT, R. S. (1998) A comparison of rapid prototyping technologies. *International Journal of Machine Tools and Manufacture,* 38**,** 1257-1287.

PILIPOVIC, A., RAOS, P. & SERCER, M. (2009) Experimental analysis of properties of materials for rapid prototyping. *International Journal of Advanced Manufacturing Technology,* 40**,** 105-115.

PODPORSKA, J., BŁAŻEWICZ, M., TRYBALSKA, B. & ZYCH, Ł. (2008) A novel ceramic material with medical application. *Processing and Application of Ceramics,* 2 [1]**,** pp 19-22.

PONCHE, R., HASCOET, J. Y., KERBRAT, O. & MOGNOL, P. (2012) A new global approach to design for additive manufacturing. *Virtual and Physical Prototyping,* 7**,** 93-105.

PORTER, J. R., HENSON, A. & POPAT, K. C. (2009) Biodegradable poly([var epsilon]-caprolactone) nanowires for bone tissue engineering applications. *Biomaterials,* 30**,** 780-788.

POUKENS, J., LAEVEN, P., BEERENS, M., KOPER, D., LETHAUS, B., KESSLER, P., VANDER SLOTEN, J. & LAMBRICHTS, I. (2010) Custom surgical implants using additive manufacturing. *Digital Dental News, 4(1). p. 72-75.* Comcord -Duesseldorf.

QUAIL, F. J., SCANLON, T. & STRICKLAND, M. (2010) Development of a regenerative pump impeller using rapid manufacturing techniques. *Rapid Prototyping Journal,* 16**,** 337-344.

QUICKPARTS (2013) SLS Materials properties. *Low-VolumePrototypes.*

RAHAMAN, M. N. (2008) *Sintering of Ceramics,* Boca Raton, CRC Press.

RAHMAN, R., HUSSAINI, H., RAHMAN, N., RAHMAN, S. A., NOR, G., AI IDRUS, S. & RAMLI, R. (2007) Facial Fractures in Kajang Hospital, Malaysia: A 5-Year Review. *European Journal of Trauma and Emergency Surgery,* 33**,** 90-95.

RAHMATI, S., AKBARI, J. & BARATI, E. (2007) Dimensional accuracy analysis of wax patterns created by RTV silicone rubber molding using the Taguchi approach. *Rapid Prototyping Journal,* 13**,** 115-122.

RAINER, A., GIANNITELLI, S., ACCOTO, D., DE PORCELLINIS, S., GUGLIELMELLI, E. & TROMBETTA, M. (2012) Load-Adaptive Scaffold Architecturing: A Bioinspired Approach to the Design of Porous Additively Manufactured Scaffolds with Optimized Mechanical Properties. *Annals of Biomedical Engineering,* 40**,** 966-975.

RAMIN, E. & HARRIS, R. A. (2009) Advanced computer-aided design for bone tissue-engineering scaffolds. *Proceedings of the Institution of Mechanical Engineers, Part H: Journal of Engineering in Medicine,* 223**,** 289-301.

RAMOS, A. M. D. A. M. & SIMOES, J. A. (2009) CAD-CAM-RTV- lost-wax casting technology for medical implants. *Rapid Prototyping Journal,* 15**,** pp. 211-215.

RASHID, H. (2014) The effect of surface roughness on ceramics used in dentistry: A review of literature. *European Journal of Dentistry,* 8**,** 571-579.

RAWLINGS, R. D., WU, J. P. & BOCCACCINI, A. R. (2006) Glass-ceramics: Their production from waste-A Review. *Journal of Materials Science,* 41**,** 733-761.

RICHARD, B., DOMINIC, E., PETER, E., ALAN, B. & ADRIAN, S. (2009) Rapid manufacture of custom-fitting surgical guides. *Rapid Prototyping Journal,* 15**,** 346-354.

RIENER, R. & HARDERS, M. (Eds.) (2012) *Virtual Reality in Medicine: Medical Model Generation,* London, Springer-Verlag.

ROEDER, R. K., CONVERSE, G. L., KANE, R. J. & YUE, W. (2008) Hydroxyapatite-reinforced polymer biocomposites for synthetic bone substitutes. *JOM,* 60**,** 38-45.

ROTHEN-WEINHOLD, A., BESSEGHIR, K., VUARIDEL, E., SUBLET, E., OUDRY, N., KUBEL, F. & GURNY, R. (1999) Injection-molding versus extrusion as manufacturing technique for the preparation of biodegradable implants. *European Journal of Pharmaceutics and Biopharmaceutics,* 48**,** 113-121.

RUFFO, M., TUCK, C. & HAGUE, R. (2006) Cost estimation for rapid manufacturing - laser sintering production for low to medium volumes. *Proceedings of the Institution of Mechanical Engineers, Part B: Journal of Engineering Manufacture,* 220**,** 1417-1427.

SABIR, M., XU, X. & LI, L. (2009) A review on biodegradable polymeric materials for bone tissue engineering applications. *Journal of Materials Science,* 44**,** 5713-5724.

SAITO, E., KANG, H., TABOAS, J., DIGGS, A., FLANAGAN, C. & HOLLISTER, S. (2010) Experimental and computational characterization of designed and fabricated 50:50 PLGA porous scaffolds for human trabecular bone applications. *Journal of Materials Science: Materials in Medicine,* 21**,** 2371-2383.

SAKR, K., FARAG, I. A. & ZEITOUN, I. M. (2006) Review of 509 mandibular fractures treated at the University Hospital, Alexandria, Egypt. *British Journal of Oral and Maxillofacial Surgery,* 44**,** 107-111.

SALMI, M., TUOMI, J., PALOHEIMO, K.-S., BJORKSTRAND, R., PALOHEIMO, M., SALO, J., KONTIO, R., MESIMAKI, K. & MAKITIE, A. A. (2012) Patient-specific reconstruction with 3D modeling and DMLS additive manufacturing. *Rapid Prototyping Journal,* 18**,** 209-214.

SANGHERA, B., NAIQUE, S., PAPAHARILAOU, Y.,AMIS, A. (2001) Preliminary study of rapid prototype medical models. *Rapid Prototyping Journal,* Vol. 7**,** pp.275 - 284.

SCHLICKEWEI, W. & SCHLICKEWEI, C. (2007) The Use of Bone Substitutes in the Treatment of Bone Defects – the Clinical View and History. *Macromolecular Symposia,* 253**,** 10-23.

SCHMIDT, B. L., KEARNS, G., GORDON, N. & KABAN, L. B. (2000) A financial analysis of maxillomandibular fixation versus rigid internal fixation for treatment of mandibular fractures. *Journal of Oral and Maxillofacial Surgery,* 58**,** 1206-1210.

SCHMITZ, J. P. (2005) Bone Substitutes in Reconstructive Implant Surgery. *Journal of Oral and Maxillofacial Surgery,* 63**,** 117-118.

SD3DPRINTING (2013) FFF vs. SLA vs. SLS: 3D Printing. *Rapid Prototyping 3D Printing.*

SEITZ, H., DEISINGER, U., LEUKERS, B., DETSCH, R. & ZIEGLER, G. (2009) Different Calcium Phosphate Granules for 3-D Printing of Bone Tissue Engineering Scaffolds. *Advanced Engineering Materials,* 11**,** B41-B46.

SEITZ, H., RIEDER, W., IRSEN, S., LEUKERS, B. & TILLE, C. (2005) Three-dimensional printing of porous ceramic scaffolds for bone tissue engineering. *Journal of Biomedical Materials Research Part B: Applied Biomaterials,* 74B**,** 782-788.

SÉQUIN, C. H. (2005) CAD tools for aesthetic engineering. *Computer-Aided Design,* 37**,** 737-750.

SHAHZAD, K., DECKERS, J., KRUTH, J.-P. & VLEUGELS, J. (2013) Additive manufacturing of alumina parts by indirect selective laser sintering and post processing. *Journal of Materials Processing Technology,* 213**,** 1484-1494.

SHAHZAD, K., DECKERS, J., ZHANG, Z., KRUTH, J.-P. & VLEUGELS, J. (2014) Additive manufacturing of zirconia parts by indirect selective laser sintering. *Journal of the European Ceramic Society,* 34**,** 81-89.

SHETTY, V., ATCHISON, K., LEATHERS, R., BLACK, E., ZIGLER, C. & BELIN, T. R. (2008) Do the Benefits of Rigid Internal Fixation of Mandible Fractures Justify the Added Costs? Results From a Randomized Controlled Trial. *Journal of Oral and Maxillofacial Surgery,* 66**,** 2203-2212.

SHIBAHARA, T., NOMA, H., FURUYA, Y. & TAKAKI, R. (2002) Fracture of mandibular reconstruction plates used after tumor resection. *Journal of Oral and Maxillofacial Surgery,* 60**,** 182-185.

SHINOHARA, N., OKUMIYA, M., HOTTA, T., NAKAHIRA, K., NAITO, M. & UEMATSU, K. (1999) Formation mechanisms of processing defects and their relevance to the strength in alumina ceramics made by powder compaction process. *Journal of Materials Science,* 34**,** 4271-4277.

SILBER, J. S., ANDERSON, D. G., DAFFNER, S. D., BRISLIN, B. T., LELAND, J. M., HILIBRAND, A. S., VACCARO, A. R. & ALBERT, T. J. (2003) Donor Site

Morbidity After Anterior Iliac Crest Bone Harvest for Single-Level Anterior Cervical Discectomy and Fusion. *Spine,* 28**,** 134-139.

SIMON, E. N. M., MERKX, M. A. W., KALYANYAMA, B. M., SHUBI, F. M. & STOELINGA, P. J. W. (2013) Immediate reconstruction of the mandible after resection for aggressive odontogenic tumours: a cohort study. *International Journal of Oral and Maxillofacial Surgery,* 42**,** 106-112.

SIMSKE, S. J., AYERS, R. A. & BATEMANT, A. (1997) Porous materials for bone engineering. *Materials Science Forum,* 250**,** pp. 151-182.

SMITH, L. (1963) CERAMIC-PLASTIC MATERIAL AS A BONE SUBSTITUTE. *Archives of surgery (Chicago, Ill. : 1960),* 87**,** 653-661.

ST JOHN, T. A., VACCARO, A. R., SAH, A. P., SCHAEFER, M., BERTA, S. C., ALBERT, T., AND HILIBRAND, A. (2003) Physical and Monetary Costs Associated With Autogenous Bone Graft Harvesting. *Am. J. Orthop.,* 32**,** 18–23.

STRATASYS (2014) compare-fdm-materials. *materials fdm.*

STRONG, D. M., FRIEDLAENDER, G.E., TOMFORD, W.W., SPRINGFIELD, D.S., SHIVES, T.C., BURCHARDT, H., ENNEKING, W.F., MANKIN, H.J. (1996) Immunologic responses in human recipients of osseous and osteochondral allografts: Fundamental and clinical immunology of the skeletal system. *Clin Orthop Relat Res.,* 326**,** 107-114.

SUN, Y., LÜ, P. & WANG, Y. (2009) Study on CAD&RP for removable complete denture. *Computer Methods and Programs in Biomedicine,* 93**,** 266-272.

SUWANPRATEEB, J., SANNGAM, R. & PANYATHANMAPORN, T. (2010) Influence of raw powder preparation routes on properties of hydroxyapatite fabricated by 3D printing technique. *Materials Science and Engineering: C,* 30**,** 610-617.

SWAPP, S. (2007) Scanning Electron Microscopy(SEM) (http://serc.carleton.edu/research education/geochemsheets/techniques/SEM.html access date: June 2013). University of Wyoming.

SZUCS, T. D. & BRABAZON, D. (2009) Effect of saturation and post processing on 3D printed calcium phosphate scaffolds. IN PRADO, M. & ZAVAGLIA, C. (Eds.) *Bioceramics 21.*

TAI, H. Y., UPTON, C. E., WHITE, L. J., PINI, R., STORTI, G., MAZZOTTI, M., SHAKESHEFF, K. M. & HOWDLE, S. M. (2010) Studies on the interactions of CO2 with biodegradable poly(DL-lactic acid) and poly(lactic acid-co-glycolic acid) copolymers using high pressure ATR-IR and high pressure rheology. *Polymer,* 51**,** 1425-1431.

TAN, K. H., CHUA, C. K., LEONG, K. F., NAING, M. W. & CHEAH, C. M. (2005) Fabrication and characterization of three-dimensional polyether–ether–ketone)/–hydroxyapatite biocomposite scaffolds using laser sintering. *Proc. IMechE. Vol. 219 Part H: J. Engineering in Medicine***,** pp. 183-194.

TAN, L., YU, X., WAN, P. & YANG, K. (2013) Biodegradable Materials for Bone Repairs: A Review. *Journal of Materials Science & Technology,* 29**,** 503-513.

TANCRED, D. C., MCCORMACK, B. A. O. & CARR, A. J. (1998) A synthetic bone implant macroscopically identical to cancellous bone. *Biomaterials,* 19**,** 2303-2311.

TESAVIBUL, P., FELZMANN, R., GRUBER, S., LISKA, R., THOMPSON, I., BOCCACCINI, A. R. & STAMPFL, J. (2012) Processing of 45S5 Bioglass® by lithography-based additive manufacturing. *Materials Letters,* 74**,** 81-84.

THOMSON, R. C., YASZEMSKI, M. J., POWERS, J. M. & MIKOS, A. G. (1996) Fabrication of biodegradable polymer scaffolds to engineer trabecular bone. *Journal of Biomaterials Science, Polymer Edition,* 7**,** 23-38.

THOMSON, R. C., YASZEMSKI, M. J., POWERS, J. M. & MIKOS, A. G. (1998) Hydroxyapatite fiber reinforced poly([alpha]-hydroxy ester) foams for bone regeneration. *Biomaterials,* 19**,** 1935-1943.

TOMECKOVA, V. & HALLORAN, J. (2012) Cure depth for photopolymerization of ceramic suspensions. *Journal of the European Ceramic Society,* Vol.30, **,** pp. 3023-3033.

TORMALA, P. (1992) Biodegradable self-reinforced composite materials: Manufacturing structure and mechanical properties. *Clin Mater,* 10**,** pp. 29-34.

TRUSCOTT, M., JANSE VAN VUUREN, M., BOOYSEN, G. & DE BEER, D. (2008) Customised patient implants : future lifeline of the medical industry. *Interim : Interdisciplinary Journal,* 7**,** 100-108.

TURNER, D. (2007) Product Development, The Lifeline of Your Company. TCT Magazine.

UMICH.EDU (2005) Bone Remodelling (http://www.ns.umich.edu/Releases/2005 /Feb05/img/bone.jpg access date: 10-10-13).

UTELA, B. R., STORTI, D., ANDERSON, R. L. & GANTER, M. Development Process for Custom Three-Dimensional Printing (3DP) Material Systems. *Journal of Manufacturing Science and Engineering,* 132**,** 011008-011008.

VAEZI, M., CHIANRABUTRA, S., MELLOR, B. & YANG, S. (2013) Multiple material additive manufacturing Part 1: a review. *Virtual and Physical Prototyping,* 8**,** 19-50.

VAEZI, M. & CHUA, C. K. (2011) Effects of layer thickness and binder saturation level parameters on 3D printing process. *International Journal of Advanced Manufacturing Technology,* 53**,** 275-284.

VAEZI, M., SAFAEIAN, D. & CHUA, C. K. (2011) Gas turbine blade manufacturing by use of epoxy resin tooling and silicone rubber molding techniques. *Rapid Prototyping Journal,* 17**,** 107-115.

VAN DE VELDE, K. & KIEKENS, P. (2002) Biopolymers: overview of several properties and consequences on their applications *Polymer Testing,* 21**,** 433-442.

VG (2012) Laser sintering LS. *Rapid Prototyping - RP.*

VISAVARUNGROJ, N. & REMON, J. P. (1992) Evaluation of maltodextrin as binding agent. *Drug Development and Industrial Pharmacy,* 18**,** 1691-1700.

VITALE-BROVARONE, C., VERNÉ, E., ROBIGLIO, L., APPENDINO, P., BASSI, F., MARTINASSO, G., MUZIO, G. & CANUTO, R. (2007) Development of glass-ceramic scaffolds for bone tissue engineering: Characterisation, proliferation of human osteoblasts and nodule formation. *Acta Biomaterialia,* 3**,** 199-208.

VOZZI, G., FLAIM, C., AHLUWALIA, A. & BHATIA, S. (2003) Fabrication of PLGA scaffolds using soft lithography and microsyringe deposition. *Biomaterials,* 24**,** 2533-2540.

WANG, P., HU, J. & MA, P. X. (2009) The engineering of patient-specific, anatomically shaped, digits. *Biomaterials,* 30**,** 2735-2740.

WARNKE, P. H., SEITZ, H., WARNKE, F., BECKER, S. T., SIVANANTHAN, S., SHERRY, E., LIU, Q., WILTFANG, J. & DOUGLAS, T. (2010) Ceramic scaffolds produced by computer-assisted 3D printing and sintering: characterization and biocompatibility investigations. *Journal of Biomedical Materials Research Part B-Applied Biomaterials,* 93B**,** 212-217.

WEBB, P. A. (2000) A review of rapid prototyping (RP) techniques in the medical and biomedical sector. *Journal of Medical Engineering & Technology,* 24**,** 149-153.

WEI, S. (2009) BioCAD in tissue science and engineering. *Computer-Aided Design and Computer Graphics, 2009. CAD/Graphics '09. 11th IEEE International Conference on.*

WHITE, G. & LYNSKEY, D. (2013) Economic Analysis of Additive Manufacturing for Final Products: An Industrial Approach. Pittsburgh, University of Pittsburgh, Swanson School of Engineering.

WHITEHOUSE, D. J. (2002) *Handbook of Surface and Nanometrology,* Boca raton, Florida, CRC Press.

WILLIAMS, R. J., BIBB, R. & EGGBEER, D. (2008) CAD/CAM-fabricated removable partial-denture alloy frameworks. *Pract Proced Aesthet Dent,* 20**,** 349-51.

WINDER, J., COOKE, R.S., GRAY, J., FANNIN, T., FEGAN, T. (1999) Medical rapid prototyping and 3D CT in the manufacture of custom made cranial titanium plates. *J Med Eng Technol. 1999 Jan-Feb;23(1):26-8.*

WOHLERS, T. (2010) *Wohlers Report 2010-3D Printing and Additive Manufacturing State of the Industry Annual Worldwide Progress Report* Wohlers Associates.

WOHLERS, T. T. (2013) *Wohlers Report 2013: Additive Manufacturing and 3D Printing State of the Industry : Annual Worldwide Progress Report,* Wohlers Associates.

WONG, M., EULENBERGER, J., SCHENK, R. & HUNZIKER, E. (1995) Effect of surface topology on the osseointegration of implant materials in trabecular bone. *Journal of Biomedical Materials Research,* 29**,** 1567-1575.

WU, Y., DU, J., CHOY, K.-L. & HENCH, L. L. (2007) Laser densification of alumina powder beds generated using aerosol assisted spray deposition. *Journal of the European Ceramic Society,* 27**,** 4727-4735.

XIAO, K., DALGARNO, K. W., WOOD, D. J., GOODRIDGE, R. D. & OHTSUKI, C. (2008) Indirect selective laser sintering of apatite–wollostonite glass–ceramic. *Proceedings of the Institution of Mechanical Engineers, Part H: Journal of Engineering in Medicine,* 222**,** 1107-1114.

XIAO, K., DYSON, J. A., DALGARNO, K. W., GENEVER, P., WOOD, D. J., GOODRIDGE, R. D. & OHTSUKI, C. (2007) Manufacture and characterisation of bioceramic tissue engineering scaffolds produced by selective laser sintering. *ASME International Conference on Manufacturing Science and Engineering.* Atlanta, GA, Amer Soc Mechanical Engineers.

YAMAMOTO, N. & SAKAI, K. (2005) Electron beam melting method for metallic material. Google Patents.

YAMAMURO, T. (2013) A/W Glass-Ceramic: Clinical Applications. IN HENCH, L. L. (Ed.) *An Introduction to Bioceramics, Second Edition.* London, Imperial College Press.

YAN, Y., LI, S., ZHANG, R., LIN, F., WU, R., LU, Q., XIONG, Z. & WANG, X. (2009) Rapid Prototyping and Manufacturing Technology: Principle, Representative Technics, Applications, and Development Trends. *Tsinghua Science & Technology,* 14**,** 1-12.

YARLAGADDA, P. K. D. V. & HOCK, T. S. (2003) Statistical analysis on accuracy of wax patterns used in investment casting process. *Journal of Materials Processing Technology,* 138**,** 75-81.

YASA, E., KRUTH, J. P. & DECKERS, J. (2011) Manufacturing by combining Selective Laser Melting and Selective Laser Erosion/laser re-melting. *CIRP Annals - Manufacturing Technology,* 60**,** 263-266.

YASZEMSKI, M. J., PAYNE, R. G., HAYES, W. C., LANGER, R. & MIKOS, A. C. (1996) Evolution of bone transplantation: molecular, cellular, and tissue
strategies to engineer human bone. *Biomaterials,* 17**,** 175-185.

YOU, Y., MIN, B. M., LEE, S. J., LEE, T. S. & PARK, W. H. (2005) In vitro degradation behavior of electrospun polyglycolide, polylactide, and poly(lactide-co-glycolide). *Journal of Applied Polymer Science,* 95**,** 193-200.

YOUNG, P. G., BERESFORD-WEST, T.B.H., COWARD, S.R.L., NOTARBERARDINO, B., WALKER,B., ABDUL-AZIZ, A. (2008) An efficient approach to converting three-dimensional image data into highly accurate computational models. *Phil. Trans. R. Soc. A,* 366 3155-3173.

ZANOTTO, E. D. (2010) A bright future for glass-ceramics. *Ceramics Org. Bulletin.*

ZHANG, H. (2004) Risk of complication associated with dental implants and implant prostheses is variable. *Journal of Evidence Based Dental Practice,* 4**,** 233-234.

ZHAO, J., CAO, W., GE, C., TAN, Y., ZHANG, Y. & FEI, Q. (2009) Research On Laser Engineering Net Shaping of thick-wall nickel based alloy parts. *Rapid Prototyping Journal,* Vol. 15 (1)**,** pp. 24-28.

ZWINGENBERGER, S., NICH,C., VALLADARES,R.D., YAO,Z., STIEHLER,M., GOODMAN,S.B. (2012) Recommendations and Considerations for the Use of Biologics in Orthopedic Surgery. *BioDrugs,* 26**,** 245-256.

Appendix A – Academic contribution.

List of publications:

KHAN, S.F., GERMAN, M., DALGARNO, K.W. Indirect Additive Manufacturing Process of Poly-Lactide-co-Glycolide. *Applied Mechanics and Materials, Trans Tech Publications Inc, USA* (accepted)

ALHARBI, N., KHAN S.F., BRETCANU, O., AND DALGARNO, K.W. Processing of Apatite-Wollastonite (AW) Glass-Ceramic for Three Dimensional Printing (3DP). *Applied Mechanics and Materials, USA, Trans Tech Publications Inc.,* (accepted)

KHAN, S.F., GERMAN, M., AND DALGARNO, K.W. (2012). Using additive manufactured tooling in the fabrication of poly (L-Lactide-co-Glycolide) implants. IN BARTOLO, P. J. E. A. (Ed.) *Virtual and Rapid Prototyping* London, Taylor & Francis Group.

KHAN, S. F., DALGARNO, K. W. (2010) Design of customised bioceramic medical implants by layered manufacturing. IN BARTOLO, P. J. E. A. (Ed.) *Innovative Developments in Design and Manufacturing.* London, Taylor & Francis Group.

KHAN, S. F., DALGARNO, K. W. (2009) Customised bioceramic medical implants by layered manufacturing. *Proceedings of the Tenth National Conference on Rapid Design, Prototyping and Manufacturing.* IN RENNIE, A., BOCKING, C. & JACOBSON, D. (Eds.). High Wycombe: MJA Print.

List of Conference and Poster presentation.

ALHARBI, N., KHAN S.F., BRETCANU, O., AND DALGARNO, K.W. (2014) Processing of Apatite-Wollastonite (AW) Glass-Ceramic for Three Dimensional Printing (3DP). *3rd International Conference on Advanced Material Engineering & Technology,* Ho Chi Minh City, Vietnam, 2014 (accepted)

KHAN, S.F., GERMAN, M., AND DALGARNO, K.W. Indirect Additive Manufacturing Process of Poly-Lactide-co-Glycolide. *3rd International Conference on Advanced Material Engineering & Technology,* Ho Chi Minh City, Vietnam, 2014 (accepted)

ALHARBI, N., KHAN, S.F., DALGARNO, K.W, Indirect Biofabrication of Apatite-wollastonite (A-W) implantable devices by three dimensional printing (3DP). *International Conference on Biofabrication*, Manchester, 2012.

KHAN, S. F., DALGARNO, KENNETH W. Additive Manufacturing (AM) Assisted Fabrication of Apatite-Wollastonite (A-W) Glass Ceramic for Medical Implants *Computer Aided Process Engineering (CAPE 2011)*, Edinburgh, Scotland, 2011.

KHAN, S.F., GERMAN, M.,DALGARNO, K.W. Using additive manufactured tooling in the fabrication of poly (L-Lactide-co-Glycolide) implants Proceeding of 5th *International Conference on Advanced Research in Virtual and Rapid Prototyping (VRAP2011*), Leiria, Portugal, 2011.

KHAN, S. F., DALGARNO, K. W. Design of customised bioceramic medical implants by layered manufacturing. *4th International Conference on Advanced Research in Virtual and Rapid Prototyping (VRAP2009*), Leiria, Portugal, 2009.

KHAN, S. F., DALGARNO, K. W. Customised bioceramic medical implants by layered manufacturing. *10th National Conference on Rapid Design, Prototyping and Manufacturing*, High Wycombe, UK, 2009.

Appendix B Data

Appendix B1 - Density and porosity measurements of AW as determine using pycnometer with data of bending tests.

	dry body		suspended	soaked body	suspended bo	soaked body		dry body	soaked bo	suspended	open porosity				
SAMPLE	weight of dry sample W1(g)	weight of density bottle m1(g)	weight of density bottle + dry sample m2d (g)	weight of density bottle + wet sample m2w (g)	weight of density bottle + dry sample + water m3d (g)	weight of density bottle + wet sample + water m3w (g)	weight of density bottle + water m4 (g)	m2d-m1	m2w-m1	m3d-m4	% apparent porosity	bulk density (g/cu cm)	density of A-W(g/cu cm)	true porosity	open porosity
F1	0.2887	17.3095	17.5982	17.6222	42.7254	42.7434	42.5609	0.2887	0.3127	0.1645	16.1943	1.9445	3.07	36.66068	44.17358
F2	0.3169	18.6419	18.9594	18.9772	43.5756	43.5898	43.3764	0.3175	0.3353	0.1992	13.0786	2.3286	3.07	24.14915	54.15767
F3	0.2719	17.3142	17.5859	17.6034	42.724	42.7319	42.56	0.2717	0.2892	0.164	13.9776	2.1662	3.07	29.43974	47.4788
F4	0.268	18.6325	18.9	18.9159	43.546	43.5553	43.381	0.2675	0.2834	0.165	13.4291	2.2552	3.07	26.54068	50.59801
F5	0.2712	17.3094	17.5808	17.6014	42.7221	42.7158	42.5554	0.2714	0.292	0.1667	16.4405	2.1621	3.07	29.5739	55.59138
F6	0.3032	18.6472	18.9501	18.9619	43.5684	43.5756	43.3762	0.3029	0.3147	0.1922	9.6327	2.4682	3.07	19.60334	49.13782
F7	0.2918	17.3102	17.6022	17.62	42.7187	42.7248	42.5436	0.292	0.3098	0.1751	13.2146	2.1639	3.07	29.51607	44.77069
F8	0.2675	18.6259	18.8934	18.9116	43.5336	43.538	43.368	0.2675	0.2857	0.1656	15.1540	2.2233	3.07	27.58048	54.94479
F9	0.3068	17.3118	17.6187	17.6387	42.7242	42.7308	42.5376	0.3069	0.3269	0.1866	14.2552	2.1835	3.07	28.87635	49.36624
F10	0.2963	18.6286	18.9246	18.9373	43.5485	43.5549	43.367	0.296	0.3087	0.1815	9.9843	2.3228	3.07	24.33772	41.02388
M3F1	0.2758	17.3106	17.5865	17.6062	42.6997	42.7009	42.5303	0.2759	0.2956	0.1694	15.6101	2.1823	3.07	28.91676	53.98302
M4F1	0.2983	18.626	18.9242	18.9427	43.5465	43.5335	43.35553	0.2982	0.3167	0.19097	14.7141	2.3675	3.07	22.88417	64.29804
M5F1	0.2716	17.3104	17.5819	17.5944	42.695	42.6982	42.52285	0.2715	0.284	0.17215	11.1757	2.4230	3.07	21.07607	53.02545
n	13	13	13	13	13	13	13	13	13	13	13	13	13	13	13
min	0.2675	17.3094	17.5808	17.5944	42.6950	42.6982	42.5229	0.2675	0.2834	0.1640	9.6327	1.9445	3.0700	19.6033	41.0239
max	0.3169	18.6472	18.9594	18.9772	43.5756	43.5898	43.3810	0.3175	0.3353	0.1992	16.4405	2.4682	3.0700	36.6607	64.2980
average	0.2868	17.9214	18.2081	18.2256	43.1021	43.1071	42.9258	0.2867	0.3042	0.1764	13.6047	2.2455	3.0700	26.8581	50.9653
sd	0.0168	0.6864	0.6913	0.6897	0.4348	0.4347	0.4289	0.0169	0.0171	0.0123	2.2024	0.1378	0.0000	4.4877	6.0557

Appendix B2- Average diameter over 3 point on test specimens.

Diameter of sintered AW

	green parts					sintered parts			
sample	dia. #1	dia. #2	dia. #3	average dia. mm	sample	dia. #1	dia. #2	dia. #3	average dia. mm
GP1	3.062	3.062	3.052	3.059	SP1	2.357	2.332	2.327	2.339
GP2	3.007	3.007	3.007	3.007	SP2	2.5	2.45	2.431	2.460
GP3	3.298	3.362	3.298	3.319	SP3	2.366	2.357	2.347	2.357
GP4	3.136	3.15	3.15	3.145	SP4	2.307	2.337	2.297	2.314
GP5	3.136	3.15	3.121	3.136	SP5	2.342	2.376	2.391	2.370
GP6	3.15	3.15	3.121	3.140	SP6	2.47	2.485	2.48	2.478
GP7	2.85	2.859	2.85	2.853	SP7	2.381	2.406	2.396	2.394
GP8	2.988	3.002	2.973	2.988	SP8	2.465	2.524	2.485	2.491
GP9	3.116	3.106	3.062	3.095	SP9	2.465	2.435	2.435	2.445
GP10	3.293	3.259	3.19	3.247	SP10	2.559	2.524	2.5	2.528
GP11	3.205	3.219	3.224	3.216	SP11	2.362	2.362	2.347	2.357
n	11	11	11	11		11	11	11	11
min	2.850	2.859	2.850	2.853		2.307	2.332	2.297	2.314
max	3.298	3.362	3.298	3.319		2.559	2.524	2.500	2.528
mean	3.113	3.121	3.095	3.110		2.416	2.417	2.403	2.412
sd	0.1327	0.1374	0.1252	0.1309		0.0792	0.0714	0.0688	0.0712

	Greenparts	*Sintered*
Mean	3.109545455	2.412060606
Standard Error	0.039454878	0.021476406
Median	3.135666667	2.394333333
Mode	#N/A	#N/A
Standard Deviation	0.130857027	0.071229179
Sample Variance	0.017123562	0.005073596
Kurtosis	0.271675587	-1.398397208
Skewness	-0.368742327	0.242122604
Range	0.466333333	0.214
Minimum	2.853	2.313666667
Maximum	3.319333333	2.527666667
Sum	34.205	26.53266667
Count	11	11
Confidence Level(95.0%)	0.087910947	0.047852414

Appendix B3- Properties of Cylindrical specimens.

Batch #1 Data of cylindrical specimens of AWGC

													8
									span L0 (mm	20		pi	3.14159
									temp	24C	humidity	0.38	
	diameter D (mm)	δ_2 (mm)	δ_1 (mm)	delta δ (mm)	F_2 (kN)	F_1(kN)	delta F(kN)	Young's Modulus E (GPa)	Max. Flexural Load Fmax (N)	Deflection at Flexural Load δ	Modulus of Rupture (Flexural strength) σ (MPa)		
F1	2.55	0.04	0.02008	0.01992	0.01117	0.00568	0.00548	22.1028	20.43	0.102	62.751		
F2	2.65	0.04	0.02008	0.01992	0.01665	0.00935	0.0073	25.2411	24.29	0.055	66.475		
F3	2.55	0.04	0.02	0.02	0.01241	0.007	0.00542	21.7414	20.7	0.072	63.580		
F4	2.55	0.04	0.02	0.02	0.01642	0.00853	0.00789	31.6665	21.4	0.051	65.730		
F5	2.65	0.04	0.02008	0.01992	0.0145	0.0073	0.00719	24.8643	22.7	0.058	62.124		
F6	2.6	0.03904	0.02004	0.019	0.01256	0.00659	0.00598	23.3731	20.4	0.061	59.113		
F7	2.6	0.04	0.02	0.02	0.01403	0.00693	0.0071	26.3577	20.5	0.056	59.402		
F8	2.5	0.04	0.02008	0.01992	0.01468	0.00729	0.00739	32.2415	18.6	0.048	60.627		
F9	2.55	0.04	0.02	0.02	0.01241	0.00643	0.00598	24.0018	21.6	0.063	66.344		
F10	2.55	0.04	0.02008	0.01992	0.01322	0.00602	0.0072	29.0203	17.3	0.054	53.137		
F11	2.35	0.04	0.02	0.02	0.00989	0.00404	0.00584	32.5303	21.1	0.073	82.804		

Batch #2 Data of cylindrical specimens of AWGC

													8
									span L_0 (mm)	20		pi	3.14159
									temp	24C	humidity	0.38	
	diameter D (mm)	δ_2 (mm)	δ_1 (mm)	delta δ (mm)	F_2 (kN)	F_1(kN)	delta F(kN)	Young's Modulus E (GPa)	Max. Flexural Load Fmax (N)	Deflection at Rupture Flexural Load δ	Modulus of Rupture (Flexural Strength) σ (MPa)		
S1	2.85	0.06776	0.04268	0.02508	0.02005	0.00663	0.01342	27.5416	42.1	0.101	92.62		
S2	2.82	0.06672	0.04	0.02672	0.01774	0.00635	0.01139	22.882	37.1	0.1	84.26		
S3	2.84	0.06696	0.0412	0.02576	0.02721	0.01494	0.01227	24.8663	31.3	0.076	69.59		
S4	3.06	0.06816	0.0424	0.02576	0.02578	0.01384	0.01193	17.9405	40.1	0.094	71.28		
S5	2.85	0.06988	0.04324	0.02664	0.01557	0.00668	0.00889	17.1816	32.8	0.102	72.16		
S6	2.95	0.067	0.04464	0.02236	0.0256	0.01399	0.0116	23.2663	35.2	0.085	69.83		
S7	2.79	0.06692	0.04028	0.02664	0.02788	0.01519	0.01269	26.6862	31.9	0.076	74.81		
S8	2.9	0.06624	0.04136	0.02488	0.02658	0.01324	0.01334	25.7352	40.9	0.092	85.41		
S9	2.56	0.065	0.04192	0.02308	0.01667	0.0083	0.00837	28.6722	20	0.075	60.71		
S10	2.86	0.0658	0.04392	0.02188	0.02087	0.01072	0.01016	23.5554	36.7	0.102	79.90		
S11	2.86	0.06436	0.04564	0.01872	0.02404	0.01657	0.00746	20.2285	36.9	0.087	80.33		

Appendix B4 –XDR and EDX analysis of sintered AW cylindrical specimens.

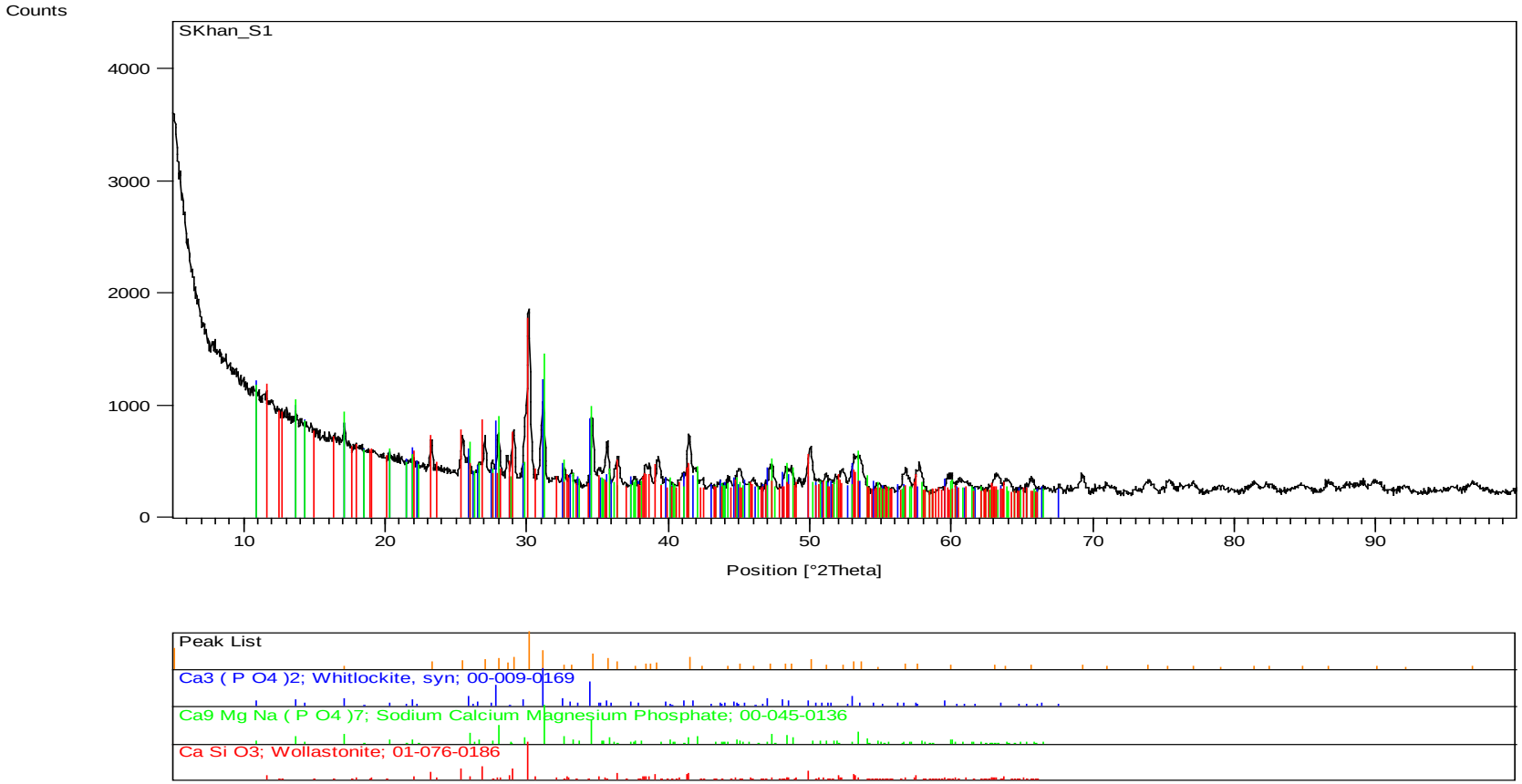

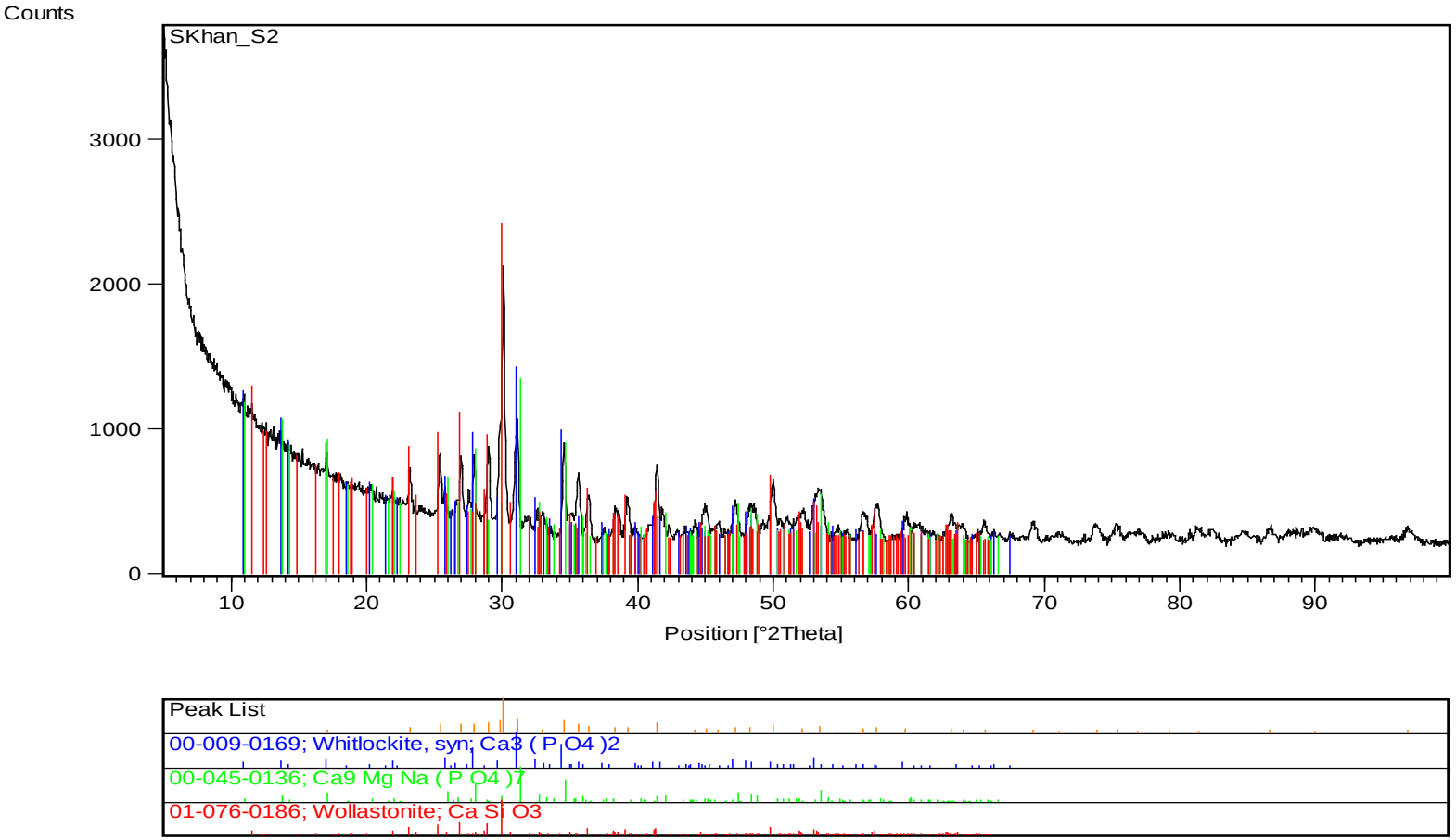
Counts
SKhan_S2
3000
2000
1000
0
10
20
30
40
50
60
70
80
90
Position [°2Theta]
Peak List
00-009-0169; Whitlockite, syn; Ca3 (P O4)2
00-045-0136; Ca9 Mg Na (P O4)7
01-076-0186; Wollastonite; Ca Si O3

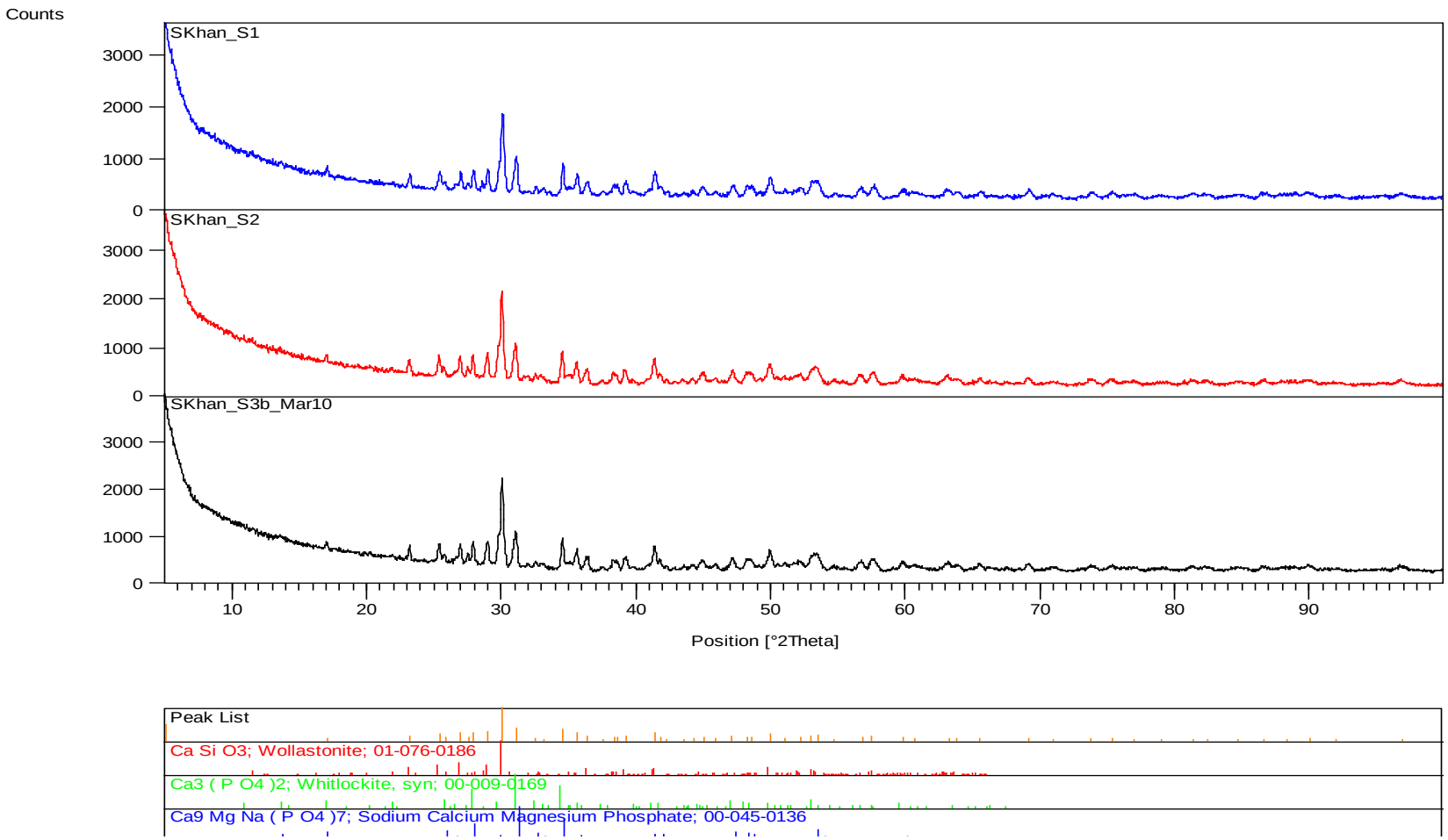
Counts
SKhan_S1
SKhan_S2
SKhan_S3b_Mar10
3000
2000
1000
0
10
20
30
40
50
60
70
80
90
Position [°2Theta]
Peak List
Ca Si O3; Wollastonite; 01-076-0186
Ca3 (P O4)2; Whitlockite, syn; 00-009-0169
Ca9 Mg Na (P O4)7; Sodium Calcium Magnesium Phosphate; 00-045-0136

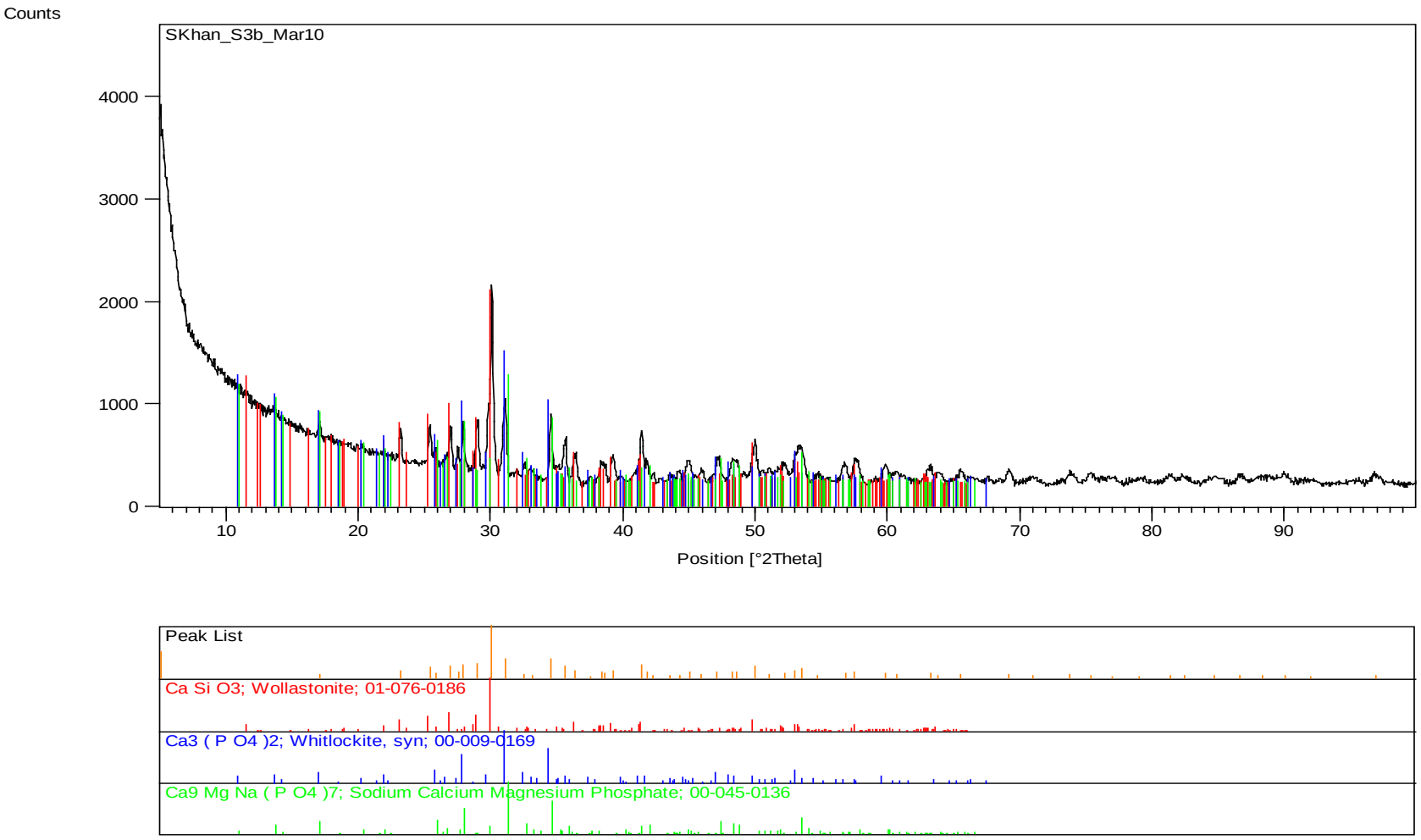
Counts
SKhan_S3b_Mar10
4000
3000
2000
1000
0
10
20
30
40
50
60
70
80
90
Position [°2Theta]
Peak List
Ca Si O3; Wollastonite; 01-076-0186
Ca3 (P O4)2; Whitlockite, syn; 00-009-0169
Ca9 Mg Na (P O4)7; Sodium Calcium Magnesium Phosphate; 00-045-0136

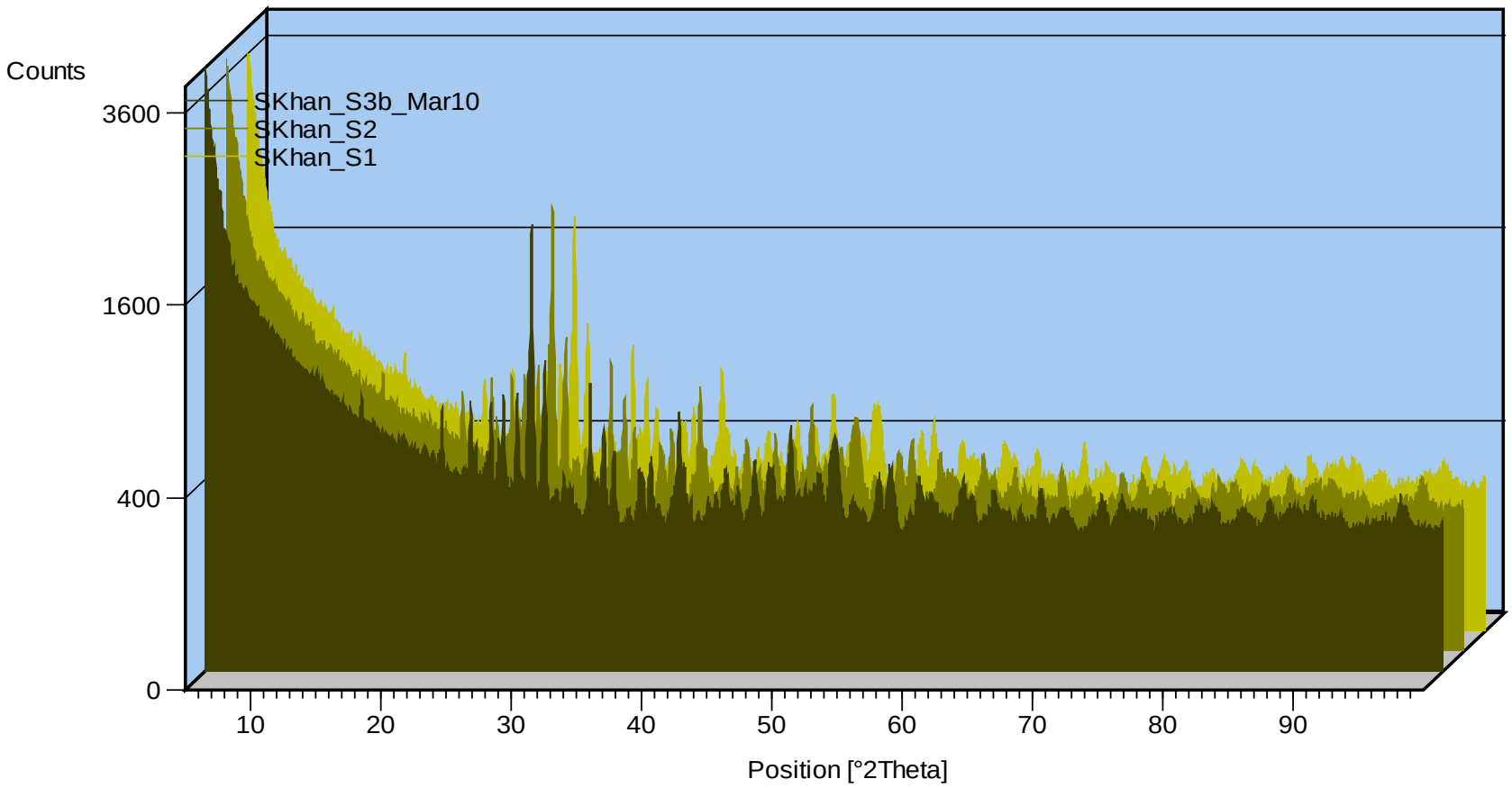
Counts
3600
1600
400
0
SKhan_S3b_Mar10
SKhan_S2
SKhan_S1
10
20
30
40
50
60
70
80
90
Position [°2Theta]

Appendix B4 - XRD analysis from PDF2 (2009)

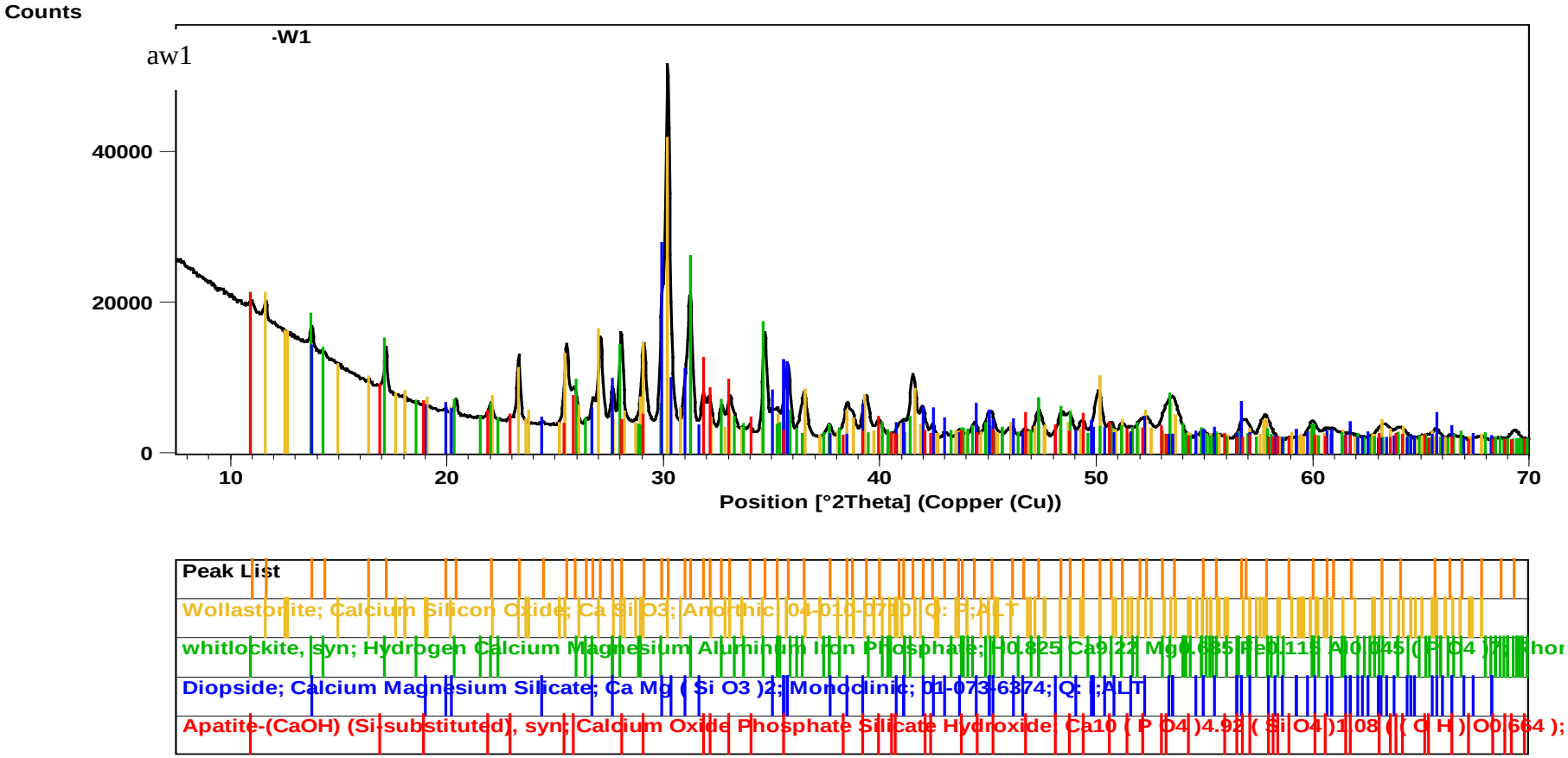

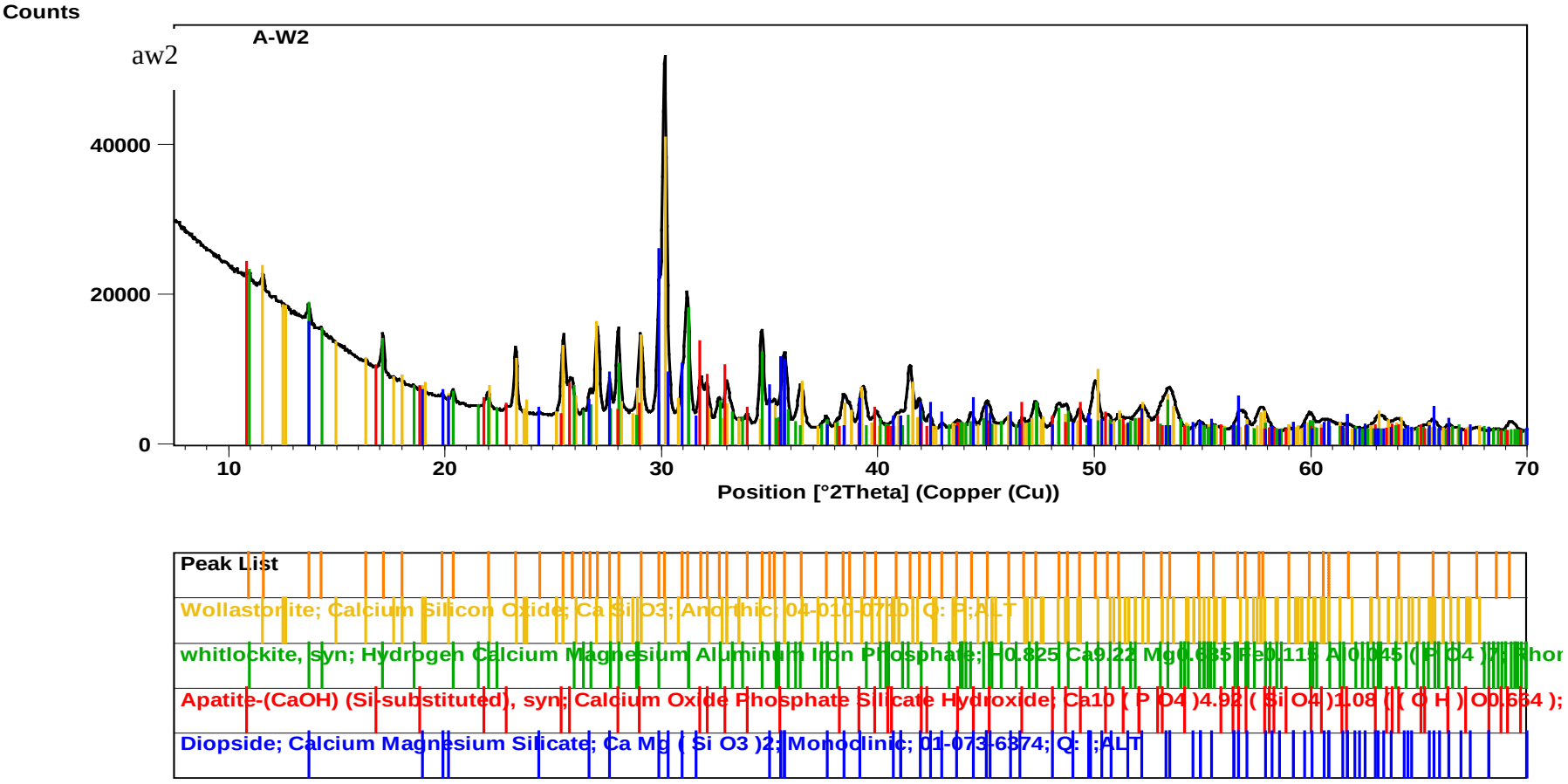
Counts
A-W2
aw2
40000
20000
0
10
20
30
40
50
60
70
Position [°2Theta] (Copper (Cu))
Peak List
Wollastonite; Calcium Silicon Oxide; Ca Si O3; Anorthic; 04-010-0710; Q: H;ALT
whitlockite, syn; Hydrogen Calcium Magnesium Aluminum Iron Phosphate; H0.825 Ca9.22 Mg0.635 Fe0.115 Al0.045 (P O4)7 Phor
Apatite-(CaOH) (Si-substituted), syn; Calcium Oxide Phosphate Silicate Hydroxide; Ca10 (P O4)4.92 (Si O4)1.08 ((O H) O0.654);
Diopside; Calcium Magnesium Silicate; Ca Mg (Si O3)2; Monoclinic; 01-073-6374; Q: ;ALT

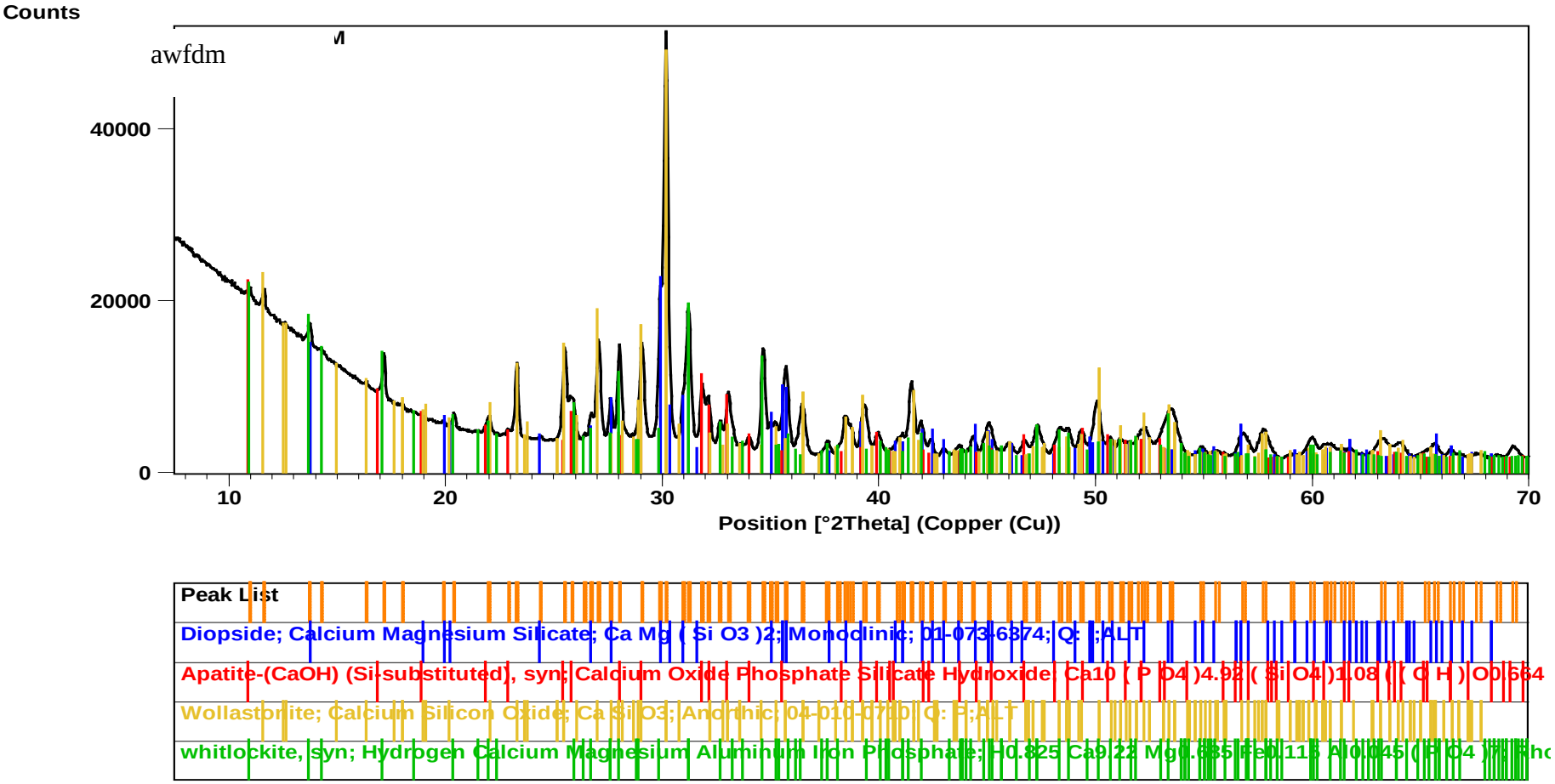
Counts
awfdm
40000
20000
0
10
20
30
40
50
60
70
Position [°2Theta] (Copper (Cu))
Peak List
Diopside; Calcium Magnesium Silicate; Ca Mg (Si O3)2; Monoclinic; 01-073-6374; Q: I;ALT
Apatite-(CaOH) (Si-substituted), syn; Calcium Oxide Phosphate Silicate Hydroxide; Ca10 (P O4)4.92 (Si O4)1.08 ((O H) O0.564
Wollastonite; Calcium Silicon Oxide; Ca Si O3; Anorthic; 04-010-0710; Q: H;ALT
whitlockite, syn; Hydrogen Calcium Magnesium Aluminum Iron Phosphate; H0.825 Ca9.22 Mg0.885 Fe0.113 Al0.045 (P O4)

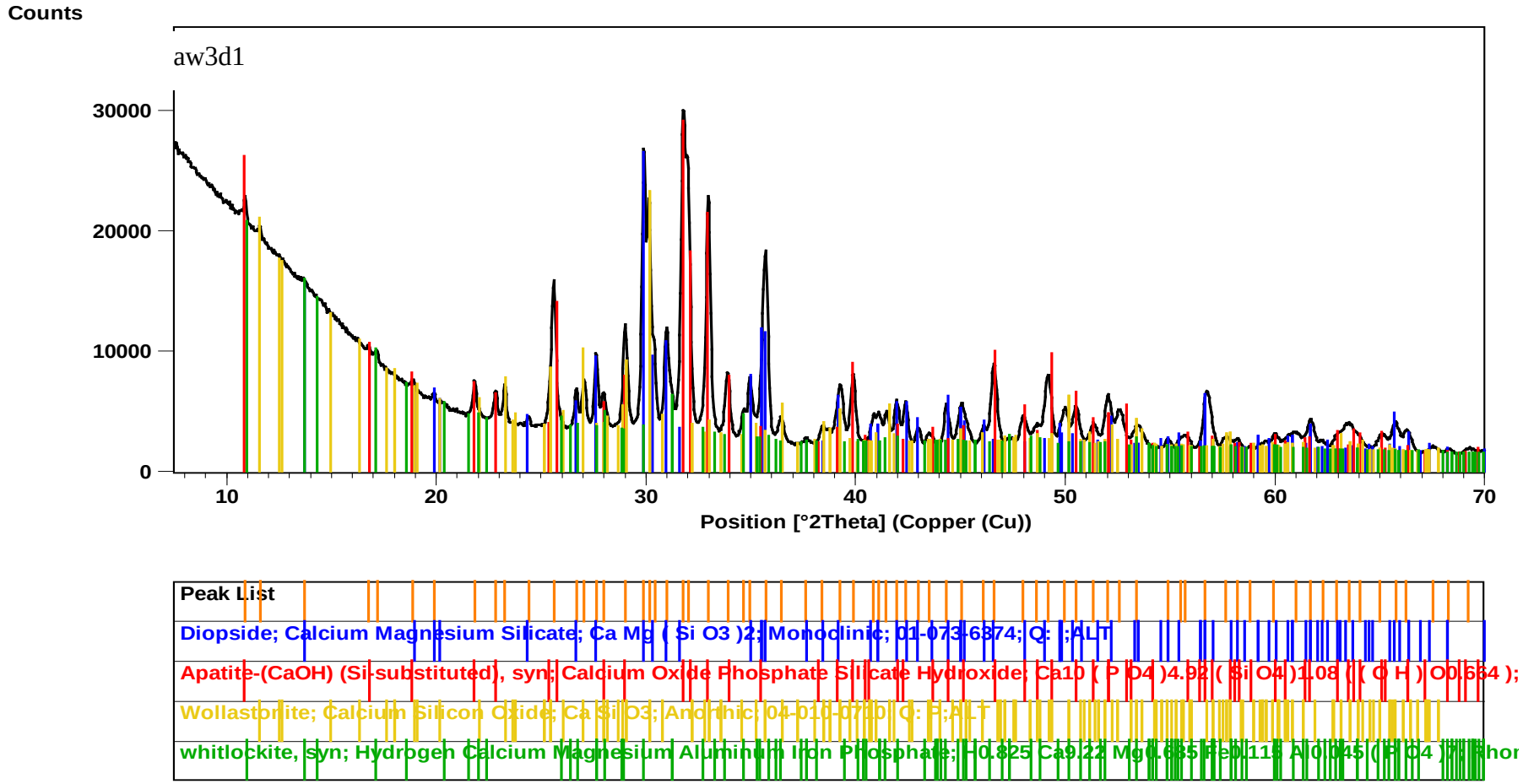
Counts
aw3d1
30000
20000
10000
0
10
20
30
40
50
60
70
Position [°2Theta] (Copper (Cu))
Peak List
Diopside; Calcium Magnesium Silicate; Ca Mg (Si O3)2; Monoclinic; 01-073-6374; Q: ;ALT
Apatite-(CaOH) (Si-substituted), syn; Calcium Oxide Phosphate Silicate Hydroxide; Ca10 (P O4)4.92 (Si O4)1.08 ((O H) O0.684);
Wollastonite; Calcium Silicon Oxide; Ca Si O3; Anorthic; 04-010-0700; Q: ;ALT
whitlockite, syn; Hydrogen Calcium Magnesium Aluminum Iron Phosphate; H0.825 Ca9.22 Mg0.685 Fe0.115 Al0.045 (P O4)7 Phor

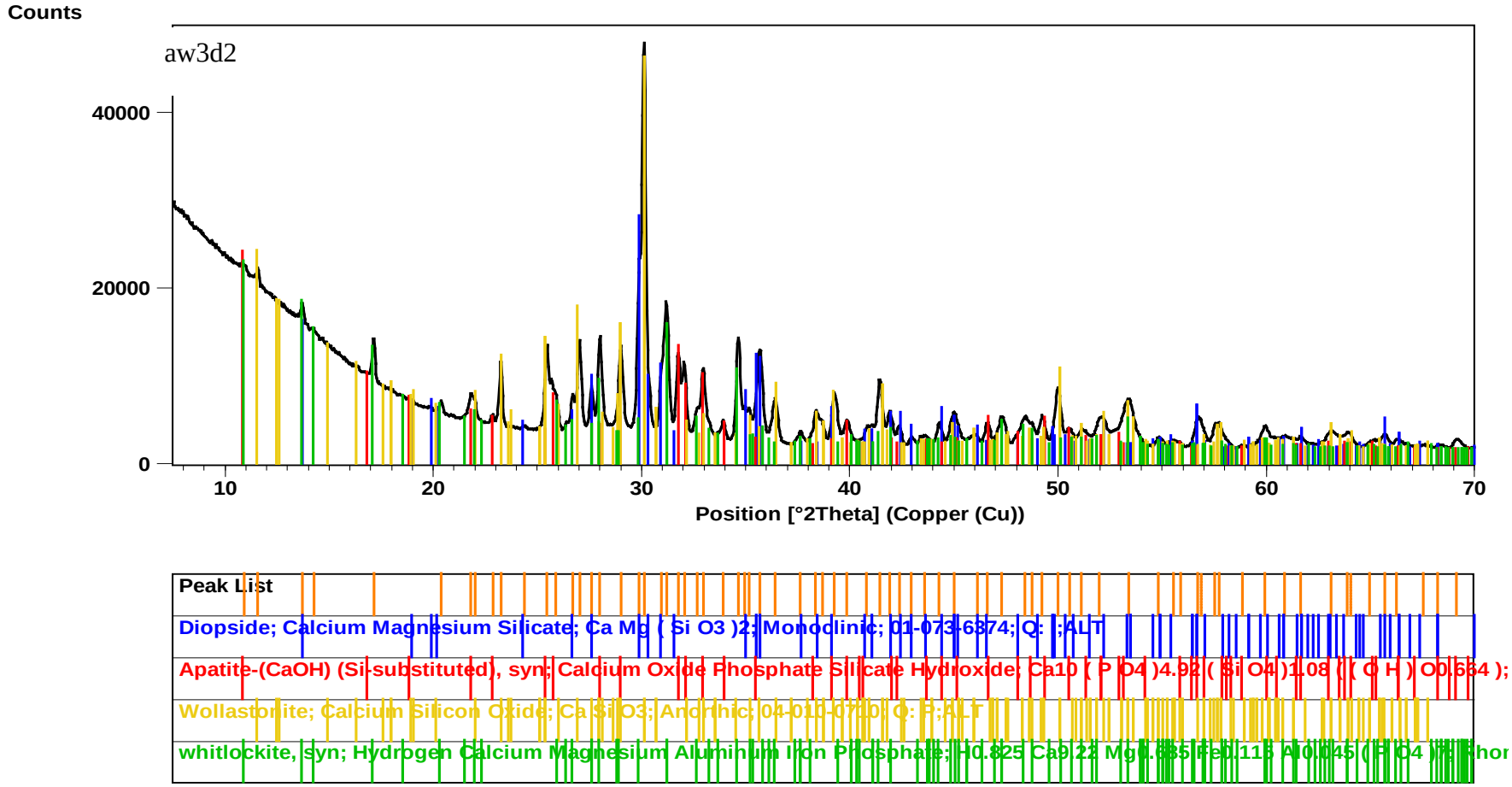
Counts
aw3d2
40000
20000
0
10
20
30
40
50
60
70
Position [°2Theta] (Copper (Cu))
Peak List
Diopside; Calcium Magnesium Silicate; Ca Mg (Si O3)2; Monoclinic; 01-073-6874; Q: ;ALT
Apatite-(CaOH) (Si-substituted), syn; Calcium Oxide Phosphate Silicate Hydroxide; Ca10 (P O4)4.92 (Si O4)1.08 ((O H) O0.634);
Wollastonite; Calcium Silicon Oxide; Ca Si O3; Anorthic; 04-010-0710; Q: P;ALT
whitlockite, syn; Hydrogen Calcium Magnesium Aluminium Iron Phosphate; H0.825 Ca9.22 Mg0.885 Fe0.113 Al0.045 (H O4)7 (Pho

aw1

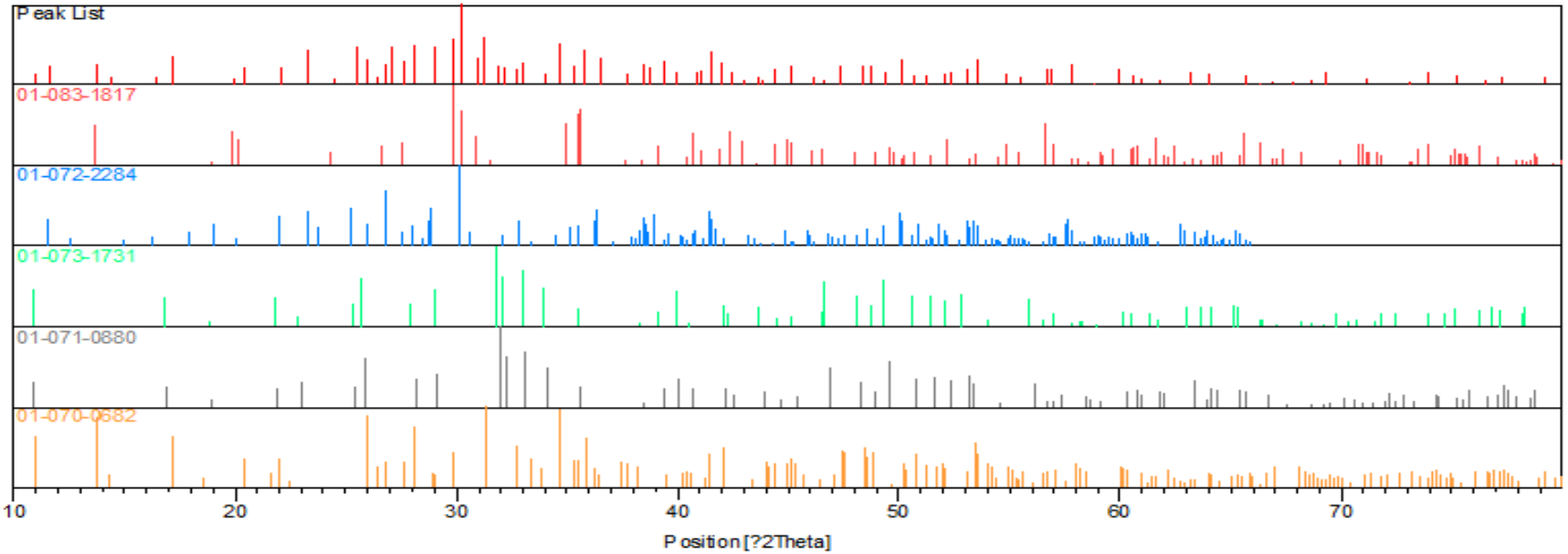

Ref. Code	Compound Name	Chemical Formula
01-083-1817	Diopside	Ca Mg Si2 O6
01-072-2284	Wollastonite 1A	Ca Si O3
01-073-1731	Hydroxylapatite	Ca5 (P O4)3 (O H)
01-071-0880	Fluorapatite	Ca5 (P O4)3 F
01-070-0682	Calcium Magnesium Pho	Ca2.81 Mg0.19 (P O4)2

aw2

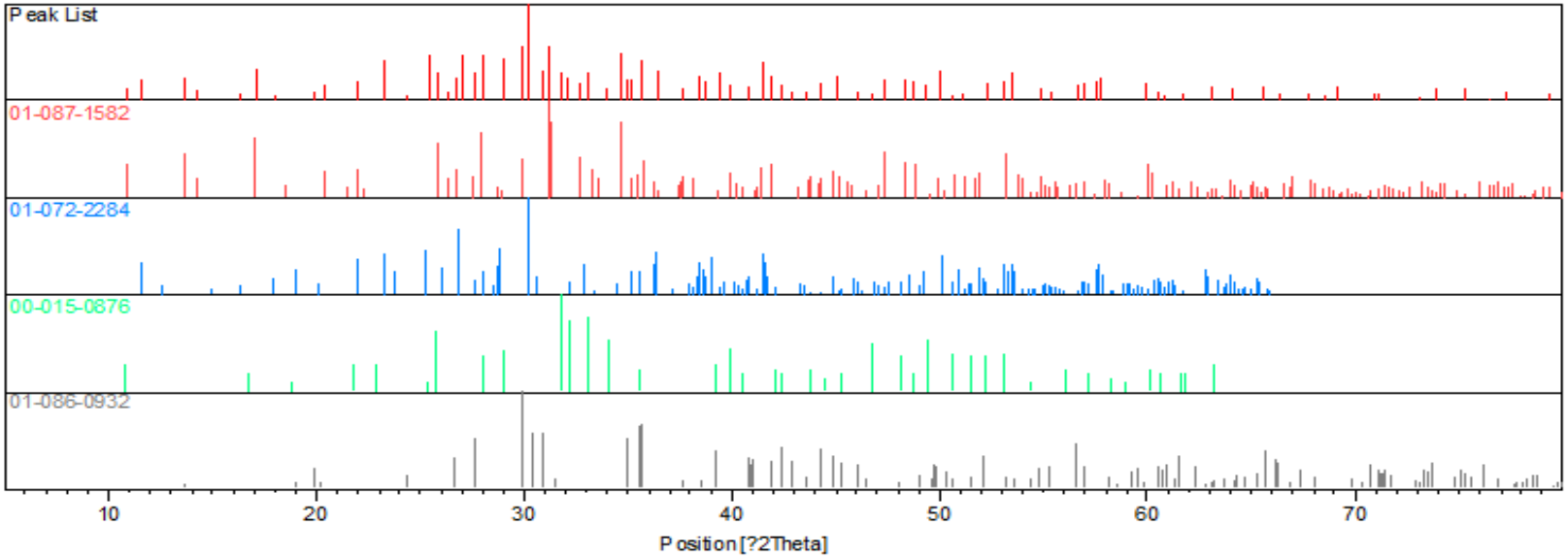

Ref. Code	Compound Name	Chemical Formula
01-087-1582	Calcium Magnesium Phosphate	(Ca2.589 Mg0.411) (P O4)2
01-072-2284	Wollastonite 1A	Ca Si O3
00-015-0876	Fluorapatite, syn	Ca5 (P O4)3 F
01-086-0932	Diopside	Ca Mg Si2 O6

awfdm

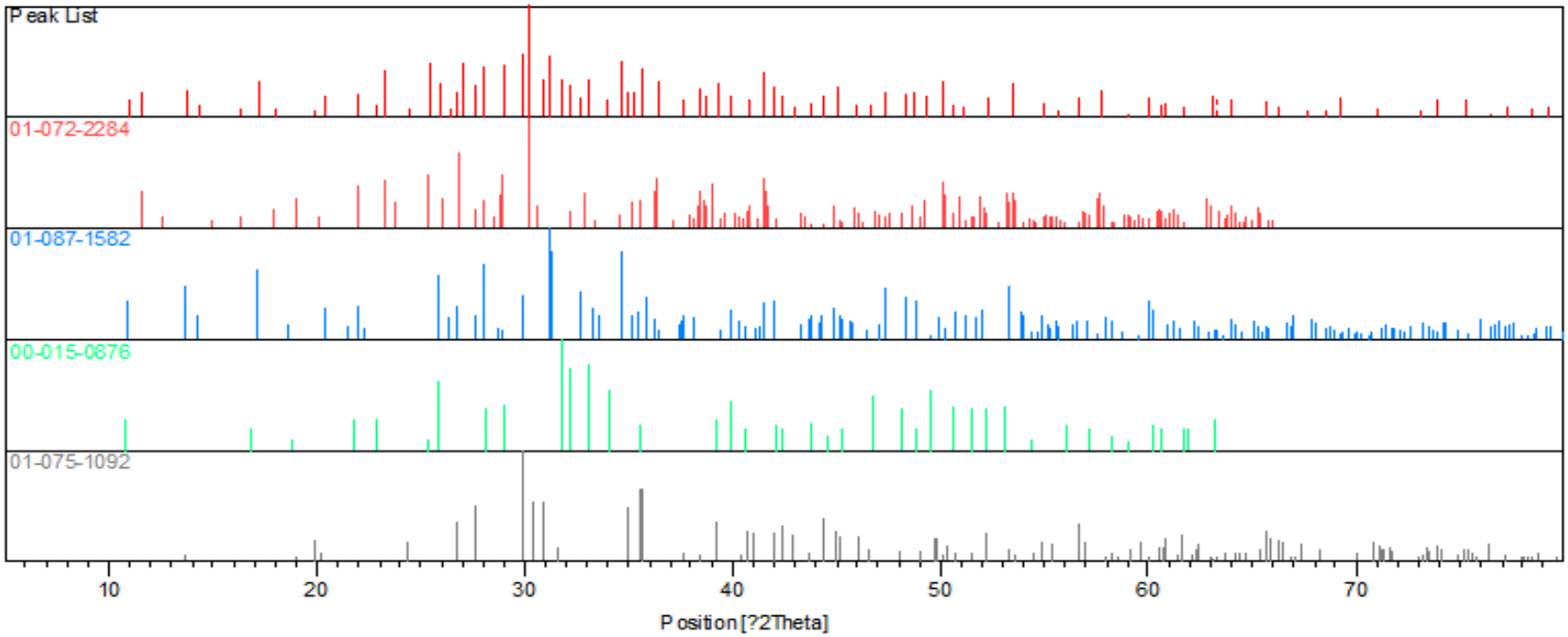

Ref. Code	Compound Name	Chemical Formula
01-072-2284	Wollastonite 1A	Ca Si O3
01-087-1582	Calcium Magnesium Phosphate	(Ca2.589 Mg0.411) (P O4)2
00-015-0876	Fluorapatite, syn	Ca5 (P O4)3 F
01-075-1092	Diopside	Ca Mg Si2 O6

Aw3d1

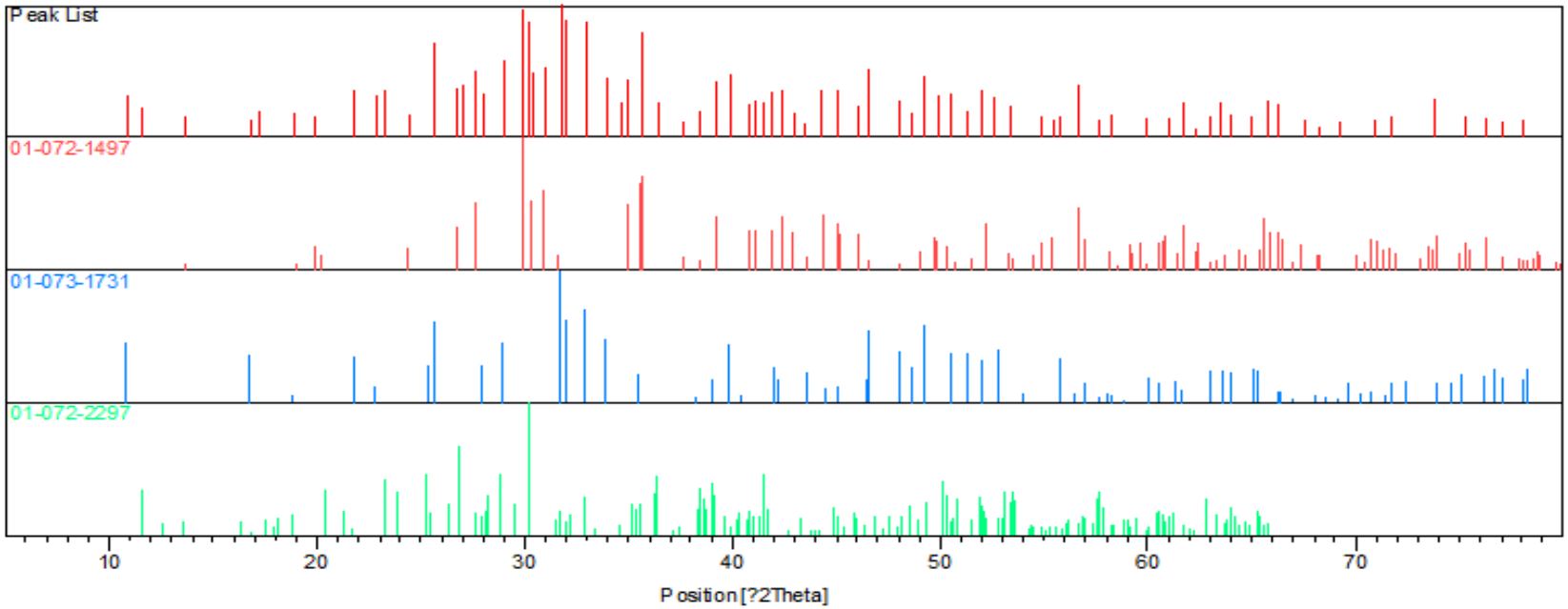

Ref. Code	Compound Name	Chemical Formula
01-072-1497	Diopside	Ca Mg Si2 O6
01-073-1731	Hydroxylapatite	Ca5 (P O4)3 (O H)
01-072-2297	Wollastonite 2\ITM\RG	Ca Si O3

aw3d2

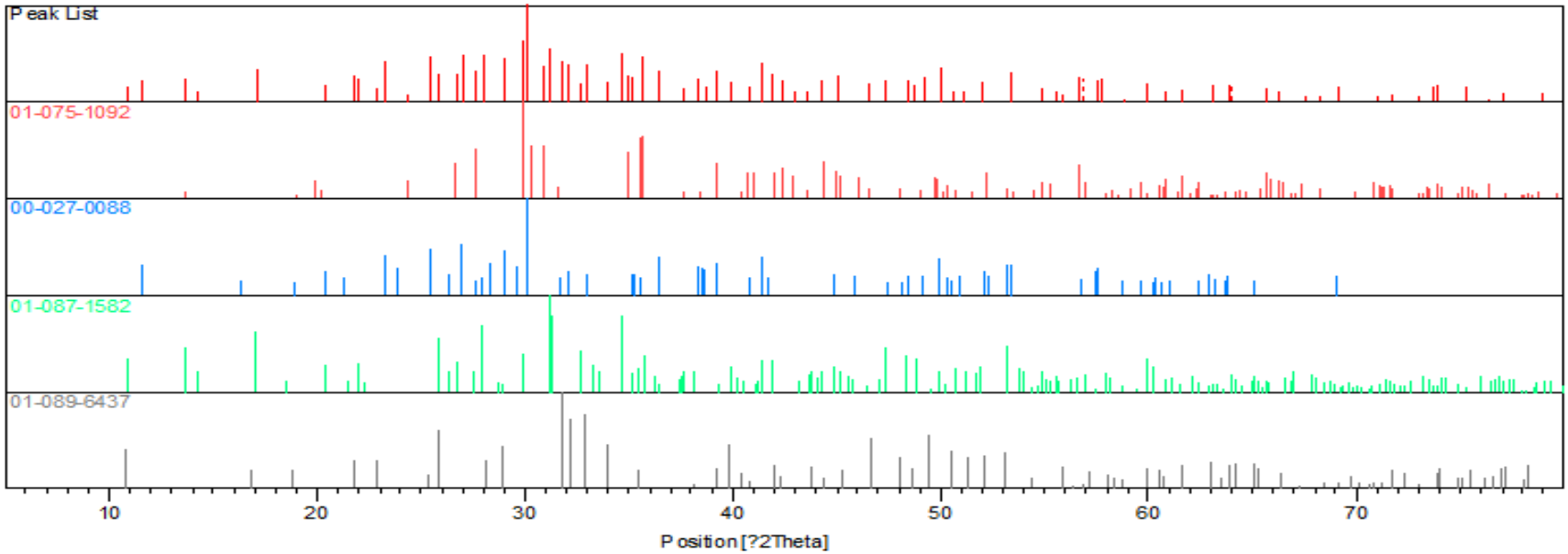

Ref. Code	Compound Name	Chemical Formula
01-075-1092	Diopside	Ca Mg Si2 O6
00-027-0088	Wollastonite-2\ITM\RG	Ca Si O3
01-087-1582	Calcium Magnesium Phosphate	(Ca2.589 Mg0.411) (P O4)2
01-089-6437	Hydroxylapatite, syn	Ca10.042 (P O4)5.952 (O H)2.292

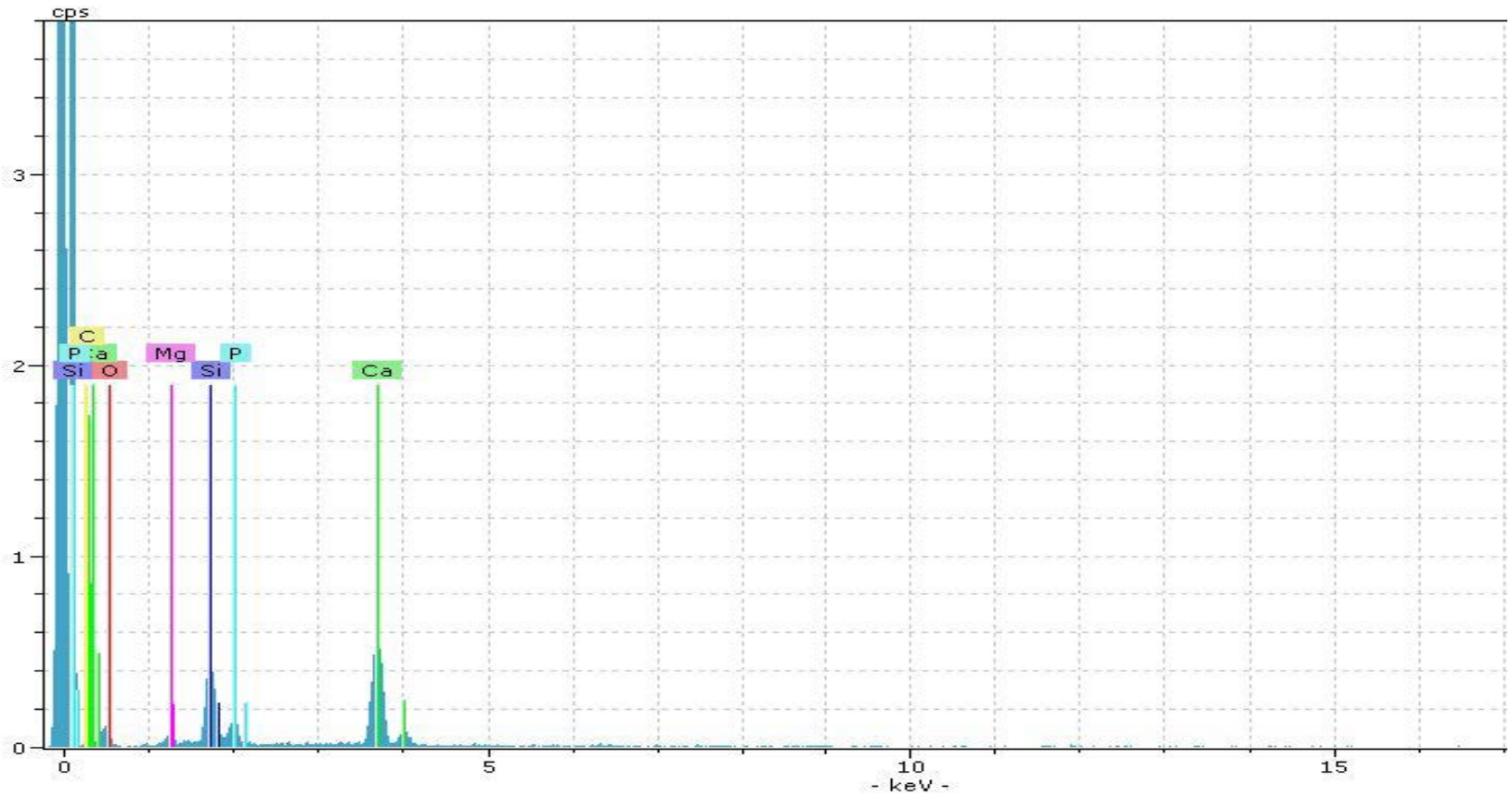

(a) Sample 1 of EDX for sintered specimen fabricated using aluminium sheet mould from the same batch of AW-PMMA powder mixture (aw1)

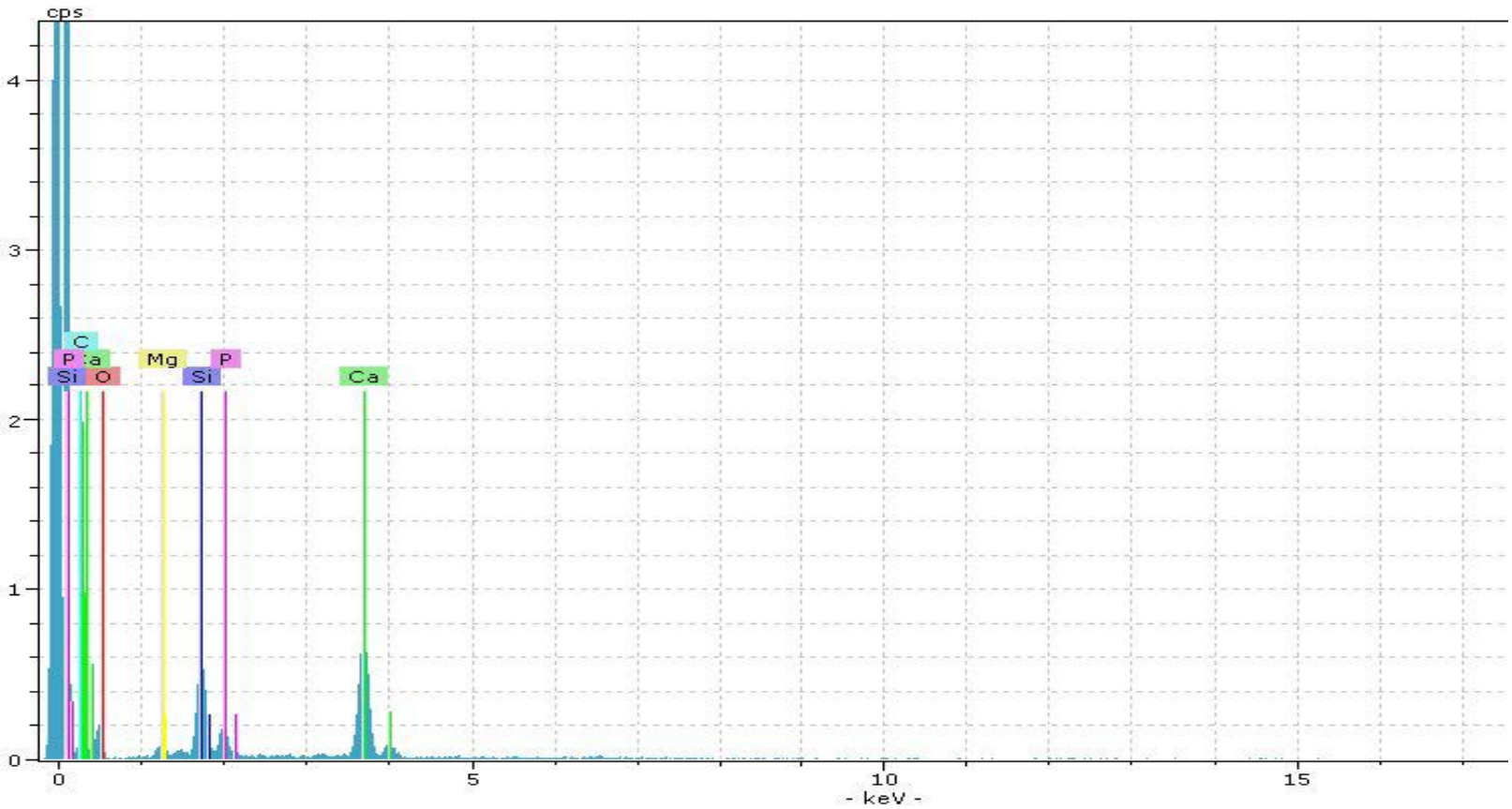

(b) Sample 2 of EDX for sintered specimen fabricated using aluminium sheet mould from the same batch of AW-PMMA powder mixture (aw2).

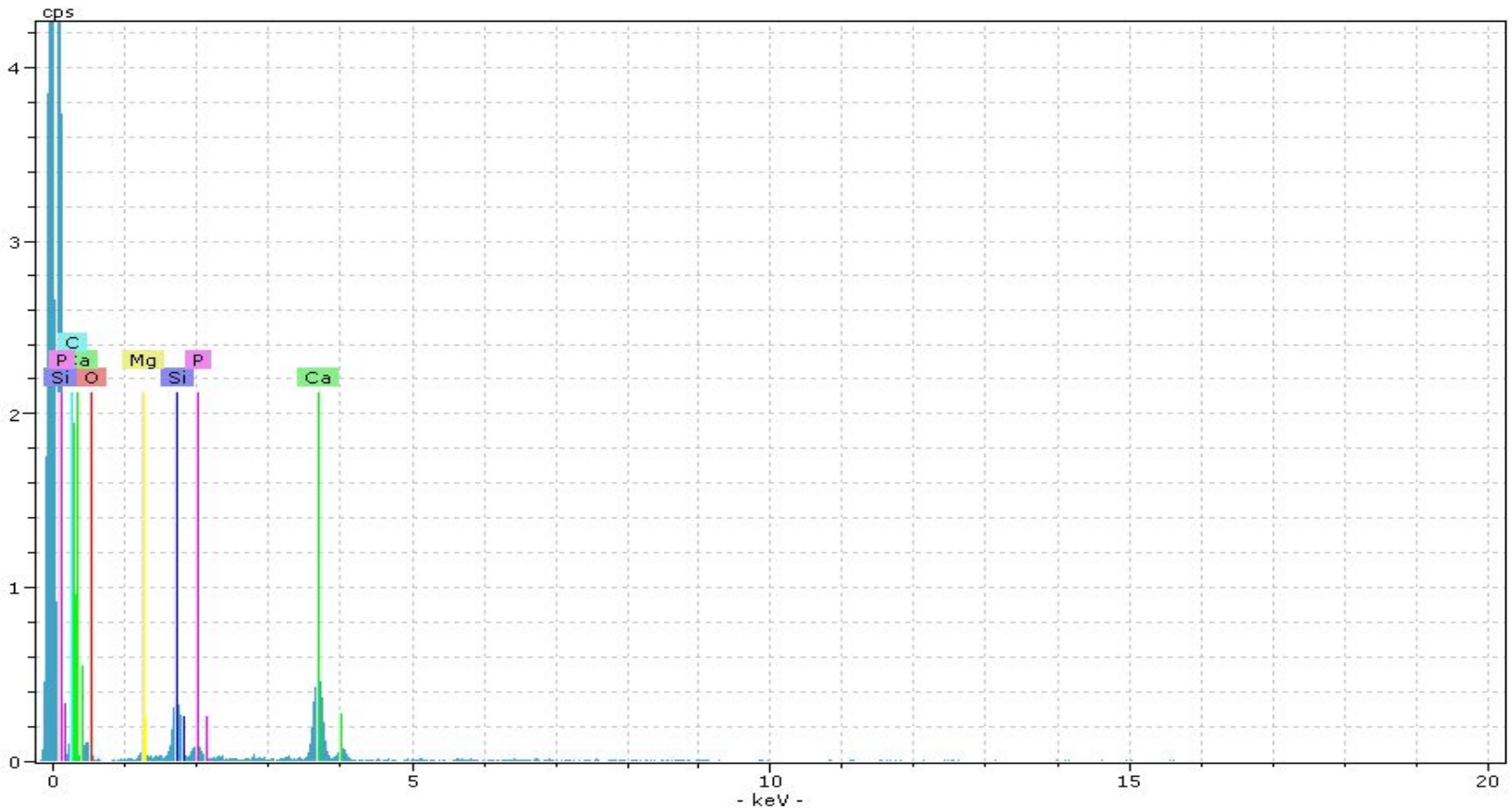

(c) Sample 3 of EDX for sintered specimen fabricated using FDM mould from the same batch of AW-PMMA powder mixture (awfdm1)

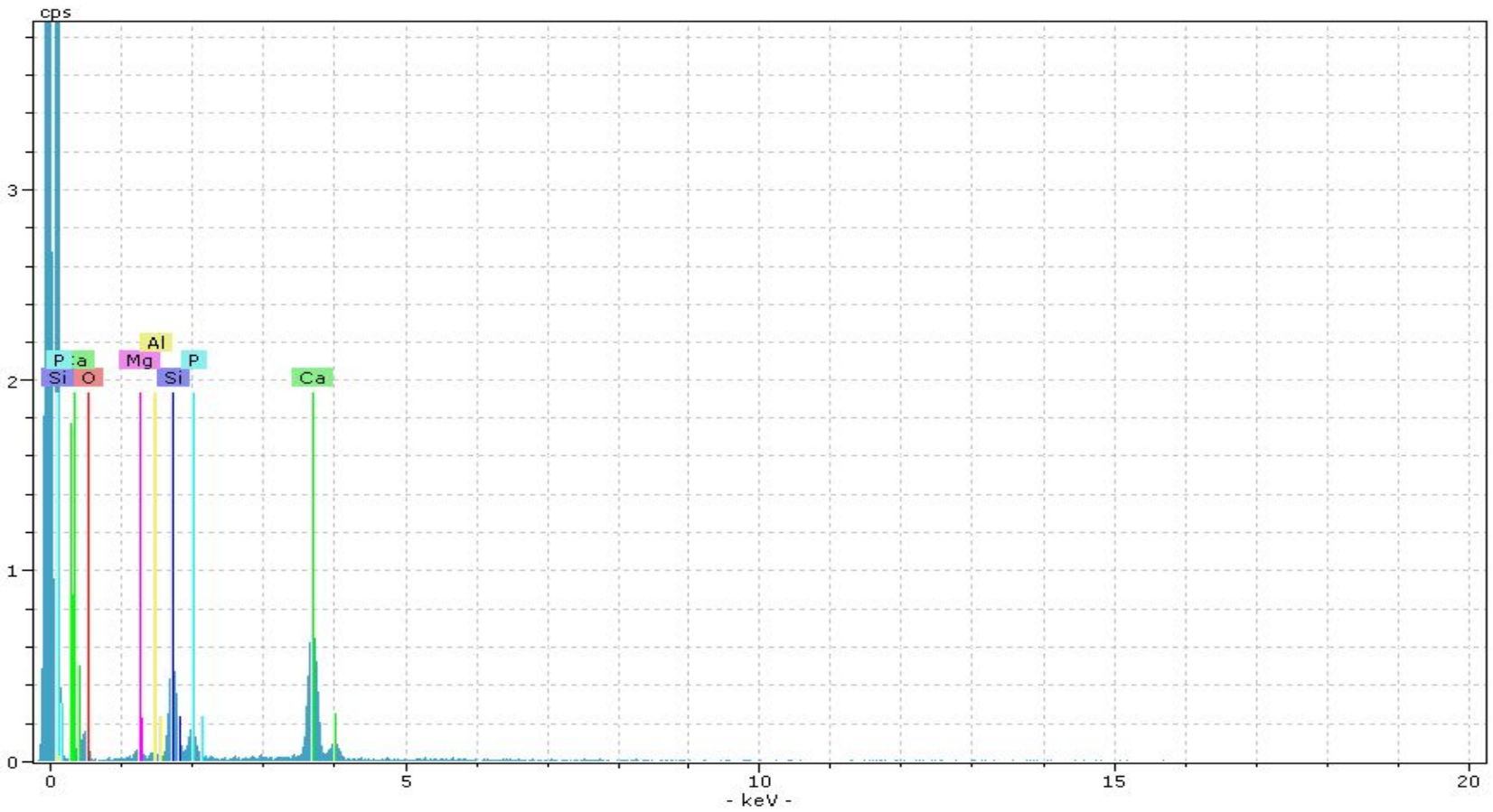

(d) Sample 4 of EDX for sintered specimen fabricated using Z-Corp 3D Printer from the same batch of AW-maltodextrine powder mixture (aw3DP1)

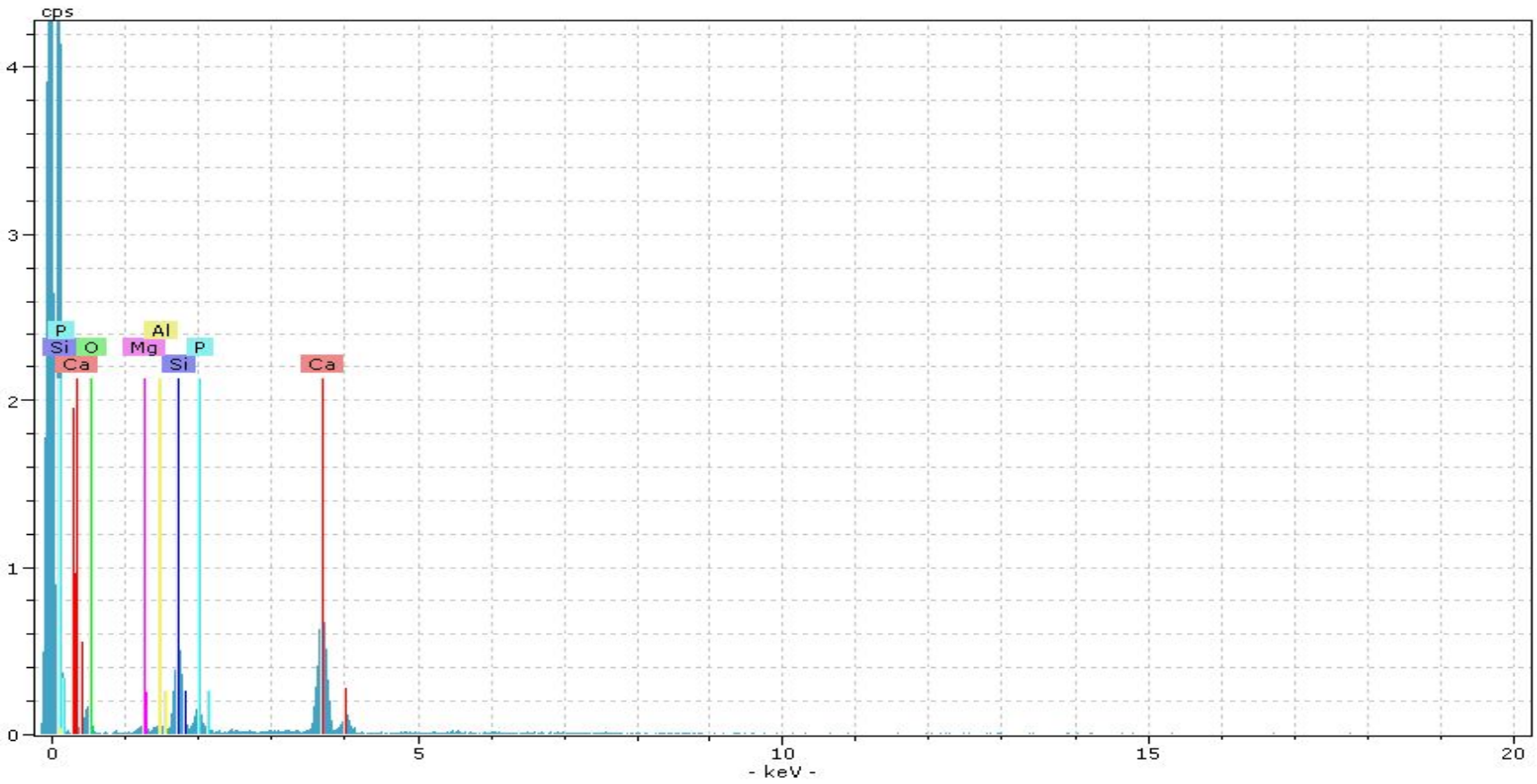

(e) Sample 1 of EDX for sintered specimen fabricated Z-Corp 3D Printer from the same batch of AW-maltodextrine powder mixture (aw3DP2)

Appendix B5 – 3DP specimens data.

Specimen	Green parts, width	thickness	Sintered parts, Not sanded,width	thickness	Sintered parts, Sanded,width	thickness					Green parts Unsintered Bending Strength MPA	Sintered parts, Not sanded, overnight in 3DP,Bending Strength MPA	Sintered parts,Sanded,overnight in room enviroment Bending Strength MPA
1	5.34	4.8275	6.15	5.55	5.3525	5.01					65.05	3224.27	2679
2	5.1575	4.915	5.9	5.54	5.2	5.1975					126.88	1158.93	1229.89
3	5.5025	5.1725	5.92525	5.32	6.11	5.045					194.39	576.88	1706.09
4	5.695	5.105	5.8775	5.505	5.21	4.7875					180.95	349.97	1961.6
5	5.545	5.065	6.2075	5.6375	5.255	4.945					164.13	513.53	1787.2
6			5.74	5.4975	5.3425	4.8325						331.48	3947.31
7			6.5275	5.6825	5.3275	5.0625						205.52	1380.49
8			6.1325	5.2525	5.12	5.1						1084.97	3934.8
9			6.26	6.0525	5.4025	5.1175						144.41	5138
10			6.1275	6.0675	5.435	5.1025						370.19	
n	5	5	10	10	10	10					5	10	9
min.	5.1575	4.8275	5.74	5.2525	5.12	4.7875					65.05	144.41	1229.89
max	5.695	5.1725	6.5275	6.0675	6.11	5.1975					194.39	3224.27	5138
Average	5.448	5.017	6.01205	5.5105	5.4255	4.997					146.28	796.015	2640.486667
s.d	0.205817	0.1419	0.228899	0.269817	0.276018	0.129781					51.98527772	919.467951	1381.192749

AppendixB6 – DSC analysis of PLGA and PLA.

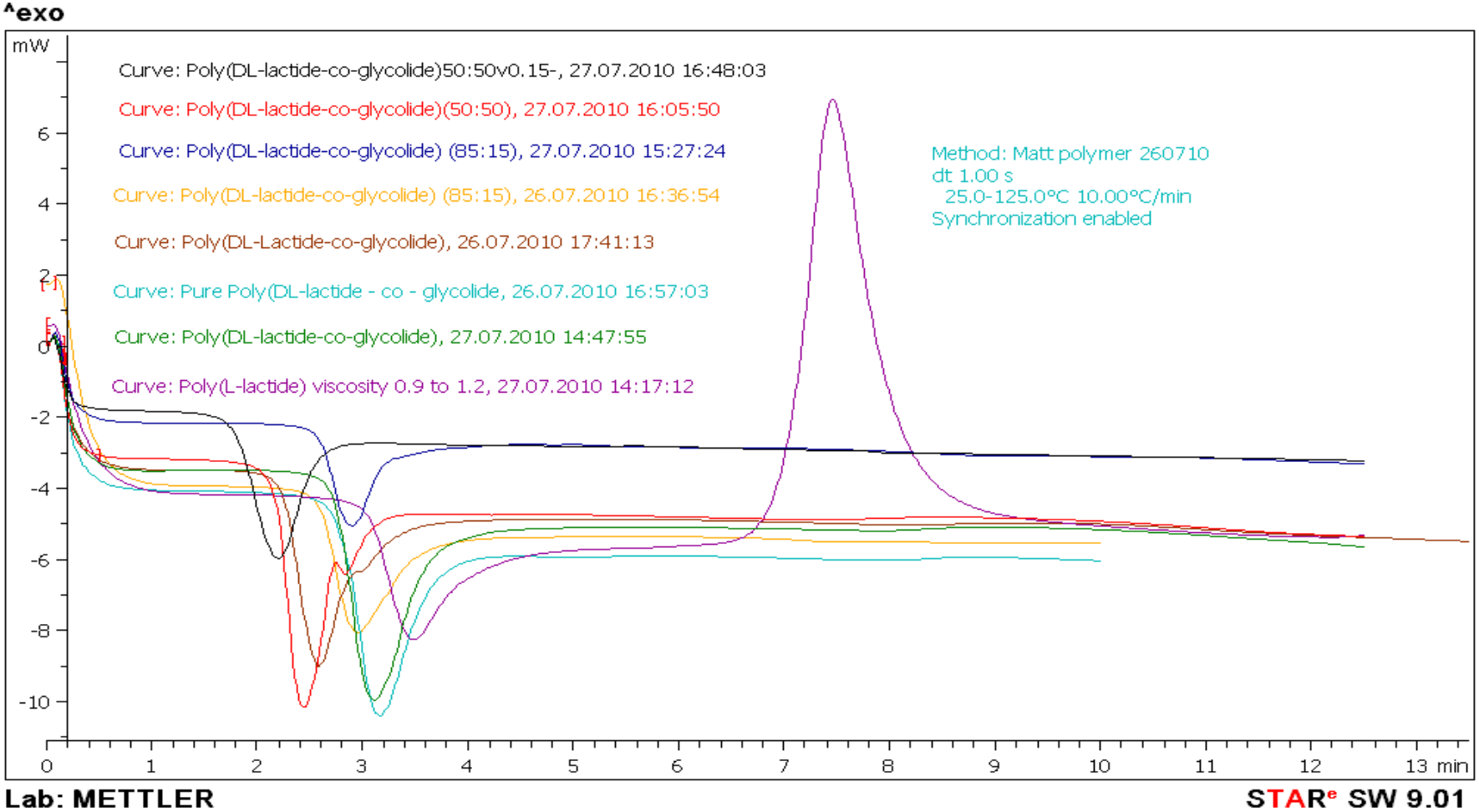

Appendix B7 - Region of energy absorb during repeated cycle of heating and cooling indicating no aging.

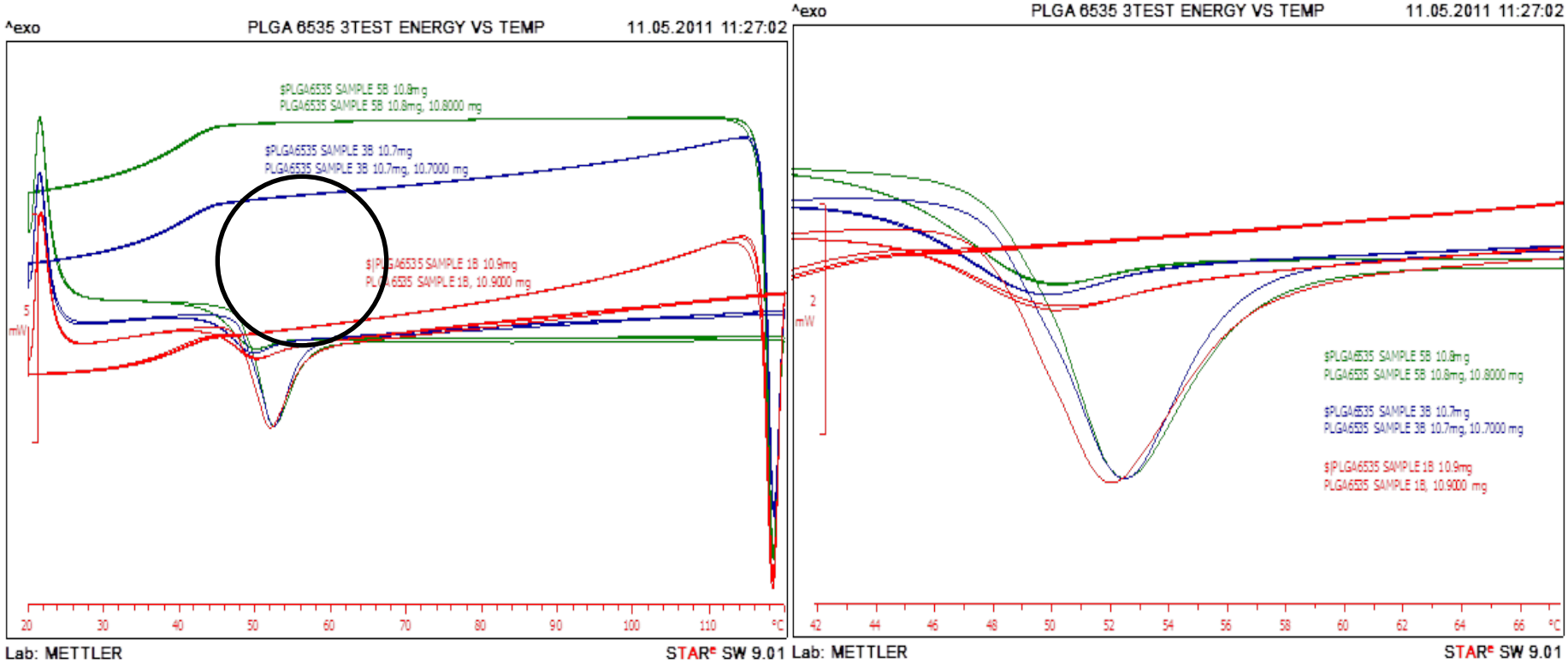

Appendix C1 Transfer mould for PLGA

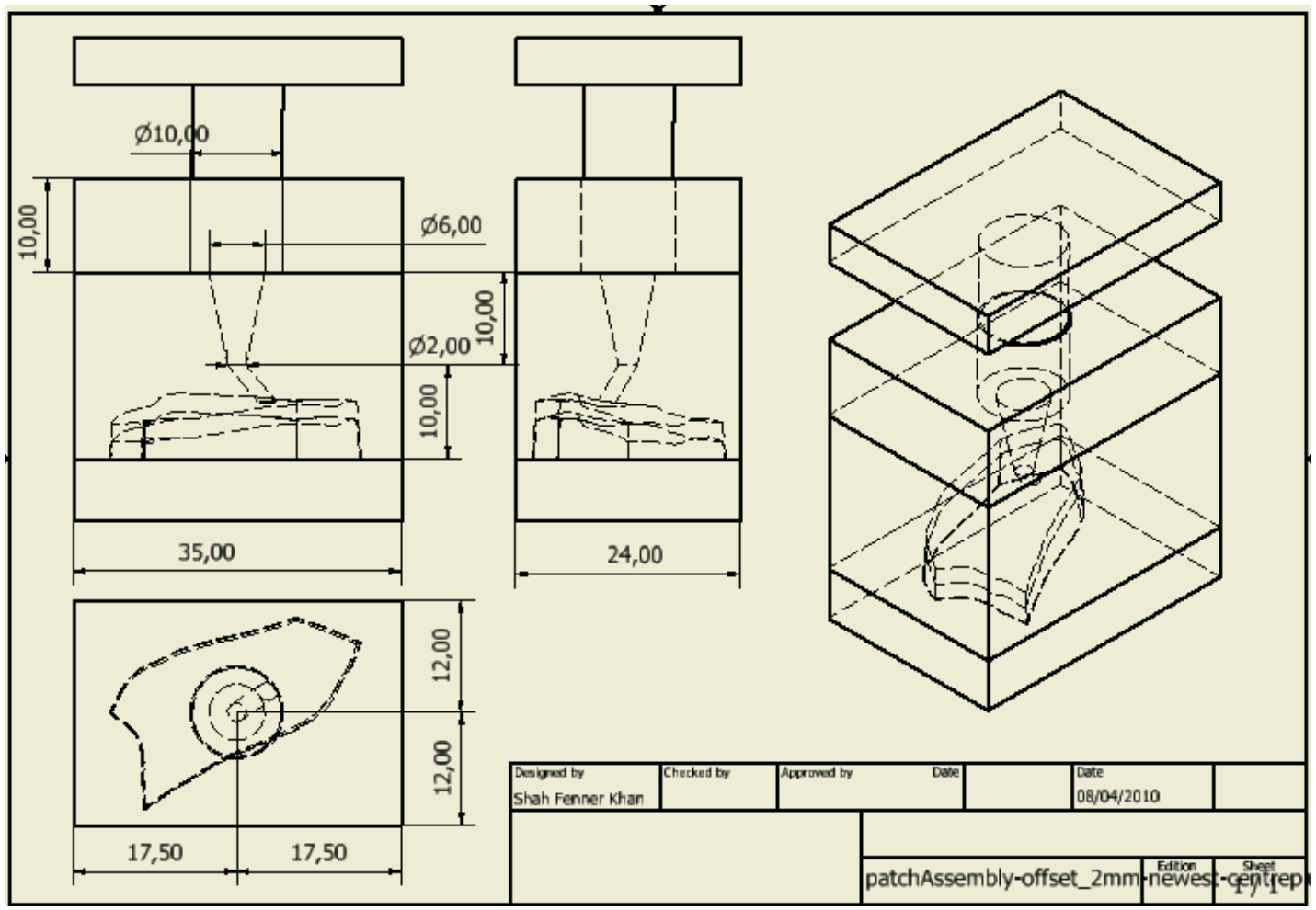

Appendix C2- Moulding box for RTV silicone.

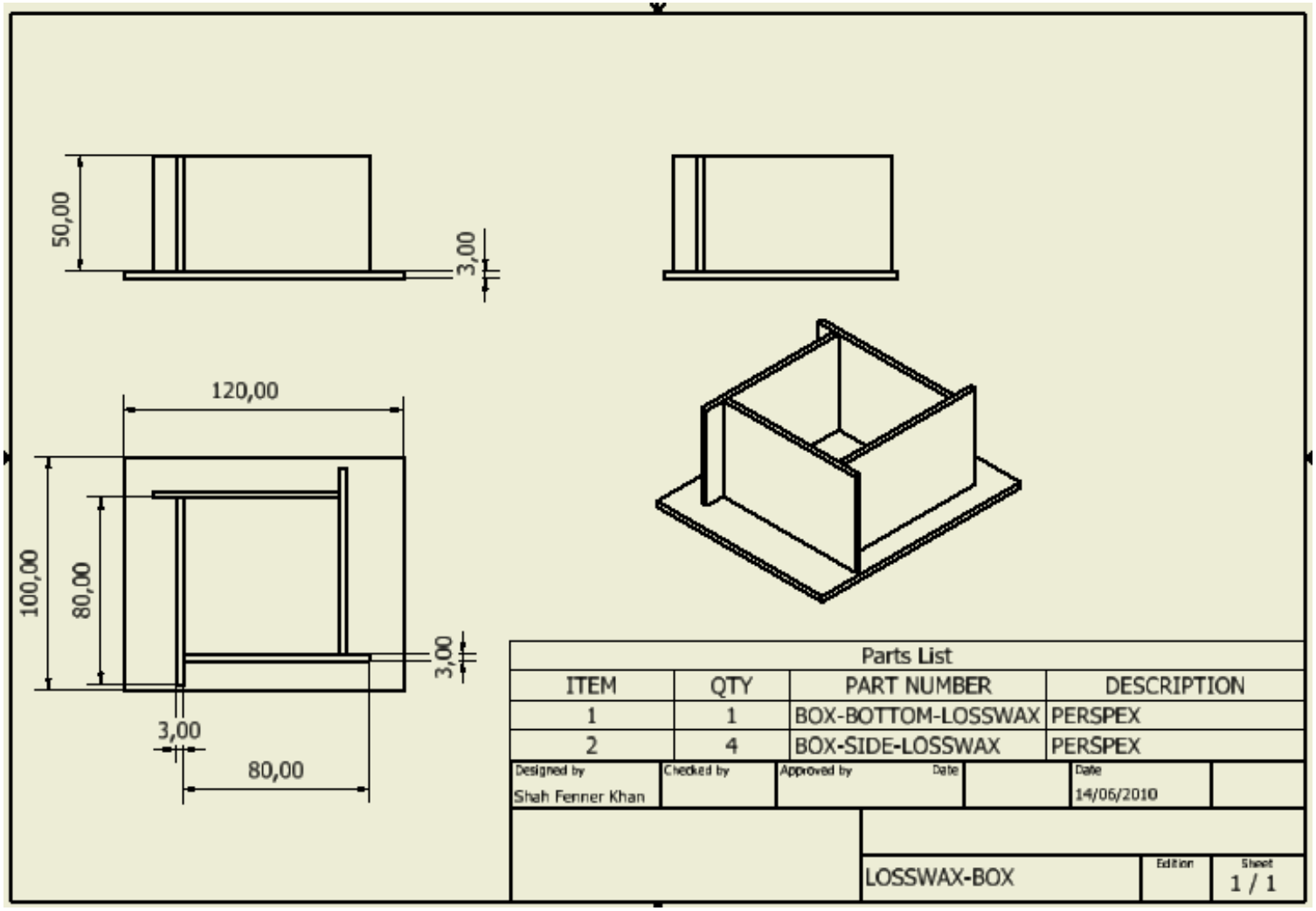

Appendix C3 - Sequences in fabricating process of AWGC implant using RTV silicone rubber moulding**.**

I. RTV silicone moulding procedure

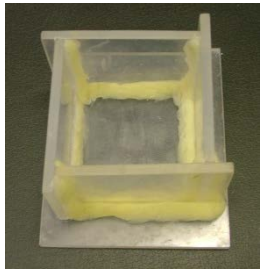 1. Moulding Box.	 2. Creating parting line on master pattern.	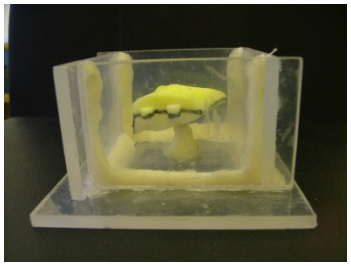 3. Placing master pattern inside moulding box.	
 4. Preparing RTV silicone.	 5. Degassing RTV silicone.	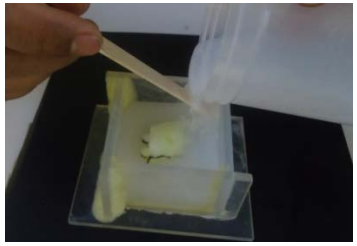 6. Pouring RTV silicone, avoid bubble by using guide.	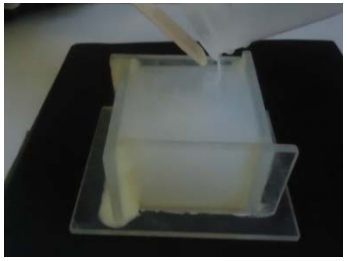 7. Fully filled mould. Setting time of 4hours for curing.

II. Demoulding of wax model from RTV silicone mould.

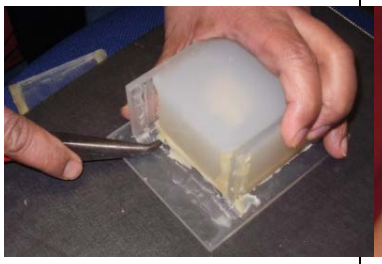 1. Removing the silicone mould after curing from mould box.	 2. Creating two half of the mould by cutting along the parting line.	 3. Exposed master pattern along the parting line.	 4. Removing the master pattern from the RTV silicone mould.	 5. Soft tooling created from RTV silicone mould.
 6. Preparing the paraffin wax	 7. Pouring the melted wax into the syringe.	 8. Injection the molten wax into the RTV mould	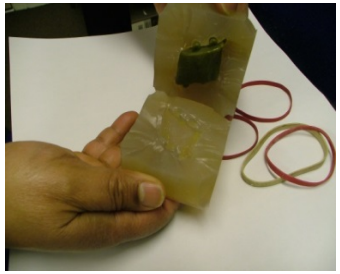 9. Removing the wax pattern from the mould.	 10. The wax pattern.

III. Casting of wax model to create AWGC BGS.

 1. Preparing the wax pattern for LWC. Attaching the spru.	 2. Setting the assembly inside a container. Cerrostone plaster is then poured in and let to set overnight.	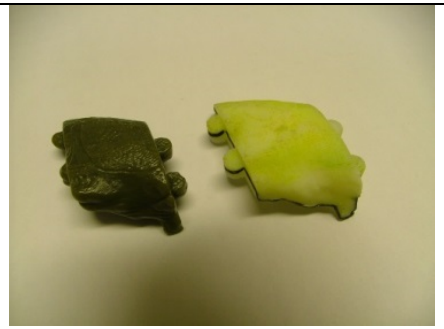 3. Comparing the wax pattern to the FDM model. Wax pattern showing high similarity with FDM model.	
 4. Wax pattern was removed by inverting the cast and heated in oven before AWGC-PMMA powder was filled into the cast.	 5. Sintering in the furnace.	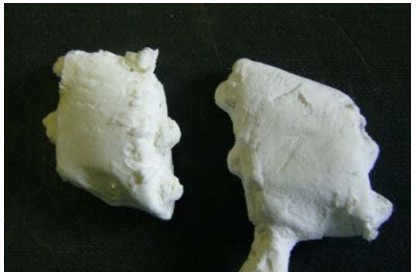 6. The fabricated AWGC artefacts.	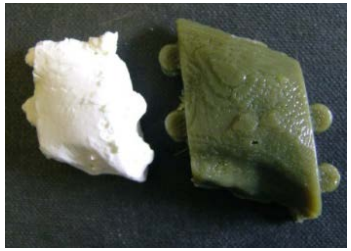 7. Comparing the fabricated AWGC artefact with the wax pattern.

-ooOooo-